

**Evaluation of Future Design Rainfall Extremes and Characteristics using Multiple-Model and  
Multiple-Scenario Climate Change Models**

by

Celyn Dezmain

A Thesis Submitted to the Faculty of

The College of Engineering and Computer Science

in Partial Fulfillment of the Requirements for the Degree of

Master of Science

Florida Atlantic University

Boca Raton, Florida

December 2013

**Evaluation of Future Design Rainfall Extremes and Characteristics using Multiple-Model and Multiple-Scenario Climate Change Models**

by

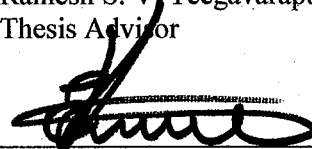
Celyn Dezmain

This thesis was prepared under the direction of the candidate's thesis advisor, Dr. Ramesh S. V. Teegavarapu, Department of Civil, Environmental and Geomatics Engineering, and has been approved by the members of his supervisory committee. It was submitted to the faculty of the College of Engineering and Computer Science and was accepted in partial fulfillment of the requirements for the degree of Master of Science.

SUPERVISORY COMMITTEE



Ramesh S. V. Teegavarapu, Ph.D., P.E.  
Thesis Advisor



Evangelos I. Kaisar, Ph.D.

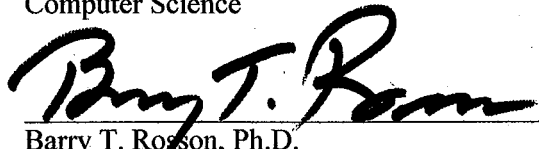


Panagiotis D. Scarlatos, Ph.D.



Yan Yong, Ph.D.  
Interim Chair, Department of Civil,  
Environmental and Geomatics Engineering

PP   
Mohammad Ilyas, Ph.D.  
Dean, College of Engineering and  
Computer Science

  
Barry T. Rosson, Ph.D.  
Dean, Graduate College

  
Date

## ABSTRACT

Author: Celyn Dezmain

Title: Evaluation of Future Design Rainfall Extremes and Characteristics using Multiple-Model and Multiple-Scenario Climate Change Models

Institution: Florida Atlantic University

Thesis Advisor: Dr. Ramesh Teegavarapu

Degree: Master of Science

Year: 2013

Climate models are common tools for developing design standards in the hydrologic field; however, these models contain uncertainties in multi-model and scenario selections. Along with these uncertainties, biases can be attached to the models. Such biases and uncertainties can present difficulties in predicting future extremes. These hydrologic extremes are believed to be non-stationary in character. Only in the recent past have model users come to terms that the current hydrologic designs are no longer relevant due to their assumption of stationarity. This study describes a systematic method of selecting a best fit model in relationship to location and time, along with the use of that best fit model for evaluation of future extremes. Rain gage stations throughout Florida are used to collect daily precipitation data used in extreme precipitation and quantitative indices. Through these indices conclusions are made on model selection and future extremes, as they relate to hydrologic designs.

**Evaluation of Future Design Rainfall Extremes and Characteristics using Multiple-Model and  
Multiple-Scenario Climate Change Models**

List of Figures .....	vii
List of Tables.....	xiii
Chapter 1 Introduction .....	1
1.1 Background.....	1
1.2 Problem Statement .....	3
1.3 Objectives .....	4
1.4 Thesis Outline .....	5
Chapter 2 Literature Review .....	6
2.1 Climate Variability and Teleconnections.....	6
2.2 Atlantic Multidecadal Oscillation (AMO) .....	7
2.3 El Niño/ La Niña Southern Oscillation (ENSO) .....	9
2.4 Pacific Decadal Oscillation (PDO) .....	11
2.5 North Atlantic Oscillation (NAO).....	12
2.6 Climate Change and Extreme Precipitation .....	13
2.6.1 Climate Projection Models.....	14
2.6.1.1 Coupled Model Intercomparison Project (CMIP).....	15
2.6.2 Variability in Extremes .....	17
2.6.3 Non-stationarity Issues.....	18
2.7 Influences on hydrologic design .....	19
Chapter 3: Methodology.....	21

3.1	Evaluation of Precipitation Extremes.....	23
3.1.1	WMO Precipitation Indices.....	23
3.1.2	Extreme Precipitation Bias Indices .....	27
3.1.2.1	Visual Bias Indices .....	27
3.1.2.2	Error Performance Measures .....	28
3.1.2.3	Contingency Measures.....	29
3.2	Bias Correction .....	32
3.2.1	Quantile Mapping (QM) .....	32
3.2.2	Uncertainty assessment of bias using resampling techniques .....	32
3.2.2.1	Bootstrap sampling .....	33
3.3	Model Selection .....	34
3.3.1	Integrated Ranking .....	34
3.3.2	Coupled Ranking.....	35
3.4	Statistical Methods.....	36
3.4.1	Parametric and Non-parametric Tests .....	36
3.4.1.1	Generalized Extreme Value (GEV) Distribution .....	36
3.4.1.2	Goodness of Fit Test: Kolmogorov-Smirnov Test: two-sample .....	37
3.5	Evaluation of Regional Precipitation Extremes .....	37
3.5.1	Depth Duration Frequency (DDF) .....	37
Chapter 4: Case Study Domain .....		39
4.1	Study Domain and Data .....	39
4.2	Data Collection and Analysis.....	42
4.2.1	Data Processing.....	43
Chapter 5: Results and Analysis.....		44
5.1	WMO Performance Measures.....	44
5.2	Bias Indices performance measures .....	56
5.2.1	Error measures performance .....	56

5.2.2	Contingency measure performance .....	56
5.3	Model Ranking .....	60
5.4	Long-term analysis of best models .....	65
5.4.1	Spatial variations of future precipitation trends .....	75
5.4.2	Incremental variations in extreme precipitation .....	75
5.4.3	Model Variation between stations .....	85
5.4.3.1	24 hour duration rainfall model variations between space and time .....	95
5.4.3.2	120 hour duration rainfall model variations between space and time .....	95
5.4.4	DDF variations with periodic time windows .....	95
5.4.5	DDF variations with expanding time window .....	96
5.4.6	Band of uncertainty between model based DDF .....	99
Chapter 6: Conclusions .....		112
6.1	Contribution of this study .....	113
6.2	Limitations of the Study.....	113
6.3	Recommendations for Future Research .....	114
Appendix A: Acronyms.....		116
Appendix B: WMO indices performance measures .....		118
Appendix C: WMO bias corrected indices performance measures .....		145
References .....		172

## List of Figures

Figure 1: AMO Index and its relation to Tropical Cyclone (Scott, 2010). .....	8
Figure 2: ENSO SST Index (Null, 2012). .....	9
Figure 3: Teleconnections between PDO and ENSO and their magnified effects (CIG C. I., 2011). .....	12
Figure 4: CO <sub>2</sub> emission concentration pathways according to the various representative concentration pathways models (Moss, et al., 2010). .....	17
Figure 5: Methodology for evaluation of downscaled precipitation from different climate change models. ....	22
Figure 6: Locations of the 31 NOAA/NWS cooperative network rain gages in Florida. ....	40
Figure 7: Variability of WMO indices for different models (2-17) and observed (1) for station 3. ....	46
Figure 8: Variability of WMO bias corrected indices for different models (2-17) and observed (1) for station 3. ....	47
Figure 9: Variability of WMO indices for different models (2-17) and observed (1) for station 8. ....	48
Figure 10: Variability of WMO bias corrected indices for different models (2-17) and observed (1) for station 8. ....	49
Figure 11: Variability of WMO indices for different models (2-17) and observed (1) for station 12. ....	50
Figure 12: Variability of WMO bias corrected indices for different models (2-17) and observed (1) for station 12. ....	51
Figure 13: Variability of WMO indices for different models (2-17) and observed (1) for station 20. ....	52
Figure 14: Variability of WMO bias corrected indices for different models (2-17) and observed (1) for station 20. ....	53
Figure 15: Variability of WMO indices for different models (2-17) and observed (1) for station 25. ....	54
Figure 16: Variability of WMO bias corrected indices for different models (2-17) and observed (1) for station 25. ....	55

Figure 17: Bias indices error performance measures. ....	57
Figure 18: Bias indices error performance measure after quantile mapping. ....	58
Figure 19: Bias indices contingency measure performance. ....	59
Figure 20: Number of times a model is selected for each performance measure. ....	61
Figure 21: Number of times a model is selected for each performance measure after quantile mapping. ....	63
Figure 22: Variability of CDD index and long-term trends in extreme precipitation.....	66
Figure 23: Variability of CWD index and long-term trends in extreme precipitation.....	67
Figure 24: Variability of RX1DAY index and long-term trends in extreme precipitation. ....	68
Figure 25: Variability of RX5DAY index and long-term trends in extreme precipitation. ....	69
Figure 26: Variability of R10 index and long-term trends in extreme precipitation. ....	70
Figure 27: Variability of R20 index and long-term trends in extreme precipitation. ....	71
Figure 28: Variability of SDII index and long-term trends in extreme precipitation. ....	72
Figure 29: Variability of PRCPTOT index and long-term trends in extreme precipitation.....	73
Figure 30: Variability of R254 index and long-term trends in extreme precipitation. ....	74
Figure 31: Variability of CDD index for long-term statistical changes in period 1(1950-1999), period 2 (2000-2049),.....	76
Figure 32: Variability of CWD index for long-term statistical changes in period 1(1950-1999), period 2 (2000-2049),.....	77
Figure 33: Variability of RX1DAY index for long-term statistical changes in period 1(1950-1999), period 2 (2000-2049),.....	78
Figure 34: Variability of RX5DAY index for long-term statistical changes in period 1(1950-1999), period 2 (2000-2049),.....	79
Figure 35: Variability of R10 index for long-term statistical changes in period 1(1950-1999), period 2 (2000-2049),.....	80
Figure 36: Variability of R20 index for long-term statistical changes in period 1(1950-1999), period 2 (2000-2049),.....	81

Figure 37: Variability of SDII index for long-term statistical changes in period 1(1950-1999), period 2 (2000-2049),.....	82
Figure 38: Variability of PRCPTOT index for long-term statistical changes in period 1(1950-1999), period 2 (2000-2049),.....	83
Figure 39: Variability of R254 index for long-term statistical changes in period 1(1950-1999), period 2 (2000-2049),.....	84
Figure 40: Variations of precipitation depths between 11 stations for 24 hour rainfall depths of a 25 year return period during 1950-1999. ....	87
Figure 41: Variations of precipitation depths between 11 stations for 24 hour rainfall depths of a 25 year return period during 2000-2049. ....	88
Figure 42: Variations of precipitation depths between 11 stations for 24 hour rainfall depths of a 25 year return period during 2050-2099. ....	89
Figure 43: Variations of precipitation depths between 11 stations for 24 hour rainfall depths of a 25 year return period during 1950-2099. ....	90
Figure 44: Variations of precipitation depths between 11 stations for 120 hour rainfall depths of a 25 year return period during 1950-1999. ....	91
Figure 45: Variations of precipitation depths between 11 stations for 120 hour rainfall depths of a 25 year return period during 2000-2049. ....	92
Figure 46: Variations of precipitation depths between 11 stations for 120 hour rainfall depths of a 25 year return period during 2050-2099. ....	93
Figure 47: Variations of precipitation depths between 11 stations for 120 hour rainfall depths of a 25 year return period during 2050-2099. ....	94
Figure 48: Variability of precipitation depths for a given 25 year return period for three 50 year intervals. ....	97
Figure 49: Variability of precipitation depths for a given 25 year return period for three expanding windows. ....	98
Figure 50: Band of uncertainty between CMIP5 model variations. ....	100
Figure 51: Band of uncertainty with comparison between observed (black) and model variations (grey). ....	101

Figure 52: Bias factor uncertainty for 24 hour duration. ....	102
Figure 53: Bias factor uncertainty for 120 hour duration. ....	103
Figure 54: Variability of precipitation depths for two durations for a return period of 25 years for observed data and model data (2000-2049) using different bias correction factors (mean factor). ....	105
Figure 55: Variability of precipitation depths for two durations for a return period of 25 years for observed data and model data (2000-2049) using different bias correction factors (lower bound factor). ..	106
Figure 56: Variability of precipitation depths for two durations for a return period of 25 years for observed data and model data (2000-2049) using different bias correction factors (upper bound factor). ..	107
Figure 57: Variability of precipitation depths for two durations for a return period of 25 years for observed data and model data (2050-2099) using different bias correction factors (mean factor). ....	108
Figure 58: Variability of precipitation depths for two durations for a return period of 25 years for observed data and model data (2050-2099) using different bias correction factors (lower bound factor). ..	109
Figure 59: Variability of precipitation depths for two durations for a return period of 25 years for observed data and model data (2050-2099) using different bias correction factors (upper bound factor). ..	110
Figure 60: Station 1 WMO indices bias evaluation. ....	119
Figure 61: Station 2 WMO indices bias evaluation. ....	120
Figure 62: Station 4 WMO indices bias evaluation. ....	121
Figure 63: Station 5 WMO indices bias evaluation. ....	122
Figure 64: Station 6 WMO indices bias evaluation. ....	123
Figure 65: Station 7 WMO indices bias evaluation. ....	124
Figure 66: Station 9 WMO indices bias evaluation. ....	125
Figure 67: Station 10 WMO indices bias evaluation. ....	126
Figure 68: Station 11 WMO indices bias evaluation. ....	127
Figure 69: Station 13 WMO indices bias evaluation. ....	128
Figure 70: Station 14 WMO indices bias evaluation. ....	129
Figure 71: Station 15 WMO indices bias evaluation. ....	130
Figure 72: Station 16 WMO indices bias evaluation. ....	131

Figure 73: Station 17 WMO indices bias evaluation.....	132
Figure 74: Station 18 WMO indices bias evaluation.....	133
Figure 75: Station 19 WMO indices bias evaluation.....	134
Figure 76: Station 21 WMO indices bias evaluation.....	135
Figure 77: Station 22 WMO indices bias evaluation.....	136
Figure 78: Station 23 WMO indices bias evaluation.....	137
Figure 79: Station 24 WMO indices bias evaluation.....	138
Figure 80: Station 26 WMO indices bias evaluation.....	139
Figure 81: Station 27 WMO indices bias evaluation.....	140
Figure 82: Station 28 WMO indices bias evaluation.....	141
Figure 83: Station 29 WMO indices bias evaluation.....	142
Figure 84: Station 30 WMO indices bias evaluation.....	143
Figure 85: Station 31 WMO indices bias evaluation.....	144
Figure 86: Station 1 WMO indices bias evaluation after quantile mapping.....	146
Figure 87: Station 2 WMO indices bias evaluation after quantile mapping.....	147
Figure 88: Station 4 WMO indices bias evaluation after quantile mapping.....	148
Figure 89: Station 5 WMO indices bias evaluation after quantile mapping.....	149
Figure 90: Station 6 WMO indices bias evaluation after quantile mapping.....	150
Figure 91: Station 7 WMO indices bias evaluation after quantile mapping.....	151
Figure 92: Station 9 WMO indices bias evaluation after quantile mapping.....	152
Figure 93: Station 10 WMO indices bias evaluation after quantile mapping.....	153
Figure 94: Station 11 WMO indices bias evaluation after quantile mapping.....	154
Figure 95: Station 13 WMO indices bias evaluation after quantile mapping.....	155
Figure 96: Station 14 WMO indices bias evaluation after quantile mapping.....	156
Figure 97: Station 15 WMO indices bias evaluation after quantile mapping.....	157
Figure 98: Station 16 WMO indices bias evaluation after quantile mapping.....	158
Figure 99: Station 17 WMO indices bias evaluation after quantile mapping.....	159

Figure 100: Station 18 WMO indices bias evaluation after quantile mapping. ....	160
Figure 101: Station 19 WMO indices bias evaluation after quantile mapping. ....	161
Figure 102: Station 21 WMO indices bias evaluation after quantile mapping. ....	162
Figure 103: Station 22 WMO indices bias evaluation after quantile mapping. ....	163
Figure 104: Station 23 WMO indices bias evaluation after quantile mapping. ....	164
Figure 105: Station 24 WMO indices bias evaluation after quantile mapping. ....	165
Figure 106: Station 26 WMO indices bias evaluation after quantile mapping. ....	166
Figure 107: Station 27 WMO indices bias evaluation after quantile mapping. ....	167
Figure 108: Station 28 WMO indices bias evaluation after quantile mapping. ....	168
Figure 109: Station 29 WMO indices bias evaluation after quantile mapping. ....	169
Figure 110: Station 30 WMO indices bias evaluation after quantile mapping. ....	170
Figure 111: Station 31 WMO indices bias evaluation after quantile mapping. ....	171

## List of Tables

Table 1: Advantages and disadvantages related to various downscaling methods (Brekke, et al., 2009). .....	3
Table 2: AMO Multidecadal Shifts. ....	9
Table 3: ENSO Recorded Years. ....	10
Table 4: CMIP5 RCP details (Moss, et al., 2010). ....	16
Table 5: Classification of observed and predicted precipitation events. ....	30
Table 6: Location of rain gages (SERCC, 2013). ....	41
Table 7: CMIP5 BCCA RCP2.6 climate models selected for initial condition analysis. ....	42
Table 8: Selected models at different sites. ....	45
Table 9: Model frequencies for each station. ....	62
Table 10: Bias Corrected model frequencies for each station. ....	64
Table 11: Stations selected for long-term analysis. ....	65
Table 12: Incremental 50 year period. ....	75
Table 13: Projected models scenario and run variations. ....	86
Table 14: Correction factors based on bootstrap resampling approach. ....	99
Table 15: Precipitation depths for different durations based on different factors. ....	104
Table 16: Band of uncertainty variations between time periods and space. ....	111

## **Chapter 1 Introduction**

### **1.1 Background**

Climate models are an important part of forecasting hydrologic events; however, they have not always been as reliable as they appear today. Accurate climate models have only been available in the recent past. With rapidly improving technology, orthodox methods of rainfall data collection, such as rain gage stations, are being combined and in some cases replaced by radar methods. With the implementation of higher maintenance on existing rain gages along with radar, rainfall data as decreased in missing data and mechanical error (Teegavarapu, 2012). Although the recent improvements in technology have enabled data recording to reach a higher level of accuracy, there is still room for improvements in the way the historical and projected data are viewed by researchers.

Up until recently, climate researchers, water resource managers, civil engineers, and hydrologists alike have viewed the climate as stationary with respect to time and space. As accurate data records went under review by leading climate organizations and researchers, it became clear that the climate is in fact non-stationary. This theory comes with grave implications on the hydrologic and water resource fields, by threatening local environments, especially urban areas, with extreme rainfall events leading to flooding or drought (Arisz & Burrell, 2006). By improving rainfall data, stormwater run-off trends can be acknowledged and local infrastructures such as retention and detention ponds, storm sewer lines, and roadways can all be appropriately modified to be better suited for changing climate.

With the climate being non-stationary, meaning that the climate is changing in frequency and intensity as time progresses, regions, on a local scale, find themselves in a struggle to elevate the level of service of hydrologic infrastructure without exhausting budgets (Hamlet, 2011). Once outdated or decrepit infrastructure is removed, engineers cannot simply replace it, because the current design standards are no

longer suited to withstand the approaching climate. In order to accommodate the changing climate, there must be a new set of design standards created. These standards will be unique on a regional level. Downscaled climate models coupled with regional historic climate data will provide analysts the necessary tools to understand and prepare for the future climate and climate extremes.

Climate models have been around for many years now and have offered themselves to water resource managers, hydrologic engineers, and climatologists in the hope to better understand and predict the future climate. There are several versions of climate modeling currently in circulation. Of the numerous models, an organization known as IPCC has developed one of the more prominent and accepted modeling methods. These models are known as General Circulation Models (GCMs) and they represent physical processes in the atmosphere, ocean, cryosphere, and land surface. GCMs depict the climate using a three dimensional grid over the globe, typically having a horizontal resolution of between 250 and 600 km, 10 to 20 vertical layers in the atmosphere and sometimes as many as 30 layers in the oceans (IPCC, 2007).

Downscaling is a process used to bring the GCMs 10 to 30 layers in the atmosphere to a local scale and also reduce the grid resolution up to an eighth degree. There are two methods to downscale climate models. The first involves nesting of regional models into GCMs. This is known as dynamic downscaling, because regional climate models (RCMs) and GCMs are both dynamic in character. The second method is statistical downscaling, which uses statistical regressions to connect local variables to driving forces in the GCMs (Wilby, et al., 2004). The advantages and disadvantages of statistical versus dynamic downscaling are listed in Table 1.

**Table 1: Advantages and disadvantages related to various downscaling methods (Brekke, et al., 2009).**

	Statistical	Dynamic
Advantages	<ul style="list-style-type: none"> <li>• Comparatively cheap and computationally efficient</li> <li>• Can provide point-scale climatic variables from GCM-scale output</li> <li>• Able to directly incorporate observations into method</li> </ul>	<ul style="list-style-type: none"> <li>• Produces responses based on physically consistent processes</li> <li>• Produces finer-resolution information from GCM-scale output that can resolve atmospheric processes on a smaller scale (for example, orographic and rain shadow effects in mountainous areas)</li> </ul>
Disadvantages	<ul style="list-style-type: none"> <li>• Does not account for non-stationarity in the predictor-predictand relationship</li> <li>• Climate system feedbacks not included</li> <li>• Dependent on GCM boundary forcing; affected by biases in underlying GCM</li> <li>• Dependent on statistical or empirical model structure and associated parameters; different models will give different results</li> </ul>	<ul style="list-style-type: none"> <li>• Computationally intensive</li> <li>• Limited number of scenario ensembles available</li> <li>• Dependent on GCM boundary forcing; affected by biases in underlying GCM</li> <li>• Dependent on RCM parameterizations; different RCMs will give different results</li> </ul>

Once the model's results are downscaled to a local resolution, they become useful to the water resource managers, hydrologic engineers and climatologist in the development and understanding local scale effects of climate change. One of the major areas that the climate change has an effect on is hydrologic design, especially in urban areas. The current standards used today were developed under the notion that climate is stationary and will mimic the past in the present and future. The fact is that climate is not stationary.

## 1.2 Problem Statement

A major concern in the hydrologic, water resources and climatology fields is the changing climate. The climate is believed to be non-stationary, opposite to prior belief. This notion will cause significant changes in the water resource and hydrologic fields and their current designs. The current design standards

will need revision to accommodate a more flexible and robust future climate. Climate models will need to be married with design parameters to better understand the future needs of urban infrastructure; however, these models are space and time specific making it difficult to develop a general methodology to correct this problem.

The use of downscaled climate models for accurate climate projections present uncertainties on temporal and spatial scales. The downscaled climate models possess a unique combination of climate model type, initial condition, and emission path scenario. Due to extreme variation of climate through space and time, the models will perform differently at different locations and times. The uncertainty of this spatial and temporal variation needs to be put to rest through a systematic comparison to rank and select a best model based on several performance measures.

### **1.3 Objectives**

This thesis reviews the uncertainties related to multiple-model and multiple-scenarios and how each model combination performs on a site and regional scale. Through a best fit model and scenario combination, the assessment of future hydrologic event will be performed. Along with this evaluation, the restructure of current hydrologic design standards, as they relate to sustainability, will be performed as needed.

The objectives of this study are as follows:

- 1) Evaluate bias corrected downscaled climate change models.
- 2) Determine the best performing model(s) through extreme precipitation and performance measure indices.
- 3) Evaluate future extremes based on best performing model(s).
- 4) Use re-sampling techniques for obtaining bias corrections factors for downscaled precipitation extremes.
- 5) Determine extent of non-stationarity on a local scale.
- 6) Assess uncertainty in hydrologic designs through future climate model projections.

## **1.4 Thesis Outline**

Organization of the contents of the thesis:

Chapter One: Provides introduction to the impacts that climate change and climate variability have on hydrologic events, specifically extreme precipitation, the problem of current hydrologic models and designs not considering the non-stationarity related to the climate along with the list of objectives for this study.

Chapter Two: Documents the existing literature on oscillations, climate change models and simulations, as well as the documented effects seen from climate change.

Chapter Three: Describes a step-by-step approach involving various methods of model selection including the evaluation of performance measures along with precipitation extremes to determine a site specific optimum model. Deviations witnessed by hydrologic events compared to projected hydrological events are noted and design standards changed accordingly.

Chapter Four: The methodology mentioned in Chapter Three is applied to a case study in order to provide real world scenarios where climate change is affecting hydrologic events. This chapter also highlights general background information needed to describe the case study region.

Chapter Five: Results from the case study are recorded and analyzed and a site specific optimum model is selected. Further analysis on the selected model to determine the accuracy of current hydrologic design standards is performed.

Chapter Six: Conclusions from the case study, as well as, contribution, limitations and recommendations for future studies are mentioned in this Chapter.

## **Chapter 2 Literature Review**

### **2.1 Climate Variability and Teleconnections**

The climate has a large influence on nearly every aspect of the Earth, from the health and well being of both plants and animals, to water resources and infrastructure design. The theory that climate is stationary has been discredited over the past years as new methods of data collection have revealed the truth on climate variability and change and their effects on the local and global environments and economies. According to the United States Geological Survey (USGS) (2012) climate variability and change are having a large effect on future hydro-climatic activity.

Climate variability refers to variations in the mean state and other statistics (such as standard deviations, the occurrence of extremes, etc.) of the climate at all spatial and temporal scales beyond that of individual weather events. Variability may be due to natural internal processes within the climate system (internal variability), or to variations in natural or anthropogenic external forcing (external variability) (IPCC, 2011). Due to climate change and variability the extreme precipitation events are believed to be increasing in both intensity and frequency, whether that is expressed through extreme floods or droughts. Because of these projections, the design and operational assumptions about water management are questioned (Brekke, et al., 2009).

With the increase in extreme precipitation also comes higher peak runoff. This increase in storm-water runoff in urban areas will present strain on the existing storm sewer infrastructure and the existing design parameters. This thesis proposes that due to climate change the preset storm-water design parameters must be reviewed and changed accordingly to match future projections for rainfall. Current water management practices may not be robust enough to cope with the impacts of the climate change on water supply reliability and flood risk (Bates, et al., 2008).

One major contributor to climate variability is a climate phenomenon known as teleconnections, which occur between multiple climatic oscillations. The teleconnections between oscillations act in both positive and negative correlations which can magnify or diminish climatic trends in local climates. This can have drastic effects on water management, for example, exceeding expected extremes in precipitation. From a prior study by Gershunov and Barnett (1998), the Pacific Decadal Oscillation (PDO) during the high phase formed a teleconnection with El Niño Southern Oscillation (ENSO) to create high extremes in precipitation for both the warm and cool phase in ENSO throughout the southern portion of the United States (Gershunov & Barnett, 1998).

During the 1930-1960 warm phase of the Atlantic Multidecadal Oscillation (AMO), the rainfall had a significant negative correlation with ENSO, whereas during the cool phases of AMO the correlation where insignificant with ENSO (Enfield, et al., 2001). Climate variability is mostly experienced on a regional scale, thus research and modeling should be done on a regional scale as well. There is reason to believe that climate extremes are increasing, but with poor data and evaluation methods it is difficult to gather accurate conclusions on the topic (RMetS, 2009).

## **2.2 Atlantic Multidecadal Oscillation (AMO)**

The Atlantic Multidecadal Oscillation is a source of variability that is expressed through sea surface temperature (SST), shifting from warm to cool, in the North Atlantic Ocean ranging approximately from 95°W-30°E and 0°-70°N (Knight, et al., 2006). The past 100 years of recorded data shows warm phases during 1860-1880 and 1940-1960, and cool phases during 1905-1925 and 1970-1990. Although warm and cool phases have been defined in the past and present, there has not been a trend related to the shifts from

warm and cool phases within AMO. The cycles are defined by temperature shifts with the rainfall remaining highly variable year to year (Obeysekera, et al., 2006); however, due to the variability in Sea Surface Temperature (SST), there is a direct relationship to the tropical storm activity on the eastern seaboard. An index of AMO's SST variability is described by Figure 1.

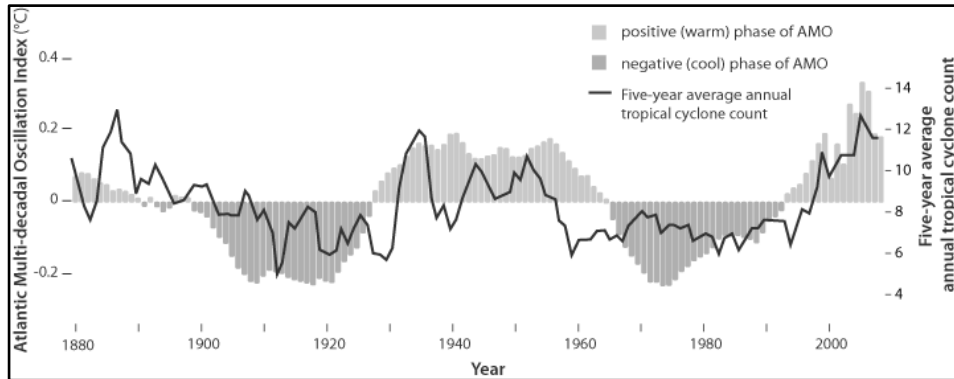


**Figure 1: AMO Index and its relation to Tropical Cyclone (Scott, 2010).**

The warm phase of AMO is producing a much higher frequency of tropical storms in the North Atlantic Ocean, while the cool phase shows a decrease in the number of tropical storms. According to Enfield, et al., (2001), AMO has a global effect with a 0.4°C range in sea surface temperature. Between AMO warm and cool phases, Mississippi River outflow varies by 10% while the inflow to Lake Okeechobee varies by 40%. These large deviations in streamflows can be caused by the effects that AMO has on local precipitation extremes. The multidecadal time periods of AMO's warm and cool phases are listed in Table 2.

**Table 2: AMO Multidecadal Shifts.**

Warm phase	Cool phase
1860-1880	1905-1925
1940-1960	1970-1990
1995-2012	

When positive (warm) phases predominate, flooding is a greater risk, while negative (cool) phases generate opposite effects. The future attempts to predict and prepare for climatic impacts will remain inaccurate if AMO is not accounted for, specifically for regions that encounter higher frequencies of tropical storms.

### 2.3 El Niño/ La Niña Southern Oscillation (ENSO)

The El/La Niño Southern Oscillation fluctuates between warm and cool phases every 3-7 years during the dry season in South and Central Florida, as well as having a global influence. Each of the two phases have opposite extreme effects on local temperature and rainfall. The warm phase generates higher rainfall and lower temperature while the cool phase generates higher temperatures and lower rainfall (Obeysekera, et al., 2006). The oscillation index is described by Figure 2.

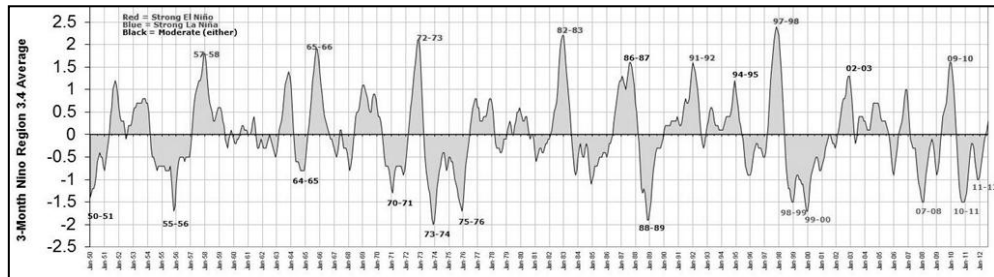


**Figure 2: ENSO SST Index (Null, 2012).**

According to the research of Ropelewski and Halpert (1986), ENSO is a contributor to surface temperature and precipitation variability throughout North America. The study revealed that 81% of the cases exhibited above normal precipitation through the southeastern portions of North America. However, there was a clear negative correlation between the ENSO event and the surface temperature within the southeastern region (Ropelewski & Halpert, 1986). ENSOs recorded phases are described by Table 3.

**Table 3: ENSO Recorded Years.**

El Niño	La Niña
1951	1950
1953	1954
1957	1955
1958	1964
1963	1967
1965	1970
1968	1971
1969	1973
1972	1974
1976	1975
1977	1983
1979	1984
1982	1988
1986	1995
1987	1998
1991	1999
1994	2000
1997	2005
2002	2007
2004	2008
2006	
2009	

Due to ENSOs rainfall extremes and the rapid phase shifts, water management is struggling to keep up with the demands. ENSO has severe effects on the hydrology of South Florida. The increases in rainfall during El Niño caused flooding in Lake Okeechobee and forced water management to discharge the excess water into the estuaries causing significant damage to the local environment. The lack of rainfall during La Niña causes droughts and water management is forced to limit water usage and implement

restrictions on the public water supply (Enfield, et al., 2001). Water management must use ENSO to make decision more suitable to the real world climate and its non-stationarity.

#### **2.4 Pacific Decadal Oscillation (PDO)**

The Pacific Decadal Oscillation is very similar to ENSO with near identical cycle patterns; however, PDO has decadal phases. PDO also does not have as much effect on the Southeast portions of the United States as ENSO does. PDO is directed more towards the North Pacific/ North American sector. The warm and cool phases of PDO have the same effects as the Warm and Cool phases of ENSO (Obeysekera, et al., 2006). Because of their close similarities, the two oscillations have strong influences over one another. The oscillations are characterized by sea surface temperatures, sea level pressure, and wind patterns (CIG C. I., 2008).

PDO has stronger effects on the Pacific North West then it does on the rest of the United States. There have recording of 10% decreases in precipitation during warm phases then in the cool phases during the water year, October 1-September 30 of the following year. While temperatures are on average 1°F higher during warm phases then in cool phases during the water year, these effects on the Pacific North West are exemplified by coinciding warm and cool phases between PDO and ENSO. The similarities between the oscillations allow for positive correlations between the two. This magnifies both precipitation and temperature effects in the local climates. The effects are demonstrated in Figure 3.

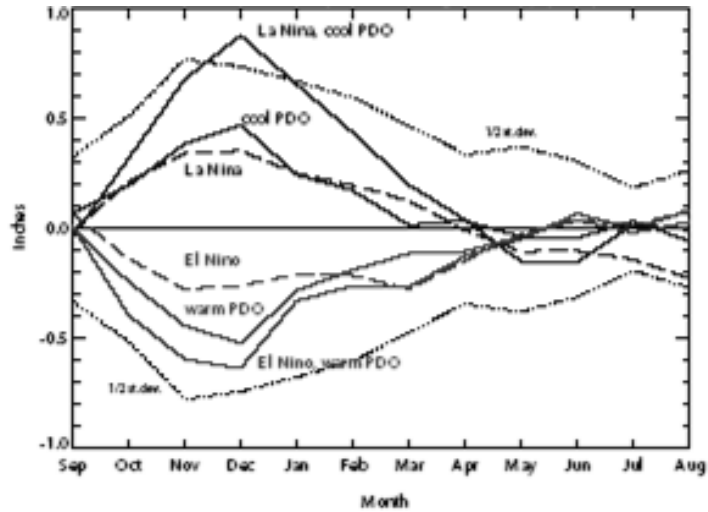


**Figure 3: Teleconnections between PDO and ENSO and their magnified effects (CIG C. I., 2011).**

The reinforcing effects that PDO and ENSO have on one another during coinciding warm or cool phases are significantly noticeable with nearly  $\pm 0.5$  inch difference in precipitation and  $1^{\circ}\text{F}$  in temperature depending on the phase. However the effects are not as significant when opposing phases in PDO and ENSO occur. There have been cases of the two oscillations cancelling each other out, but it is not consistent in time or space (CIG C. I., 2011).

## 2.5 North Atlantic Oscillation (NAO)

Hurrell (2003) states that the North Atlantic Oscillation is the prevailing climatic oscillation in the North Atlantic Region, North America to Europe, Asia, and Africa. NAO refers to swings in the atmospheric sea level pressure difference between the Arctic and the subtropical Atlantic that is most noticeable during the boreal cold season (November–April) and are associated with changes in the mean wind speed and direction. Such changes alter the seasonal mean heat and moisture transport between the Atlantic and the neighboring continents, as well as the intensity and number of storms, their paths, and their weather (Hurrell, et al., 2003).

Due to the drastic pressure differences produced by NAO's positive phase, there are generally stronger westerly winds throughout the middle grounds of the North Atlantic region. These strong westerly winds result in warm and wet winters in the Eastern USA and Europe and cold and dry winters in Canada and Greenland (Rosenzwei, et al., 2011). The effects of NAO are generally strongest in the winter, December through March, but will prevail throughout the year. The negative phase of NAO has opposing effects than that seen during the positive phase. The results are weaker and eastward subtropical high and a weaker Iceland low (Rosenzwei, et al., 2011). This generates winds moving west to east and will bring colder and drier winters to the eastern USA.

Durkee, et al. (2007) performed a study where seasonal phases of the NAO are compared to changes in the frequency and distribution of winter season (December–March) precipitation-type observations for the years 1961–2001 in the eastern U.S. Statistically significant increases in the frequency of rain observations across the study region are associated with positive NAO phases (Durkee, et al., 2007). The study encompasses a network of 100 stations to measure rain or snow fall. Stations are located throughout the eastern portion of the U.S. The northern portion of the study area saw a 24% increase in rainfall between positive and negative NAO phases, with the remainder of the stations experiencing at least a 20% increase in rainfall between phases. The snowfall observations were not as significant; however, they did experience increases of at least 8% of snowfall (Durkee, et al., 2007). The water management division must heed the results of this study to better develop and prepare for future water management practices. With a 20% shift in rainfall frequency between NAO phases, there can be drastic fluctuations in stream flows causing flooding or drought in local watersheds.

## **2.6 Climate Change and Extreme Precipitation**

Due to present day infrastructure reaching its maximum yield performance the study of climate change and its effects on water resources has become a hot topic. With the increasing frequency and duration of extreme precipitation, there is concern that infrastructure will experience more frequent failure, in particular urban drainage. The difficulties and uncertainties that present themselves with urban drainage are in both temporal and spatial scales. The current climate models represent coarse grids for long-term

forecasts. The water resources field is interested in the short term and local scale effects that climate change has on urban drainage, sewer systems, and flooding. In order to accommodate these needs, global climate models must be downscaled to a local scale. It is important to follow the climate models as they are updated and compared to local scale rainfall extremes. The results of the climate models will be beneficial to hydrologic planners and designers in upgrading infrastructure to accommodate the effects of future climate change (Willems, et al., 2011).

Madsen, et al., (2012) composed a report on the causes and effects of global warming in light of the growing concern of its effects of hydrologic events. Extreme rainfall and storm events were highlighted as some of the effects global warming has on local and global scales. The rising temperature is directly related to the increases seen in the intensity, frequency and durations of rainfall events. Rain stations around the country have been used to predict trends in rainfall caused by global warming. These trends show a 30% increase in extreme storm events and a 10% increase in the rainfall over the past 60 years. These trends could increase exponentially if there is no action taken to decrease the pollution generated by the burning of fossil fuels, which in return releases CO<sub>2</sub> into the atmosphere (Madsen, et al., 2012).

### **2.6.1 Climate Projection Models**

Most commonly used for precipitation projections is the GCMs. Only GCMs have the potential to provide geographically and physically consistent estimates of regional climate change which are required in impact analysis, thus fulfilling IPCC's criterion 2 (Viner, 2011). There are five criteria that must be fulfilled to consider a scenario possible. The five criteria are:

Criterion 1: Consistency with global projections. The model scenarios should be consistent with a broad range of global warming projections based on increased concentrations of greenhouse gases. This range is variously cited as 1.4°C to 5.8°C by 2100, or 1.5°C to 4.5°C for a doubling of atmospheric CO<sub>2</sub> concentration (otherwise known as the "equilibrium climate sensitivity").

Criterion 2: Physical plausibility. The model scenarios should be physically plausible; that is, they should not violate the basic laws of physics. Hence, changes in one region should be physically consistent

with those in another region and globally. In addition, the combination of changes in different variables (which are often correlated with each other) should be physically consistent.

Criterion 3: Applicability in impact assessments. The model scenarios should describe changes in a sufficient number of variables on a spatial and temporal scale that allows for impact assessment. For example, impact models may require input data on variables such as precipitation, solar radiation, temperature, humidity and wind speed at spatial scales ranging from global to site and at temporal scales ranging from annual means to daily or hourly values.

Criterion 4: Representative. The model scenarios should be representative of the potential range of future regional climate change. Only in this way can a realistic range of possible impacts be estimated.

Criterion 5: Accessibility. The model scenarios should be straightforward to obtain, interpret and apply for impact assessment. Many impact assessment projects include a separate scenario development component which specifically aims to address this last point. The DDC and this guidance document are also designed to help meet this need (IPCC, 2011). These criteria are used to develop climate models.

#### ***2.6.1.1 Coupled Model Intercomparison Project (CMIP)***

GCM is on a global level and needs to be downscaled in order to be useful for any regional level precipitation or temperature model. GCMs are downscaled to what is known as Bias Corrected Statistical Disaggregation (BCSD) models which are downscaled from the GCMs at 2° pixel to 1/8° pixel and are displayed as monthly projections, or Bias Corrected Constructed Analog (BCCA) models which are daily projections with similar downscaling. There are currently 134 downscaled climate models available by BCCA that include: 21 GCMs, 4 emission scenarios (RCP2.6, RCP4.5, RCP6.0, RCP8.5), and ensemble runs 1 to 12. Each of these models is different and will perform better or worst depending on the study domain and scenario chosen.

CMIP Phase 3 (CMIP3) paved the way in the study of climate change and water resource management and still provides accurate data recordings and projection models for research. The selection of the scenario and model will greatly affect the outcomes; however, the results will be beneficial in

providing insight on the effects of multiple-model and multiple-scenario uncertainties. The most commonly used scenario, for CMIP3, is the doubling of CO<sub>2</sub> emissions from 2000-2050, scenario A1b. This climate scenario is predicted to increase rainfall intensities by 15%-20% or cutting storm design return periods in half (Arisz & Burrell, 2006).

As time moves forward so does technology and with this technology, there becomes a desire for more efficient climate projection models. CMIP Phase 5 (CMIP5) was created, utilizing a parallel process in developing new circulation models in order to reduce turnaround time and increase efficiency. The new models come with new and improved "scenarios" although they are now known as Representative Concentration Pathways (RCPs), which display interest in not only concentration levels, but also emission paths. CMIP5 utilizes a peer to peer methodology by removing the IPCC from the process allowing more mobility and speed. There are benefits to using CMIP5, such as extended projections and fewer data gaps (Moss, et al., 2010). CMIP5 utilizes four versions of RCPs: RCP2.6, RCP4.5, RCP6.0, RCP8.5. These pathways represent various concentration pathways that are described in Table 4.

**Table 4: CMIP5 RCP details (Moss, et al., 2010).**

Name	Radiative forcing	Concentration (ppm)	Pathway	Model providing RCP*
RCP8.5	>8.5 W m <sup>-2</sup> in 2100	>1,370 CO <sub>2</sub> equiv. in 2100	Rising	MESSAGE
RCP6.0	~4.5 W m <sup>-2</sup> at stabilization after 2100	~850 CO <sub>2</sub> equiv. (at stabilization after 2100)	Stabilization without overshoot	AIM
RCP4.5	~6 W m <sup>-2</sup> at stabilization after 2100	~600 CO <sub>2</sub> equiv. (at stabilization after 2100)	Stabilization without overshoot	GCAM
RCP2.6	Peak ~3 W m <sup>-2</sup> before 2100 and then decline	Peak at ~490 CO <sub>2</sub> equiv. before 2100 and then decline	Peak then decline	IMAGE

The pathways describe extremes at each end of the spectrum. The worst case being RCP8.5, where the concentration steadily increases without stabilization or decline, and the best case being RCP2.6, where the concentrations peak before 2100 and decline afterwards displayed in Figure 4.

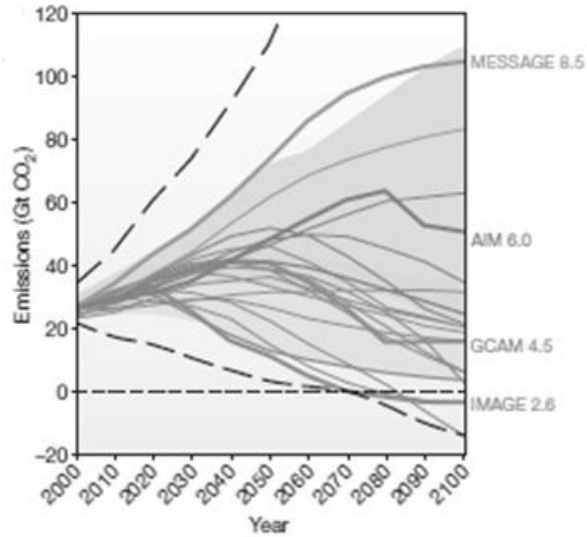


**Figure 4: CO<sub>2</sub> emission concentration pathways according to the various representative concentration pathways models (Moss, et al., 2010).**

These variations in models and scenarios are cause for concern when selecting a suitable model. There is large uncertainty related to model selection when the variations have high deviations from one another. A study by Teegavarapu (2013) discusses model selection and the uncertainties associated with it. Climate change models present limitations on the assessment of uncertainties with climate change. Uncertainties such as extreme precipitation have influences on hydrologic design and water resources and will need proper modeling in order to reduce biases and missed predictions.

### **2.6.2 Variability in Extremes**

Anthropogenic changes to the environment have drastic effects on the climate and local hydrologic cycle. The dramatic increase of CO<sub>2</sub> over the past years is expected to continue to increase by two fold during this century. With these increased CO<sub>2</sub> emissions, increases in hydrological and climatic extremes are expected. General Circulation Models predict additional increases in mean global temperature by 1.1 to 6.4 degrees Celsius (IPCC, 2007). The global atmospheric circulation and hydrologic processes patterns are predicted to increase in mean annual precipitation and inter- and intra-annual variability of precipitation

(Easterling, et al., 2000). Nearly all GCMs show slight to moderate increases in rainfall extremes (IPCC, 2007) and (Zhang, et al., 2007).

There are uncertainties on both projected and observed extreme precipitation. Observed extreme precipitation has high variability in both temporal and spatial scales. Florida is especially susceptible to these variations because of its' vast amounts of large water bodies and its' vulnerability to hydrologic storm events. The water bodies found in and surrounding the state of Florida produce increased humidity and more likelihood of a precipitation event. This factor combined with the characteristically high landfall rate of tropical storms, creates a high variability for extreme rainfall through the state.

### **2.6.3 Non-stationarity Issues**

Stationarity of rainfall statistical characteristics is a fundamental assumption in hydrologic infrastructure design that may not be valid in an era of changing climate. Hydrologic infrastructure design is normally based on the concept of a design storm event, either historical or synthetic (Denault, et al., 2002). Typical design standards for hydrologic structures come from Intensity Duration Frequency (IDF) curves. These curves commonly assume climatic stationarity in their design where mean and standard deviations remain constant over time. These assumptions can greatly affect a hydraulic design as time passes.

The non-stationarity of climate also generally implies non-stationarity of hydrologic extremes (Jain & Lall, 2001). The southeast region of the U.S is experiencing climate change effects such as rising temperature, sea level rise, and higher frequency of extreme precipitation. Possible forms of non-stationarity caused by climate change are (1) change in distribution as a whole (average value increases while the variability remains unchanged); (2) change in the variability while the average values remain the same; and (3) changes in both the average and the variability of the variable over time (Lemmen, et al., 2007), (Mailhot & Duchesene, 2010). These attributes of climate change have already produced real world damages on the economy and ecosystem. In 2011, Texas experienced prolonged temperature rises that shortened the cattle season, as well as increased wildfires throughout the state (Melillo & Peterson, 2009). Higher storm frequencies will generate stronger storm surges, flooding the low lying coastal infrastructure

(Arisz & Burrell, 2006). The existing infrastructure of local regions experiencing significant hydrologic changes must be updated to accommodate the changing climate.

Previously mentioned, rainfall has increased by 10% over the past 60 years and is expected to continue increasing. The consequences of the effects of climate change are a decreasing level of service for drainage infrastructure, increased risk of flooding, and environmental damages resulting from channel destabilization (Arisz & Burrell, 2006). With hydrologic infrastructure both costly and time consuming to update and adapt to the changing climate and the existing urbanization leaving little room for expansion, there must be creative ideas presented to help solve the problem of aging infrastructure. There are two types of storm drainage systems: major and minor. The major systems convey water on a larger scale over land and consist of retention and detention ponds, catchments, open channels, and etc. Whereas the minor systems are underground pipelines and storm sewer drains. Both must be updated to consider the non-stationarity of the climate. An increase in research and monitoring are needed to help fill gaps in the advancement of water resource planning. There will always be uncertainties associated with non-stationarity, but these can provide improvements in understanding climate change and the effects it has on hydrologic design and water resources (Brekke, et al., 2009).

## **2.7 Influences on hydrologic design**

Design criteria for stormwater infrastructure have strong connections to the assumption that the probability distribution of precipitation extremes is statistically stationary. This makes climate and climate change have large influences on hydrologic design (Rosenburg, et al., 2010). Urban drainage design should incorporate the climatic change that is expected to occur during the life span of the structure. This takes non-stationarity into design consideration. The translation of climate projections into planning assumptions such as supplies, demands, flood risks, and infrastructure safety can greatly improve the outcomes in future (Brekke L. , 2013). One way is to (1) incorporating the anthropogenic assumption from local communities into GCM, (2) downscaling these models to local scales, (3) applying the downscaled models to hydrologic extremes and, (4) accepting an acceptable flood risk (Nielsen, 2011).

Intensity Duration Frequency (IDF) curves are common tools in the hydrologic design fields. These curves allow engineers to design for expected rainfall intensities for a given storm event. However, these curves in most regions have not been updated for many years, even decades. This leads to inaccurate hydrologic infrastructure. Many IDF curve users such as civil engineers, consultants, and water resource managers have concerns that the climate change may have presented changes in “older” curves (Mailhot & Duchesene, 2010). These curves are essential for planning infrastructure safety and flood risk reduction. The supplementation of historical climate information into the future climate might be expected, but planning assumptions are instead related to projections of future precipitation; however, there is not one best approach yet to developing the relationship between hydrologic planning and the future climate projections (Brekke L. , 2013).

### **Chapter 3: Methodology**

It is known that precipitation is highly correlated to regional characteristics at a local scale. In order to statistically preserve precipitation data when applied to climate models, certain characteristics must be incorporated. The GCMs grid size range from 150km-300km, which is not applicable for local scale analysis. There are downscaled climate models, CMIP, at  $1/8^\circ$  or 13.89km grid size to assist local characteristics to become relevant in the precipitation data applied. CMIP5 utilizes a variety of scenarios and initial conditions to mimic regional characteristics. The climate conditions are represented through 21 climate models, each with four emission pathway options and multiple initial condition scenarios. In order to determine which model and pathway combination is best suited for a particular region, the historic precipitation extremes must be compared to the project extremes. This will allow the selection of general circulation models through quantitative, statistical, and visual indices, thus leading to updated local hydrologic infrastructure. The proposed methodology using different indices for selection of a best model and resampling approach for evaluation of biases is shown in Figure 5.

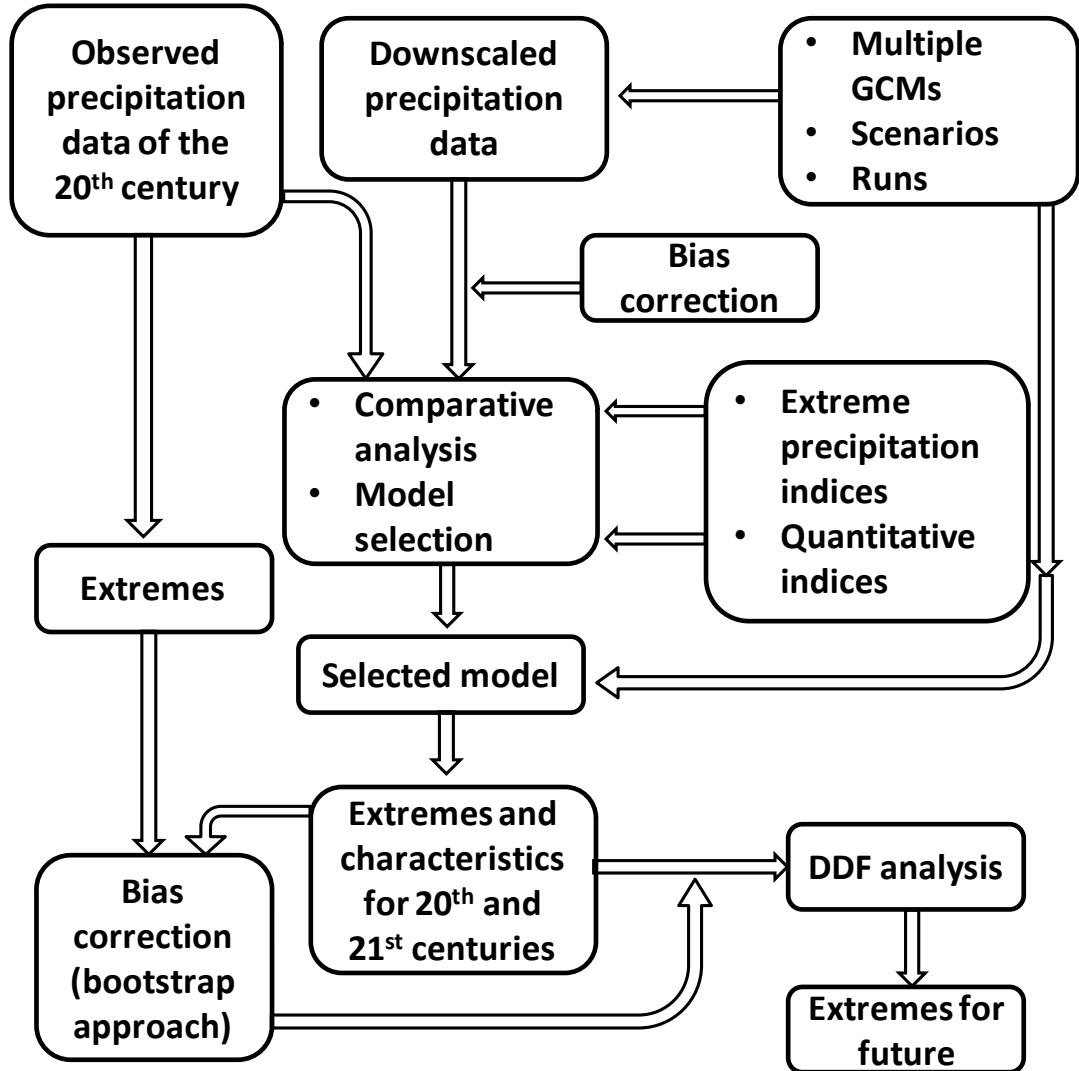


Figure 5: Methodology for evaluation of downscaled precipitation from different climate change models.

### 3.1 Evaluation of Precipitation Extremes

The analysis of precipitation extremes has been conducted on historical data as well as projected model data, known as GCMs. These models are climate models, CMIP5, that have accounted for highly probable scenarios or emission paths that are likely to occur in the future. The objective is to determine which model is performing the best by producing the least error when compared to the observed historical data. There have been many indices and error functions used in the climate and hydrologic fields to compare, quantitatively and qualitatively, models and observed data. The most suited indices come from a study by the World Meteorological Organization (WMO) in 2009. This study created 11 precipitation indices that will allow researchers to better understand the behavior of precipitation extremes in their region of study through standardized quantitative analysis. However, in order to determine, statistically and visually, whether there are any biases in the climate models, there will be several bias indices applied to the historical data to detect them. These bias indices were adopted from a study for the South Florida Water management District (SFWMD) performed by Teegavarapu (2012). This study defines 21 bias indices to detect biases in the precipitation data.

#### 3.1.1 WMO Precipitation Indices

The WMO precipitation indices are based on physical characteristics of the observed and historic model rainfall. These indices provide insight on the behavior of extreme rainfall at a regional scale, which in return can help reduce natural disaster, caused by flooding or drought, in urbanized areas. These physical indices can be applied to hydrologic design criteria and planning. Depending on the outcome of the indices, a best fit climate model can be determined. The extreme precipitation indices adopted from WMO, (2009) are as follows:

***RX1DAY***, *Maximum one day precipitation*: The first index, *RX1DAY*, is used to calculate the highest precipitation amount in a one-day period. This index allows maximum daily rainfall events to be calculated for a given time period, whether that is a month, year, or decade. Hydrologic designs can use this extreme rainfall index to determine what a maximum daily rainfall event could yield in the future.

Let  $RR_{ij}$  be the daily precipitation amount on day  $i$  and period  $j$ . The maximum one-day value for period  $j$  is:

$$RX1DAY_j = \max(RR_{ij}) \quad \forall j \quad (1)$$

***RX5DAY***, *Maximum five day precipitation*: Similar to ***RX1DAY***, ***RX5DAY*** calculates the highest precipitation amount in a five day period. This index can lend itself to how stormwater will accumulate as land becomes saturated and infrastructure meets maximum capacity caused by prolonged storm events.

Let  $RR_{kj}$  be the daily precipitation amount for the five-day interval  $k$  and in period  $j$ , where  $k$  is defined by the last day. The maximum five-day values for period  $j$  are:

$$RX5DAY_j = \max(RR_{kj}) \quad \forall j \quad (2)$$

***SDII***, *Simple daily intensity index*: ***SDII*** is a mean precipitation index that only considers wet days, rainfall above 1mm in depth, through a mean calculation. The index will define the average rainfall experienced in a region over a given period of time, determining a baseline intensity for stormwater drainage design.

Let  $RR_{ij}$  be the daily precipitation amount on wet day  $w$  ( $RR \geq 1$  mm) in period  $j$ . If  $W$  represents the number of wet days in  $j$  then the simple precipitation intensity index:

$$SDII_j = \sum_j (RR_{wj}) / W \quad (3)$$

**R10mm, Heavy precipitation days:** This index is used to count the number of days were the daily precipitation meets or exceeds 10mm. This stormwater threshold is considered to be a product of heavy precipitation.

Let  $RR_{ij}$  be the daily precipitation amount on day  $i$  and in period  $j$ . Count the number of days where:

$$RR_{ij} \geq 10mm \quad \forall i, \forall j \quad (4)$$

**R20mm, Very heavy precipitation days:** Similar to R10mm index, R20mm is a count of days that receive a daily precipitation of 20mm or greater. This stormwater threshold is considered to be a product of very heavy precipitation.

Let  $RR_{ij}$  be the daily precipitation amount on day  $i$  and in period  $j$ . Count the number of days where:

$$RR_{ij} \geq 20mm \quad \forall i, \forall j \quad (5)$$

**Rnnmm:** Rather than having a preset threshold, Rnnmm allows the user to assign an arbitrary threshold value that may be relevant to the case study or area of interest.

Let  $RR_{ij}$  be the daily precipitation amount on day  $i$  and in period  $j$ . Count the number of days where:

$$RR_{ij} \geq nn \text{ mm} \quad \forall i, \forall j \quad (6)$$

**CDD**, *Consecutive dry days*: By counting the maximum length of dry spell, defined as daily rainfall less than 1mm, this index determines the maximum frequency of consecutive dry days.

Let  $RR_{ij}$  be the daily precipitation amount on day  $i$  and in period  $j$ . Count the largest number of consecutive days where:

$$RR_{ij} < 1mm \quad \forall i, \forall j \quad (7)$$

**CWD**, *Consecutive wet days*: Similar to CDD, CWD counts the maximum stretch of wet days, defined by having a daily rainfall greater than 1mm.

Let  $RR_{ij}$  be the daily precipitation amount on day  $i$  and in period  $j$ . Count the largest number of consecutive days where:

$$RR_{ij} \geq 1mm \quad \forall i, \forall j \quad (8)$$

**R95pTOT**: The 95<sup>th</sup> percentile of precipitation of wet days, rainfall greater than 1mm. This index will sum the precipitation of top 5% of the wettest day out of wet days.

Let  $RR_{wj}$  be the daily precipitation amount on a wet day  $w$  ( $RR \geq 1$  mm) in period  $j$  and let  $RR_{wn}95$  be the 95<sup>th</sup> percentile on wet days in the base period  $n$  (1961-1999). Then  $R95pTOT_j = \text{sum}(RR_{wj})$ , where:

$$RR_{wj} \geq RR_{wn}95 \quad \forall j \quad (9)$$

**R99pTOT**: Similar to R95TOT, R99TOT will sum the precipitation of top 1% of the wettest days out of wet days.

Let  $RR_{wj}$  be the daily precipitation amount on a wet day  $w$  ( $RR \geq 1$  mm) in period  $j$  and let  $RR_{wn}99$  be the 99<sup>th</sup> percentile on wet days in the base period  $n$  (1961-1999). Then  $R99pTOT_j = \sum(RR_{wj})$ , where:

$$RR_{wj} \geq RR_{wn}99 \quad \forall j \quad (10)$$

**PRCTOT**: the PRCTOT index takes the total precipitation in wet days, rainfall greater than 1mm, within the preset period of time.

Let  $RR_{wj}$  be the daily precipitation amount on a wet day  $w$  ( $RR \geq 1$ mm) in period  $j$ . Then:

$$PRCTOT_j = \sum_j (RR_{wj}) \quad \forall j \quad (11)$$

### 3.1.2 Extreme Precipitation Bias Indices

Bias within precipitation data can be evaluated through comparison of model and observed data. A study performed by Teegavarapu (2012) developed and selected appropriate bias indices considering methods commonly used in hydrologic model evaluation. There are three general categories of bias indices that have been selected: visual, error performance measures, and quantitative indices.

#### 3.1.2.1 Visual Bias Indices

Visual indices will be applied in order to gain a better understanding of the behavior of both observed and model data sets, as well as the comparison of the two. Time series plots are a primary visual aid in the understanding of any data recorded of a period of time. By utilizing the time series plots the raw data will depict any outliers in extreme precipitation, positive or negative slopes in the data, and/or the characteristics of variability. Box plots, along with residual error and nonexceedance plots, provide the evaluation of basic statistics unique to a data set, as well as, the under or over estimation of two data sets.

### 3.1.2.2 Error Performance Measures

#### Mean error

Mean error (ME) is the measure of the average magnitude of error between observed ( $\theta_o$ ) and predicted ( $\theta_p$ ) data for each model,  $m$ , out of a total of  $N$  models, for each day,  $i$ . This index; however, has limitations due to the preservation of the sign of each value. The cancellation of positive and negative values may occur leading to an over or underestimation of the overall error. The ME index can be useful in the determination of overall reliability.

$$ME_i = \frac{1}{N} \sum_{m=1}^N (\theta_{o,m} - \theta_{p,m}) \quad \forall m, \forall i \quad (12)$$

#### Mean absolute error

Mean absolute error (MAE) measure the average magnitude of absolute error. By applying the absolute sign to the index, the possibility of positive and negative values cancelling each other is dismissed. The MAE index is not sensitive to outliers and can be useful in the determination of overall accuracy.

$$MAE_i = \frac{1}{N} \sum_{m=1}^N |\theta_{o,m} - \theta_{p,m}| \quad \forall m, \forall i \quad (13)$$

#### Root mean square error

Root mean square error (RMSE) measures the square root of the mean of squared residuals. Because the index applies a square power to the error residual, outliers will be magnified; however, this measure preserves the units that are seen in the observed or predicted values.

$$RMSE_i = \sqrt{\frac{1}{N} \sum_{m=1}^N (\theta_{o,m} - \theta_{p,m})^2} \quad \forall m, \forall i \quad (14)$$

### **Nash Sutcliffe Efficiency Coefficient**

Nash sutcliffe efficiency coefficient (NSEC) can be described as a qualitative measure; however, this index does utilize aspects of error performance measures. NSEC is partly a qualitative measure because it compares the predicted values to the average value of the observed, thereby determining whether the predicted values are, in fact, outperforming a mean baseline model.

$$NSEC_i = 1 - \frac{\sum_{m=1}^N (\theta_{o,m} - \theta_{p,m})^2}{\sum_{m=1}^N (\theta_{o,m} - \bar{\theta}_o)^2} \quad \forall m, \forall i \quad (15)$$

### **Correlation Coefficient**

Correlation coefficient ( $\rho$ ) will be used to measure the linear association between observed and predicted data. This measure can be generated through ordinary correlation coefficient methods, where  $S_o$  and  $S_p$  are the observed and predicted standard deviations.

$$\rho = \frac{1}{N-1} \sum_{m=1}^N \frac{(\theta_{o,m} - \bar{\theta}_o)}{S_o} \frac{(\theta_{p,m} - \bar{\theta}_p)}{S_p} \quad \forall m \quad (16)$$

#### **3.1.2.3 Contingency Measures**

In order to understand the interaction between the observed and predicted data, a contingency classification method will be applied. The key assessments to be classified will be the correct predictions of wet days, the correct prediction of dry days, the rate of misses or false alarms by predictions, and the rate of agreement between observed and predicted. A contingency table is used to classify precipitation events as shown in Table 5.

**Table 5: Classification of observed and predicted precipitation events.**

Observed Precipitation	Predicted Precipitation	
	$\theta_o > 0$	$\theta_p > 0$ [ <i>Hits</i> ]
$\theta_o = 0$	$\theta_p > 0$ [ <i>Misses</i> ]	$\theta_p = 0$ [ <i>Correct Negatives</i> ]

$$\text{if}(\theta_{o,i} > 0, \theta_{p,i} > 0), \text{then } C_{11}^i = 1, \text{ else } C_{11}^i = 0 \quad (17)$$

$$\text{if}(\theta_{o,i} > 0, \theta_{p,i} = 0), \text{then } C_{10}^i = 1, \text{ else } C_{10}^i = 0 \quad (18)$$

$$\text{if}(\theta_{o,i} = 0, \theta_{p,i} > 0), \text{then } C_{01}^i = 1, \text{ else } C_{01}^i = 0 \quad (19)$$

$$\text{if}(\theta_{o,i} = 0, \theta_{p,i} = 0), \text{then } C_{00}^i = 1, \text{ else } C_{00}^i = 0 \quad (20)$$

$$C_{11} = \sum_{i=1}^N C_{11}^i \quad \forall i \quad (21)$$

$$C_{10} = \sum_{i=1}^N C_{10}^i \quad \forall i \quad (22)$$

$$C_{01} = \sum_{i=1}^N C_{01}^i \quad \forall i \quad (23)$$

$$C_{00} = \sum_{i=1}^N C_{00}^i \quad \forall i \quad (24)$$

### Concordance

The concordance index that is also referred to as proportion correct (PC) gives the fraction of all wet days and dry days correctly estimated based on model precipitation data given observed precipitation data, where  $c_{11}$ ,  $c_{10}$ ,  $c_{01}$ , and  $c_{00}$  are observed and predicted contingency for wet-wet, wet-dry, dry-wet, and dry-dry.

$$\text{Concordance} = \frac{c_{11} + c_{00}}{c_{11} + c_{01} + c_{10} + c_{00}} \quad (25)$$

### **Error rate**

The error rate gives the fraction of all wet and dry events incorrectly estimated based on model precipitation data given observed precipitation data.

$$\text{Error Rate} = \frac{c_{01} + c_{10}}{c_{11} + c_{01} + c_{10} + c_{00}} \quad (26)$$

### **Sensitivity**

Sensitivity is also referred to as success rate. It provides information about what fraction of the wet events obtained by model precipitation estimates that were actually observed based on precipitation observations.

$$\text{Sensitivity} = \frac{c_{11}}{c_{11} + c_{10}} \quad (27)$$

### **Specificity**

Specificity provides information about the fraction of dry events obtained by model precipitation estimates that were actually observed as dry events based on precipitation observations.

$$\text{Specificity} = \frac{c_{00}}{c_{10} + c_{00}} \quad (28)$$

## 3.2 Bias Correction

The climate model data downloaded can experience a dry bias that can skew the predicted data values by decreasing the statistical mean. By applying a bias correction to the overall data, the goal is to adjust the predicted values to better simulate the observed data.

### 3.2.1 Quantile Mapping (QM)

The quantile-based mapping methods applied to this study are adopted from a study performed by Teegavarapu (2013). These methods are widely used for correcting the biases in both downscaled precipitation and temperature datasets obtained from general circulation model (GCM) simulations. The quantile-mapping method (Panofsky and Brier, 1968) is widely used in numerous hydrologic simulations and climate change impact studies (Wood, et al., 2002). Although this method tries to adjust all the moments of the estimated data, the major drawback is its dependence on a stationarity assumption for corrections. The method uses the observed cumulative distribution function (CDF) of data from the training period to correct data from the test period with an assumption that the future distribution of data follows that of past observed data. The correction method is expressed by equation 29,

$$\theta_i^{bce} = F_o^{-1}(F_e^v(\theta_i^e)) \quad \forall i \quad (29)$$

Where,  $F_o$  is the CDF of the observed data derived from the training dataset and  $F_e^v$  is the CDF from the testing dataset based on estimated precipitation data. The variable  $\theta_i^{bce}$  is the bias-corrected estimate of precipitation for any time interval  $i$  from the testing dataset obtained by following two steps: 1) estimated values of precipitation are used to develop a CDF and the non-exceedence probability  $F_e^v(\theta_i^e)$  is obtained for each value of  $\theta_i^e$  and 2) corrected estimate ( $\theta_i^{bce}$ ) using the inverse of the observed CDF for the value of non-exceedence probability obtained in step 1 (Teegavarapu, 2013).

### 3.2.2 Uncertainty assessment of bias using resampling techniques

Precipitation data, especially extreme events, are likely to contain a high level of uncertainty, specifically related to a bias between observed and predicted data. These uncertainties are related to

variations in time, space, and model selection. In order to assess the uncertainty of the bias without compromising the integrity of climates non-stationarity, resampling techniques are used.

### 3.2.2.1 *Bootstrap sampling*

Bootstrap sampling approach, adopted from Teegavarapu, et al., (2013), describes a method of resampling from a single data set in order to produce multiple datasets to create a robust collection of samples from a relatively small sample set (Efron & Gong, 1983). These samples contain similar distributions and statistics because they are generated from the same parent sample. The purpose of bootstrap sampling is to ultimately generate a confidence interval to help with inferences on the sample data set (Efron & Tibshirani, 1993). The notations and procedures developed by Davison & Hinkley (1997) were adopted for this study. The sample values  $y_1, y_2, \dots, y_n$  are thought of as the outcomes of independent and identically distributed (iid) random variables  $Y_1, Y_2, \dots, Y_n$  whose cumulative distribution function (CDF) is denoted by  $F$ . The estimate of  $F$  denoted by  $\hat{F}$  is obtained using data  $y_1, y_2, \dots, y_n$  (Teegavarapu, et al., 2013). In order to obtain the confidence intervals desired the following steps will be used:

- Bootstrap (re) sample  $y_1^*, y_2^*, \dots, y_n^* \sim \hat{F}$  are obtained from the original samples allowing repetitions.
- $\hat{F}$ , an estimator of  $F$  is obtained nonparametrically using empirical distribution function (EDF) of the original data, i.e, by placing a probability of '1/n' at each data value from sample  $y_1, y_2, \dots, y_n$ .
- Sample mean statistic  $\hat{\theta}^*$  is computed from bootstrap sample  $y_1^*, y_2^*, \dots, y_n^*$ .
- The above steps are repeated ' $N$ ' times, to obtain  $N$  sample means  $\hat{\theta}_1^*, \hat{\theta}_2^*, \dots, \hat{\theta}_N^*$ . The practical size ' $N$ ' depends on the tests to be run on the data.

A study performed by Chernick (2007) recommends a size ' $N$ ' of 1000 and 10,000 for evaluating the sample statistics and confidence intervals, which will be used in this study. After  $N$  samples are obtained, normally approximated confidence intervals are computed for the uncertainty assessment. If  $\hat{\theta}$

(estimated mean of original data) is approximately normal, then  $\hat{\theta} \sim N(\theta + \beta, v)$  (Teegavarapu, et. al., 2013). The confidence interval (CI) of  $\theta$  for known bias ( $\beta = \beta(F)$ ) and variance ( $v = v(F)$ ) (Davison and Hinkley, 1997) is given by:

$$CI = \hat{\theta} - \beta \pm Z_{\alpha} \cdot v^{\frac{1}{2}} \quad (30)$$

$$\text{where, } \beta(F) \doteq \beta(\hat{F}) \doteq b = \overline{\theta^*} - \hat{\theta} \quad (31)$$

$$v(F) \doteq v(\hat{F}) \doteq \frac{1}{N-1} \sum_{i=1}^N (\hat{\theta}_i^* - \overline{\theta^*})^2 \quad (32)$$

The variable  $\overline{\theta^*}$  is the mean of  $\hat{\theta}_1^*, \hat{\theta}_2^*, \dots, \hat{\theta}_N^*$  and  $Z_{\alpha}$  is the  $\alpha$  quantile of the standard normal distribution. If a confidence interval of 95% were to be used, the  $\alpha=0.025$  and  $Z_{\alpha} = -1.96$ . The confidence interval generated will define the uncertainty of the bias between observed and model data.

### 3.3 Model Selection

A selection procedure will be implemented to the projected model data to determine the best model(s). Each model holds unique characteristics within a case study. After applying WMO, bias, and contingency indices to the observed and predicted data, both raw and bias corrected data, there will be a best performing model; however, some models will outperform in error measures, while other models will achieve greater accuracy in precipitation extremes. The goal is to find the model that is performing well in all categories. A series of statistical test can be performed to rank the models.

#### 3.3.1 Integrated Ranking

To begin the procedure, the model values must be converted into a standard expression in order to fairly judge the outcomes. By taking the absolute error (AE) of the extreme precipitation indices, WMO, and contingency measures, all the indices, WMO, bias, or contingency, can be seen as relevant to each other.

$$AE = \sum_{i=1}^N |l_{o,m} - l_{p,m}| \quad \forall m \quad (33)$$

Where,  $l_{o,m}$ , is the observed precipitation for a given model,  $m$ , after any given index is applied and similarly,  $l_{p,m}$ , for predicted precipitation. The integrated approach in selecting or ranking the climate models involves the evaluation of individual indices. By taking each index separately and determining the least error (LE) model, an array of best fit models can be generated. With this array of best fit models, a model must be selected that is outperforming overall. Given the array of best fit models, the mode of this array will determine the overall best model (BM).

$$mode = 1 + \left( \frac{f_s}{f_p + f_s} * c \right) \quad (34)$$

Where 1 defines the lower limit of the modal class and  $c$  is the width of the class interval. The frequency of class succeeding and the frequency of the class preceding the modal class are defined as:  $f_s$  and  $f_p$ . This process will be repeated for each of the indices individually to determine the OM. This integrated approach will allow insight on extreme precipitation, biases between observed and predicted values relates to space throughout Florida. Although the integrated ranking method provides insight on the models, there need a single model selected for future analysis. To do this a coupled ranking approach will be used.

### 3.3.2 Coupled Ranking

Similarly to the integrated ranking the AE, Equation 16, will be taken of each model for each index. However, instead of finding the LE, Equation 17, of each station and index, the AE values for each index will be normalized and range from 0 to 1.

$$Normalized(AE_m) = \frac{AE_m}{AE_{max}} \quad \forall m \quad (35)$$

Where,  $i$ , is defining the index being normalized. Now that the indices are relative, the 19 indices used can be compiled and summed into one overall index. From this ultimate index, the mode will be taken to determine the overall best model(s).

### **3.4 Statistical Methods**

Extreme precipitation has been used as a foundation to the understanding of general statistical extremes. Many extreme distributions have been developed to capture the characteristics of extreme hydrologic events. In order to determine a best fitting distribution one can use several parametric or non-parametric statistical tests.

#### **3.4.1 Parametric and Non-parametric Tests**

Parametric tests require the data sets to follow a specific distribution in order for the test to produce accurate results. However, it is not always the case that the distribution is known for a data set. The data must first undergo non-parametric tests to determine distributions and other statistical characteristics of the data.

##### **3.4.1.1 Generalized Extreme Value (GEV) Distribution**

Extreme precipitation has been found to follow GEV in many cases. This distribution contains similar characteristics to extreme precipitation such as: heavy tails, temporal and spatial dependence, as well as, temporal cycles. GEV is a three parameter function and as given by Equation 36.

$$f(x; \mu, \sigma, \gamma) = \begin{cases} \exp \left\{ - \left[ \frac{1 + \gamma(x - \mu)}{\sigma} \right]^{\frac{-1}{\gamma}} \right\}, \\ \left\{ 1 + \frac{\gamma(x + \mu)}{\sigma} \right\} > 0 \quad \gamma \neq 0, \\ \exp \left\{ - \exp \left[ - \frac{(x - \mu)}{\sigma} \right] \right\}, \quad \gamma = 0 \end{cases} \quad (36)$$

The three parameters  $\mu$ ,  $\sigma$ , and  $\gamma$  represent location, scale, and shape. These parameters are typically found through a likelihood ratio test. Maximum Likelihood Estimator (MLE) is a parameter vector that maximizes the likelihood function. The likelihood function defines the probability density function (PDF) that is most likely to have produced the original data through an inverse function of the data vector ( $x$ ) and the parameter vector (MLE) (Katz, et al., 2002).

#### 3.4.1.2 Goodness of Fit Test: Kolmogorov-Smirnov Test: two-sample

The two sample KS test is commonly used in the hydrologic field, due to continuous distributions, as a non-parametric test to measure the gap between fitted and empirical CDF curves. The two sample KS test can be used on two data sets as well. The null hypothesis assigned to the KS test is that the fitted and empirical data are of the same distribution (Wilks, 2006).

### 3.5 Evaluation of Regional Precipitation Extremes

The evaluation of precipitation extremes will provide input on the hydrologic design. There will be further data collection involved in this section of the methodology. The data range will be extended to 1950-2099 and only the best models, selected through the ranking process mentioned earlier in this chapter, will be used. Also model scenario and initial runs will be evaluated to determine variations between them.

#### 3.5.1 Depth Duration Frequency (DDF)

DDF is a commonly used tool in the hydrologic field that determines the maximum depth from a given return period, typically 25 years, and duration. A 25 year return period is a practical return period used for baseline hydrologic design standards. Of course, higher return periods will produce a more robust

design along with higher costs. The DDF will use rainfall duration data sets fitted to GEV distribution using the parameters from MLE and two sample KS test (Overeem, et al., 2008). Intensity Duration Frequency (IDF) curves can also be created through the results from the DDF values.

## **Chapter 4: Case Study Domain**

The objective of this case study application is to select the best downscaled GCMs on a regional scale. In doing so the best model will be used to evaluate hydrologic planning and design for that specific region and determine whether or not the current hydrologic design standards will hold up to the future climate as it changes. The methodology described in Chapter 3 is used to evaluate precipitation extremes at different sites (i.e. rain gages) in Florida.

### **4.1 Study Domain and Data**

Florida, described by Carpenter & Provorse (1998), is geographically located in a highly susceptible region of the United States for extreme precipitation events. Located in the south eastern region, specifically 79° 48' to 87° 38' west longitude 24° 30' to 31° north latitude, Florida is 500 miles long and 160 miles wide at its most distant points. Florida is bordered by Georgia and Alabama to the north, Alabama and the Gulf of Mexico on the west, and surrounded by the Atlantic Ocean to the south and to the east. Florida covers 65,758 square miles, making it the 22nd largest of the 50 states. The highest point in Florida is Britton Hill, Lakewood Park in Walton County and is only 345 feet above sea level located in the Florida Panhandle, with the lowest point being sea level where Florida meets the Atlantic Ocean and the Gulf of Mexico. Florida has more than 1260 miles of coastline-more than any other state in the continental United States (Riorbdan, 2008). With the exceptionally low elevation, a high tropical storm landfall rate, and increased contact with both fresh and salt water, Florida is highly susceptible to extreme hydrologic events making it difficult to predict future climate. National Oceanic and Atmospheric Administration (NOAA) and Nation Weather Service (NWS) has strategically located a cooperative network of 306 rain stations, both active and inactive, throughout the state of Florida. These stations can be described as rain gages or stations, interchangeably, throughout this thesis. Of these stations, 31 have been selected for data collection and analysis for this case study. Locations of these 31 stations are shown in Figure 6 and listed in Table 6.

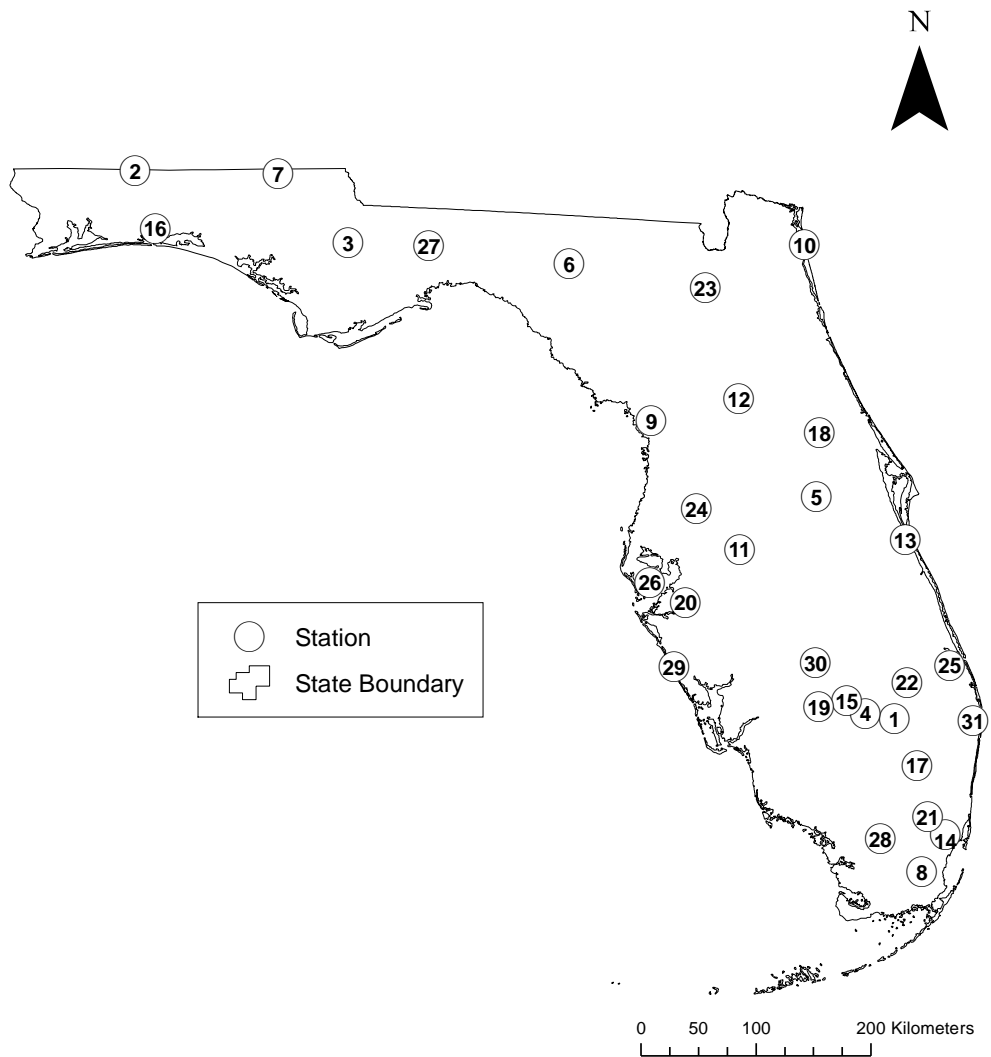


**Figure 6: Locations of the 31 NOAA/NWS cooperative network rain gages in Florida.**

The 31 Florida rain gage stations depicted in Figure 6 are captured within a 1/8° grid created by the downscaled data. Each grid contains climate data; whichever grid the rain gage is encompassed by shares its data with the station. Each of the 31 stations is therefore theoretically relocated to the center of the encompassing grid.

**Table 6: Location of rain gages (SERCC, 2013).**

Rain gage ID	Latitude	Longitude
1	26.700	-80.717
2	30.983	-86.650
3	30.418	-84.986
4	26.742	-80.940
5	28.434	-81.325
6	30.250	-83.259
7	30.958	-85.533
8	25.500	-80.500
9	29.025	-82.616
10	30.400	-81.417
11	28.021	-81.922
12	29.200	-81.931
13	28.096	-80.631
14	25.791	-80.316
15	26.840	-81.087
16	30.531	-86.492
17	26.334	-80.537
18	28.933	-81.300
19	26.790	-81.304
20	27.609	-82.348
21	25.930	-80.454
22	26.983	-80.617
23	30.068	-82.193
24	28.338	-82.260
25	27.117	-80.283
26	27.763	-82.626
27	30.393	-84.353
28	25.761	-80.824
29	27.101	-82.436
30	27.135	-81.330
31	26.685	-80.099

## 4.2 Data Collection and Analysis

The collection of previously bias corrected and downscaled GCM's began at [gdo-dcp.ucllnl.org](http://gdo-dcp.ucllnl.org), which is a downscaled bias corrected data archive provided by several climatological and hydrological organizations and groups, where downscaled CMIP5 climate projections and historical data are archived for analytical and exploratory measures by the public. The purpose these organizations provide this archived data is to allow the assessment of potential climate change impacts on the natural and social systems, local to regional projection uncertainty, and risk based exploration of planning and policy responses framed by potential climate changes exemplified by these projections (Maurer, et al., 2007). For convenience of the case study, a unique list of model IDs is used, listed in Table 7.

**Table 7: CMIP5 BCCA RCP2.6 climate models selected for initial condition analysis.**

CMIP5 Model	Case Study Model ID
bcc-csm1-1	2
canesm2	3
ccsm4	4
csiro-mk3-6-0	5
gfdl-cm3	6
gfdl-esm2g	7
gfdl-esm2m	8
ipsl-cm5a-lr	9
ipsl-cm5a-mr	10
miroc-esm	11
miroc-esm-chem	12
miroc5	13
mpi-esm-lr	14
mpi-esm-mr	15
mri-cgcm3	16
noresm1-m	17

The 16 models are defined as 2 through 17 with the notion that the observed data set is defined as 1. These data sets will be used for initial analysis to identify the best model or models based on the ranking procedure described in the methodology chapter, and will use emission pathway RCP2.6 with first initial condition.

#### **4.2.1 Data Processing**

Once data was collected, Mathworks Matlab, Microsoft Excel and Windows Notepad were used to generate workbooks and text file. These files were configured in a way to allow for systematic index calculations to occur. The process to select the best model will begin with the historical data and model data coinciding with emission pathway RCP2.6 and first initial condition. By beginning with historical data, it will prevent bias models from misleading the performance of the predicted data. The models will be compared through 19 indices mentioned in chapter three's methodology. The best model(s) will then continue analysis on the projected climate data from 2000-2099.

## Chapter 5: Results and Analysis

### 5.1 WMO Performance Measures

Both the observed and predicted data have been calculated through the 9 WMO indices. The statistical characteristics of each of the 16 climate models have been compared to determine the performance of each model. An arbitrary selection of 5 rain gage stations, 3, 8, 12, 20, and 25, has been made to depict the variation from the panhandle through to South Florida. A series of boxplot matrixes are listed where, the comparison of the observed data (labeled as 1 on the x-axis) and the predicted data (labeled as 2 through 17 on the x-axis) show a dry bias throughout the extreme precipitation indices. This is determined by the observed median being consistently under estimated. In order to correct this dry bias seen through the predicted data, the quantile mapping method of bias correction was applied to the raw data. The WMO indices performance after bias correction, as expected, improved the predicted values and raised the median of each model and index to reduce the gap between the observed and predicted data. From the boxplots of the WMO measures, seen in Figure 7 through Figure 16, the model data experiences variations between each other but deviations are not excessive. Between the five stations and regions associated with them, the highest performing models are shown in Table 8.

**Table 8: Selected models at different sites.**

Rain gage station ID	Region	Best Model ID
3	Northwest (Panhandle)	15
6	North Central	10
12	East Central	12
20	Tampa Bay	12
25	South East	14

The results seen in Table 8 describe the spatial variability seen throughout Florida. The variations in models throughout the regions in Florida describe that model selection for hydrologic research and design is an important factor for an accurate design. This is a preliminary evaluation on site specific model selection, and an in depth ranking for the entire state of Florida will be performed in the sections to come. Any further insight on the remaining 26 rain gage stations can be met in Appendix B and Appendix C.

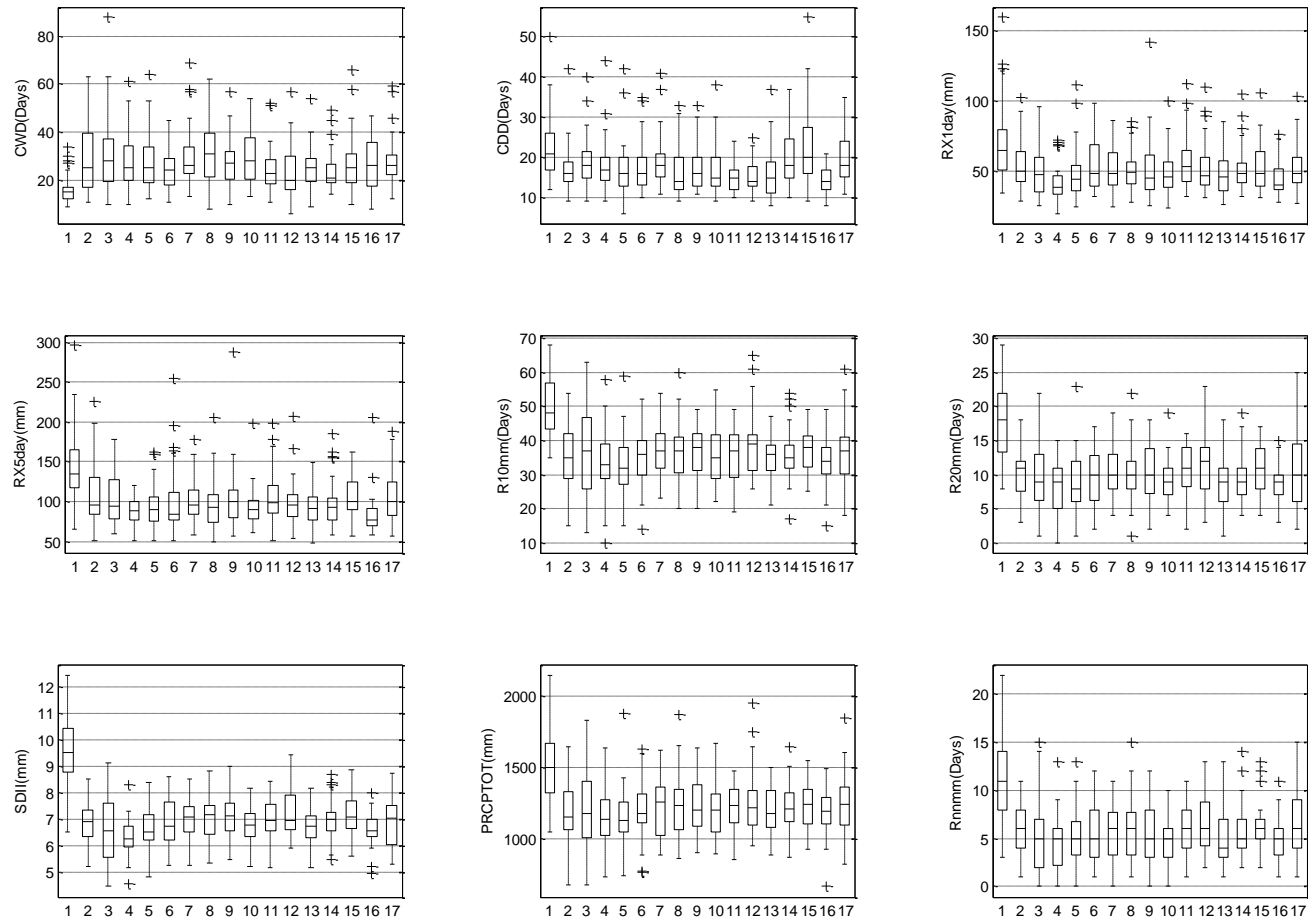


**Figure 7: Variability of WMO indices for different models (2-17) and observed (1) for station 3.**

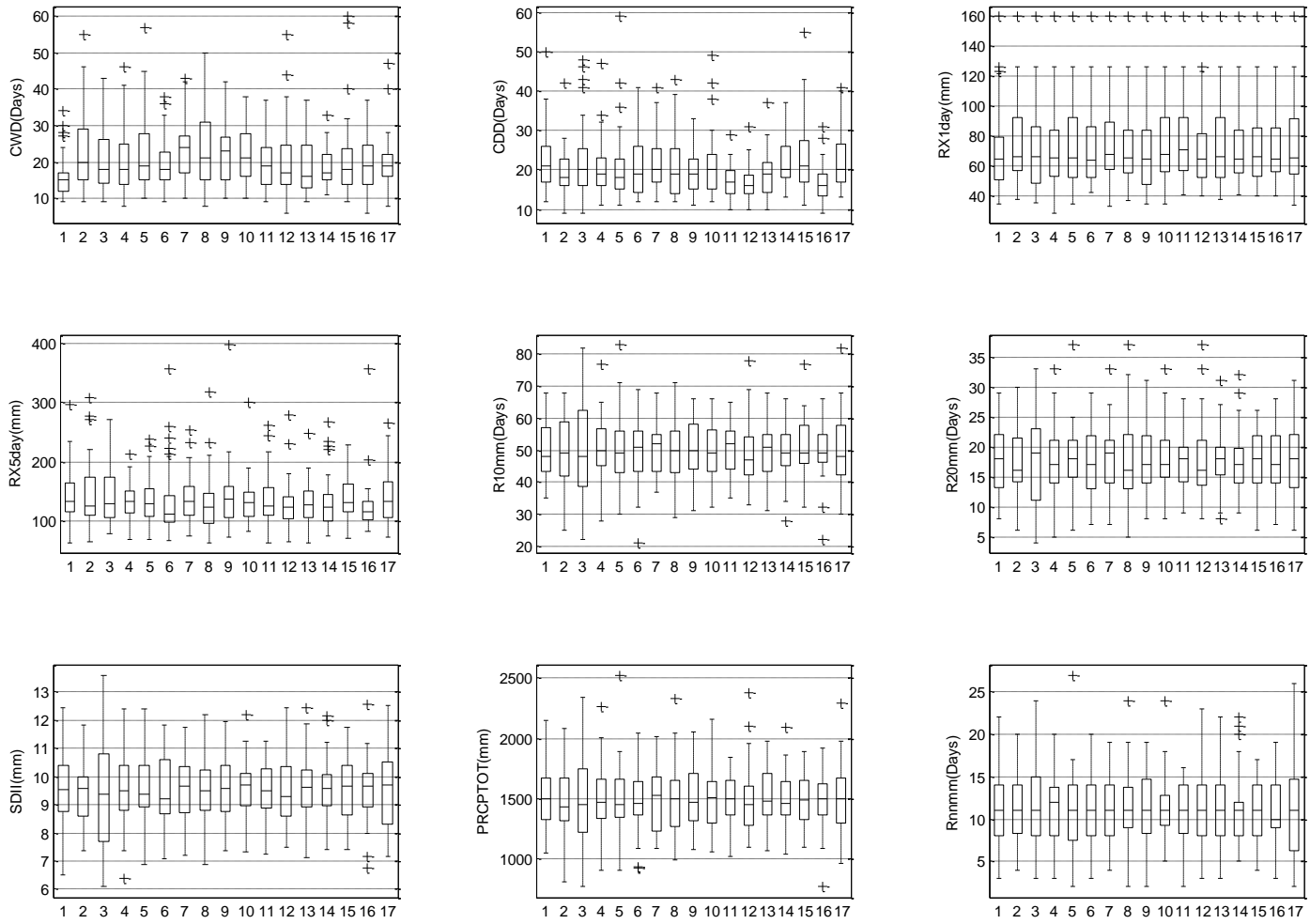
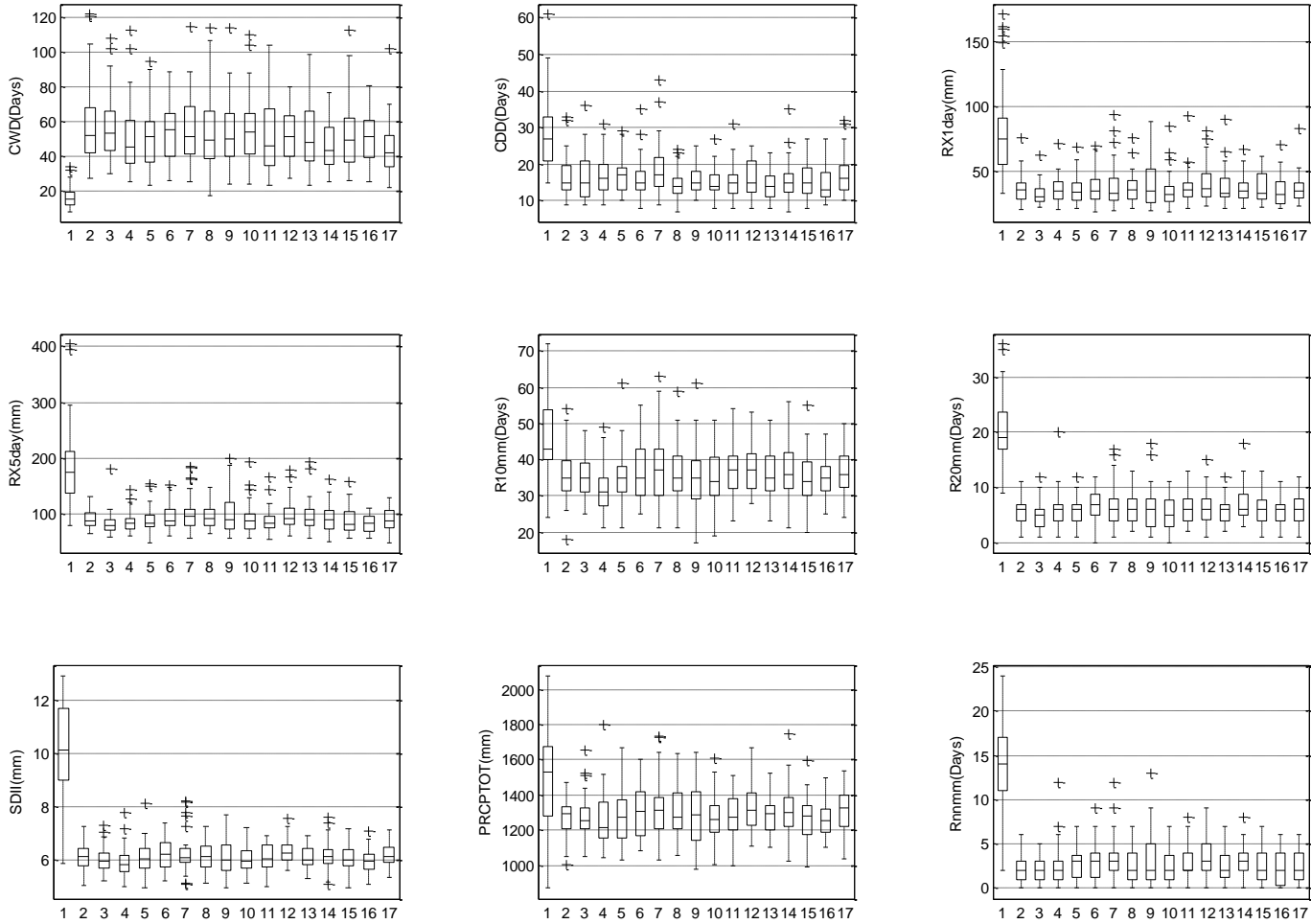
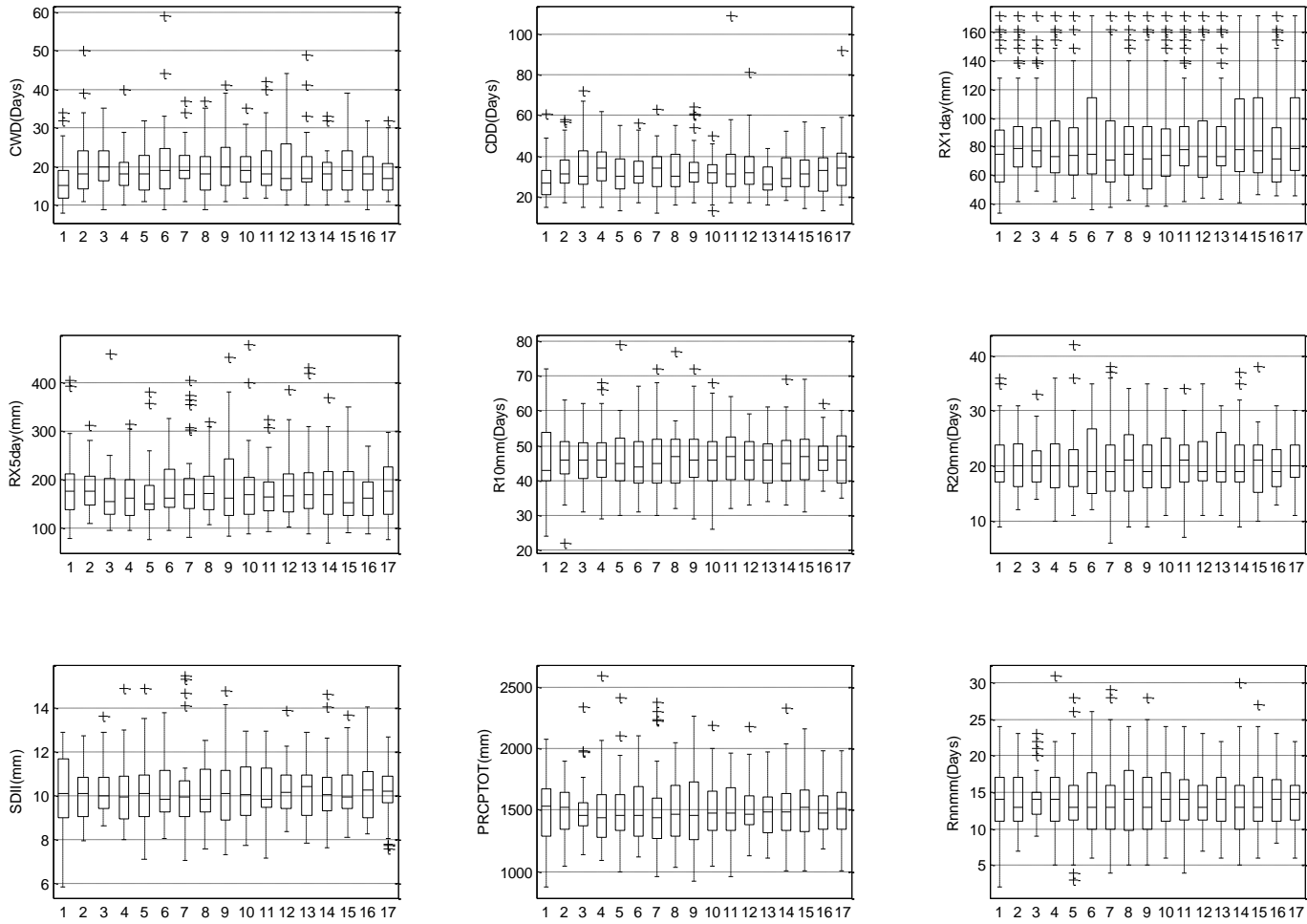


Figure 8: Variability of WMO bias corrected indices for different models (2-17) and observed (1) for station 3.



**Figure 9: Variability of WMO indices for different models (2-17) and observed (1) for station 8.**



**Figure 10: Variability of WMO bias corrected indices for different models (2-17) and observed (1) for station 8.**

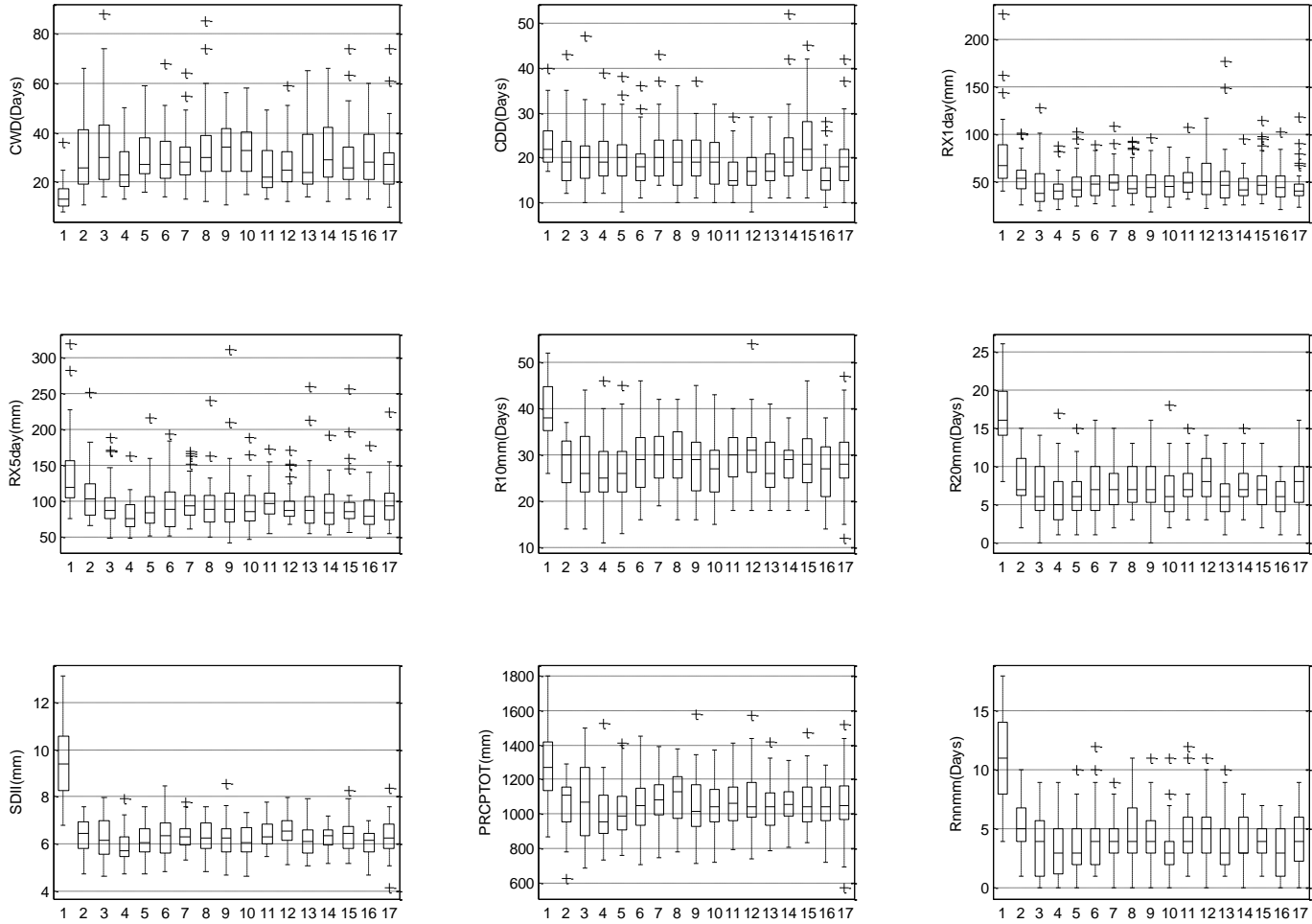


**Figure 11: Variability of WMO indices for different models (2-17) and observed (1) for station 12.**

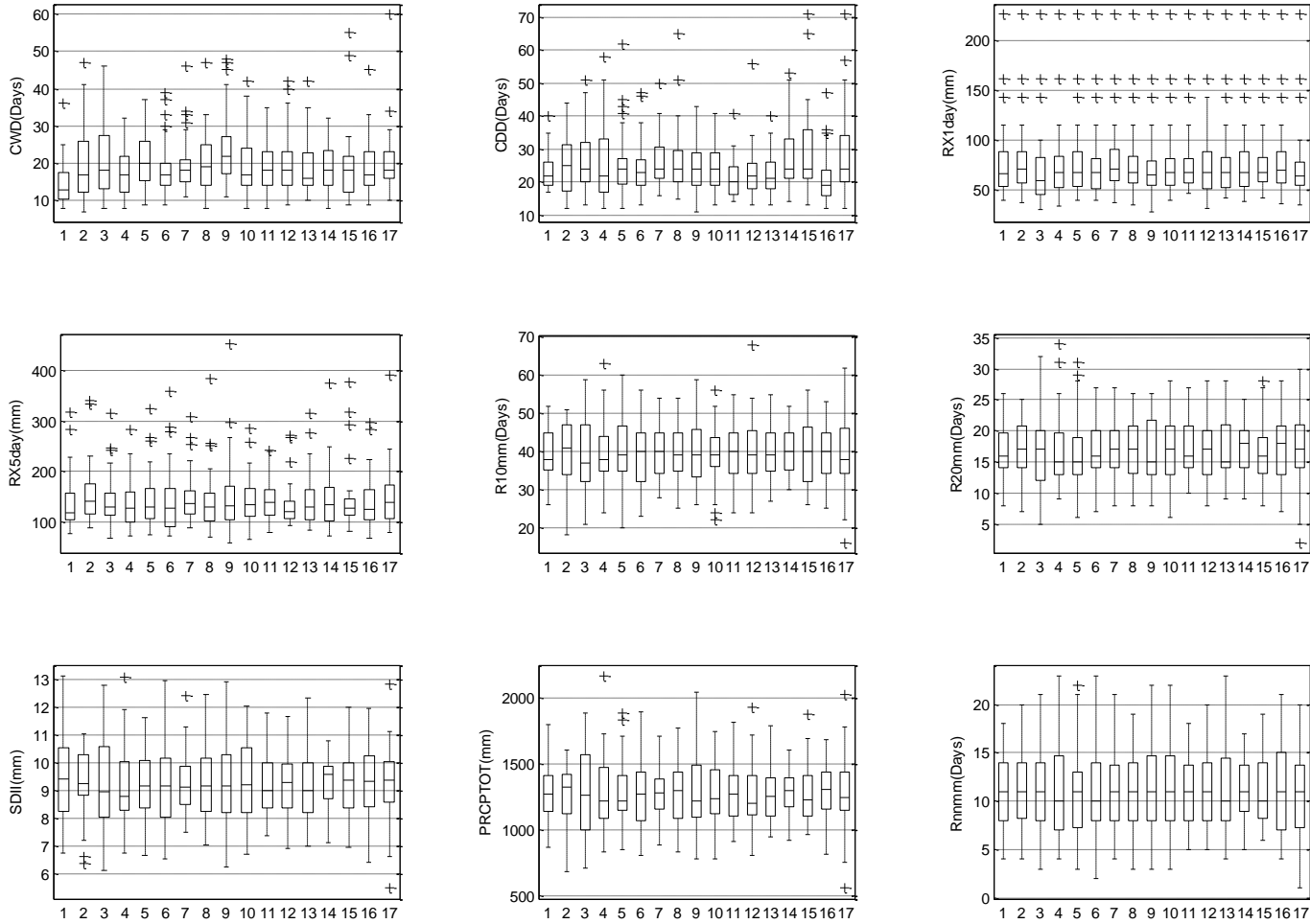


**Figure 12: Variability of WMO bias corrected indices for different models (2-17) and observed (1) for station 12.**

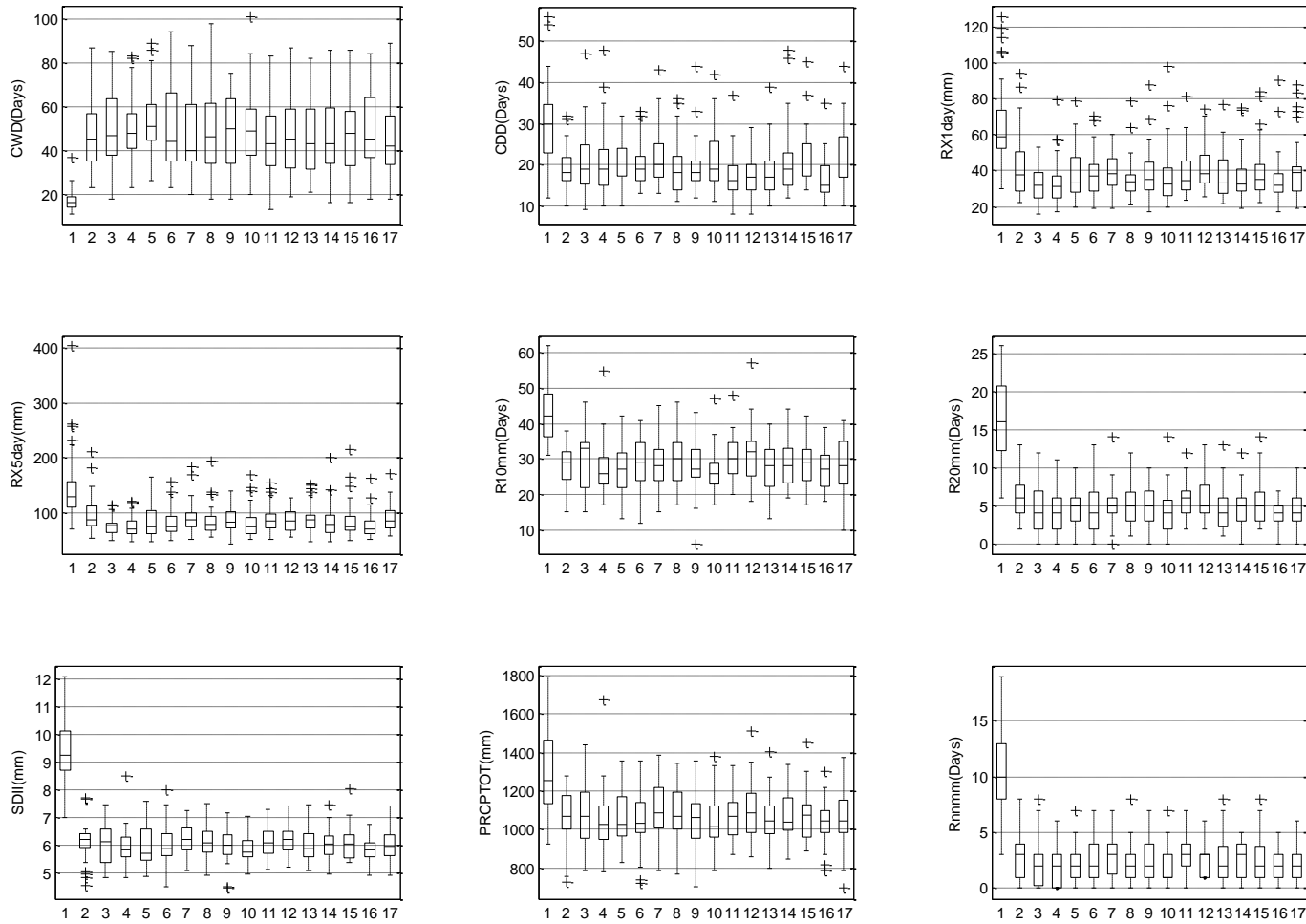


**Figure 13: Variability of WMO indices for different models (2-17) and observed (1) for station 20.**

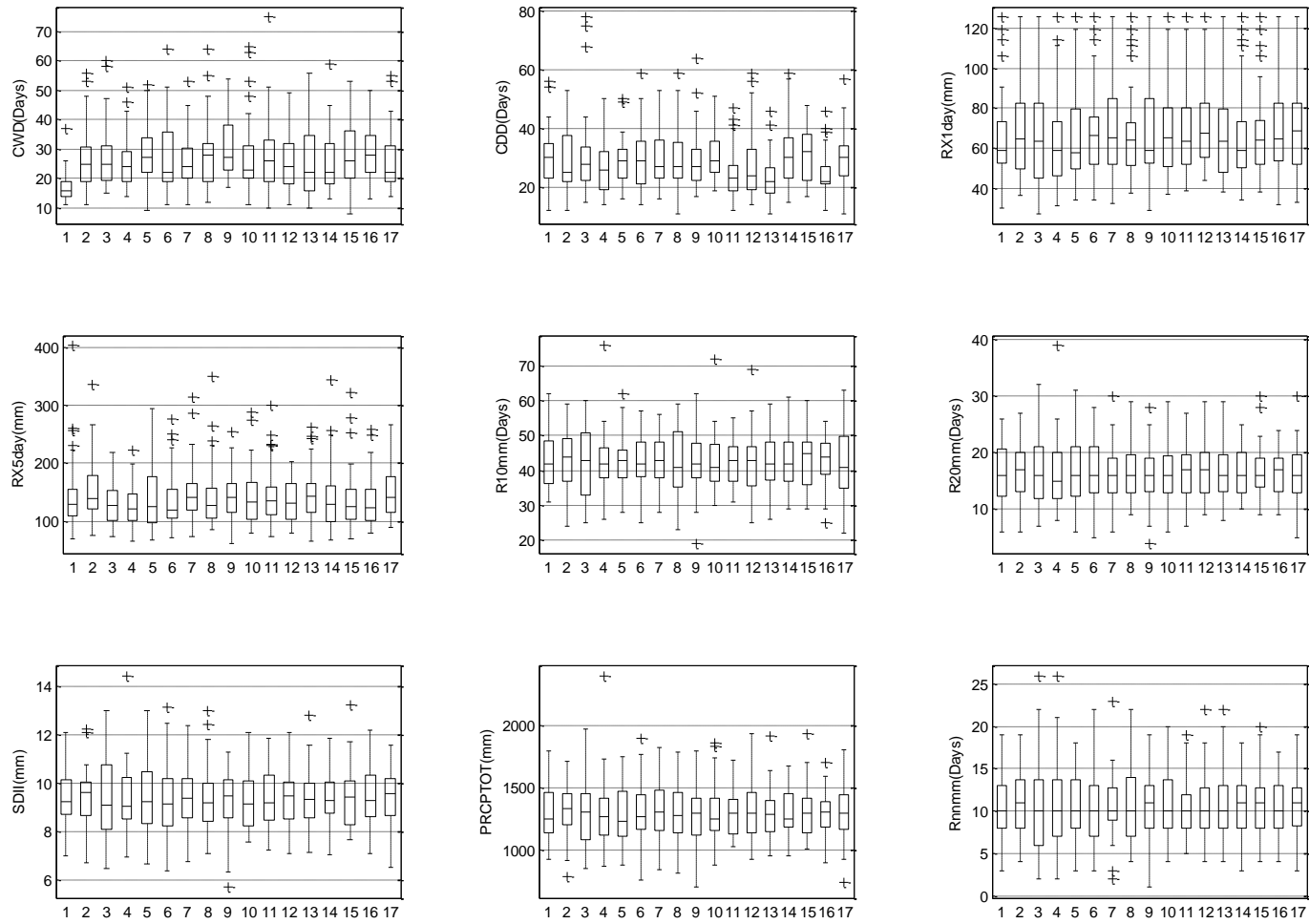


**Figure 14: Variability of WMO bias corrected indices for different models (2-17) and observed (1) for station 20.**

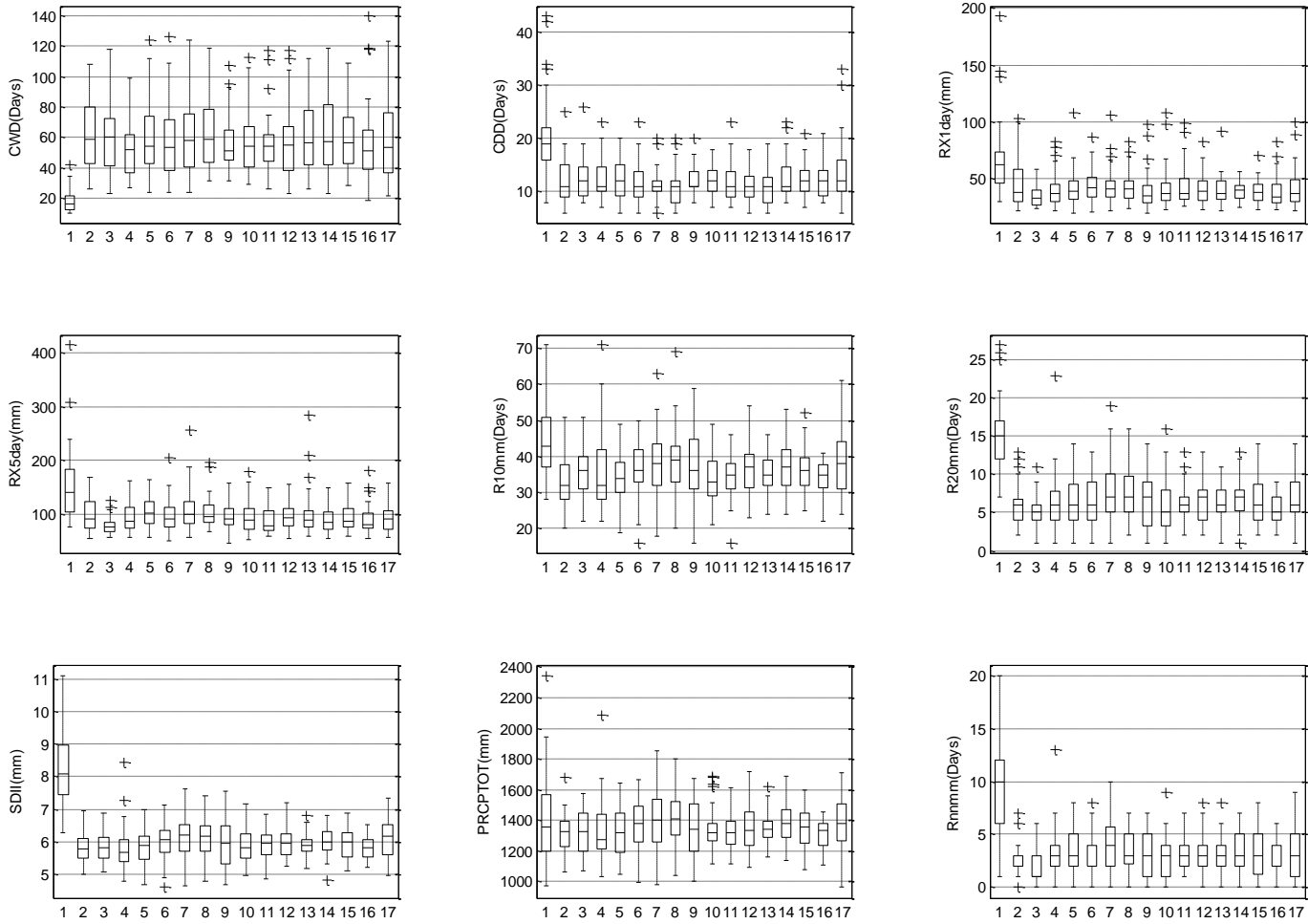


Figure 15: Variability of WMO indices for different models (2-17) and observed (1) for station 25.

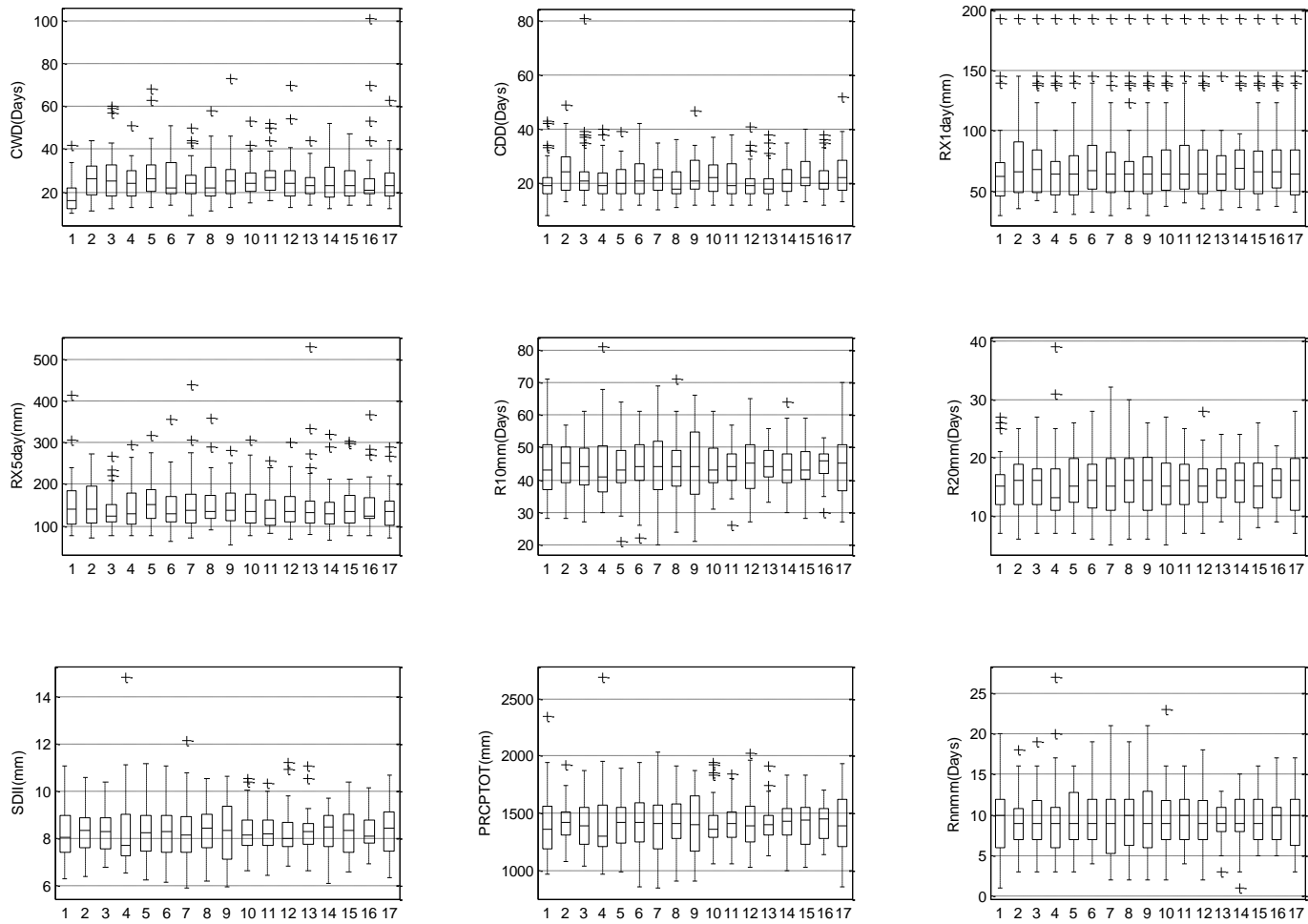


Figure 16: Variability of WMO bias corrected indices for different models (2-17) and observed (1) for station 25.

## **5.2 Bias Indices performance measures**

Bias indices consist of error measures between observed and predicted, as well as, contingency measures, as previously mentioned in Chapter Three.

### **5.2.1 Error measures performance**

The error measures were taken as a daily gross error for the entire date range, 1961 to 1999. This allowed for a single value to be applied to each station and model combination. The error measures will allow insight into the model with the lowest tendency for mistake. Figure 17 and Figure 18 assist in the visual interpretation of error performance of the observed and predicted precipitation values. The error values are significantly decreased after quantile mapping is applied to raw data. .

### **5.2.2 Contingency measure performance**

The concordance measure demonstrates an above average performance in the agreement between the observed and model data sets. This is unusual due to the strong dry bias related to the model data; although, could be caused by similar patterns between depth values in the models and depth values in the observed data. The error rate describes misses and false alarms as below average. The sensitivity and specificity are describing correctly predicted wet and dry days. The sensitivity index show 66% of actual positives are correctly identified, meaning the model is capturing positive rainfall correctly above average. The specificity index shows 55% of zero rainfall is correctly identified.

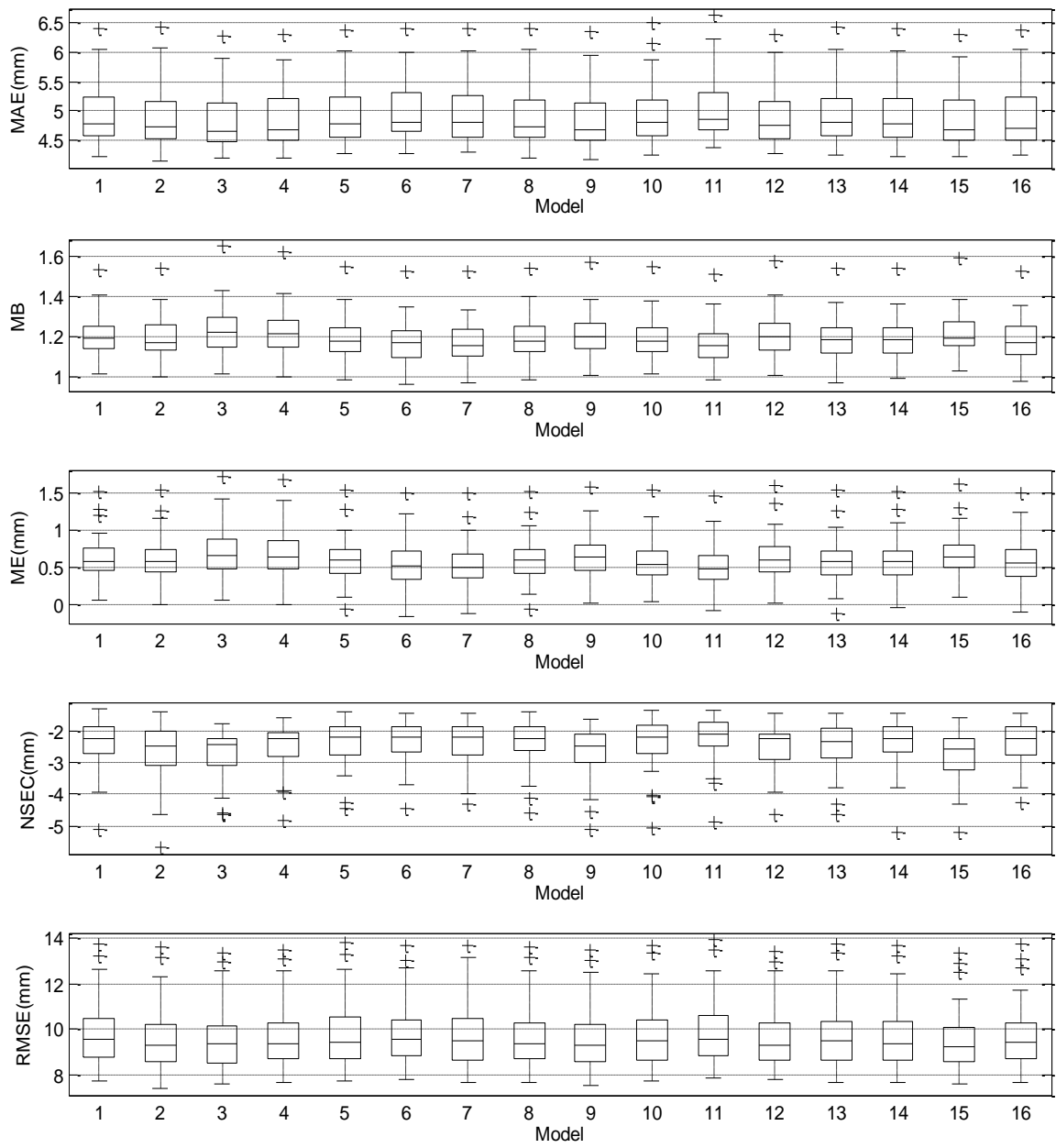


**Figure 17: Bias indices error performance measures.**

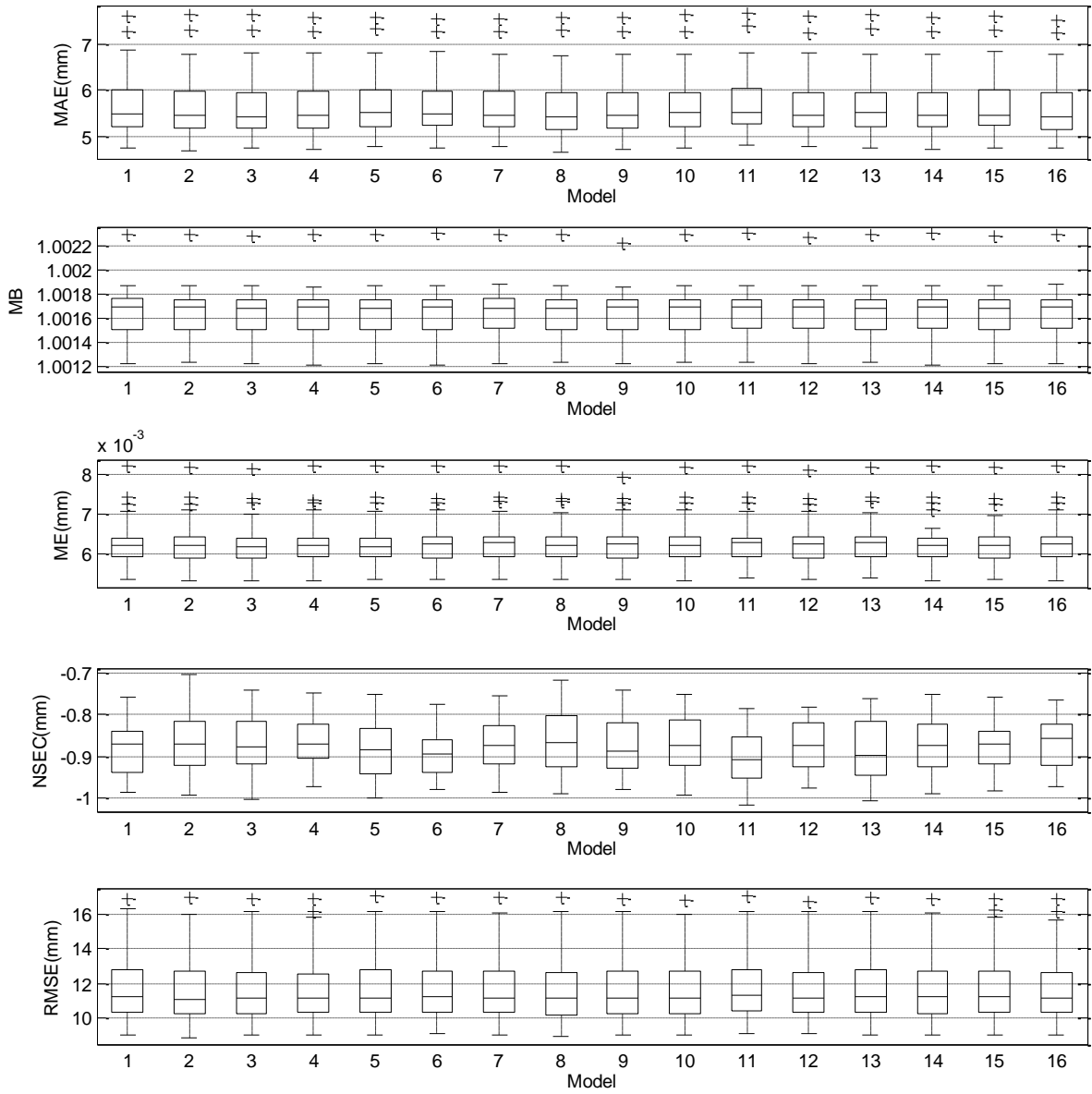


**Figure 18: Bias indices error performance measure after quantile mapping.**

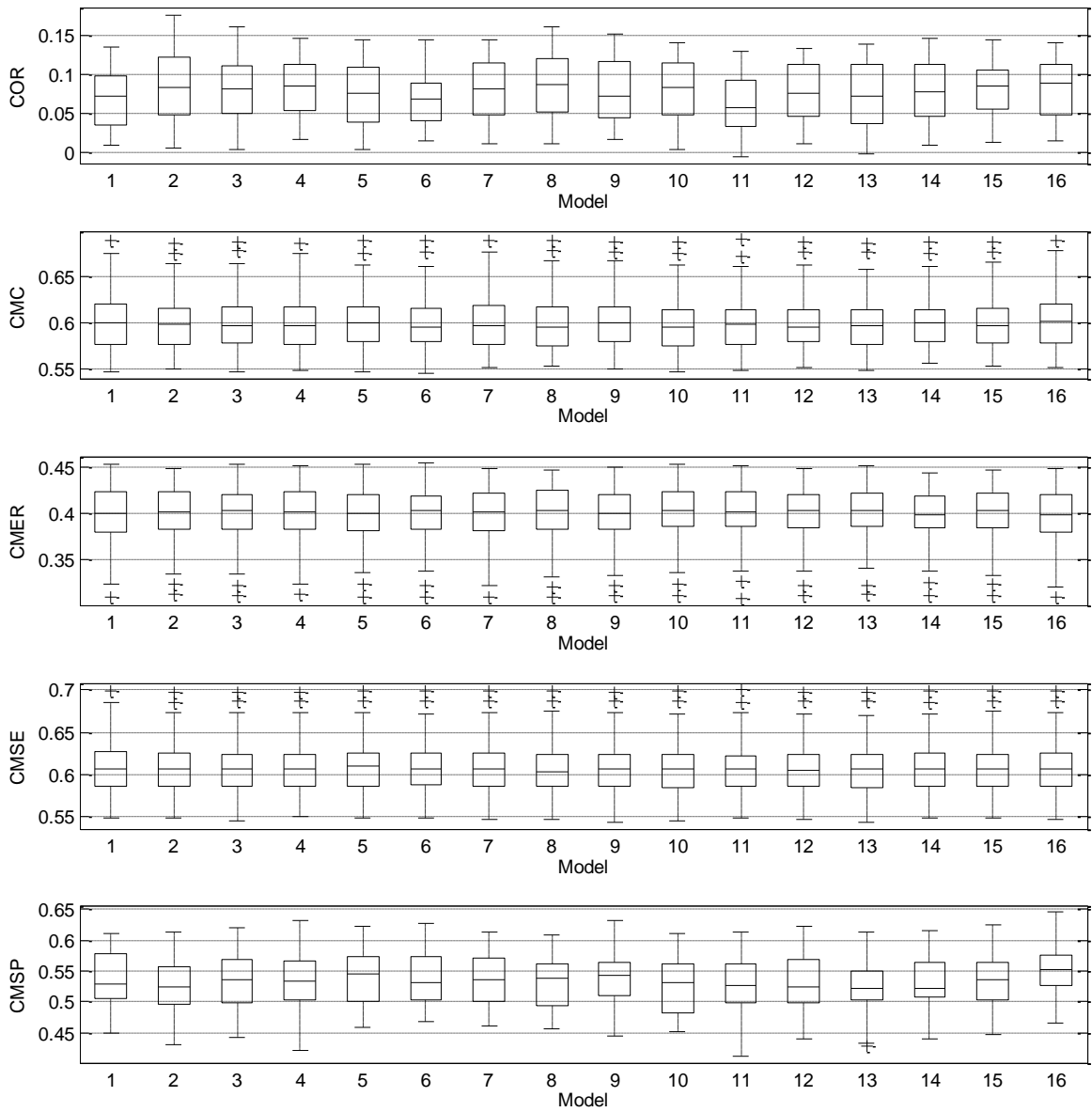


**Figure 19: Bias indices contingency measure performance.**

### 5.3 Model Ranking

The ranking of the models is based will describe the frequency analysis of each of the 16 models in the seven methods of ranking. Of the seven ranking methods, mentioned in Chapter Three's methodologies, a histogram matrix was used to describe the results. Gathered from Figure 20, there are two prevailing models, 12 and 14. Similarly, the bias corrected histogram matrix, seen in Figure 21, has model 12 and model 14 as the top two ranked models as well. The performance of the models based on individual stations as demonstrated in Table 9, and for bias corrected results, Table 10. Model 12 represents the BCCA CMIP5 model known as MIROC\_ESM\_CHEM. This model was developed by the Japan Agency for Marine and Earth Science Technology, Atmosphere and Ocean Research Institute and the National Institute for Environmental Studies. While model 14 represents the BCCA CMIP5 model known as MPI-ESM-LR. This model was developed by Max Planck Institute for Meteorology (MPI-M) Florida. These models share similar backgrounds as they are both Earth System Models (ESM). These models relate to the study of the Earth and its interaction with the surrounding atmosphere, cryosphere, and hydrosphere (Claussen, 1998). The capabilities of ESMs to incorporate the hydrosphere allow the models to perform well in extreme precipitation research.

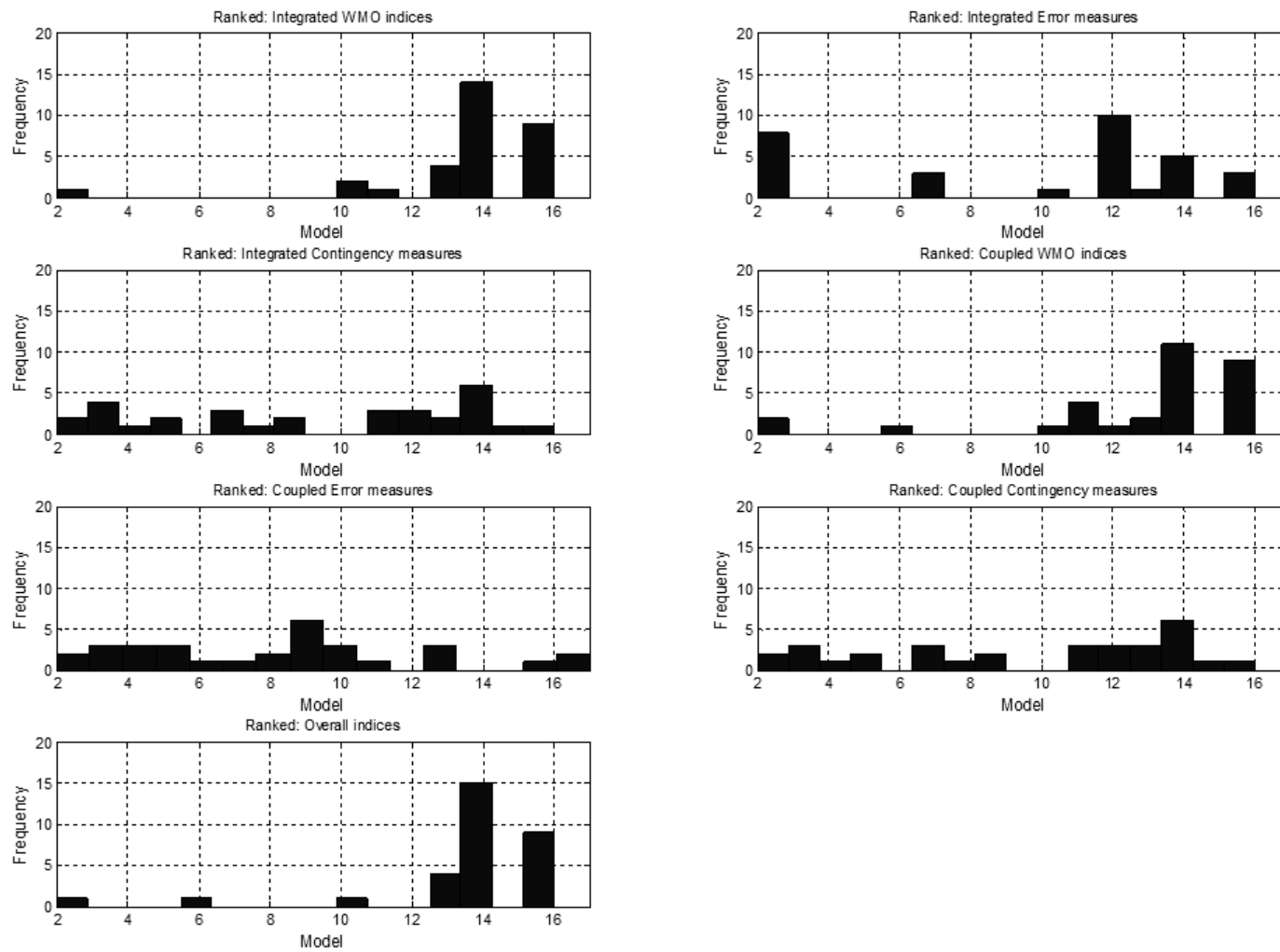


Figure 20: Number of times a model is selected for each performance measure.

**Table 9: Model frequencies for each station.**

Station ID	Coupled			Integrated			Overall
	WMO	Bias	Contingency	WMO	Bias	Contingency	
1	12	7	14	12	12	13	12
2	12	12	11	12	12	11	12
3	15	12	12	15	15	12	11
4	7	7	9	5	9	9	12
5	4	12	14	6	6	14	11
6	14	12	7	14	11	7	14
7	12	11	11	2	11	11	11
8	12	12	7	14	14	7	12
9	14	12	12	14	14	12	14
10	12	12	3	12	14	3	12
11	11	12	2	11	11	2	11
12	12	12	13	11	11	13	12
13	8	8	8	8	8	8	8
14	7	7	14	14	14	15	14
15	12	12	14	12	7	14	12
16	12	14	11	12	12	11	12
17	7	7	5	13	14	5	14
18	12	12	3	8	8	1	12
19	12	12	14	8	8	14	12
20	12	12	14	12	12	16	12
21	14	7	14	14	14	14	14
22	12	7	14	12	17	14	14
23	8	8	13	12	14	13	8
24	11	12	9	11	11	9	11
25	7	7	12	14	14	12	14
26	12	12	4	7	7	14	12
27	12	12	7	2	11	7	12
28	12	12	3	13	12	3	12
29	12	12	5	7	12	5	12
30	8	6	4	12	8	14	7
31	17	17	2	17	7	2	7

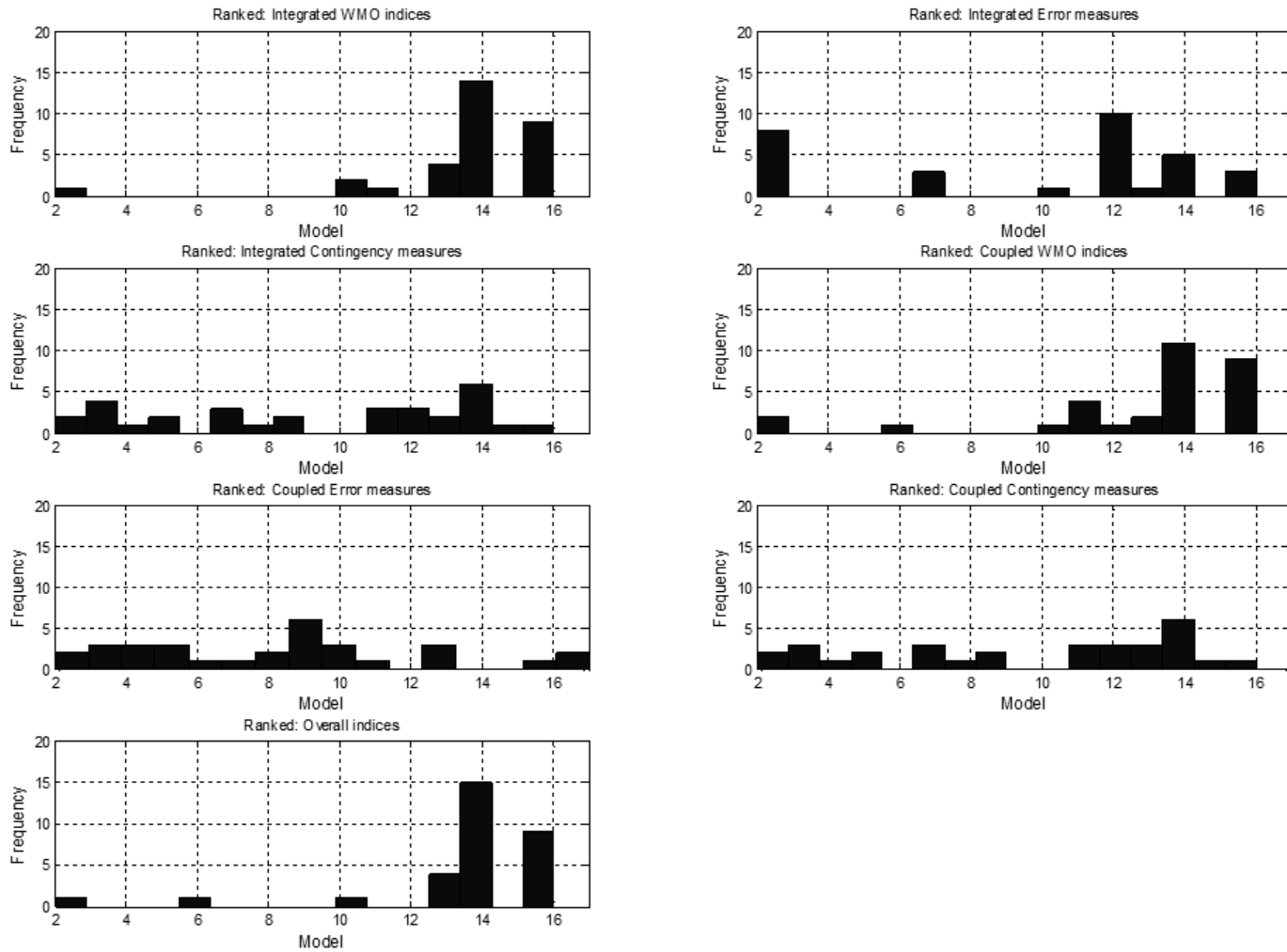


Figure 21: Number of times a model is selected for each performance measure after quantile mapping.

**Table 10: Bias Corrected model frequencies for each station.**

Station ID	Coupled			Integrated			Overall
	WMO	Bias	Contingency	WMO	Bias	Contingency	
1	14	7	14	11	13	13	14
2	16	14	11	6	8	11	16
3	16	2	12	16	4	12	16
4	2	16	9	2	9	9	2
5	14	12	14	12	3	14	14
6	10	14	7	16	5	7	10
7	16	14	11	16	10	11	16
8	13	2	7	13	2	7	13
9	14	12	12	14	9	12	14
10	14	10	3	14	10	3	14
11	16	12	2	16	9	2	16
12	14	12	13	2	9	13	14
13	14	2	8	14	5	8	14
14	14	12	15	14	9	15	14
15	16	16	14	16	9	14	16
16	16	14	11	16	7	11	16
17	16	7	5	16	5	5	16
18	16	12	3	14	6	3	16
19	14	13	14	11	3	14	14
20	14	12	16	14	11	16	14
21	14	2	14	14	16	14	14
22	14	2	14	14	4	14	14
23	14	14	13	14	8	13	14
24	11	12	9	11	2	9	14
25	13	2	12	16	3	12	13
26	14	12	4	14	17	4	14
27	10	12	7	10	13	7	6
28	13	16	3	13	4	3	13
29	13	2	5	11	17	5	13
30	16	7	3	16	10	14	16
31	14	2	2	14	13	2	14

#### 5.4 Long-term analysis of best models

With the two best models selected for Florida, the extended projections of predicted daily precipitation were collected from 1950 to 2099. These extended data sets will be collected for 11 stations randomly selected throughout the state. The stations will act as representatives for the remaining 20 stations. By collecting an extended date range, the models will be able to depict trends and variations on a long-term climate forecast. The 11 stations are described in Table 11.

**Table 11: Stations selected for long-term analysis**

Rain gage ID	Latitude	Longitude
3	30.418	-84.986
6	30.250	-83.259
8	25.500	-80.500
12	29.200	-81.931
13	28.096	-80.631
16	30.531	-86.492
19	26.79	-81.304
20	27.609	-82.348
23	30.068	-82.193
25	27.117	-80.283
28	25.761	-80.824

From these 11 stations, where the case study IDs are used for convenience of the extended analysis, there are variations in regional long-term trends. The trends are mixed and do show variations throughout the state. There are specific stations that are reacting consistently to extreme precipitation intensity, frequency, or duration. Station 3, 16, and 23 are all located in the panhandle region of Florida and all experience similar increases in extreme precipitation events. Oppositely the stations located in the central and southern regions are experiencing decreasing or stable trends. The resulting trends as described by Figure 22 to Figure 30. These trends are known to have a dry bias related to them; however, there is no bias correction associated to these results due to non-stationarity.

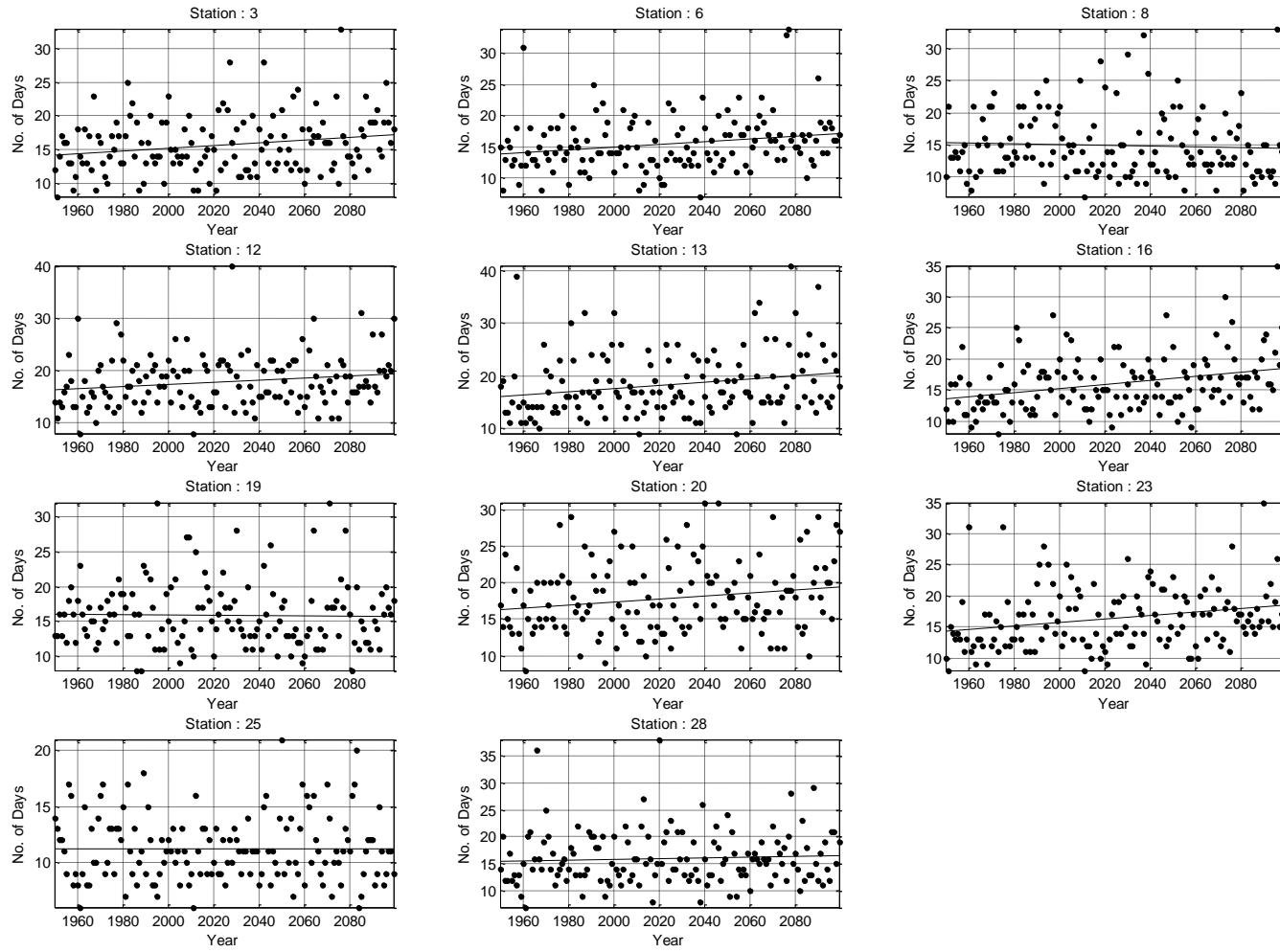


Figure 22: Variability of CDD index and long-term trends in extreme precipitation.

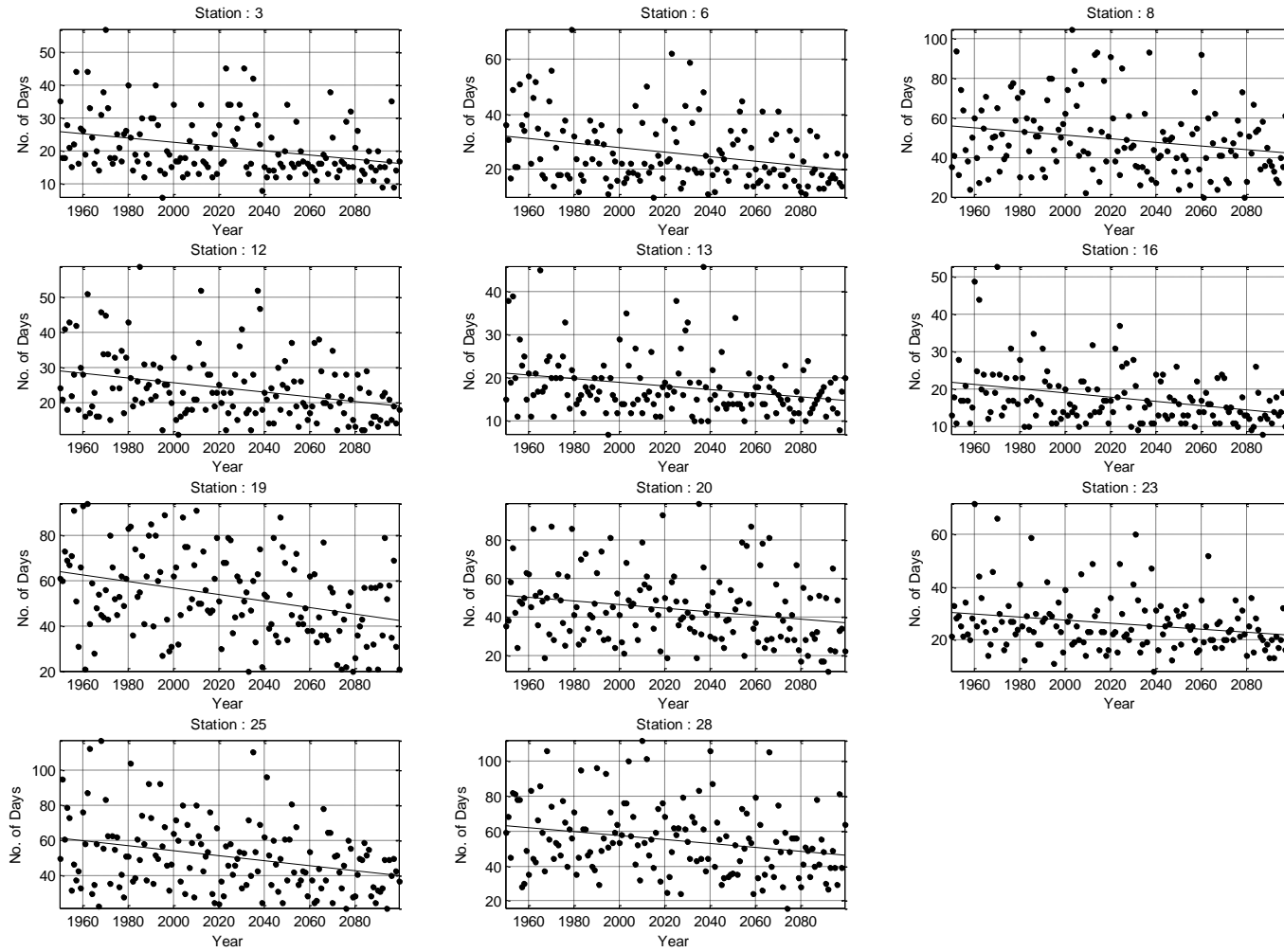


Figure 23: Variability of CWD index and long-term trends in extreme precipitation.

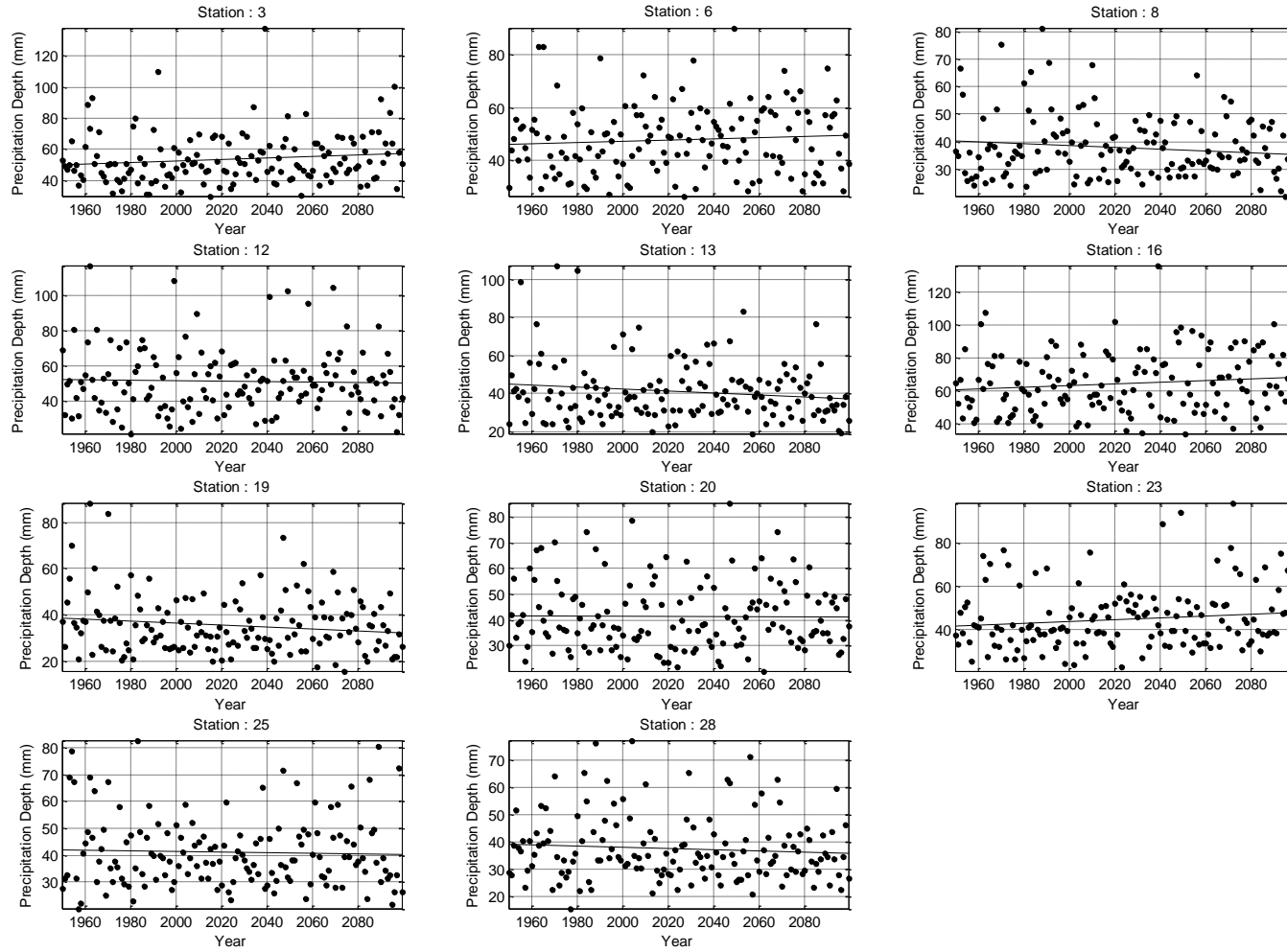


Figure 24: Variability of RX1DAY index and long-term trends in extreme precipitation.

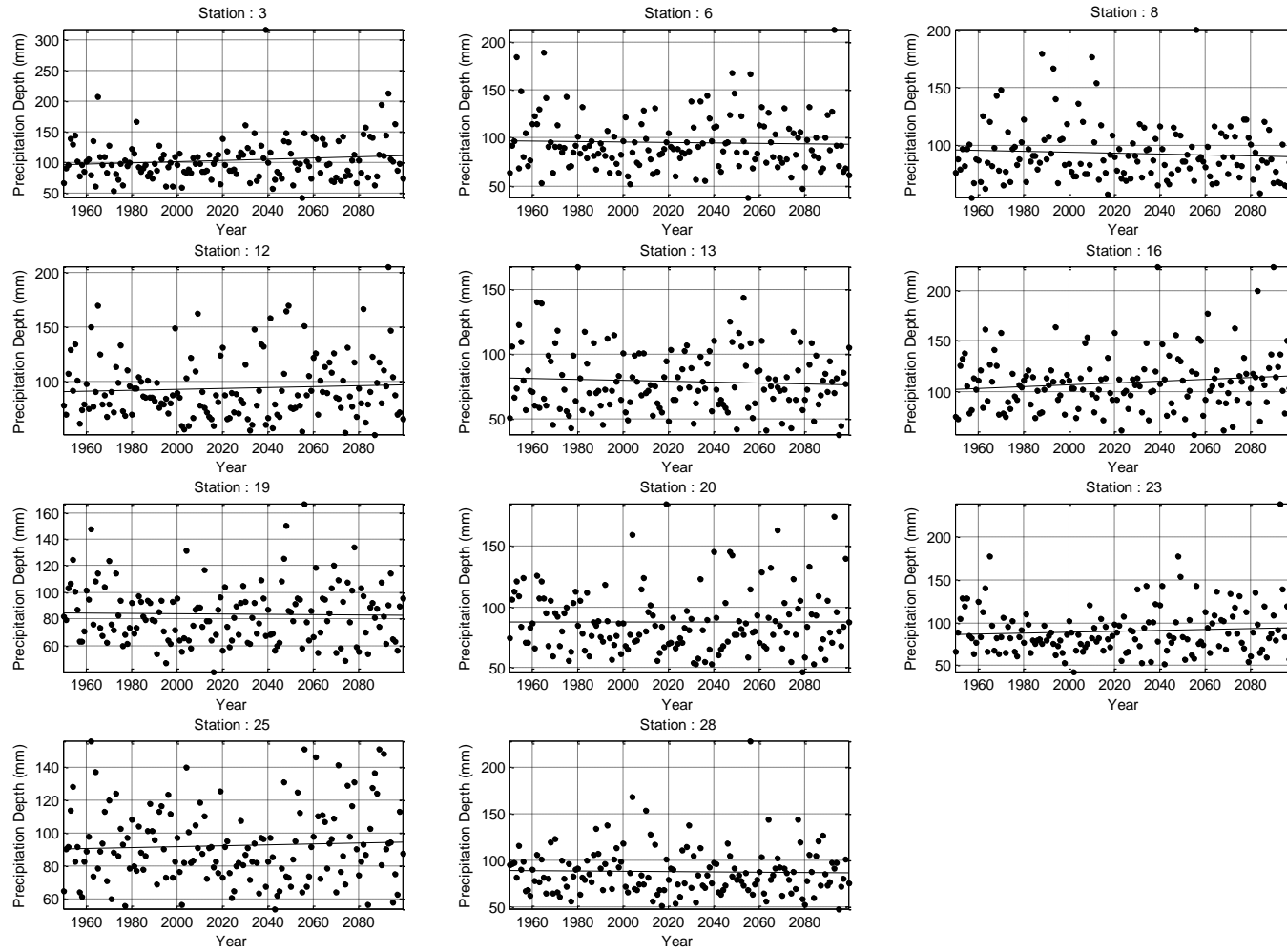


Figure 25: Variability of RX5DAY index and long-term trends in extreme precipitation.

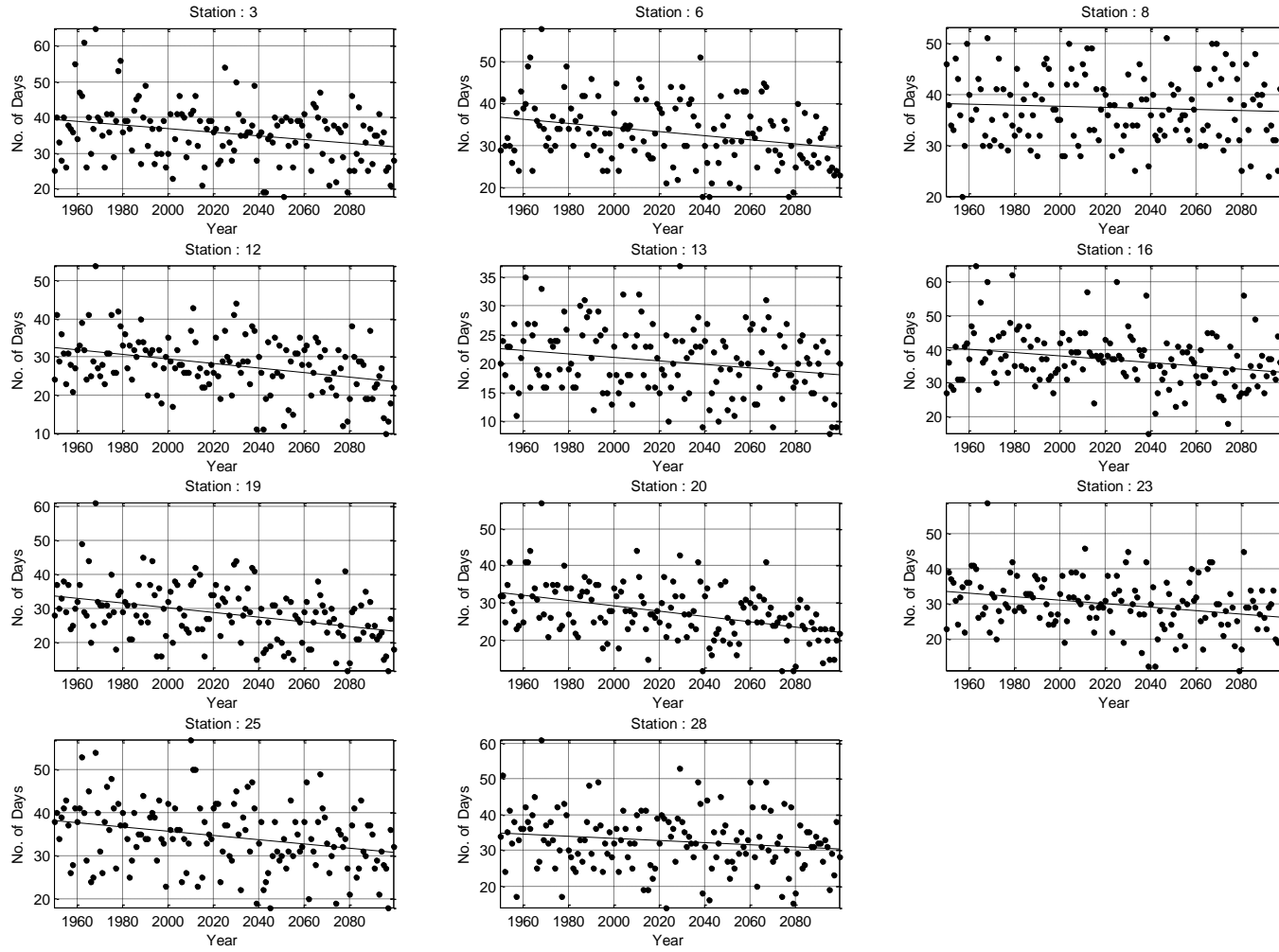
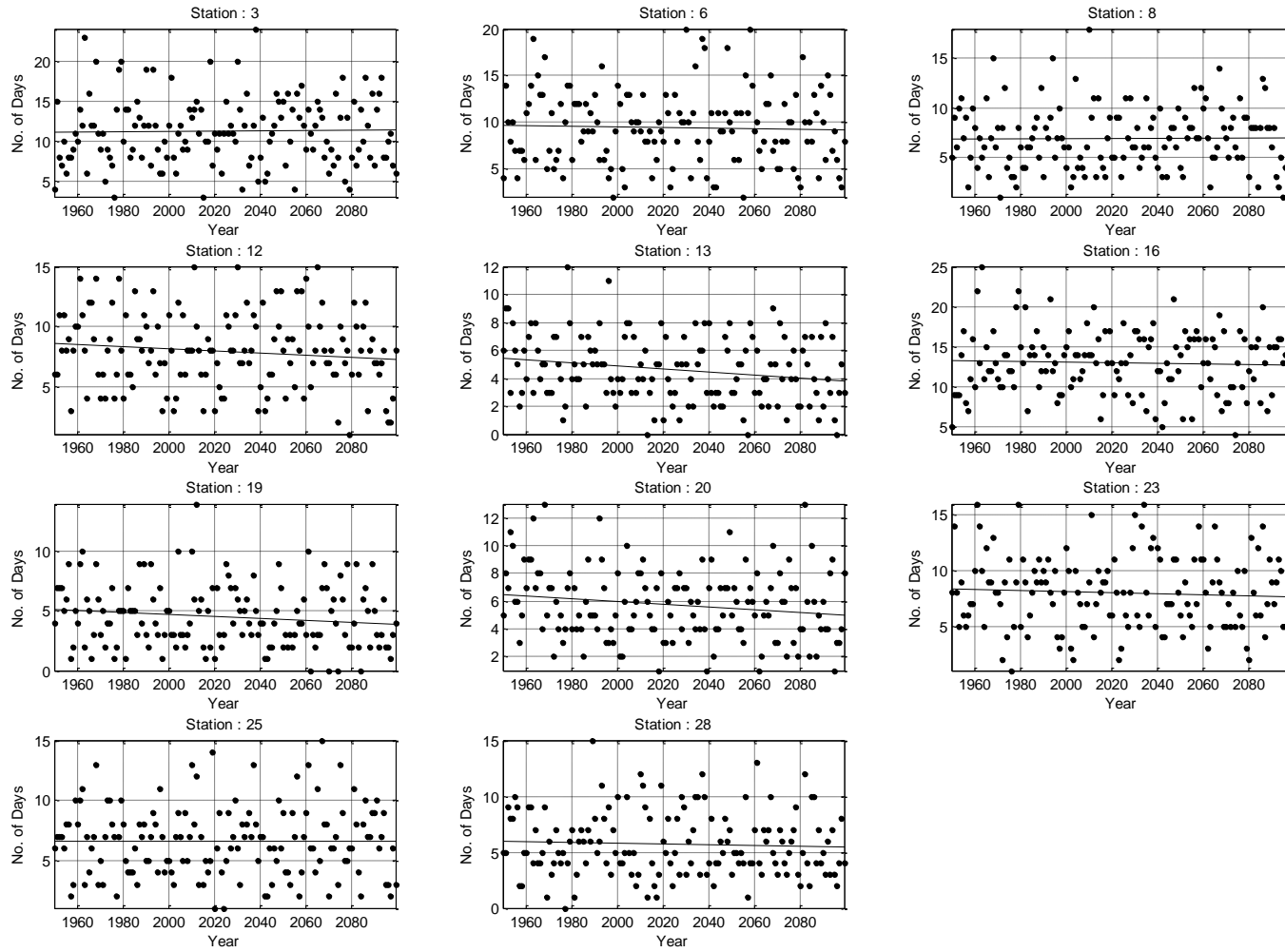


Figure 26: Variability of R10 index and long-term trends in extreme precipitation.



**Figure 27: Variability of R20 index and long-term trends in extreme precipitation.**

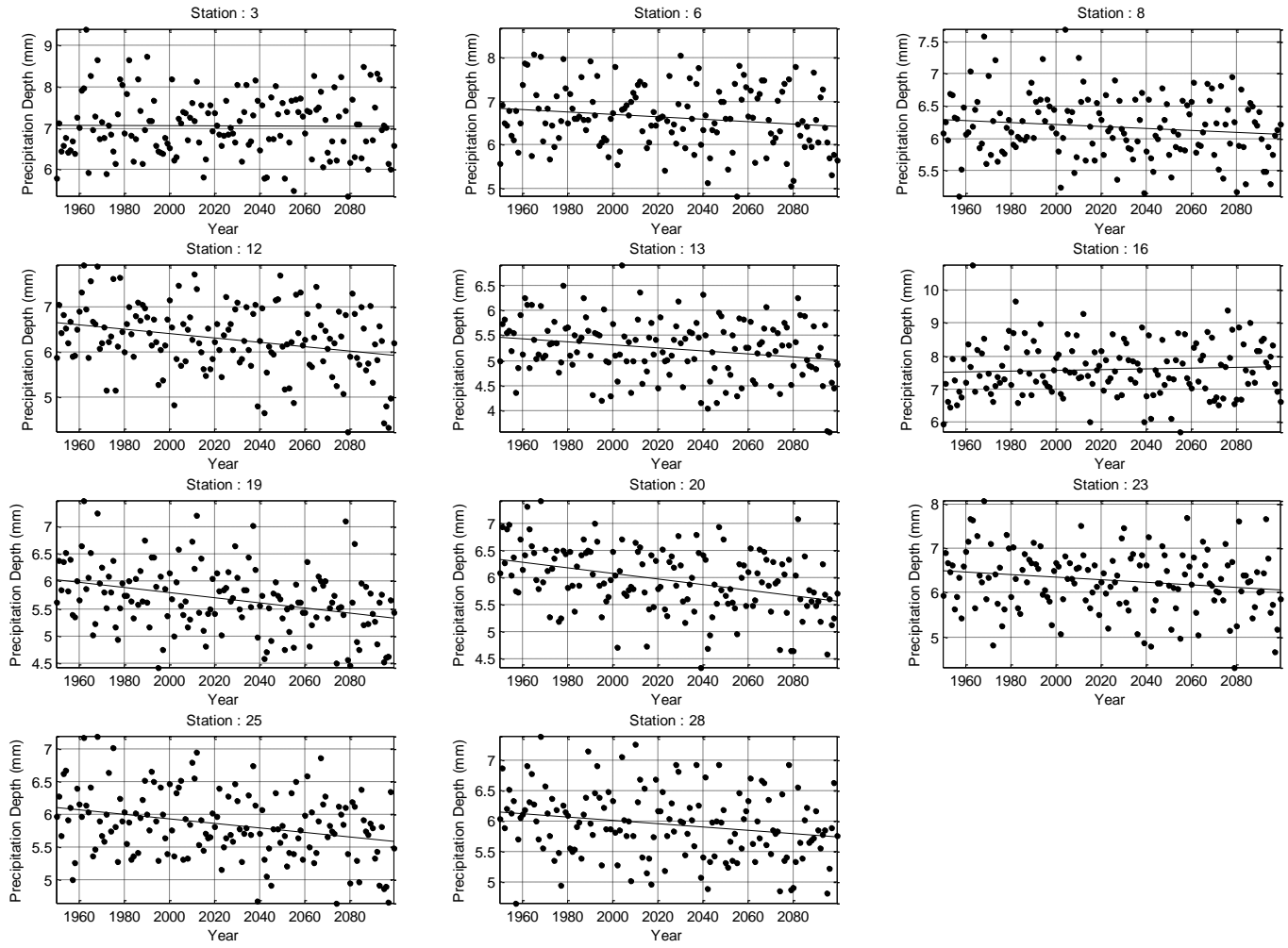


Figure 28: Variability of SDII index and long-term trends in extreme precipitation.

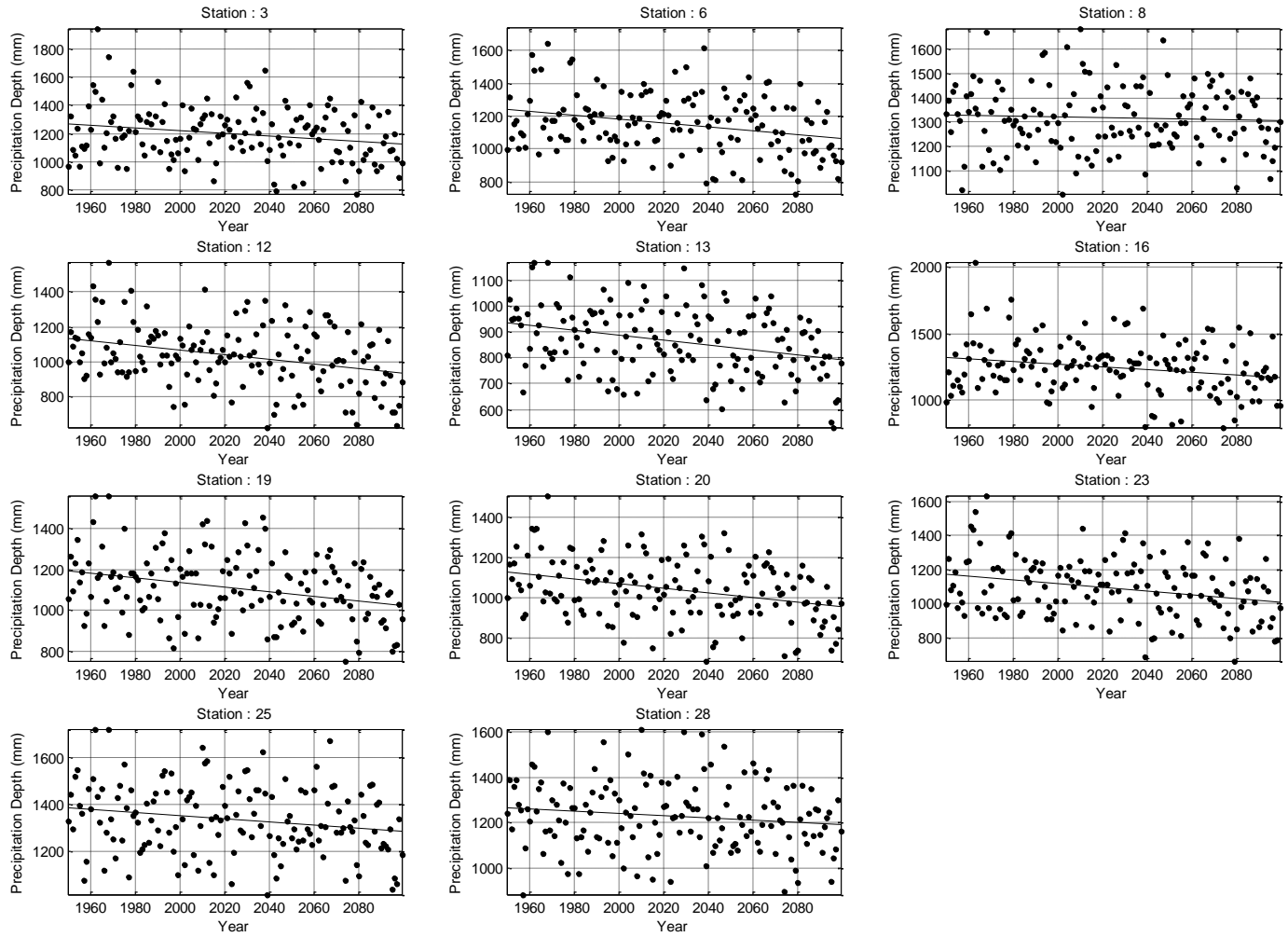


Figure 29: Variability of PRCPTOT index and long-term trends in extreme precipitation.

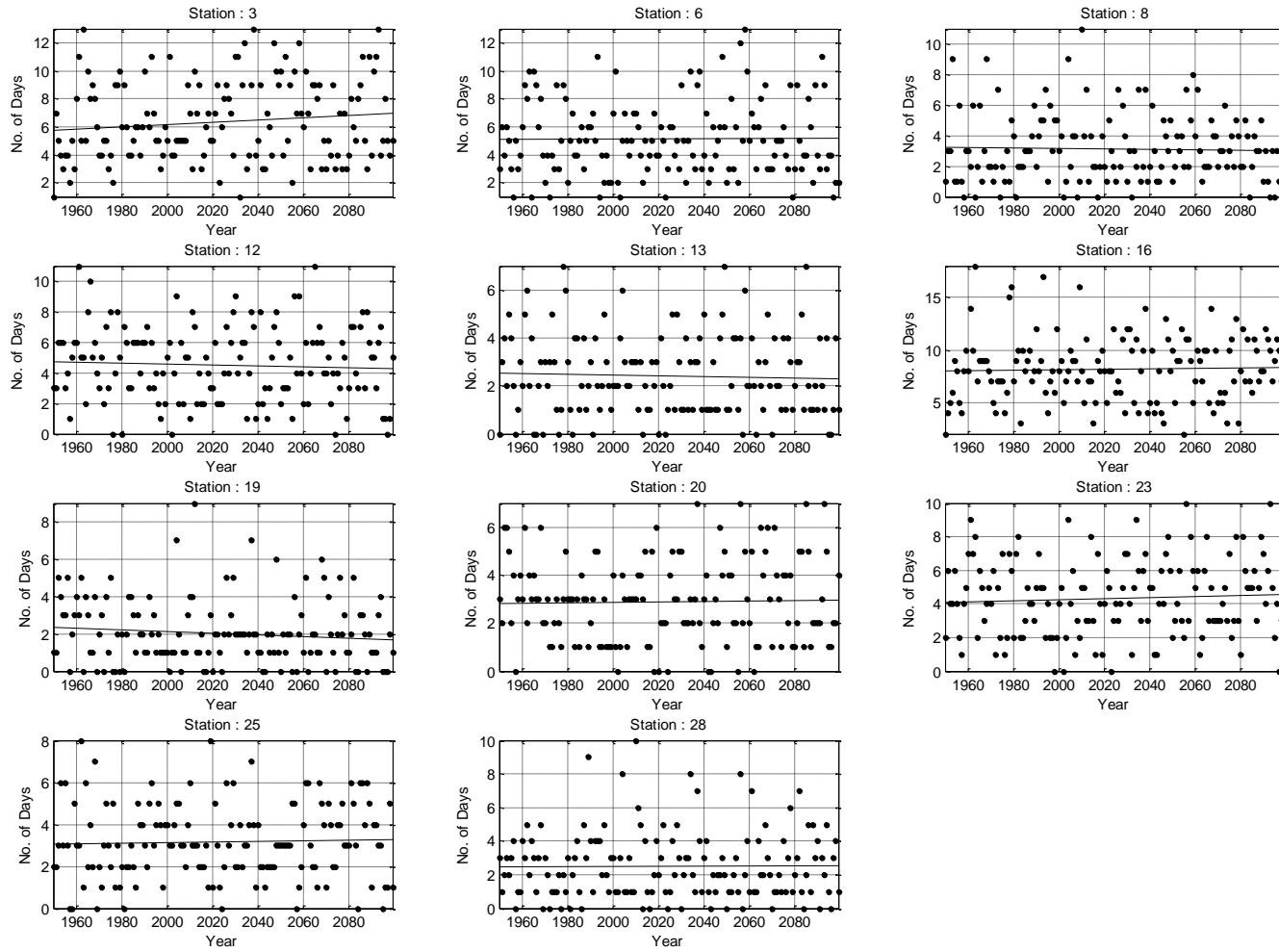


Figure 30: Variability of R254 index and long-term trends in extreme precipitation.

#### 5.4.1 Spatial variations of future precipitation trends

Of the 11 stations, the overall performance indicates that there is a steady decrease in precipitation totals and extremes throughout Florida in the next 100 year. There are; however, regional variations in trends and their characteristics. For the extreme intensity indices, RX1DAY and RX5DAY, the trends show the panhandle region increasing during extreme rainfall, RX1DAY, as well as a prolonged extreme rainfall event, RX5DAY. Although increases were seen in the panhandle for both indices, RX5DAY showed a milder slope indicating less deviation from present conditions in extended extreme rainfall events, seen in Figure 24 and Figure 25.

Precipitation indices R10, R20, and R254 are used to depict the models reaction to future frequencies. The frequency of rainfall events is generally decreasing, but the models do deviate in certain regions and stations as the threshold precipitation depth is increased. By doing so the models show that higher intensity events, R254, will be more common in the panhandle region and parts of south Florida, but there will decreases in the number of moderate to mild, R10 and R20, rainfall events in the next 100 years, seen in Figure 26, Figure 27, and Figure 30.

#### 5.4.2 Incremental variations in extreme precipitation

The 150 year period, 1950-2099, taken for this study is defining a declining trend. There is uncertainty on how and when this trend is occurring. By splitting the time period into three 50 year periods the behavior of the projections can be understood. Table 12 defines the three time periods used.

**Table 12: Incremental 50 year period.**

Period	Dates
1	1950-1999
2	2000-2049
3	2050-2099

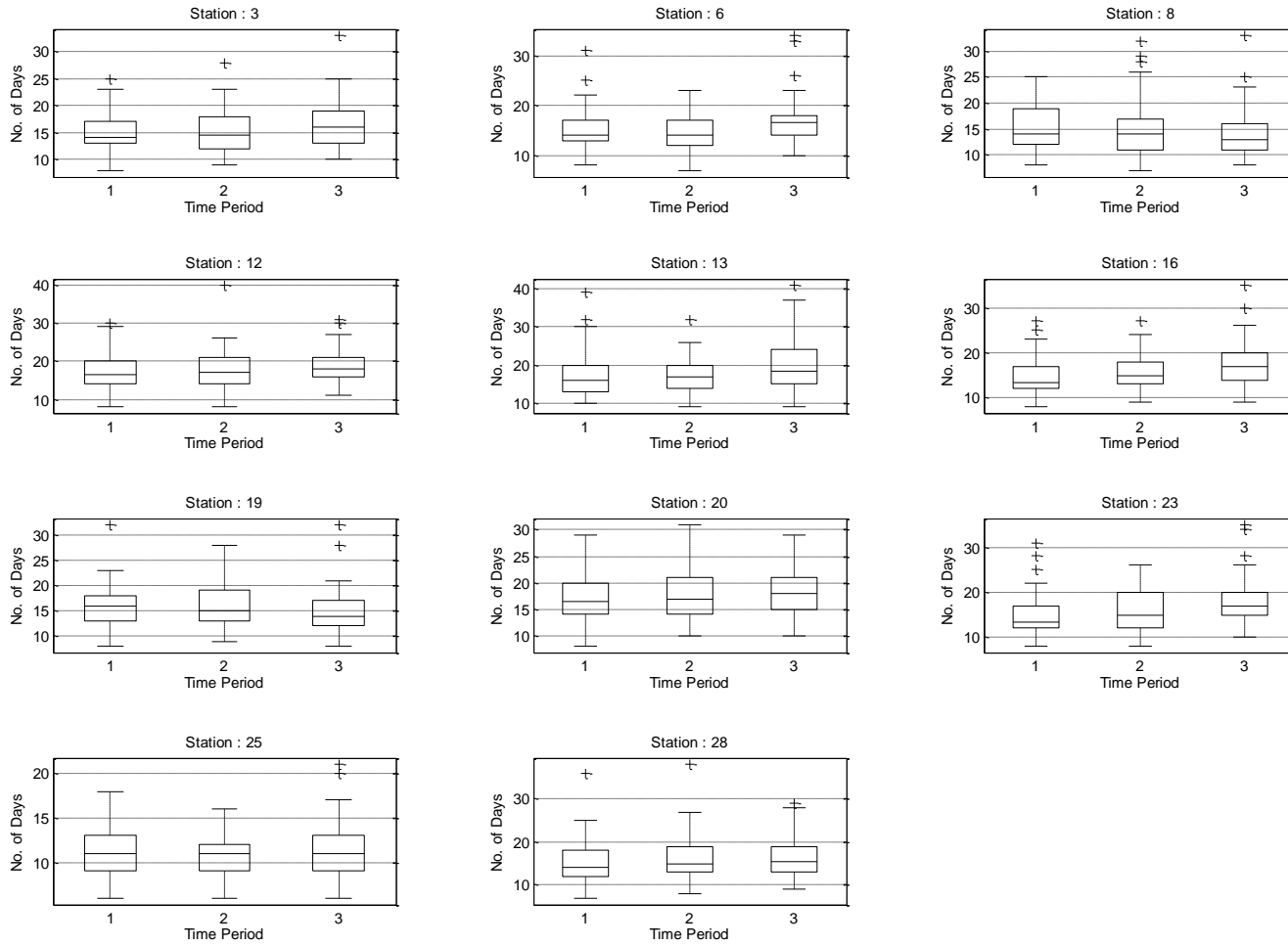


**Figure 31: Variability of CDD index for long-term statistical changes in period 1(1950-1999), period 2 (2000-2049), and period 3 (2050-2099).**

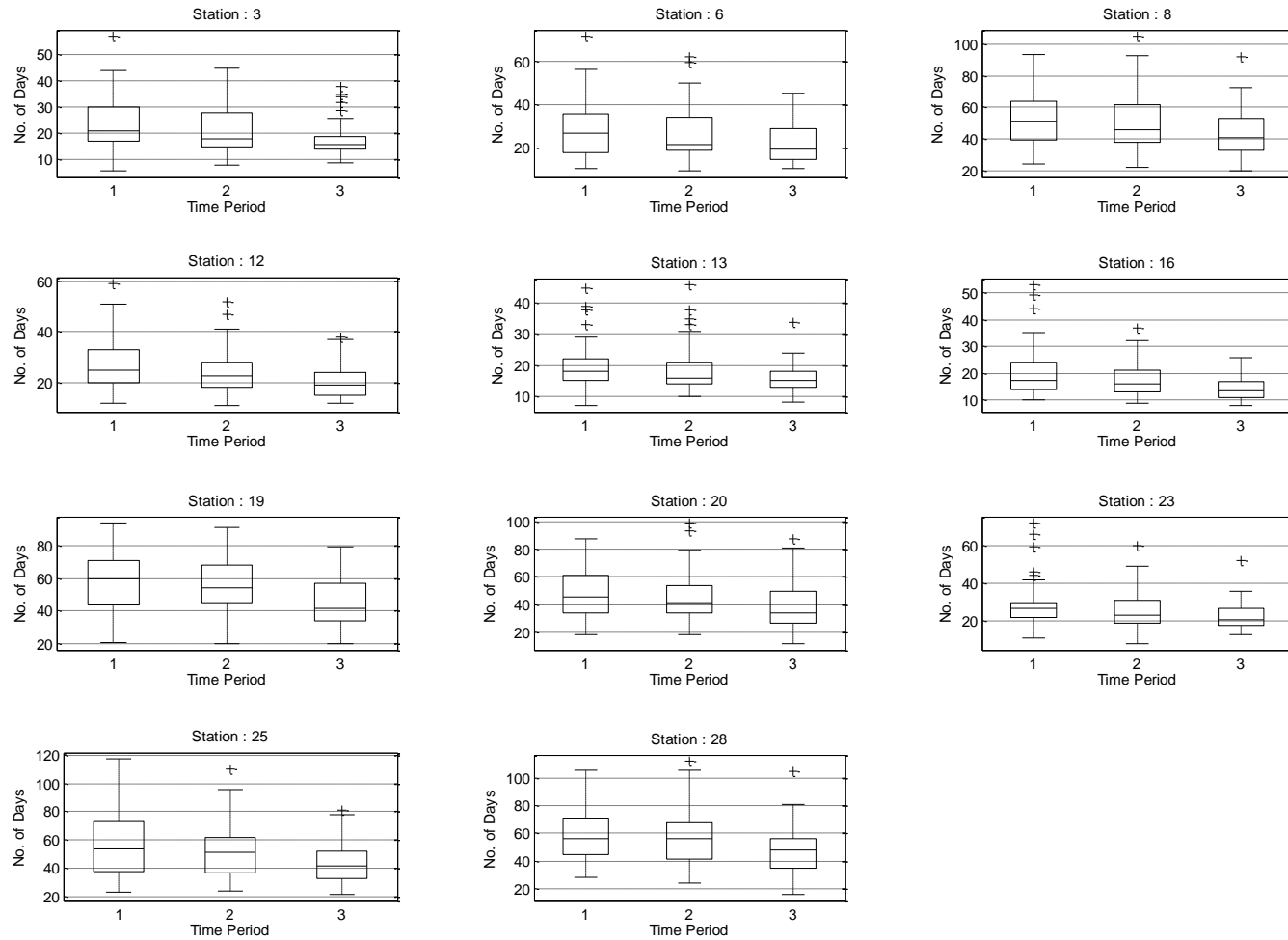


**Figure 32: Variability of CWD index for long-term statistical changes in period 1(1950-1999), period 2 (2000-2049), and period 3 (2050-2099).**

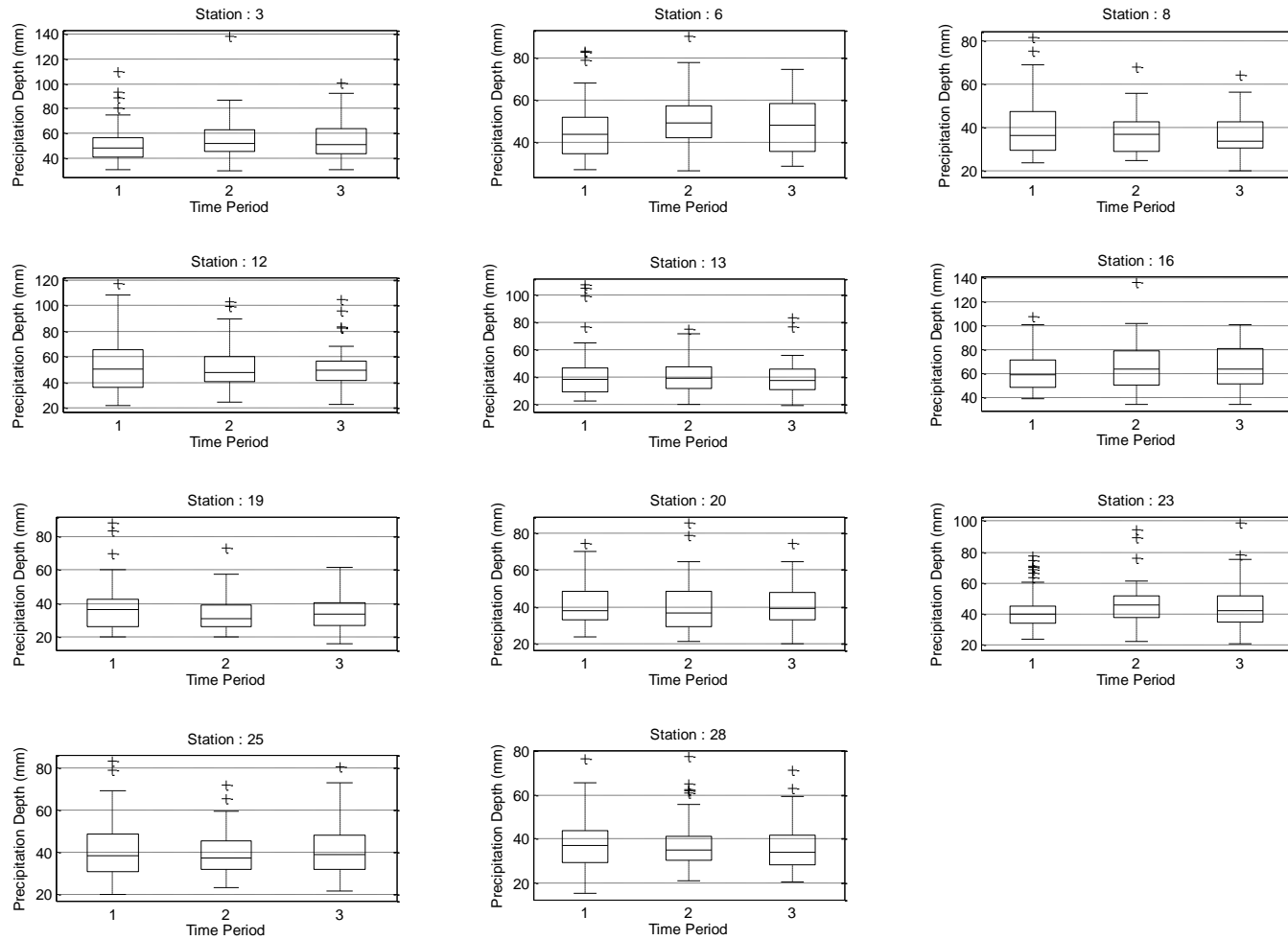


**Figure 33: Variability of RX1DAY index for long-term statistical changes in period 1(1950-1999), period 2 (2000-2049), and period 3 (2050-2099).**

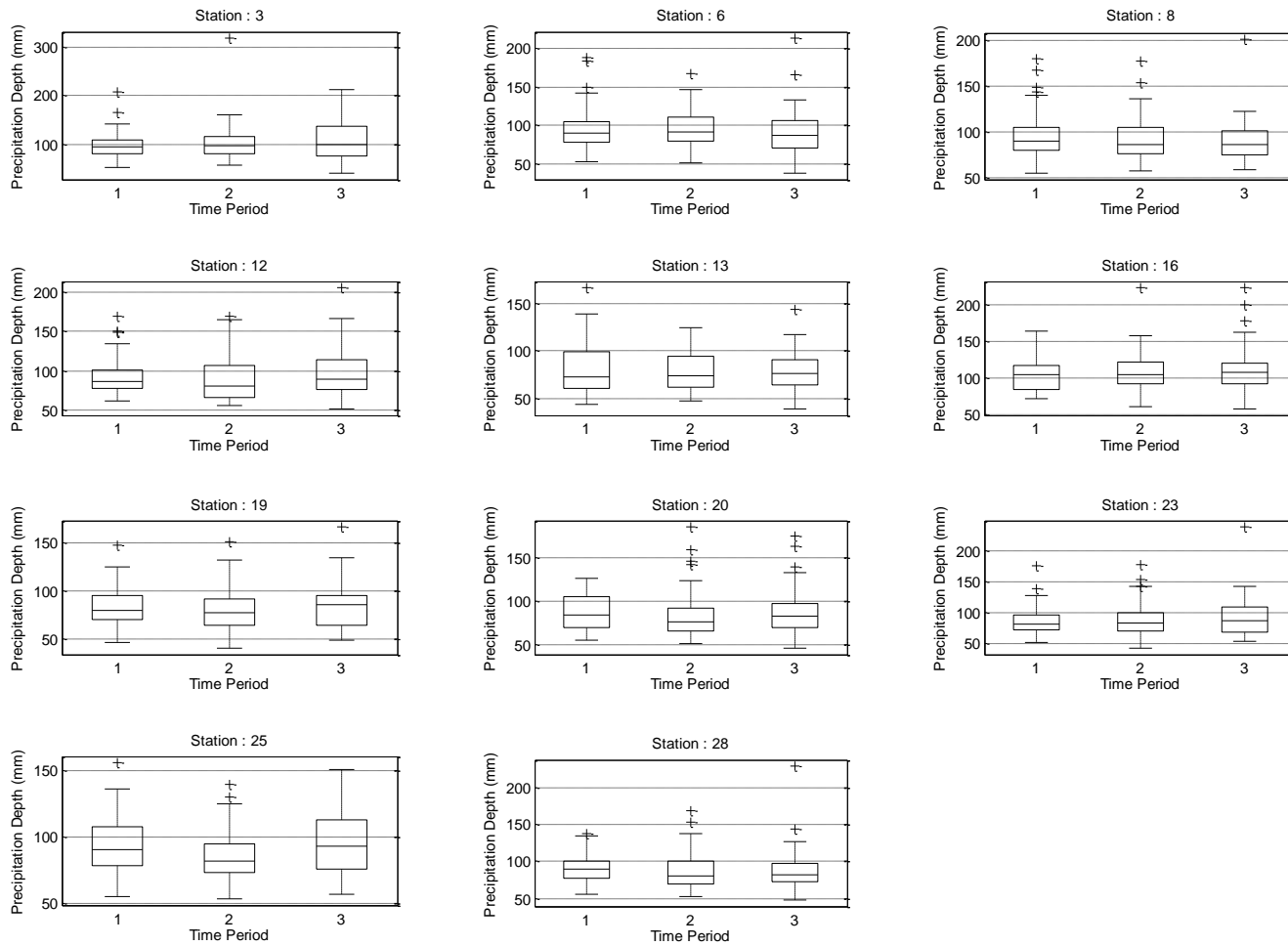


**Figure 34: Variability of RX5DAY index for long-term statistical changes in period 1(1950-1999), period 2 (2000-2049), and period 3 (2050-2099).**

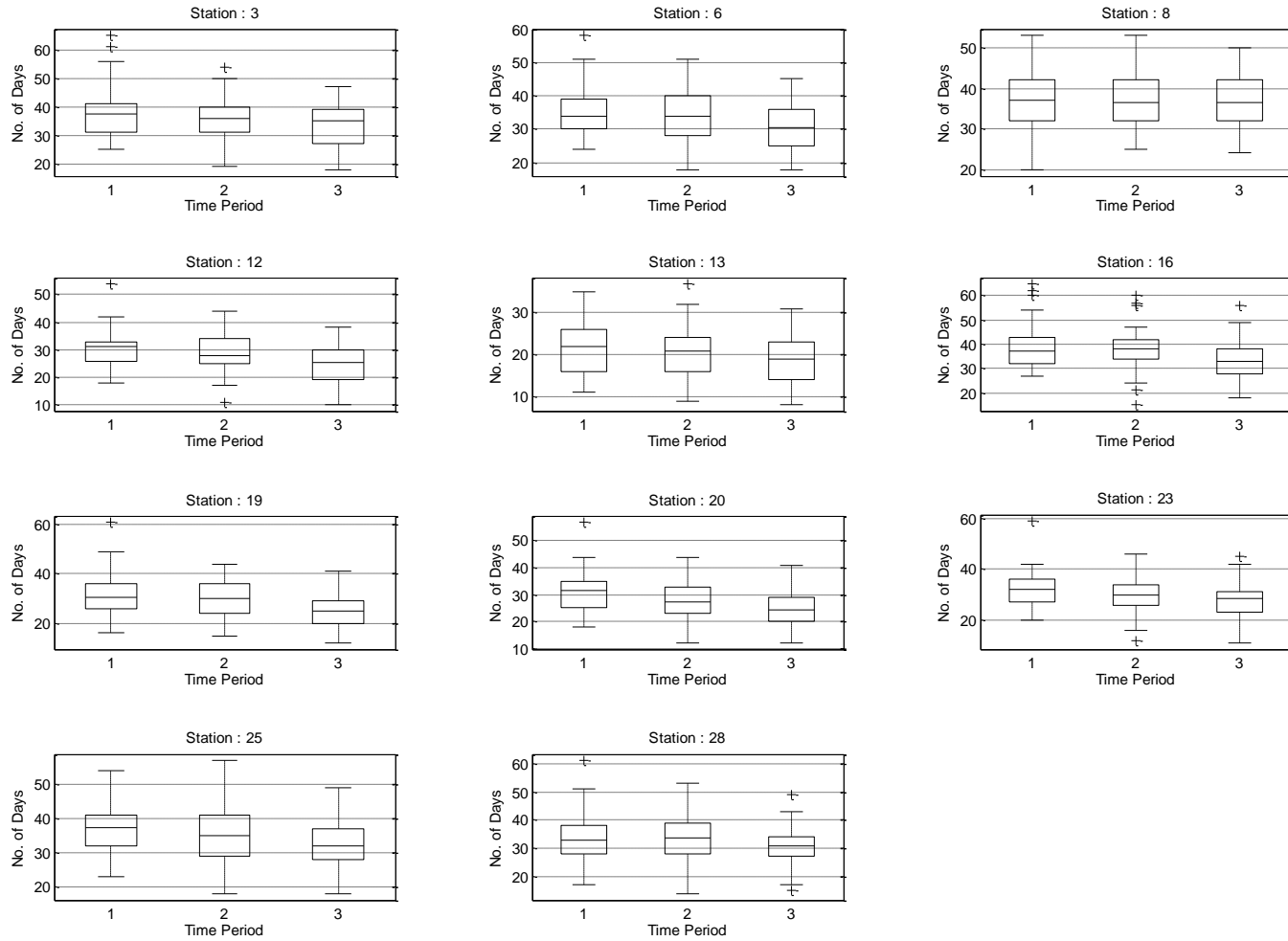


**Figure 35: Variability of R10 index for long-term statistical changes in period 1(1950-1999), period 2 (2000-2049), and period 3 (2050-2099).**

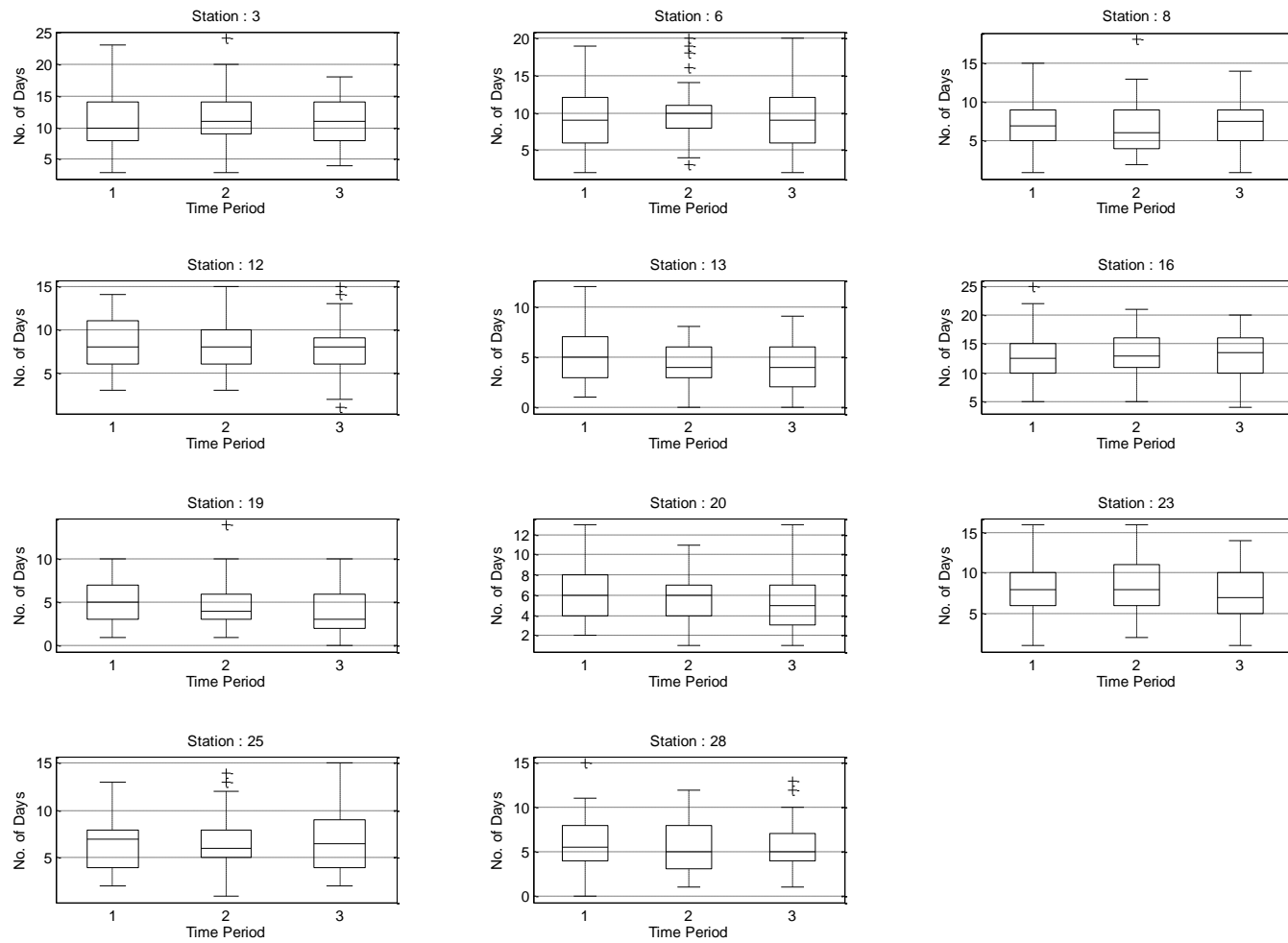


**Figure 36: Variability of R20 index for long-term statistical changes in period 1(1950-1999), period 2 (2000-2049), and period 3 (2050-2099).**

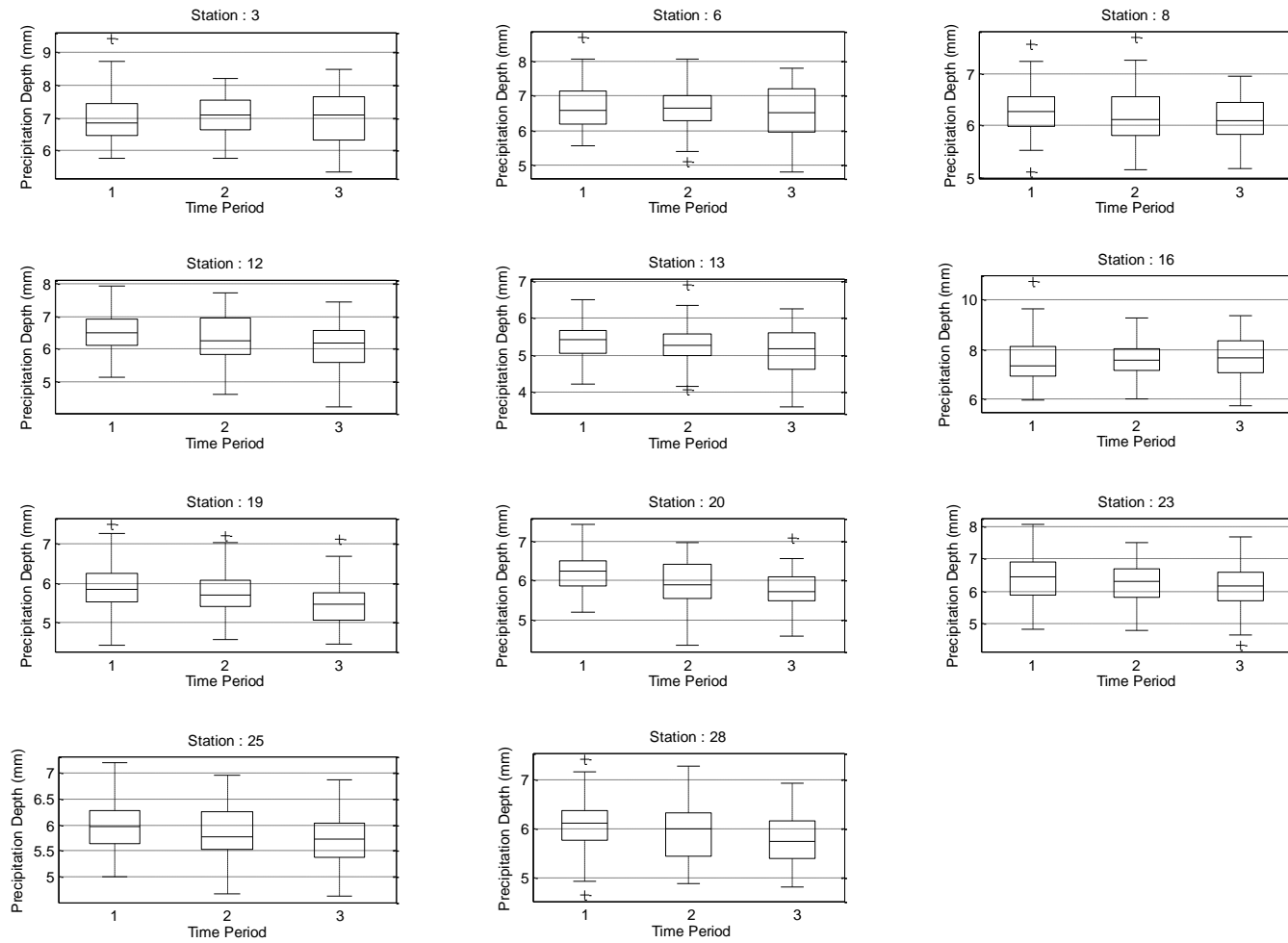


**Figure 37: Variability of SDII index for long-term statistical changes in period 1(1950-1999), period 2 (2000-2049), and period 3 (2050-2099).**

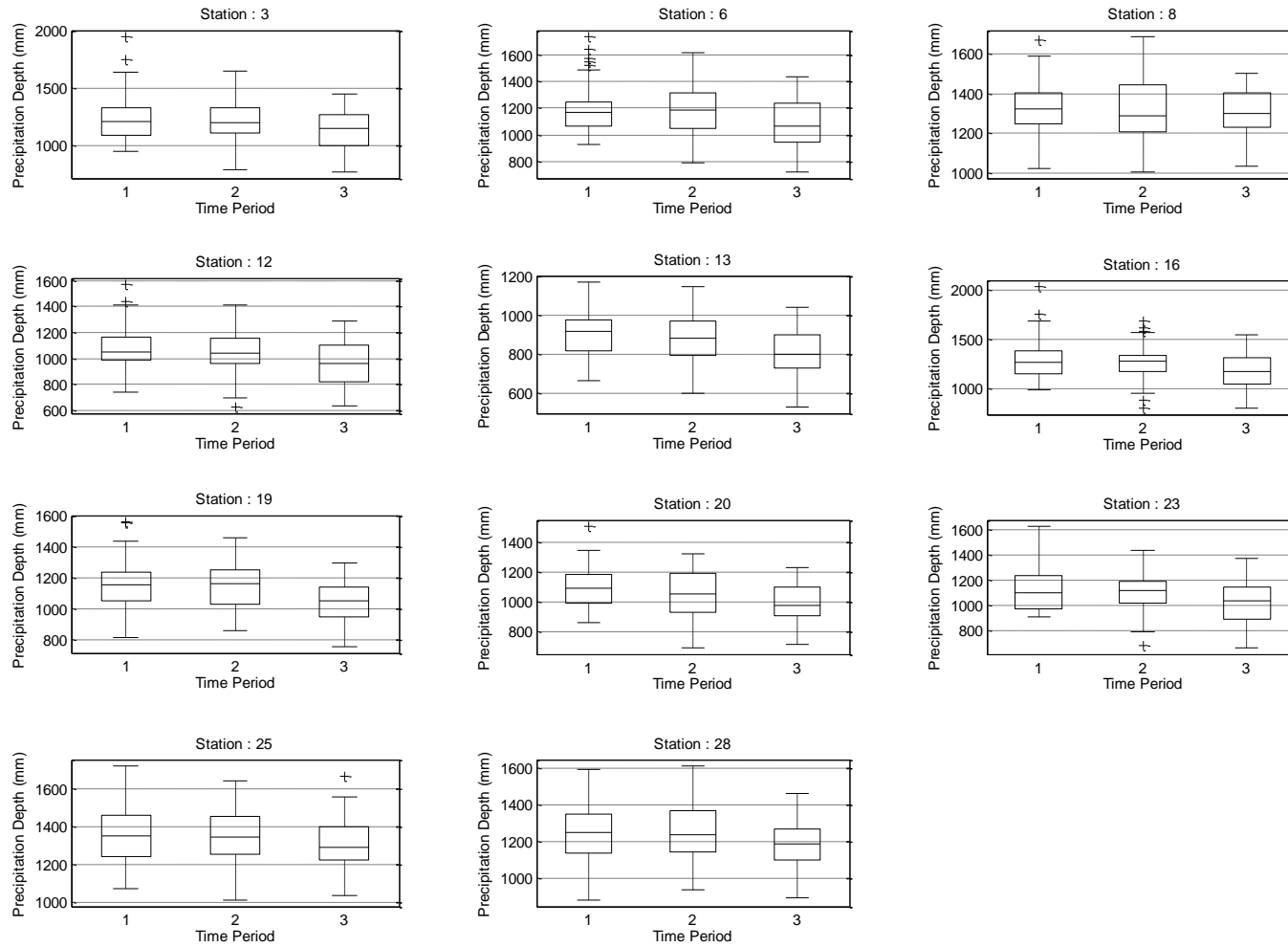


**Figure 38: Variability of PRCPTOT index for long-term statistical changes in period 1(1950-1999), period 2 (2000-2049), and period 3 (2050-2099).**

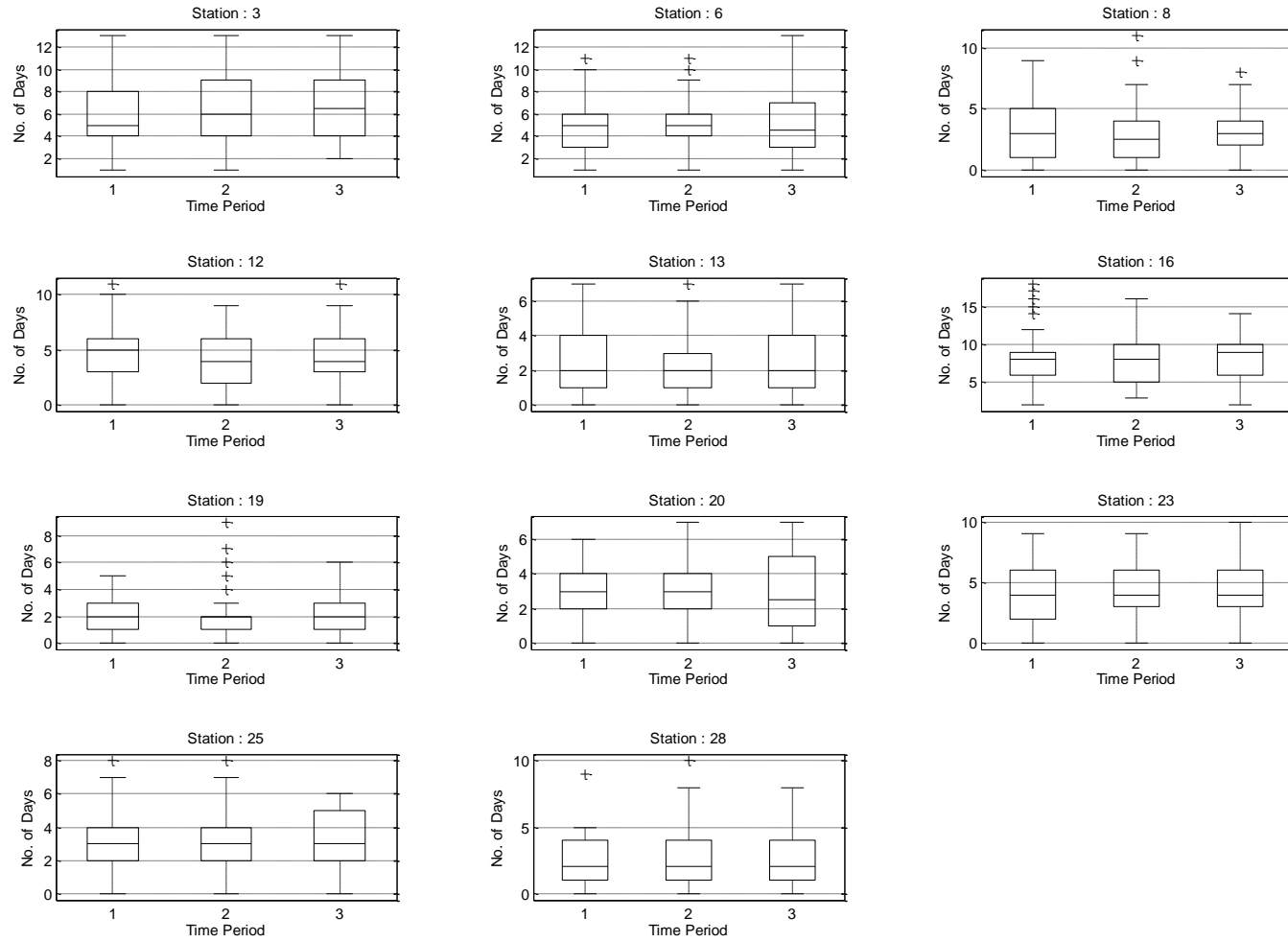


**Figure 39: Variability of R254 index for long-term statistical changes in period 1(1950-1999), period 2 (2000-2049), and period 3 (2050-2099).**

Larger deviations are observed in extremes during the final period, 3. Uncertainties caused by non-stationarity can be the source of these increased deviations. The trends show the panhandle region along with parts of South Florida experiencing slight increases in extreme precipitation events and their frequencies. These shifts in regional extreme precipitation trends are caused by a split in climate zones over Florida, where the panhandle, northern, and central regions are described by continental climate zone: humid subtropical. The remaining regions, Southern, south east, and south west are described by Equatorial climate zones: Rainforest, Monsoon, and Savannah which are adopted from Köppen-Geiger climate zones.

#### **5.4.3 Model Variation between stations**

There were a total of 13 variations between model 12 and model 14. These variations involve different scenarios and initial condition selected for the two models. A list of model variations is given in Table 13. The deviations between each of the 13 variations can be misleading if the incorrect scenario is selected. The user must recognize the band of uncertainty between the model and scenario combinations and determine which is useful to the case study.

There temporal variations that have been applied to show if the models are more or less variable during certain periods compared to an overall variation. The four temporal scales of DDF variations are (1) 24 hour duration at a 25 year return period from data ranging from 1950-2099, (2) 24 hour duration at a 25 year return period from data in three 50 year increments, (3) 120 hour duration at a 25 year return period from data ranging from 1950-2099, (4) 120 hour duration at a 25 year return period from data in three 50 year increments. The band of uncertainty based on 13 variations of models is described for each station by Figure 40 to Figure 47.

**Table 13: Projected models scenario and run variations.**

Model ID	CMIP5 Model	RCP	Run
12.1	miroc-esm-chem	2.6	1
12.2	miroc-esm-chem	4.5	1
12.3	miroc-esm-chem	6.0	1
12.4	miroc-esm-chem	8.5	1
14.5.1	mpi-esm-lr	2.6	1
14.5.2	mpi-esm-lr	2.6	2
14.5.3	mpi-esm-lr	2.6	3
14.6.1	mpi-esm-lr	4.5	1
14.6.2	mpi-esm-lr	4.5	2
14.6.3	mpi-esm-lr	4.5	3
14.7.1	mpi-esm-lr	8.5	1
14.7.2	mpi-esm-lr	8.5	2
14.7.3	mpi-esm-lr	8.5	3

Models 12 and 14 consist of all available scenarios and runs for the given model. The use of all available scenarios and runs will allow for the assessment of uncertainty related to multiple models, multiple scenarios, and multiple runs.

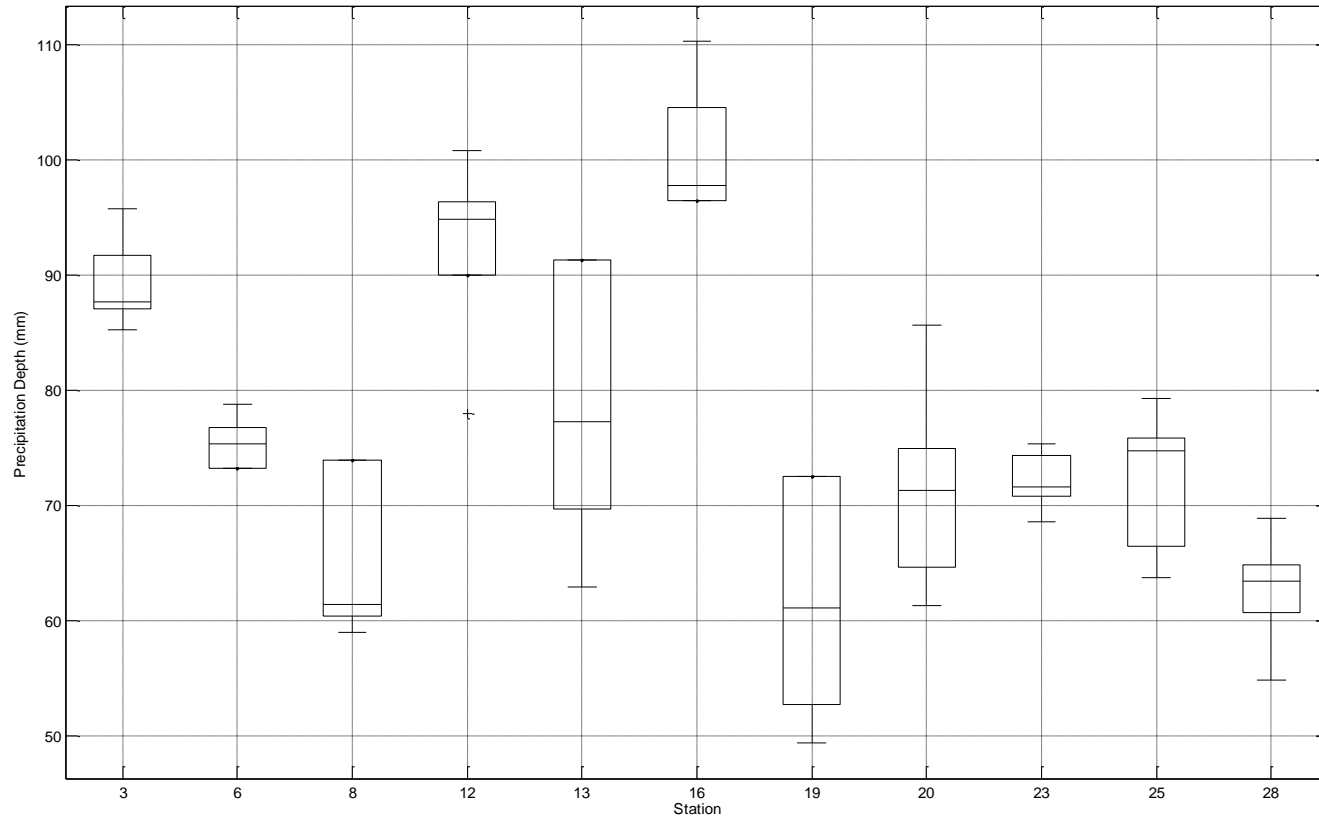


**Figure 40: Variations of precipitation depths between 11 stations for 24 hour rainfall depths of a 25 year return period during 1950-1999.**

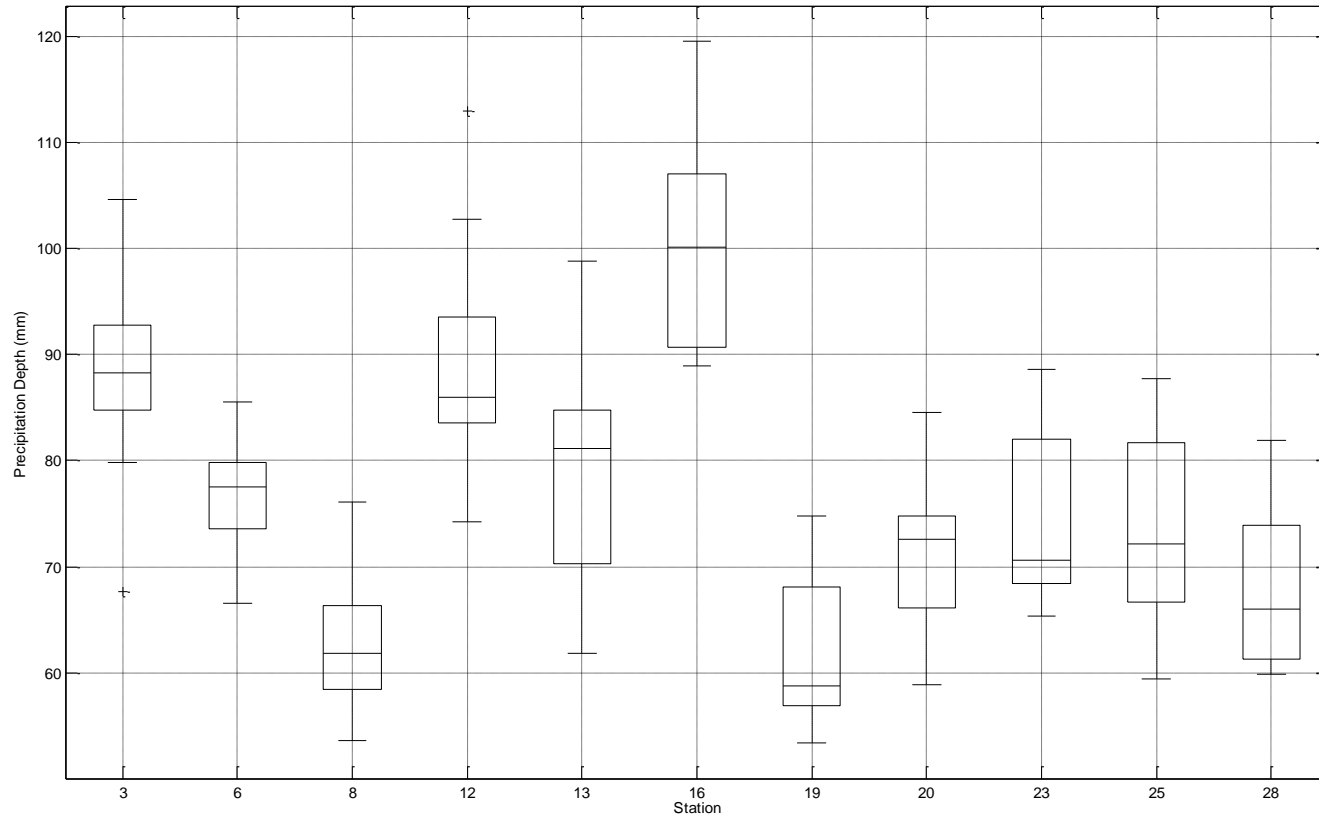


**Figure 41: Variations of precipitation depths between 11 stations for 24 hour rainfall depths of a 25 year return period during 2000-2049.**

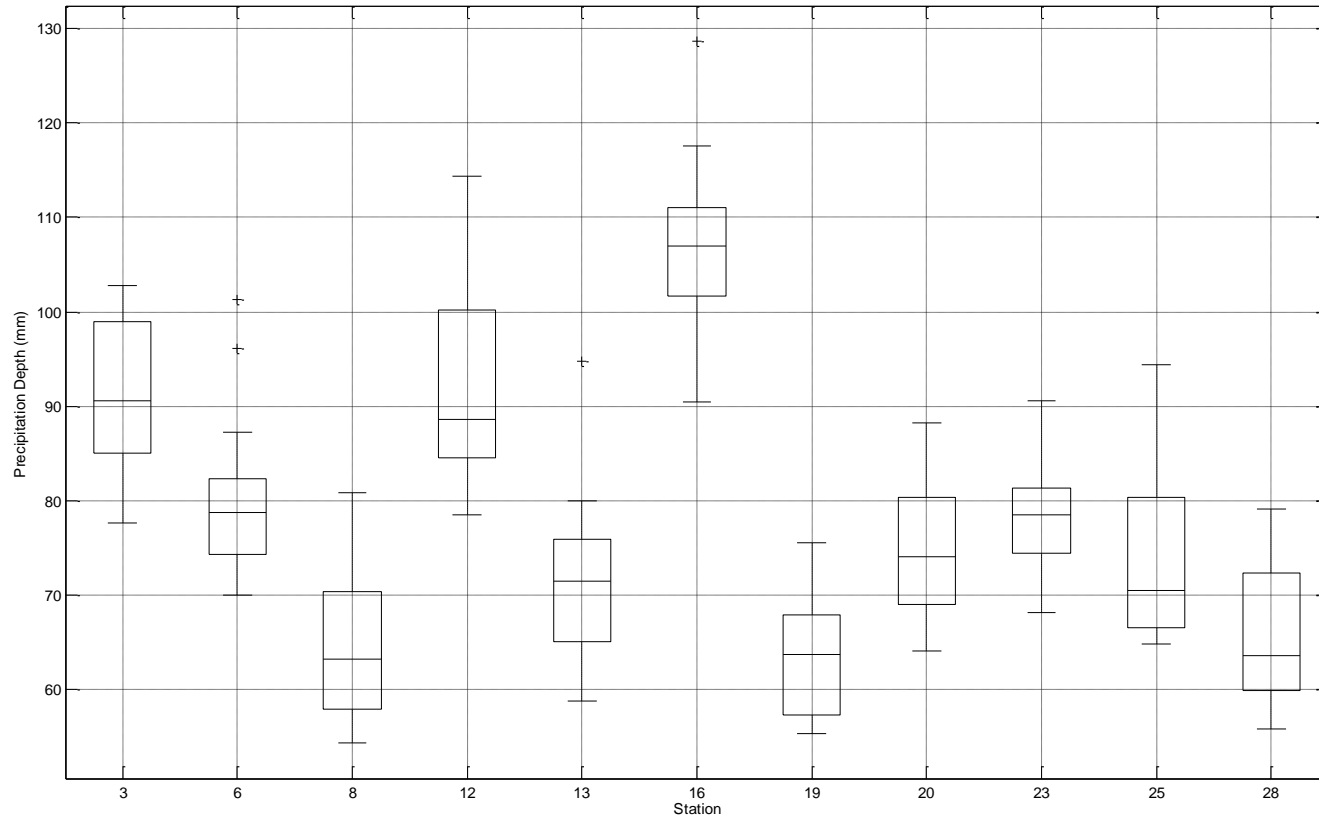


**Figure 42: Variations of precipitation depths between 11 stations for 24 hour rainfall depths of a 25 year return period during 2050-2099.**

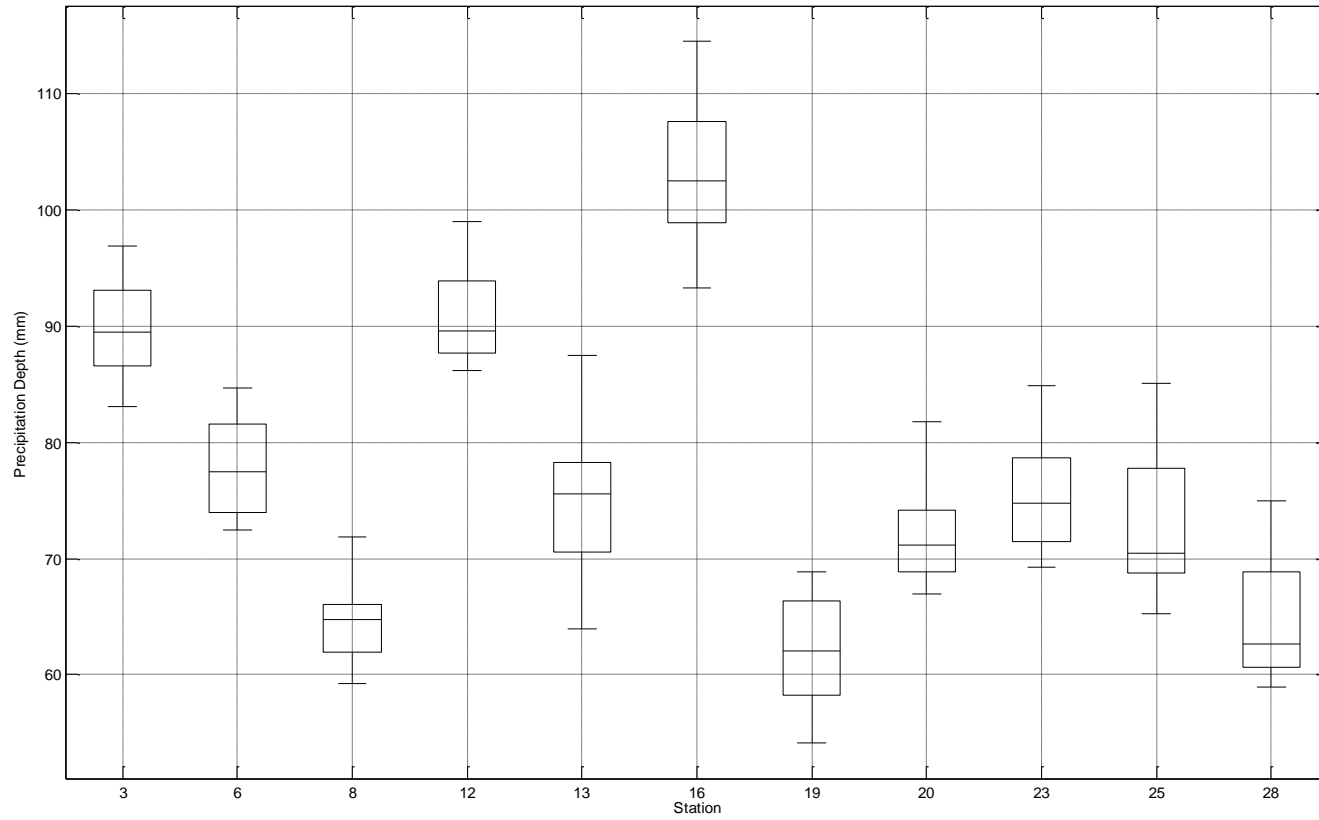


**Figure 43: Variations of precipitation depths between 11 stations for 24 hour rainfall depths of a 25 year return period during 1950-2099.**

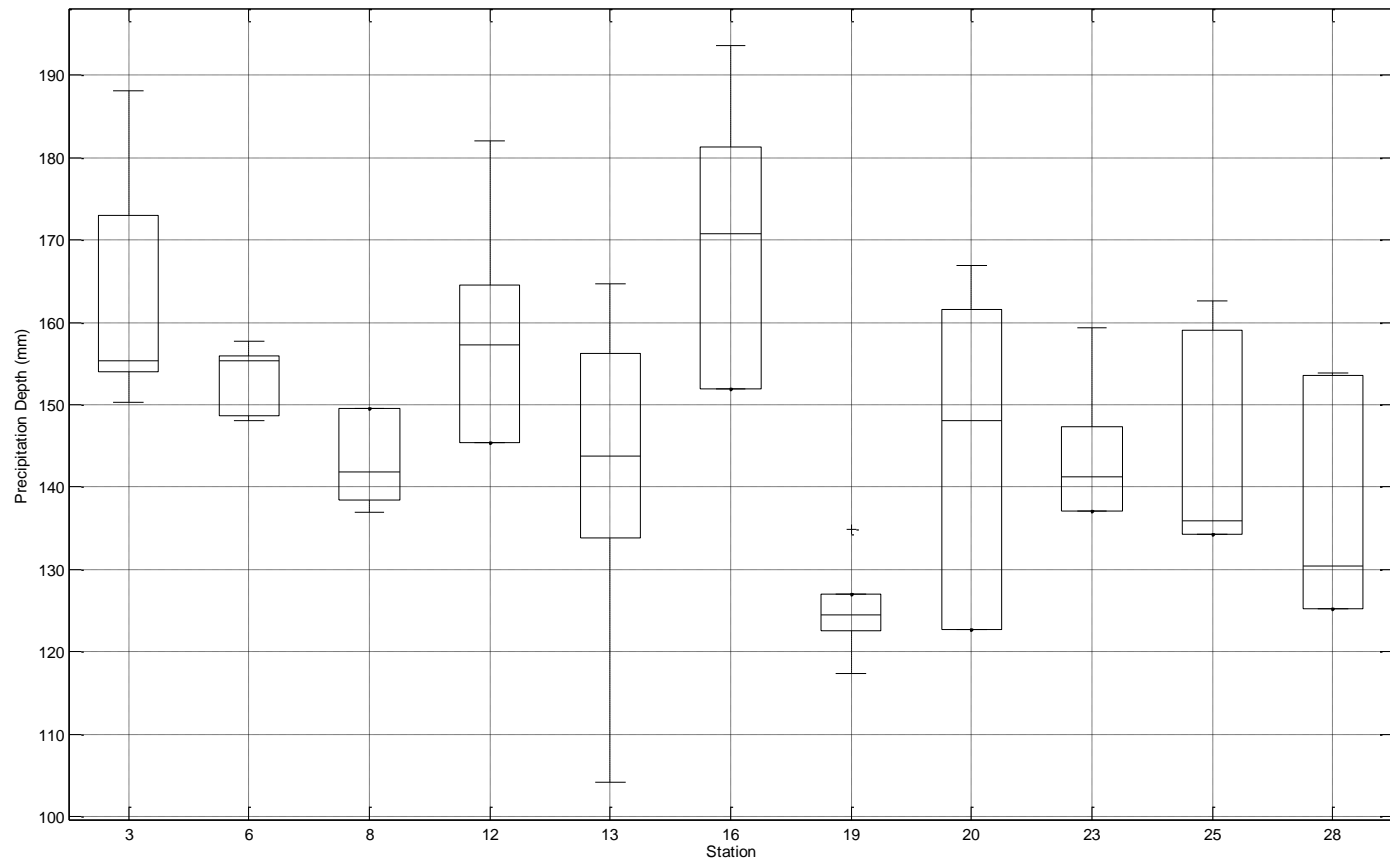


**Figure 44: Variations of precipitation depths between 11 stations for 120 hour rainfall depths of a 25 year return period during 1950-1999.**

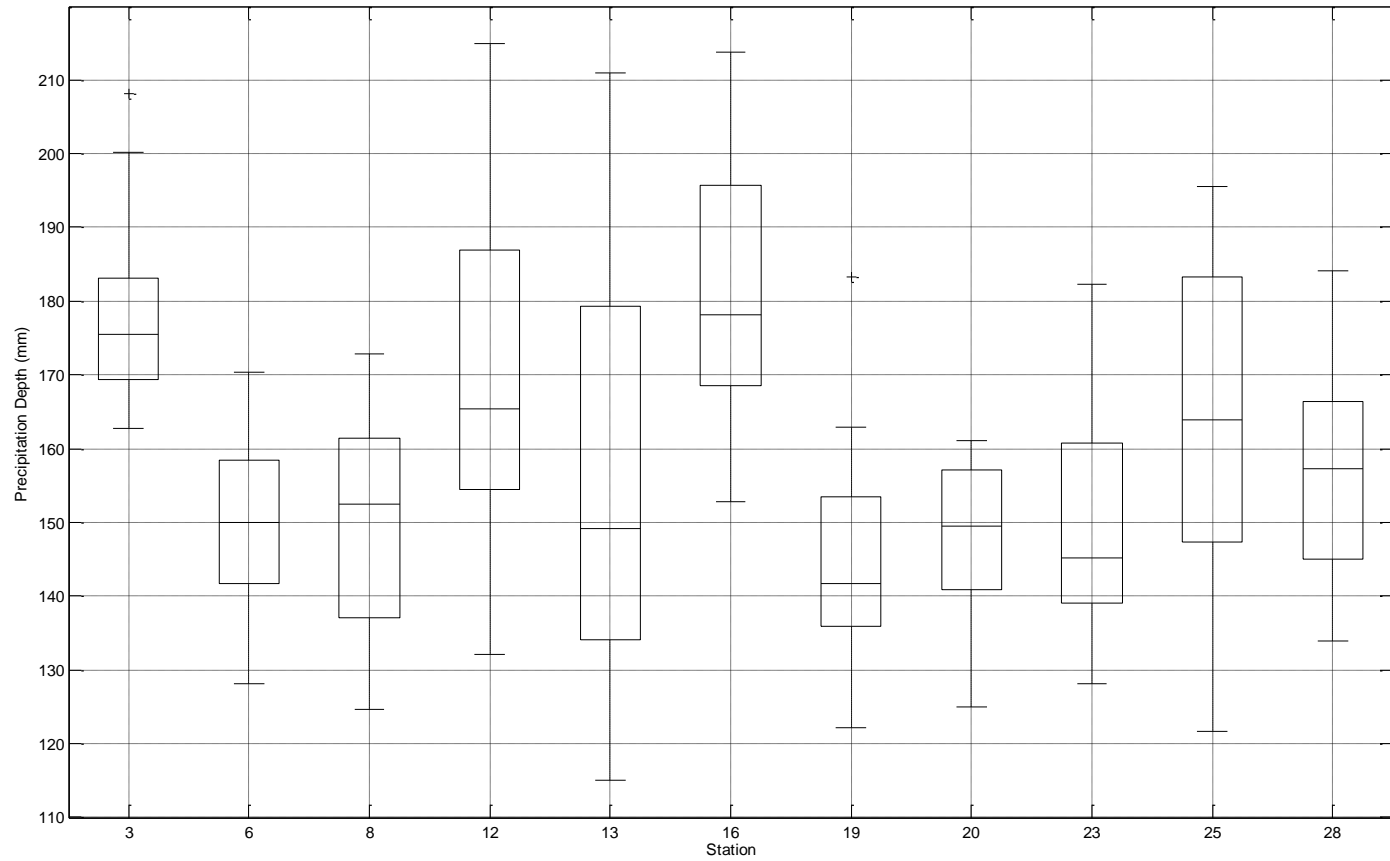


**Figure 45: Variations of precipitation depths between 11 stations for 120 hour rainfall depths of a 25 year return period during 2000-2049.**

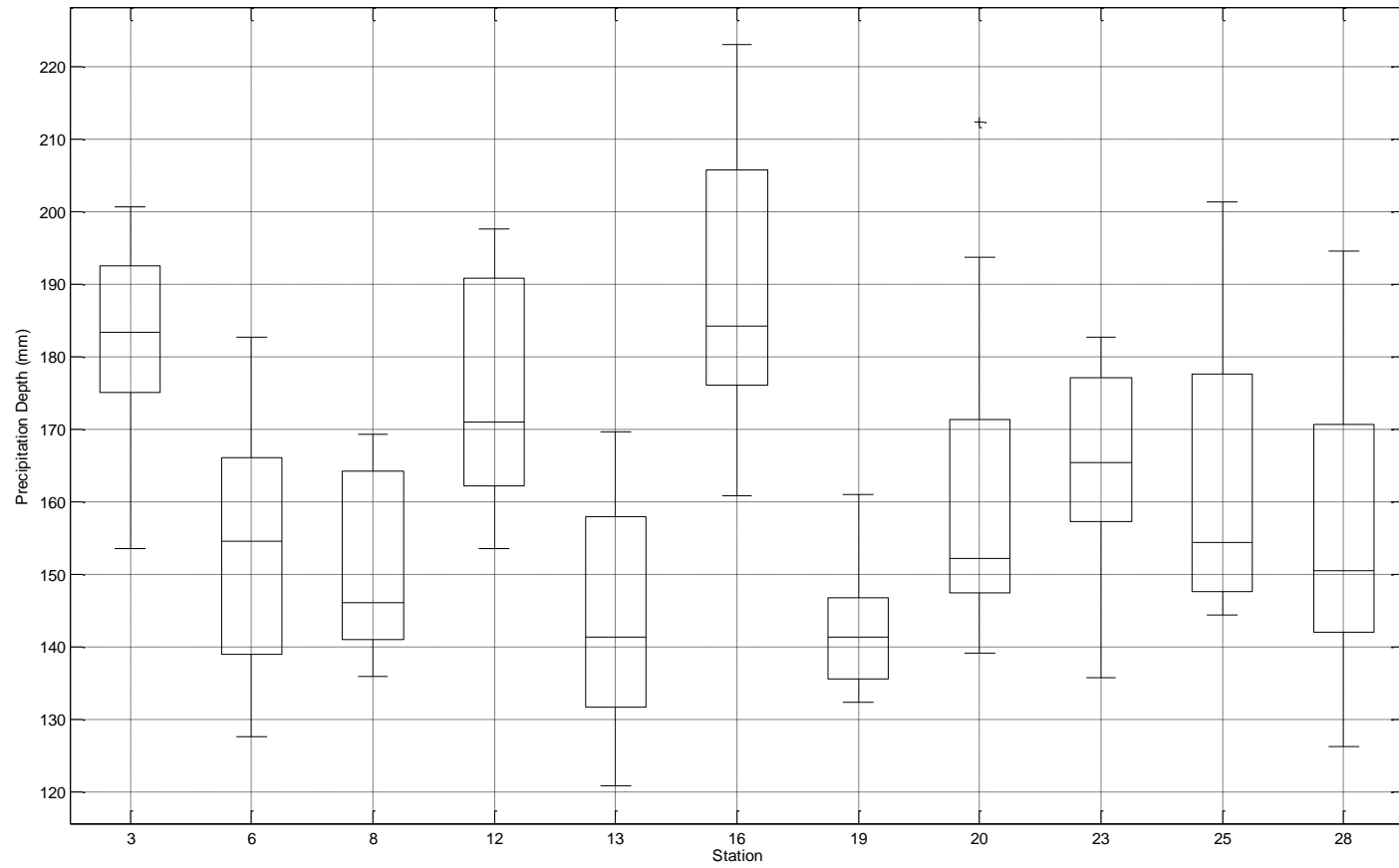


**Figure 46: Variations of precipitation depths between 11 stations for 120 hour rainfall depths of a 25 year return period during 2050-2099.**

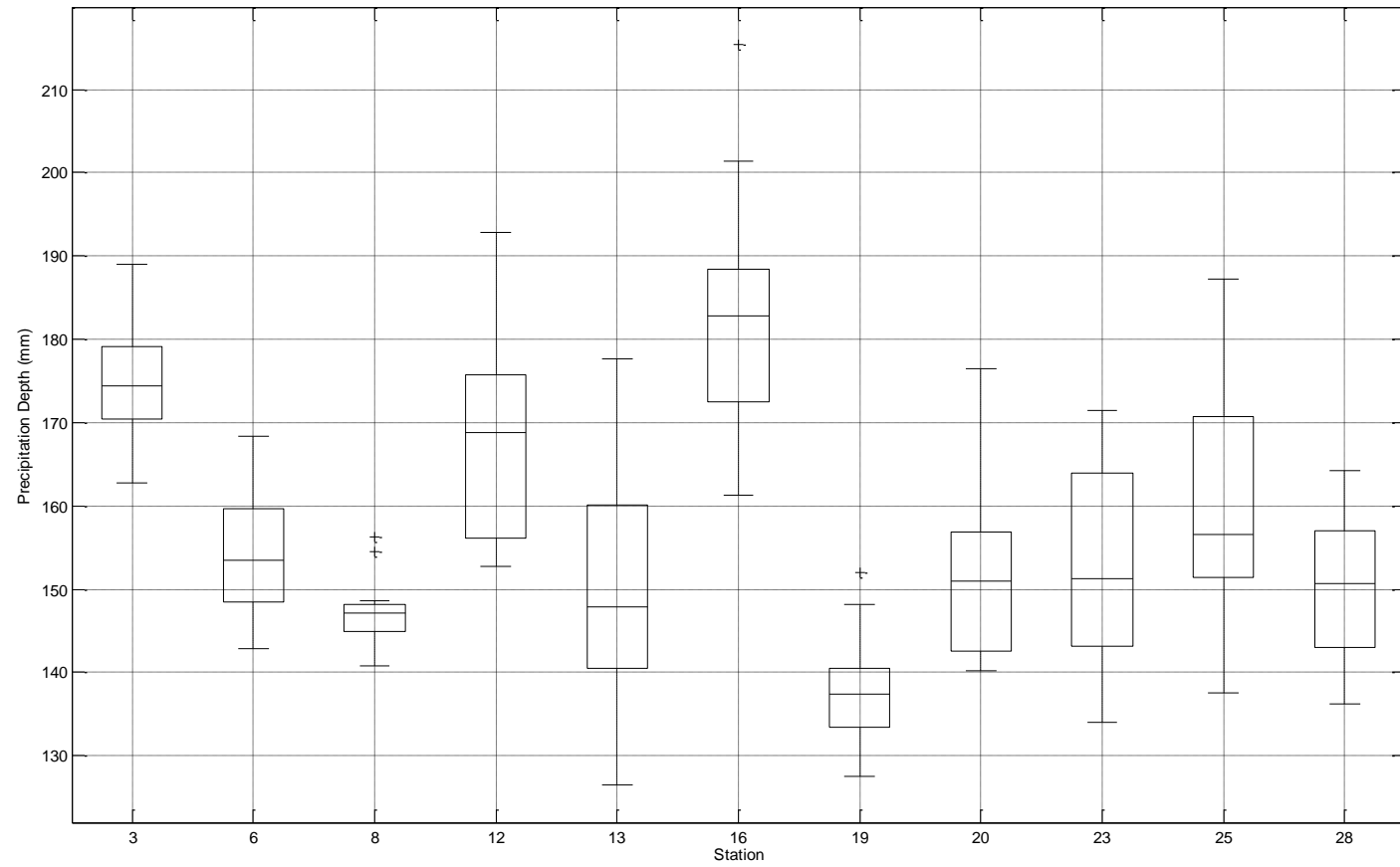


**Figure 47: Variations of precipitation depths between 11 stations for 120 hour rainfall depths of a 25 year return period during 1950-2009.**

#### **5.4.3.1 24 hour duration rainfall model variations between space and time**

The variations in models range both in time and space. The two durations, 24 hour and 120 hour, were split into three 50 year periods to determine if the models increase in deviation as time progresses. From Figure 48 and Figure 49, the 24 hour duration rainfall depths experience the largest gaps between the highest or most robust model and the lowest or most conservative model during the latter two periods, 2000-2049 and 2050-2099. This is expected due to increasing uncertainties the farther into the future the models predict. The highest model variations according to space is seen in station 13, which is located in the central east region, and the lowest variations seen in station 6, which is located in panhandle region. This means that the panhandle will be affected most by poor model selection due to its smaller performance range, while the central east region will experience a more drastic change between model selections.

#### **5.4.3.2 120 hour duration rainfall model variations between space and time**

Similarly to the 24 hour duration models, the 120 hour duration experiences the largest deviations between the most robust and most conservation models as the models predict further into the future. However, the 120 hour duration experiences several decreases from period 2, 2000-2049, to period 3, 2050-2099. These decreases are seen in station 8, 12, 13, 19, 23, and 25. These stations are located throughout Florida excluding the panhandle. The highest model variations according to space is seen in station 16, which is located in the panhandle, and the lowest variation is seen in station 8, which is located in the south east. This means that as durations increase the model variability shifts in space. The panhandle will be more sensitive to model selection in higher durations and the south east will be less susceptible to poor model selection in higher durations.

#### **5.4.4 DDF variations with periodic time windows**

The projected data extends from 1950-2099. A moving window was taken for the DDF to determine whether the depths experience periodic trends over three 50 year periods. From Figure 48, there are spatial variations in the trends that the DDFs are experiencing. Several stations, 12, 13, and 19, experience decreasing mean precipitation depths between the three 50 year periods. These stations are located in the central and central east regions of the state. Stations 25 and 28 experience a peak and decline

scenario in the mean precipitation depths, meaning the near future may produce increased depths but will decrease thereafter. As for the extremes, all stations experience increases in depths over the three periods. This describes an overall increase in precipitation intensities for the State of Florida. Several outliers were captured in the plots having mixed results.

#### **5.4.5 DDF variations with expanding time window**

The expanding window acts as a cumulative sum over three periods: (1) 1950-2000, (2) 1950-2050, and (3) 1950-2099. These three windows will act as a real world trend analysis by incorporating the historic data. With the inclusion of the historic data into the last two periods, there were slight changes in the trends. The extreme depths were the most affected by the inclusion of historic data. Where previously, the extreme depth were all increasing, now there are several with decreases or a peak and decline scenario. Stations 12, 13, and 20 show decreases in extreme depths, however; stations 3 and 19 show a peak and decline scenario for the extreme depths. These trends are given by Figure 49.

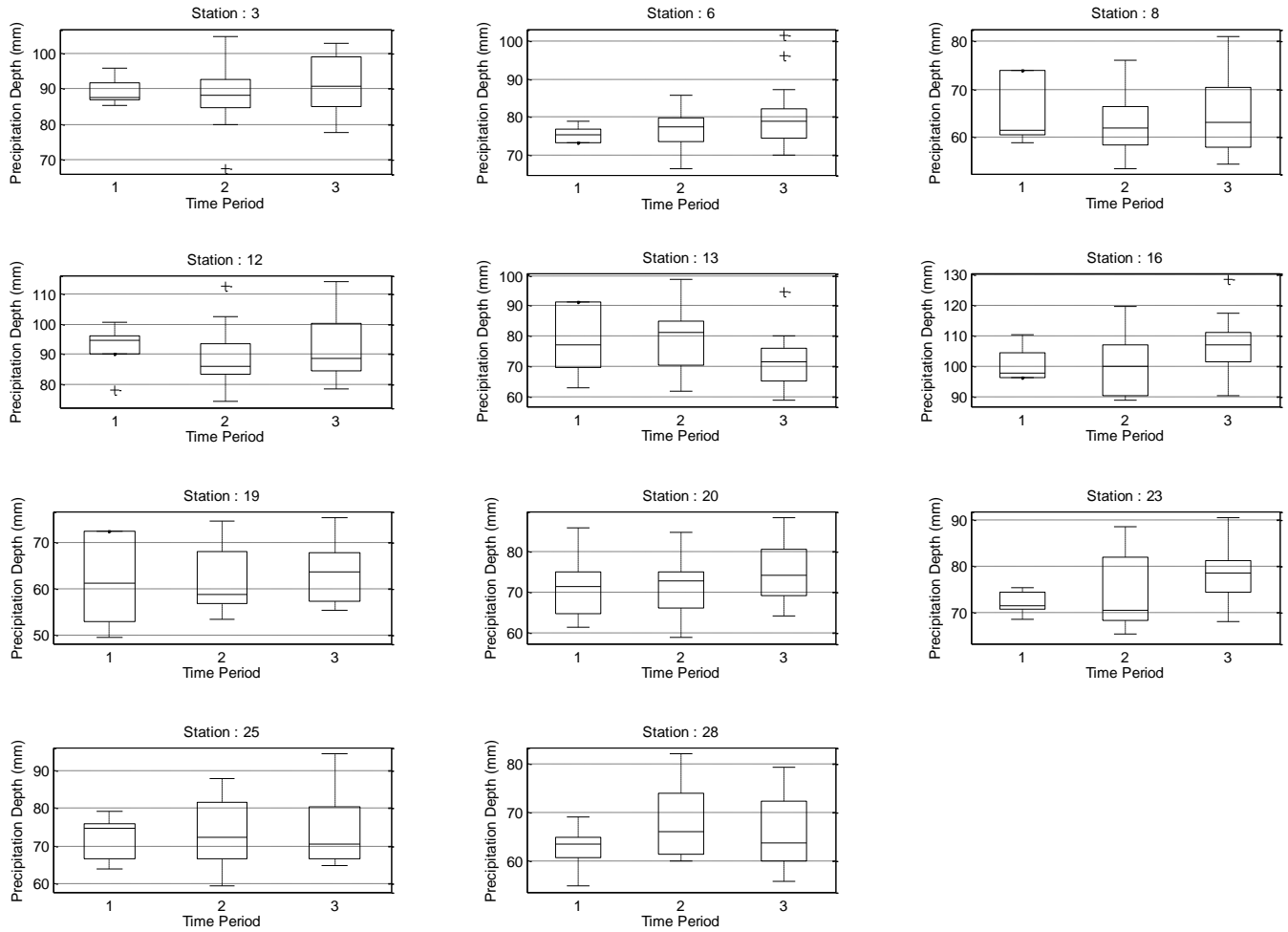


**Figure 48: Variability of precipitation depths for a given 25 year return period for three 50 year intervals.**

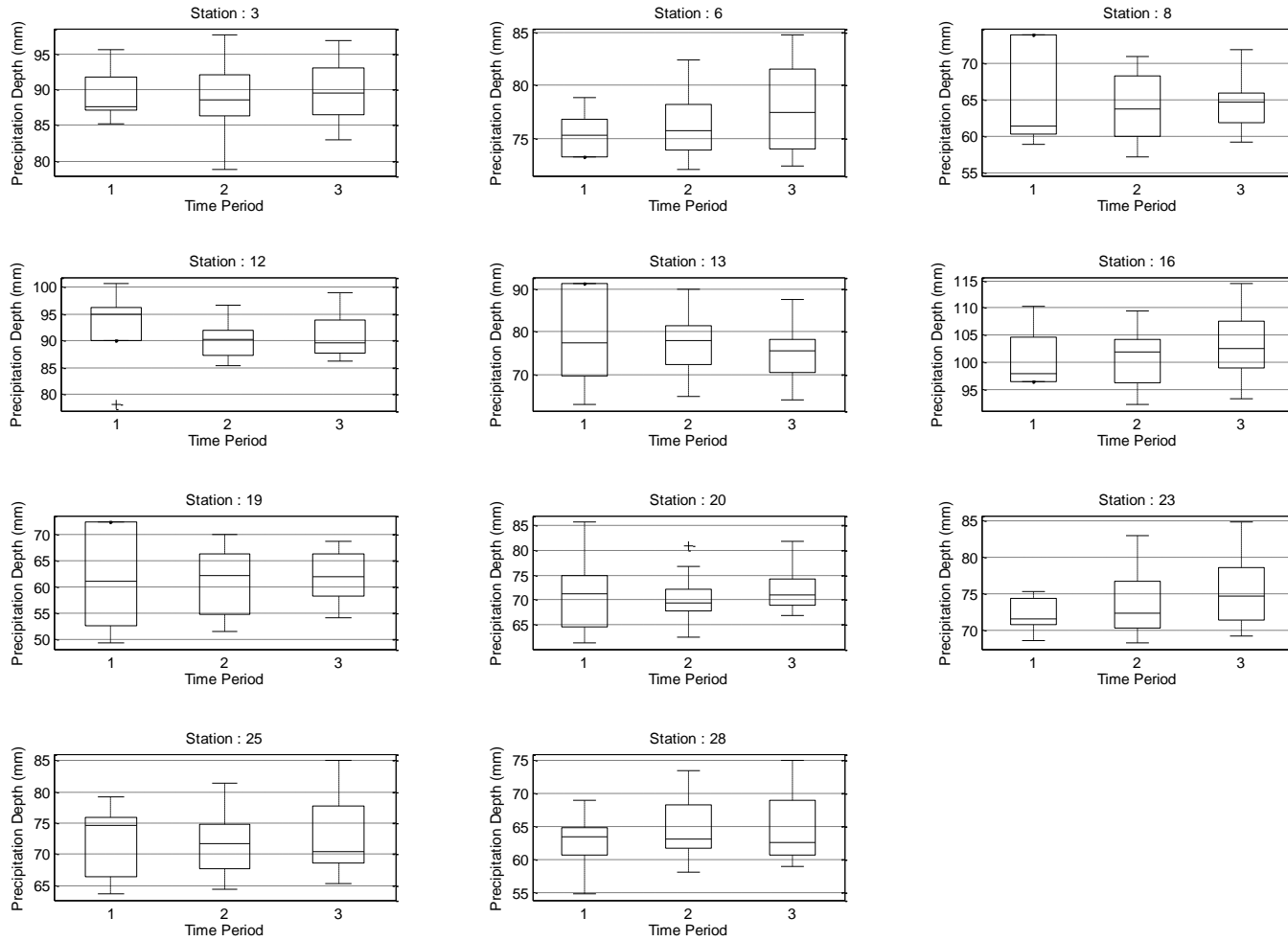


**Figure 49: Variability of precipitation depths for a given 25 year return period for three expanding windows.**

#### 5.4.6 Band of uncertainty between model based DDF

The band of uncertainty defines the range that occurs between the upper and lower bounds, most robust and most conservative models. The band of uncertainty for the 13 model variations are described for each station by Figure 50. There are two durations plotted, 24 hour and 120 hour for 25 year depths. The band of uncertainty increases as the duration increases from 24 hours to 120 hours. This demonstrates the higher uncertainty with longer durations of precipitation events. This increase in uncertainty as duration increases is seen over most of the state excluding station 8, located in South Florida, which has a tight grouping in both durations.

When the 13 models are plotted against the observed data from 1961-1999, there is an overwhelming dry bias. A method known as bootstrap sampling is used to determine an average factor that the stations are under performing. This factor value was found to have varying ranges, depending on the station location. Figure 51 shows the dry bias before the bootstrap correction factors were applied. These correction factors are listed in Table 14.

**Table 14: Correction factors based on bootstrap resampling approach.**

Stations	24 hour			120 hour		
	Mean factor	Lower bound	Upper bound	Mean factor	Lower bound	Upper bound
3	1.51	1.39	1.63	1.57	1.47	1.68
6	1.42	1.31	1.54	1.53	1.40	1.66
8	2.33	2.15	2.51	2.02	1.88	2.17
12	1.78	1.59	1.97	1.56	1.45	1.67
13	2.43	2.24	2.62	2.00	1.86	2.15
16	1.80	1.67	1.94	1.88	1.72	2.04
19	1.54	1.46	1.62	1.53	1.45	1.61
20	1.80	1.69	1.91	1.80	1.67	1.94
23	1.49	1.38	1.60	1.49	1.39	1.59
25	1.75	1.60	1.90	1.73	1.60	1.86
28	1.91	1.76	2.06	1.83	1.71	1.95

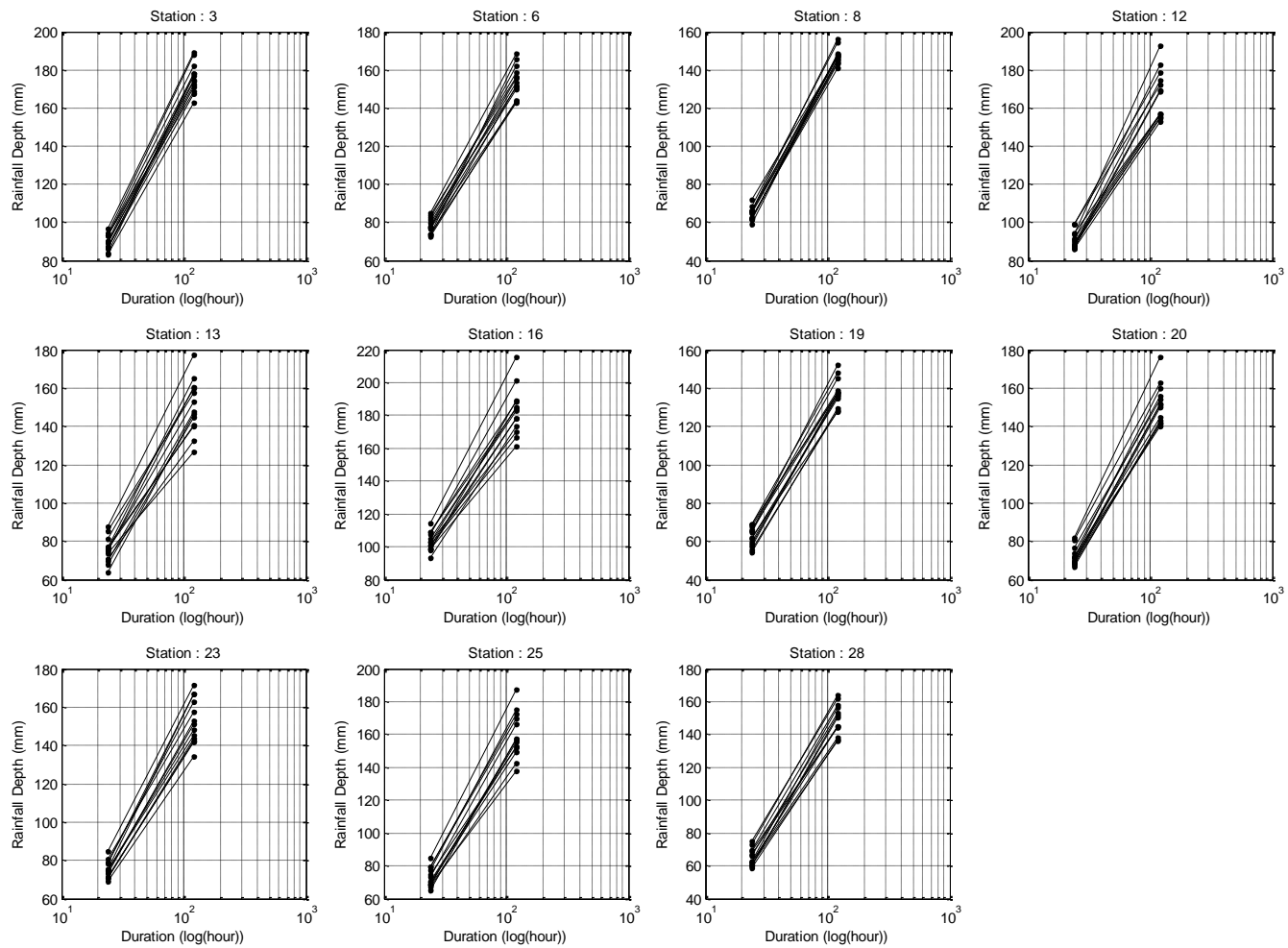


Figure 50: Band of uncertainty between CMIP5 model variations.

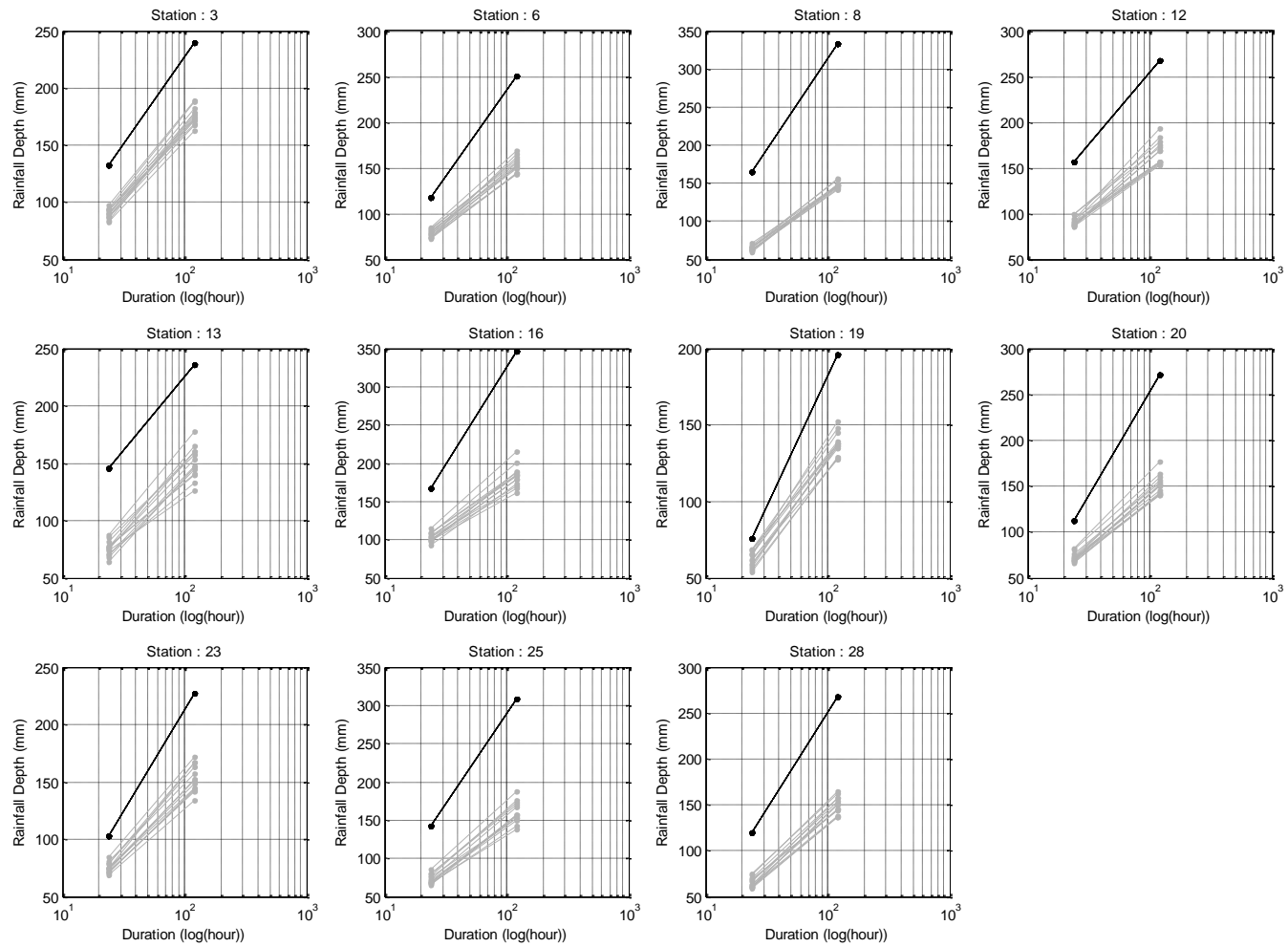


Figure 51: Band of uncertainty with comparison between observed (black) and model variations (grey).

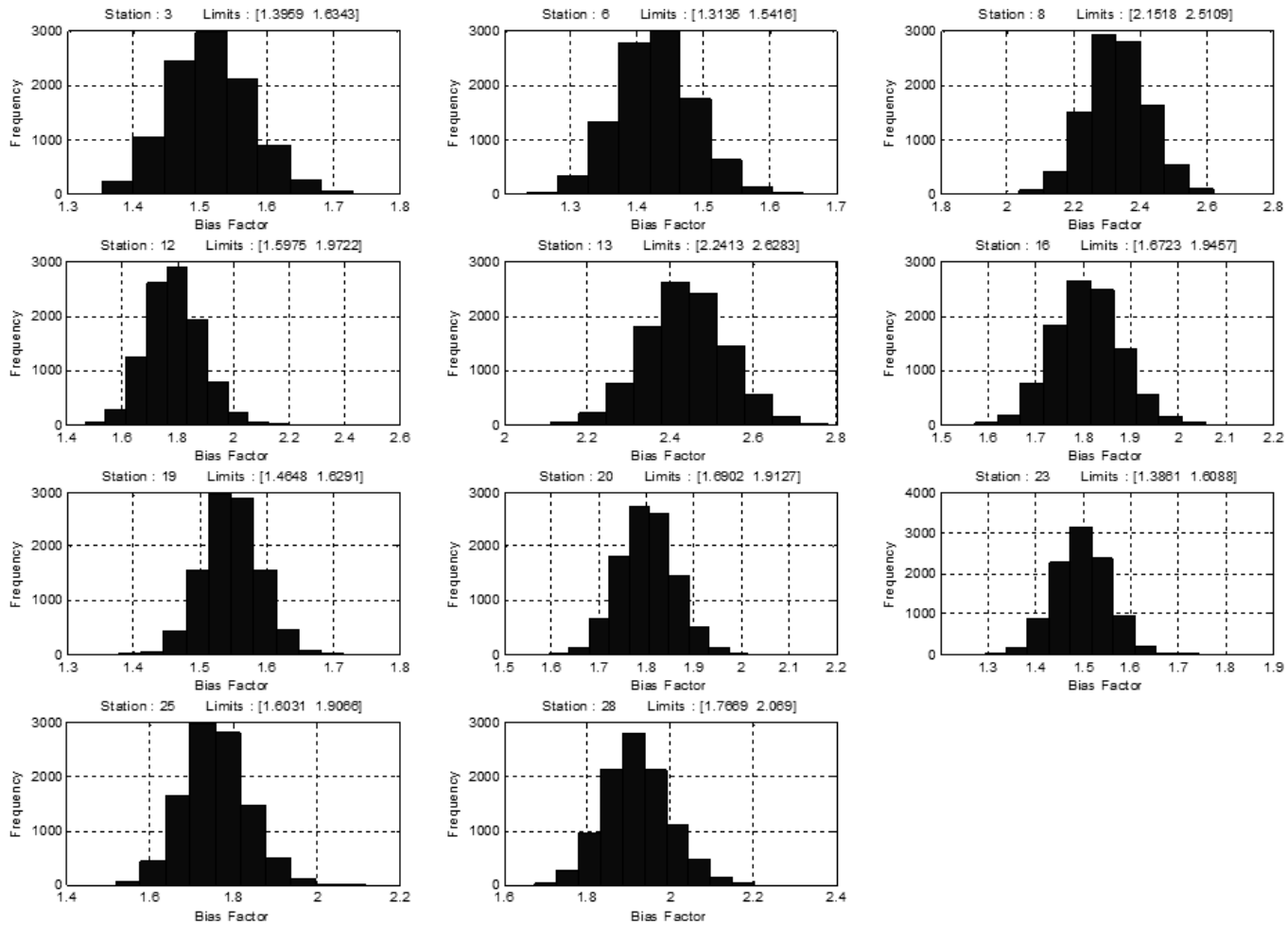


Figure 52: Bias factor uncertainty for 24 hour duration.

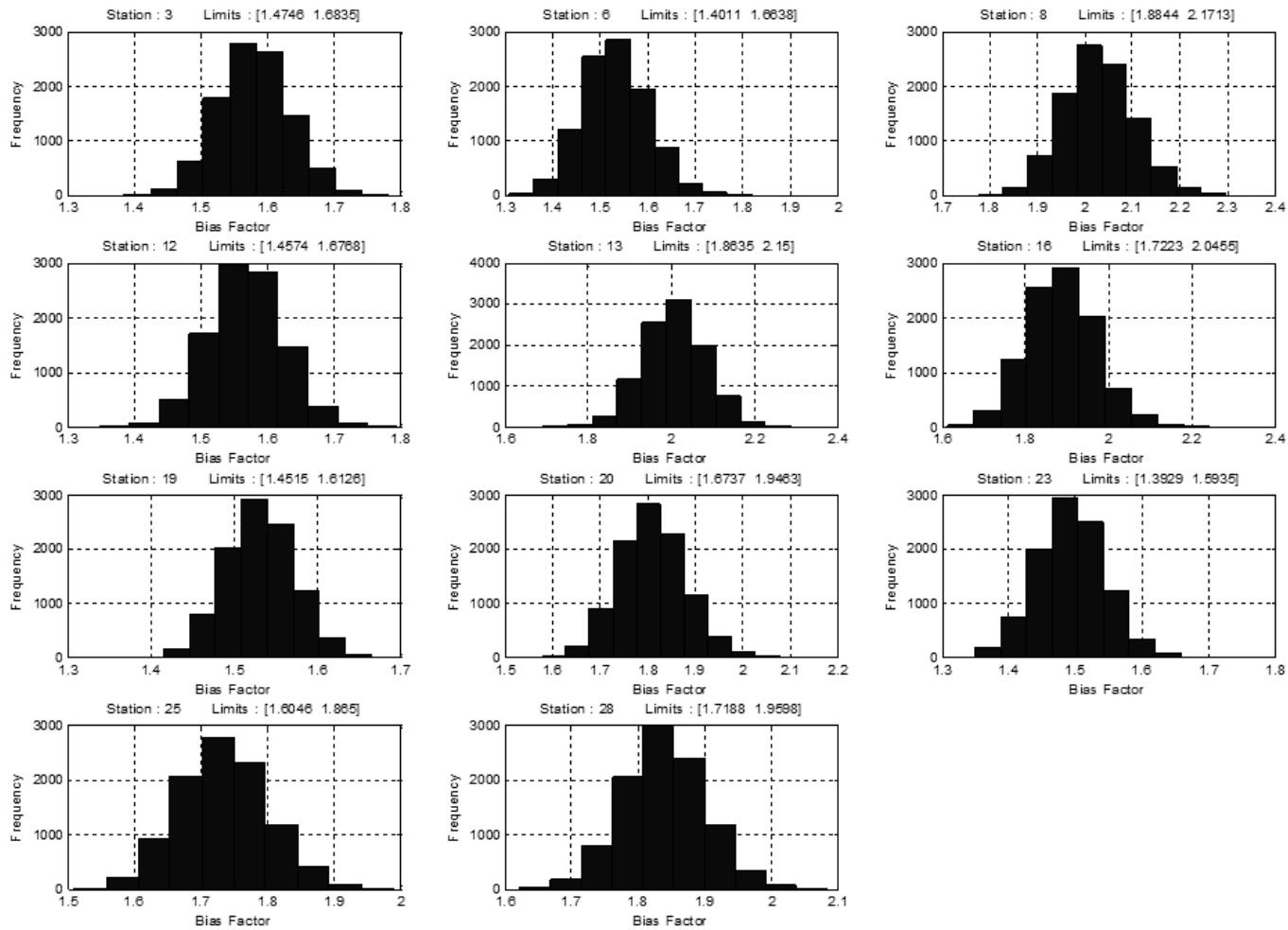


Figure 53: Bias factor uncertainty for 120 hour duration.

After the bootstrap sampling correction factors were applied to the model data, the DDF curve was recreated seen in Figure 54 through Figure 59. The bootstrap factor significantly raised the model data to relate to the observed data; however, there is uncertainty associated between the lower, mean, and upper bound factors. The simultaneous plotting of observed and model data allows the user to use the observed data as a reference point when viewing the behavior of the models. Uncertainty between time intervals and bias corrected models is listed in Table 15.

**Table 15: Precipitation depths for different durations based on different factors.**

2000-2049			
Duration	Mean factor	Lower bound	Upper bound
24	133.5971	123.0589	144.2782
120	196.2588	181.2877	211.2349
2050-2099			
24	135.7833	123.4598	148.3419
120	204.4398	179.163	228.521

There is more uncertainty associated to the far future, 2050-2099, as opposed to the near future, 200-2049. The uncertainty experiences more variations in when the upper bound correction factor is applied, with a 3.9% increase between 2000-2049 and 2050-2099 for the 120 hour duration and 1.4% increase in 24 hour duration. These increases are expected due to the variability characteristics related to precipitation and time. There are also spatial uncertainties associated with the depths. The Because of poor spatial resolution, point scale, it is difficult to target regional design criteria that need improvement. These uncertainties between time intervals and between space are described by Table 16.

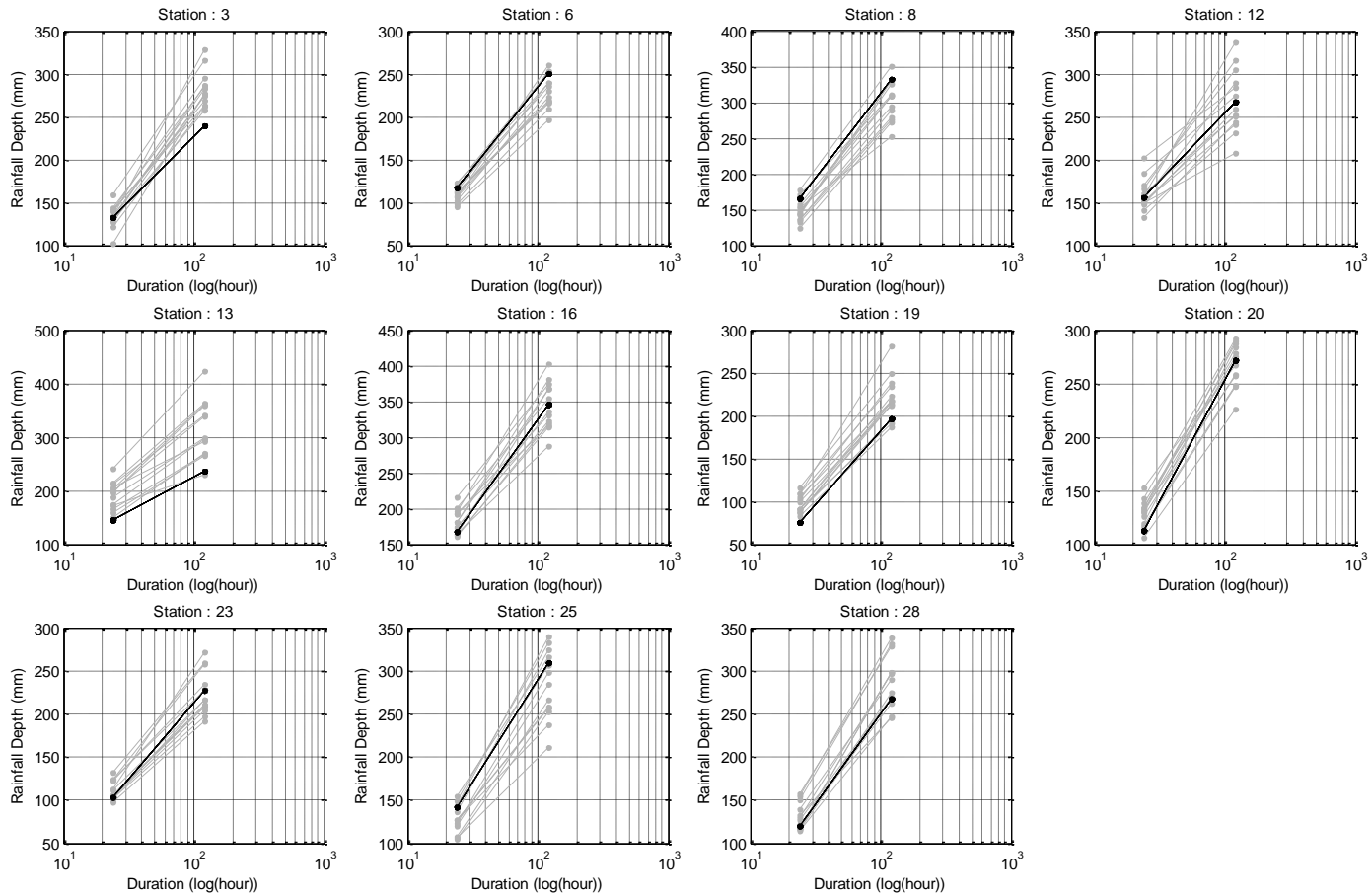


**Figure 54: Variability of precipitation depths for two durations for a return period of 25 years for observed data and model data (2000-2049) using different bias correction factors (mean factor).**

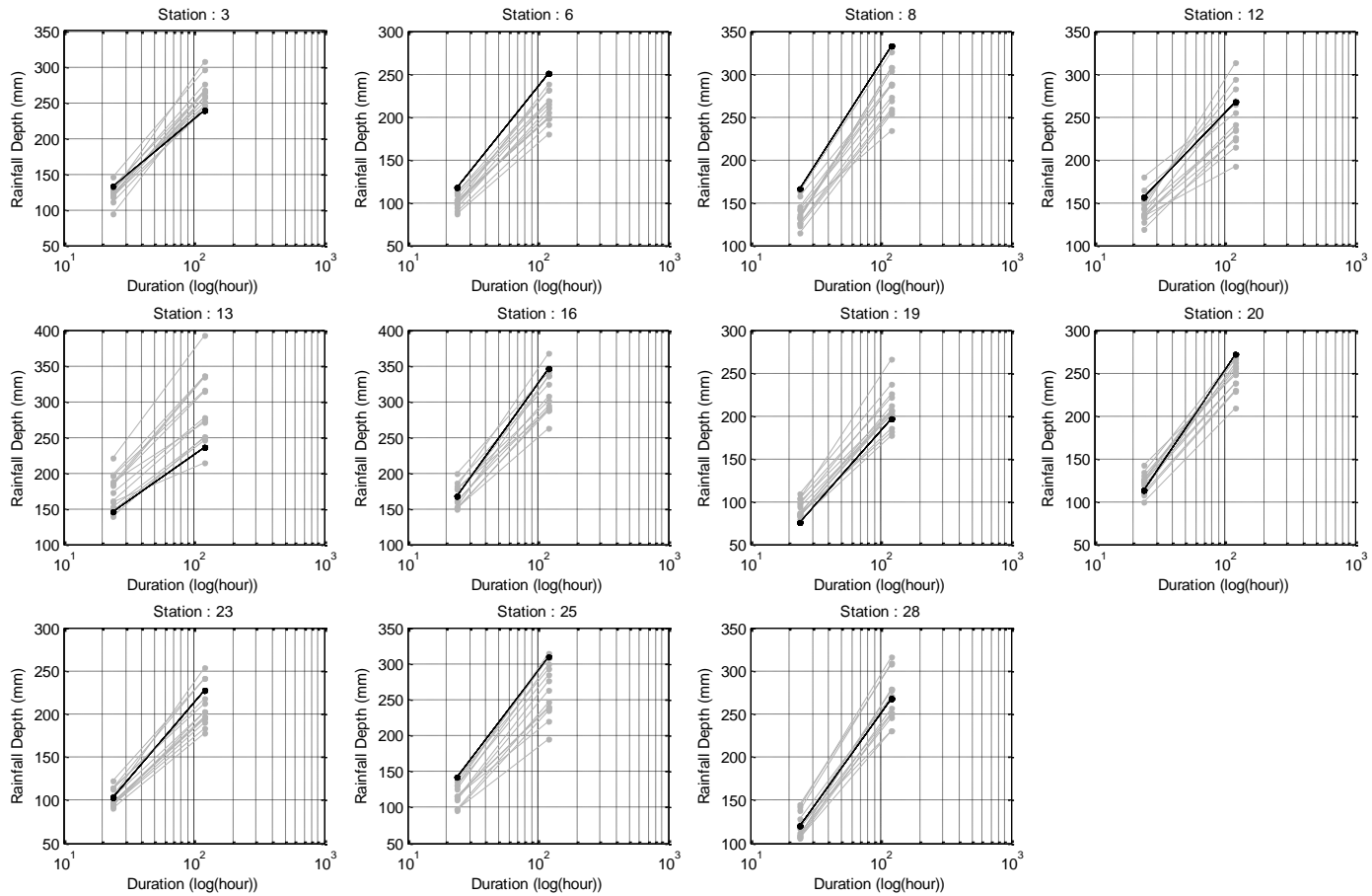


**Figure 55: Variability of precipitation depths for two durations for a return period of 25 years for observed data and model data (2000-2049) using different bias correction factors (lower bound factor).**

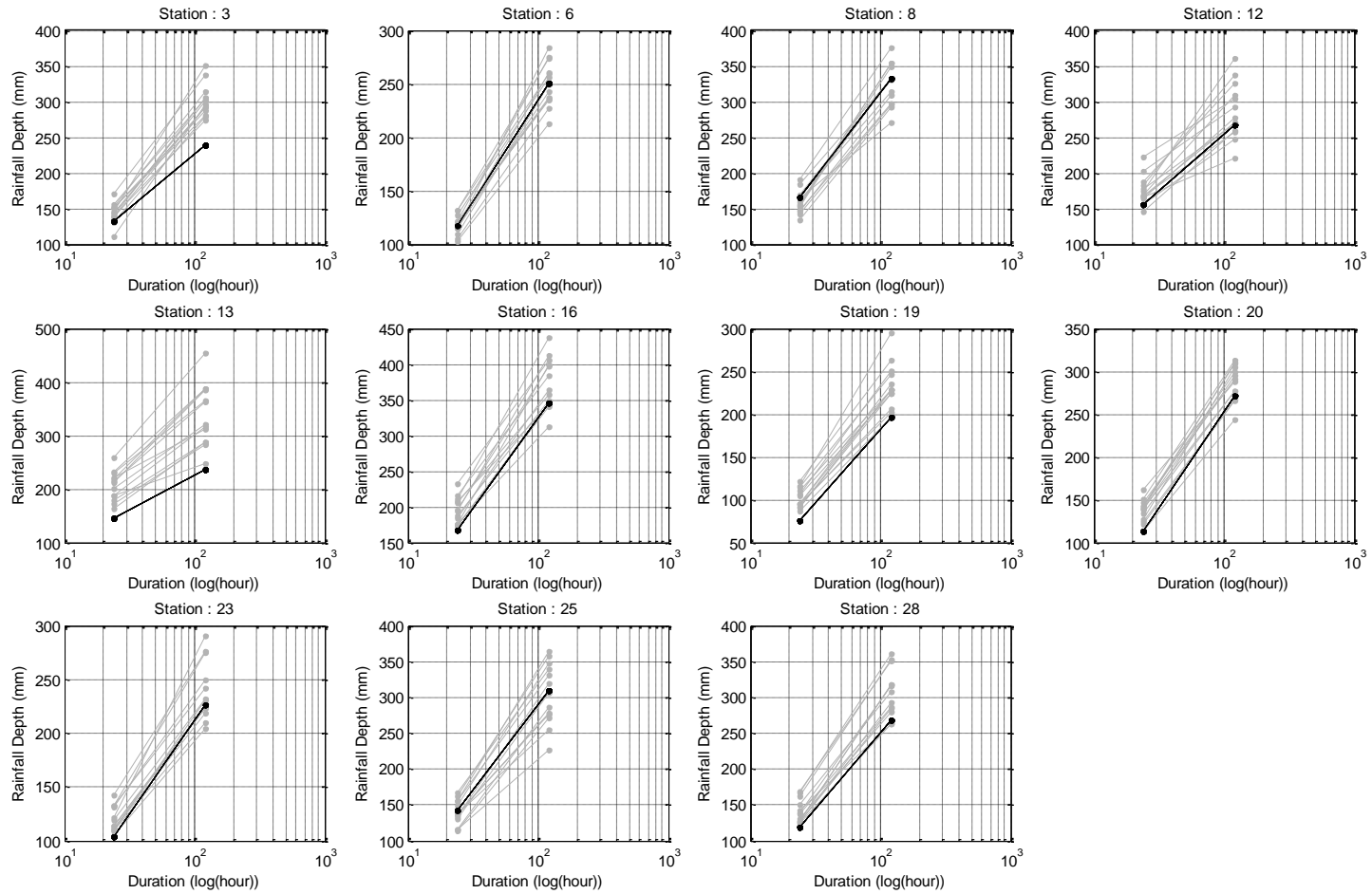


**Figure 56: Variability of precipitation depths for two durations for a return period of 25 years for observed data and model data (2000-2049) using different bias correction factors (upper bound factor).**

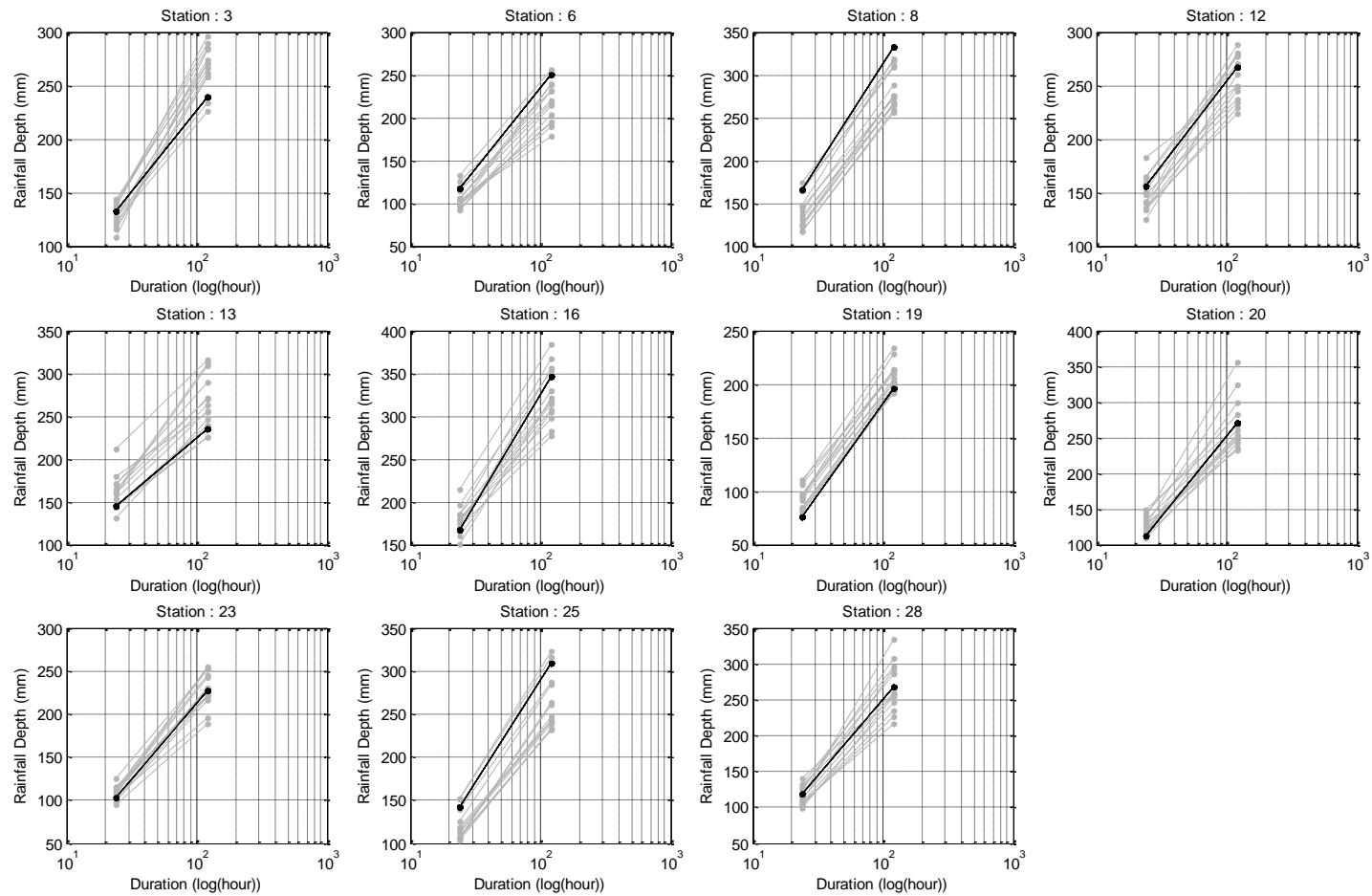


**Figure 57: Variability of precipitation depths for two durations for a return period of 25 years for observed data and model data (2050-2099) using different bias correction factors (mean factor).**

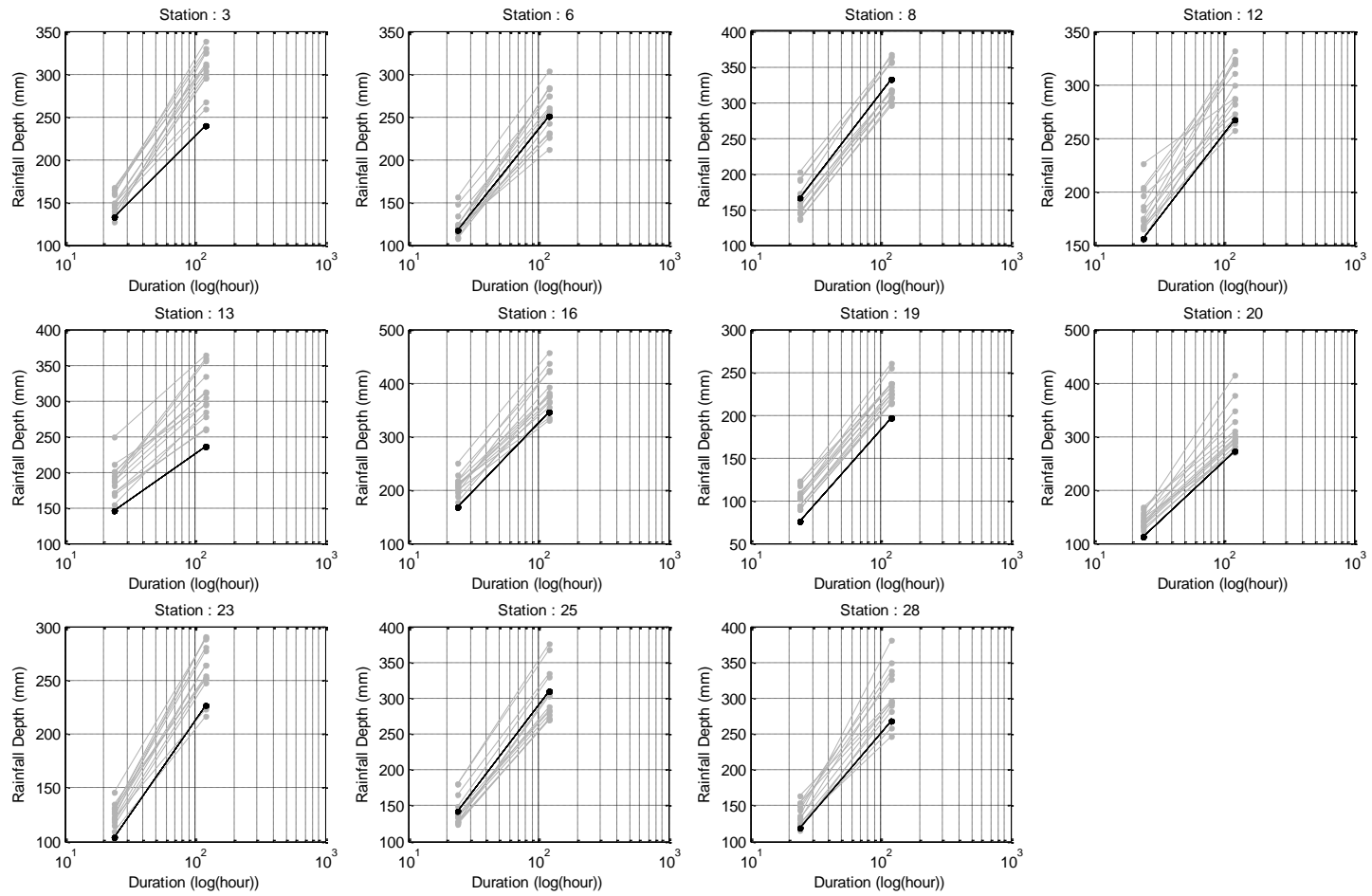


**Figure 58: Variability of precipitation depths for two durations for a return period of 25 years for observed data and model data (2050-2099) using different bias correction factors (lower bound factor).**

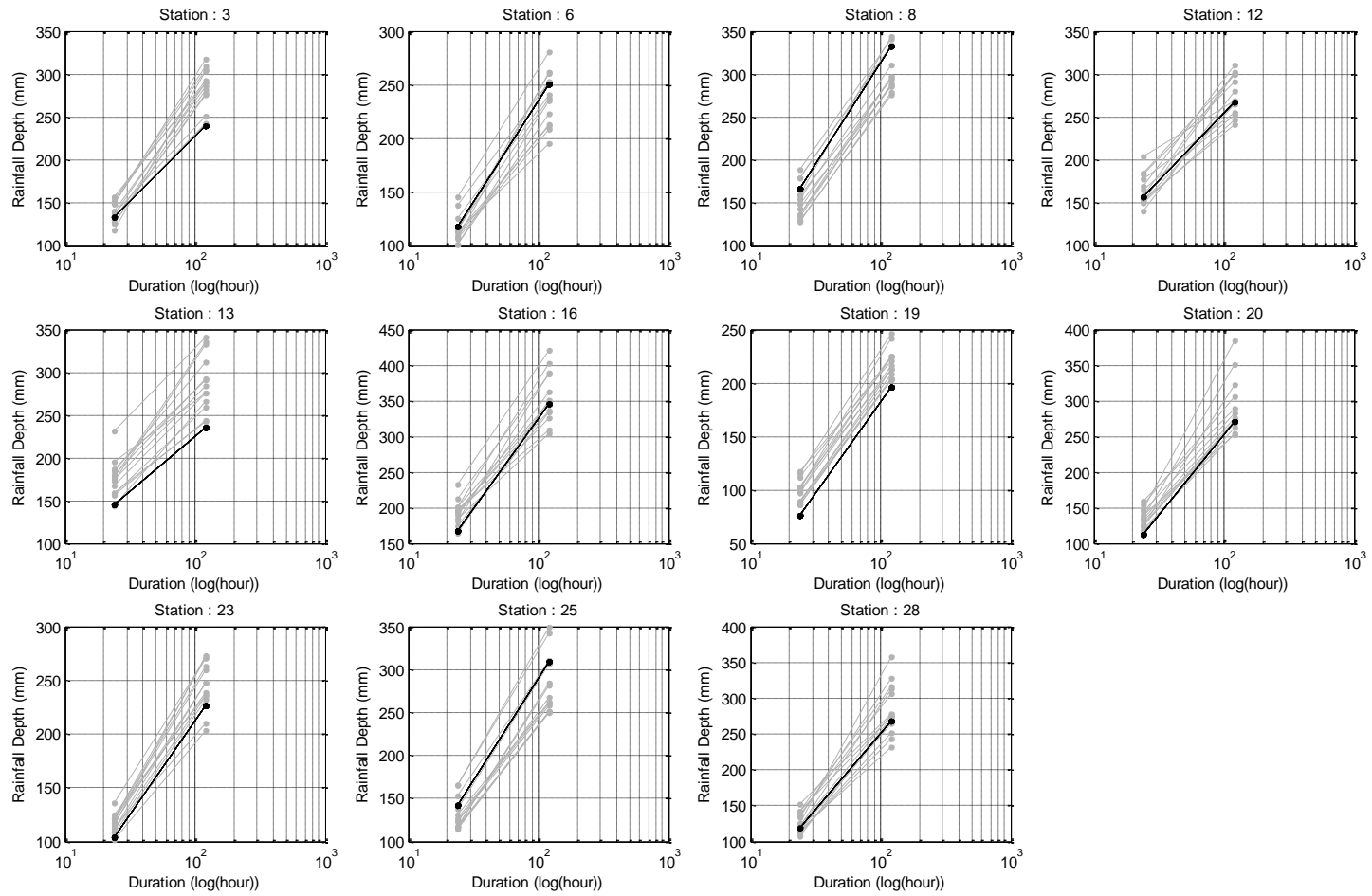


**Figure 59: Variability of precipitation depths for two durations for a return period of 25 years for observed data and model data (2050-2099) using different bias correction factors (upper bound factor).**

**Table 16: Band of uncertainty variations between time periods and space.**

2000-2049			
Durations	Mean factor	Lower bound	Upper bound
24	42.25716	38.909	45.55996
120	92.30651	86.27233	98.37325
2050-2099			
Durations	Mean factor	Lower bound	Upper bound
24	44.80363	41.25371	48.30546
120	125.6439	117.4304	133.9017

There is a spatial uncertainty of 15% related to the 120 hour duration throughout Florida. The uncertainty is constant throughout the State because the stations are cooperative. This uncertainty is expected due to the high variability of precipitation over the State of Florida. The large amounts of water bodies, tropical climate, and low topography along with a varying climate, allows precipitation to obtain a spontaneous nature in return causing more spatial uncertainties.

## **Chapter 6: Conclusions**

The study utilized a total of 16 GCMs and experienced a significant variation between the models. The variability of the models is highly correlated to the site selection. Each of the 31 rain gage stations used in the study achieved a best fitting model. There were; however, reoccurring models over several stations. The model(s) with the highest reoccurrence were chosen to represent Florida as a whole. The models observed through the case study to be the most likely to represent Florida's future extreme were miroc-esm-chem and mpi-esm-lr.

The study revealed significant dry biases through the climate models predictions. As mentioned throughout the thesis, it is believed that the climate is non-stationary. This assumption presents difficulties in a proper bias correction procedure. Currently bias correction that incorporate non-stationarity into their algorithms are hard to develop and almost nonexistent. Due to the lack of appropriate bias correction methods, the study was forced to use corrections based on the observed data using quantile mapping and bootstrap resampling methods. These methods helped remove the dry bias, but there is uncertainties related to them because the future climate is unknown due to non-stationarity.

To determine whether the future extremes are increasing or decreasing, an extended projection of extreme rainfall depths was assembled. These depths, before bias correction, experienced significant decreasing trends. However, after bias correction, the future extremes did experience increases from the observed historical data depending on the model, scenario, and station combination. The major contributor to the variations was the model scenario and location selection. DDF analysis, based on these future extremes, was performed and a band of uncertainty was described for each station. Depending on a robust or conservative selection, hydrologic design may not match current standards.

## **6.1 Contribution of this study**

Climate change is an important variable in the analysis of extreme precipitation. Precipitation extreme can be studied through climate models, one of which being GCMs. These models are low resolution models that can be downscaled into higher resolution, or local scale, models known as Region Climate Models (RCMs). The models are developed using varying initial conditions and emission scenarios. These variations can affect the performance of the models differently as time and space change and in return create uncertainties in model results. These uncertainties result in misleading future hydrologic extremes which are generally used in the development of hydrologic design standards.

Along with uncertainties from model selection, there is growing concern over non-stationarity issues related to climate and climate change. Hydrologic design is strongly based on the belief that the climate is stationary. With the increased realization and eye witness accounts of real world events caused by climate change, water resource managers, civil engineers, hydrologists, and consultants alike are expressing concern that the current design standards will be or are now outdated. There is little to no large scale recall on hydrologic design standards on a local scale.

In this study, site specific precipitation depths have been collected from multiple downscaled climate models. The essential downscaled BCCA CMIP5 models have been compared and analyzed through a series of extreme precipitation, contingency, and error measure indices. This comparison was against historical observed precipitation data to help distinguish the best model(s) by a least error method. The methodology was applied to the case study domain, Florida, and ultimately determined the best climate model for site specific locations. The model(s) then were used to determine the effects of climate change and non-stationarity on a point scale. Any trends experienced by precipitation extremes were applied to the development of updated DDF curves to help improve the accuracy of hydrologic design standards.

## **6.2 Limitations of the Study**

The case study applied to the methodologies produced a specific set of results; however, the methodology is generalized in order to apply to a variety of case studies. There are several limitations in techniques of data collection, spatial resolution, data processing, and data analysis.

- Climate model: The study used a single type of downscaled climate modeling known as CMIP5. These models are statically downscaled GCMs to a 1/8<sup>th</sup> degree grid resolution. From the CMIP5 models, 16 BCCA, daily time scale, models were selected. These models are variations of the GCMs after downscaling. By only using one type of climate model downscaling it presents higher uncertainty of true model trends for future projections.
- Temporal resolution: Extreme precipitation increases in variability as the temporal window increases. This study used a daily temporal scale throughout the analysis. Daily values allow for decadal projection but are too large for detailed hydrologic design analysis.
- Spatial resolution: A point scale spatial resolutions limits the study by increasing uncertainties in spatial variation of intensities. Rainfall is highly variable throughout space. The assumption that the point scale data can represent a large area, such as Florida, can present uncertainties in the results. Point scale also has trouble representing the large amount of water bodies, tropical storm landfall, and minimal topography present in Florida.
- Bias corrections: The bias correction, quantile mapping, used in this case study proved to be a useful method of correction, but there remain uncertainties in the analysis of existing bias. Different bias correction techniques can be applied to help understand the existing bias. Because the climate is non-stationary, the bias correction factors developed from the comparison of observed and predicted data will have a level of uncertainty due to the unknown future. Historical distributions cannot be expected to represent the future distributions if the future climate is expected to change.

### **6.3 Recommendations for Future Research**

If the application of the developed methodology is requested for another case study, the following recommendations should be considered due to limitations mentioned previously in this section. The expansion of available climate models is recommended to help evaluate uncertainty in the models. These models could apply finer resolutions in temporal scales. The study utilized a daily time scale and was limited to 24 hour increments for DDF analysis. By using hourly, or finer, temporal scale a better

understanding of the short term intensities and frequencies will be better met. Finer resolution time scales could help evaluate variability in the results and, the data could achieve a higher correlation and lower uncertainty in the evaluation of hydrologic design durations. Bias correction techniques that account for non-stationarity issues would be significant in the evaluation of future extremes. When these bias corrections become more assessable and readily available for the public, it would be a great addition in the analysis. Also future studies intended on using the methodology, the study recommends a grid scale. A grid scale will better capture the variability of precipitation and allow for interpolations of large areas.

## Appendix A: Acronyms

ENSO	El Niño/La Niña Southern Oscillation
PDO	Pacific Decadal Oscillation
NAO	North Atlantic Oscillation
AMO	Atlantic Multidecadal Oscillation
NOAA	National Oceanic and Atmospheric Administration
IPCC	Intergovernmental Panel on Climate Change
SFWMD	South Florida Water Management District
IDF	Intensity Duration Frequency
GCM	General Circulation Model
SRES	Special Report on Emissions Scenarios
BCCA	Bias-Corrected and Constructed Analog
BCSD	Bias Corrected and Spatial Disaggregation
USGS	United States Geological Survey
CIMAS	Cooperative Institute for Marine and Atmospheric Studies
CDF	Cumulative Distribution Function
PC	Positive Correct
DDF	Depth Duration Frequency
BM	Best Model
CMIP	Coupled Model Intercomparison Project
RCP	Representative Concentration Pathway

GEV	Generalized Extreme Value
QM	Quantile Mapping
KS-TEST	Kolmogorov–Smirnov test
MLE	Maximum Likelihood Estimator
ME	Mean Error
MAE	Mean Absolute Error
MB	Multiplicative Bias
RMSE	Root Mean Square Error
NSEC	Nash Sutcliffe Efficiency Coefficient
COR	Correlation Coefficient
LE	Least Error
AE	Absolute Error
CDD	Consecutive Dry Days
CWD	Consecutive Wet Days
RX1DAY	Maximum One Day Precipitation
RX5DAY	Maximum Five Day Precipitation
R10	Precipitation Exceeding 10mm Threshold
R20	Precipitation Exceeding 20mm Threshold
R254	Precipitation Exceeding 25.4mm Threshold
PRCPTOT	Total Precipitation
SDII	Standard Daily Intensity Index
CMSE	Contingency Measure for Sensitivity
CMSP	Contingency Measure for Specificity
CMC	Contingency Measure for Conductivity
CMER	Contingency Measure for Error
SST	Sea Surface Temperature

Appendix B: **WMO indices performance measures**

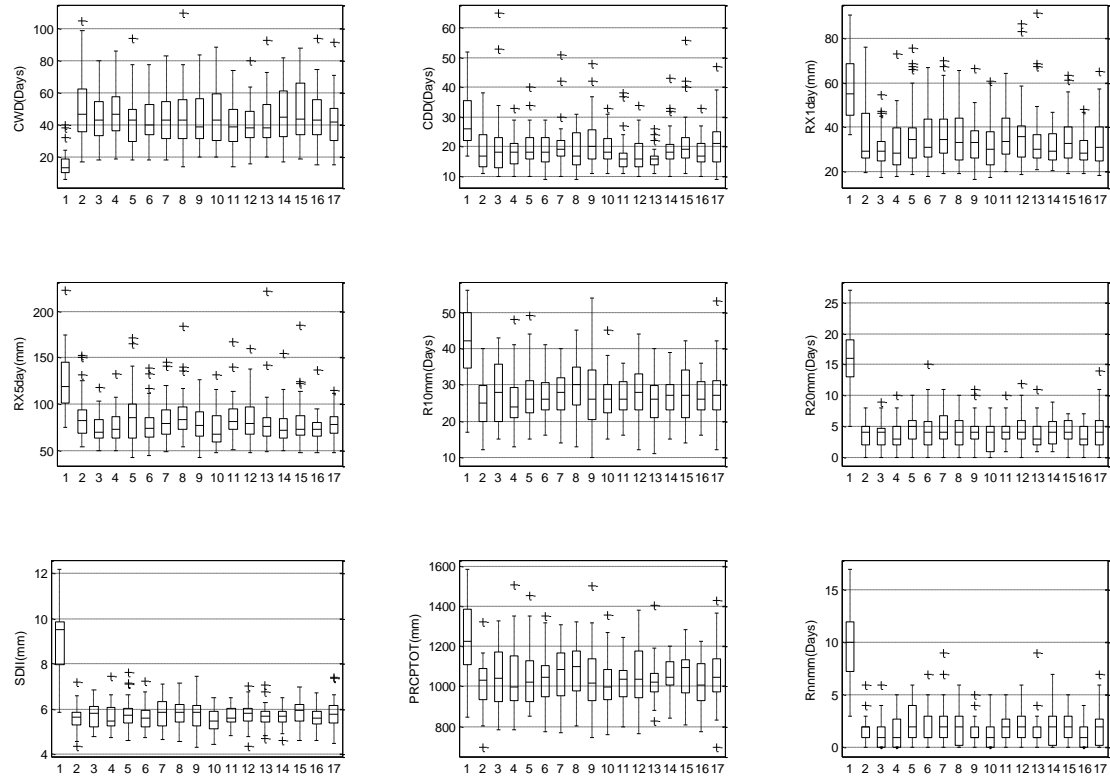


Figure 60: Station 1 WMO indices bias evaluation.

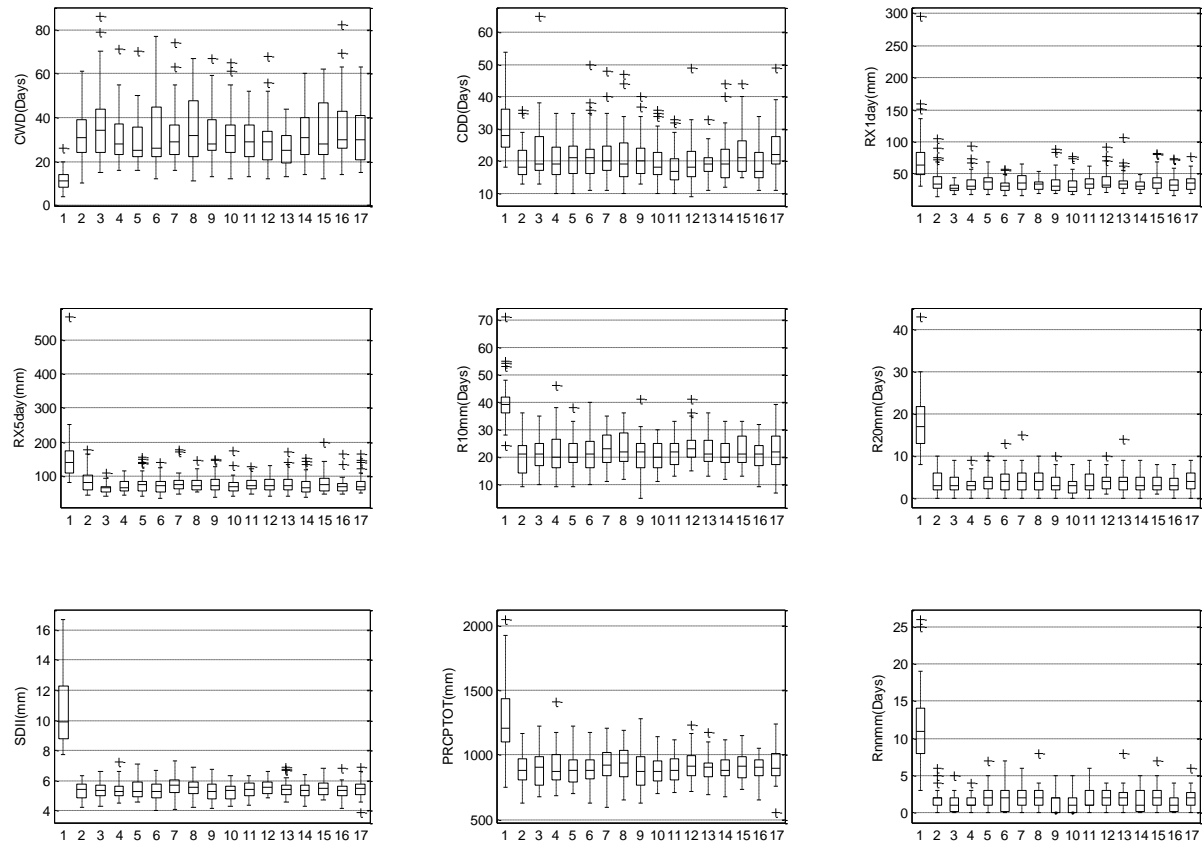


Figure 61: Station 2 WMO indices bias evaluation.

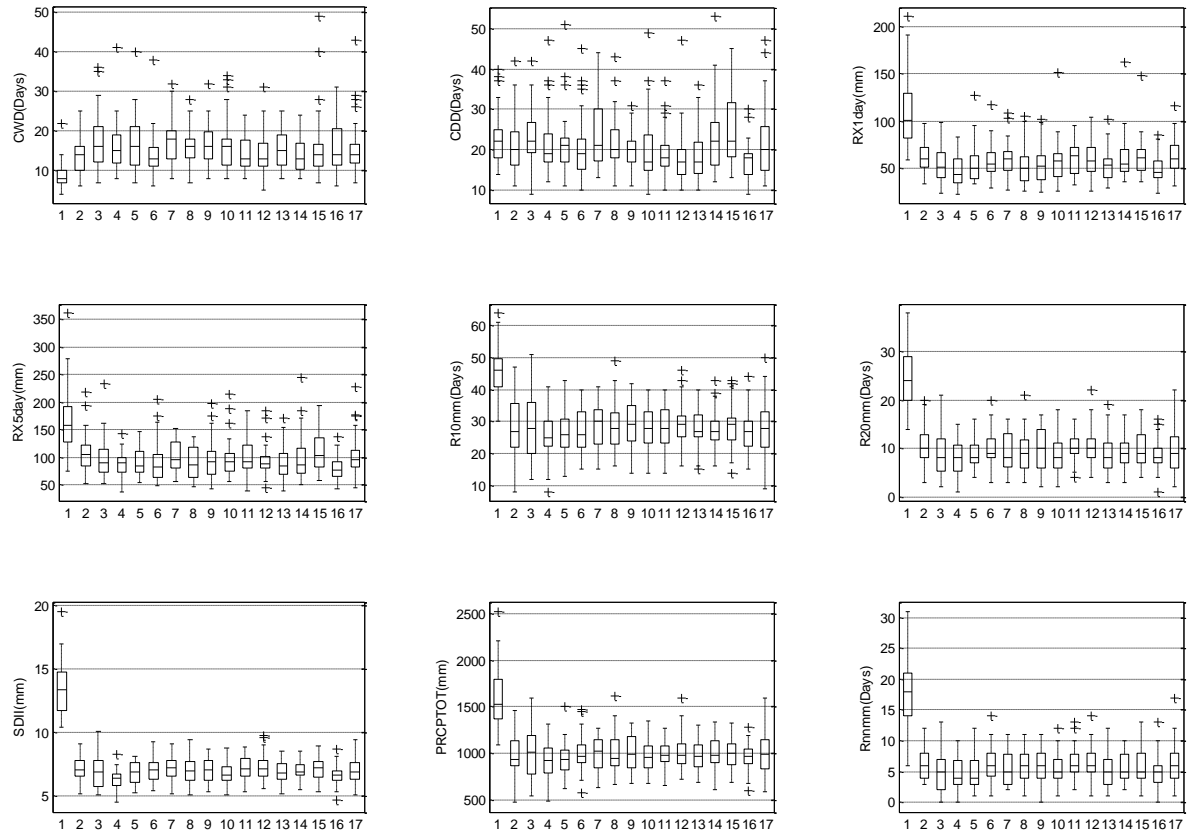
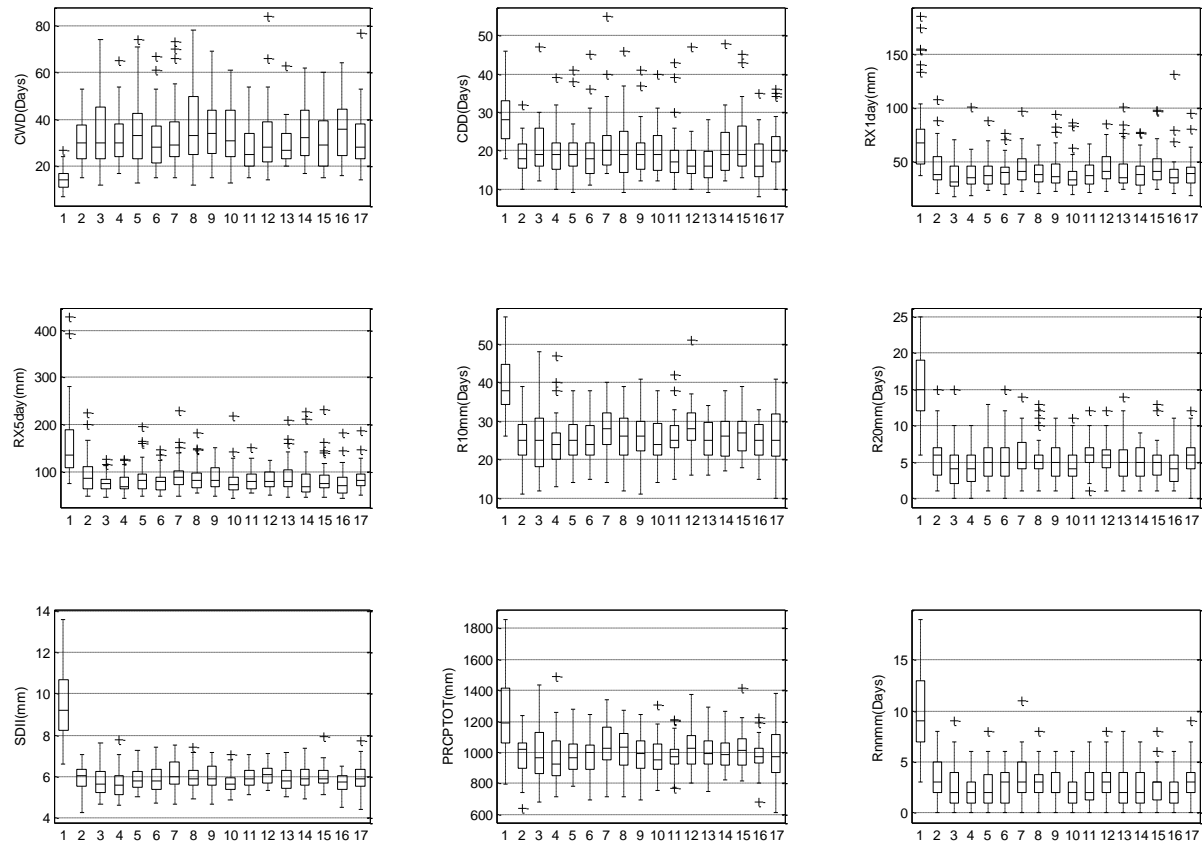


Figure 62: Station 4 WMO indices bias evaluation.



**Figure 63: Station 5 WMO indices bias evaluation.**

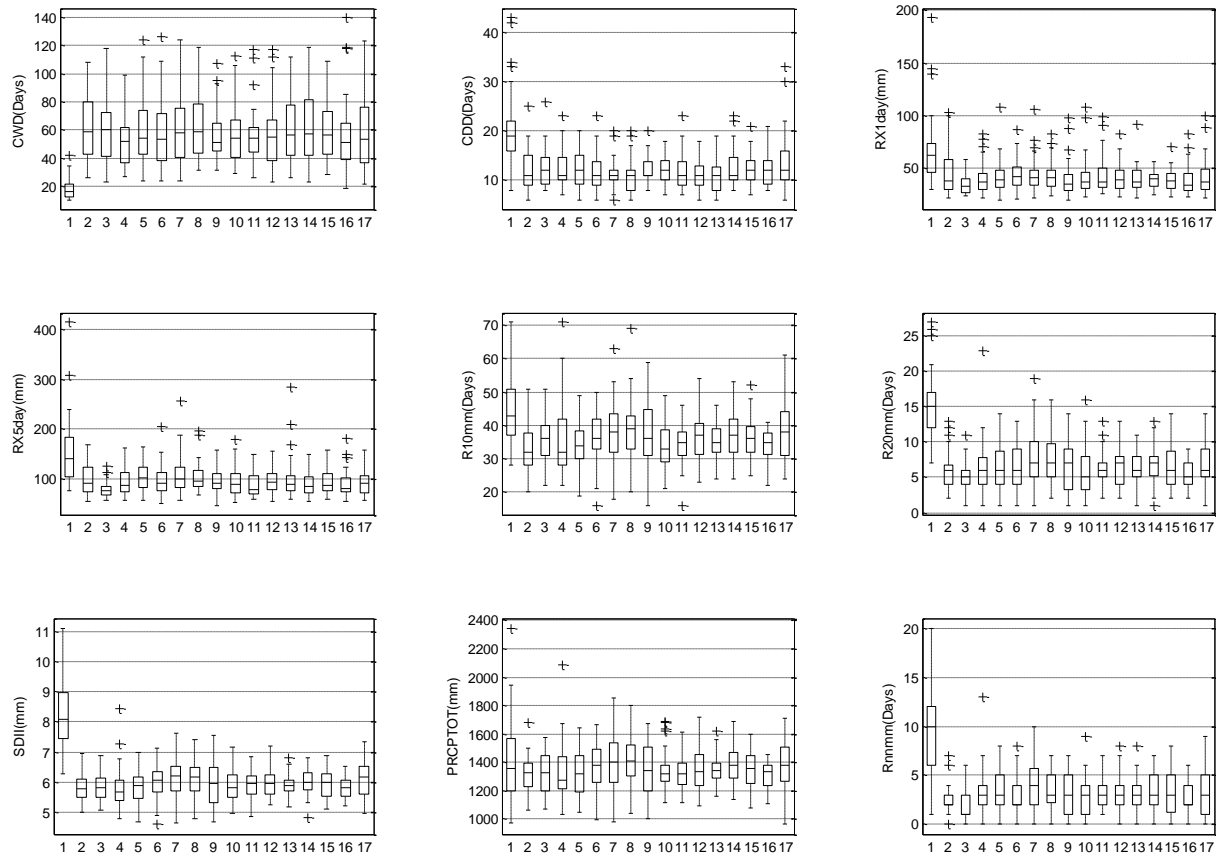


Figure 64: Station 6 WMO indices bias evaluation.

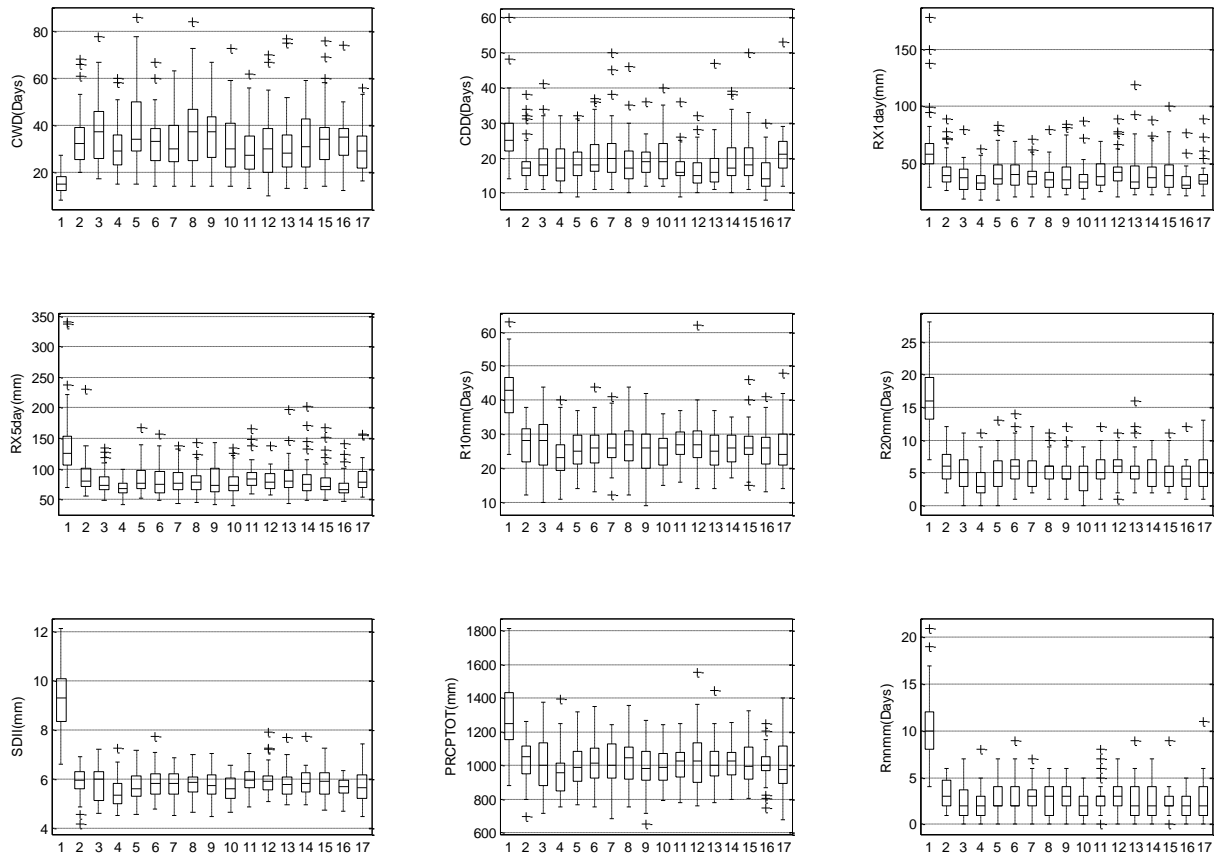


Figure 65: Station 7 WMO indices bias evaluation.

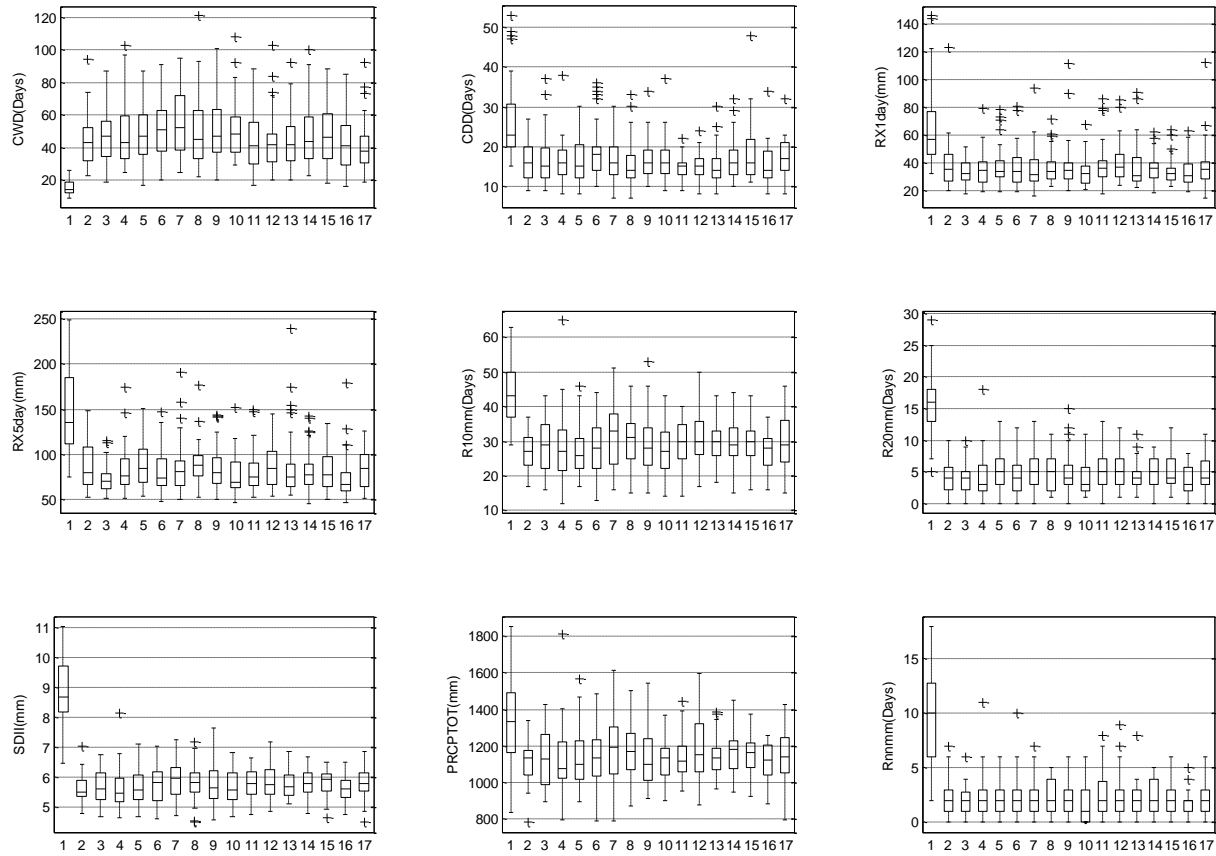


Figure 66: Station 9 WMO indices bias evaluation.

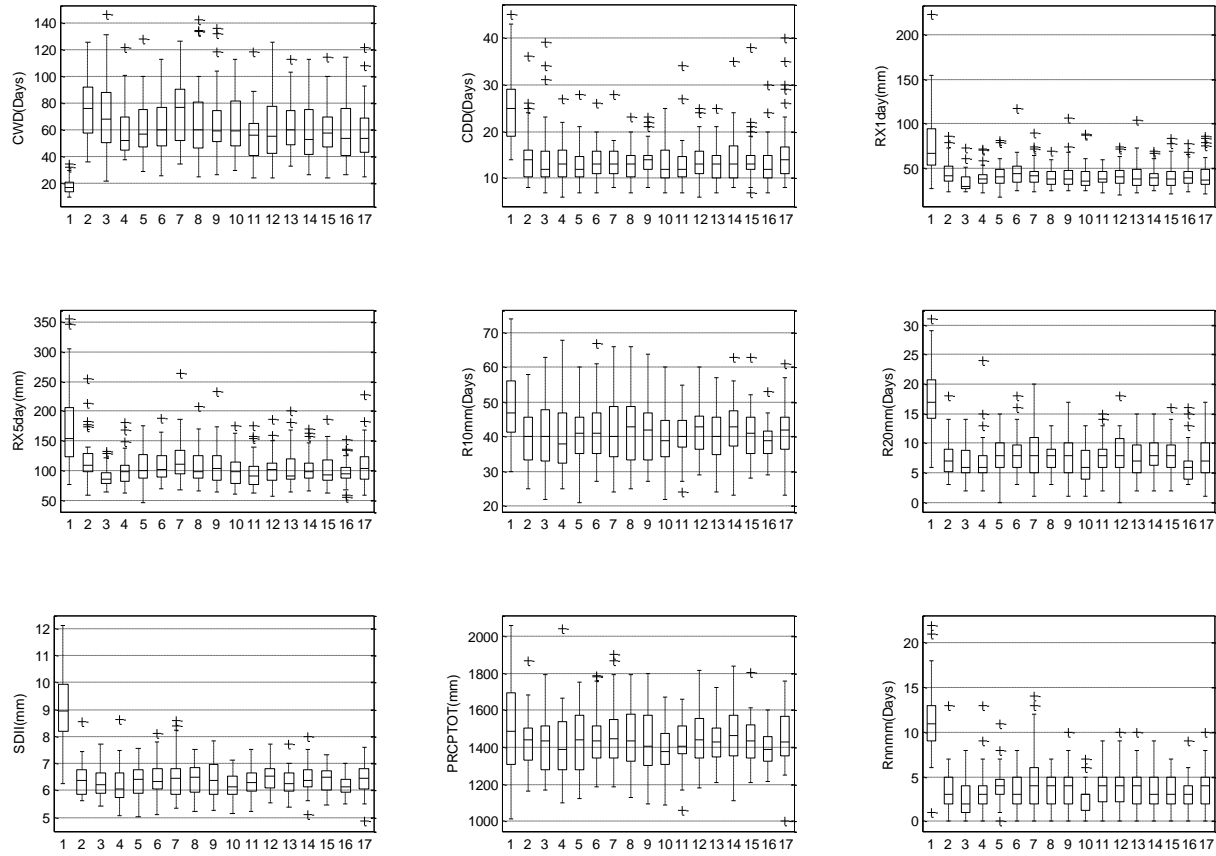


Figure 67: Station 10 WMO indices bias evaluation.

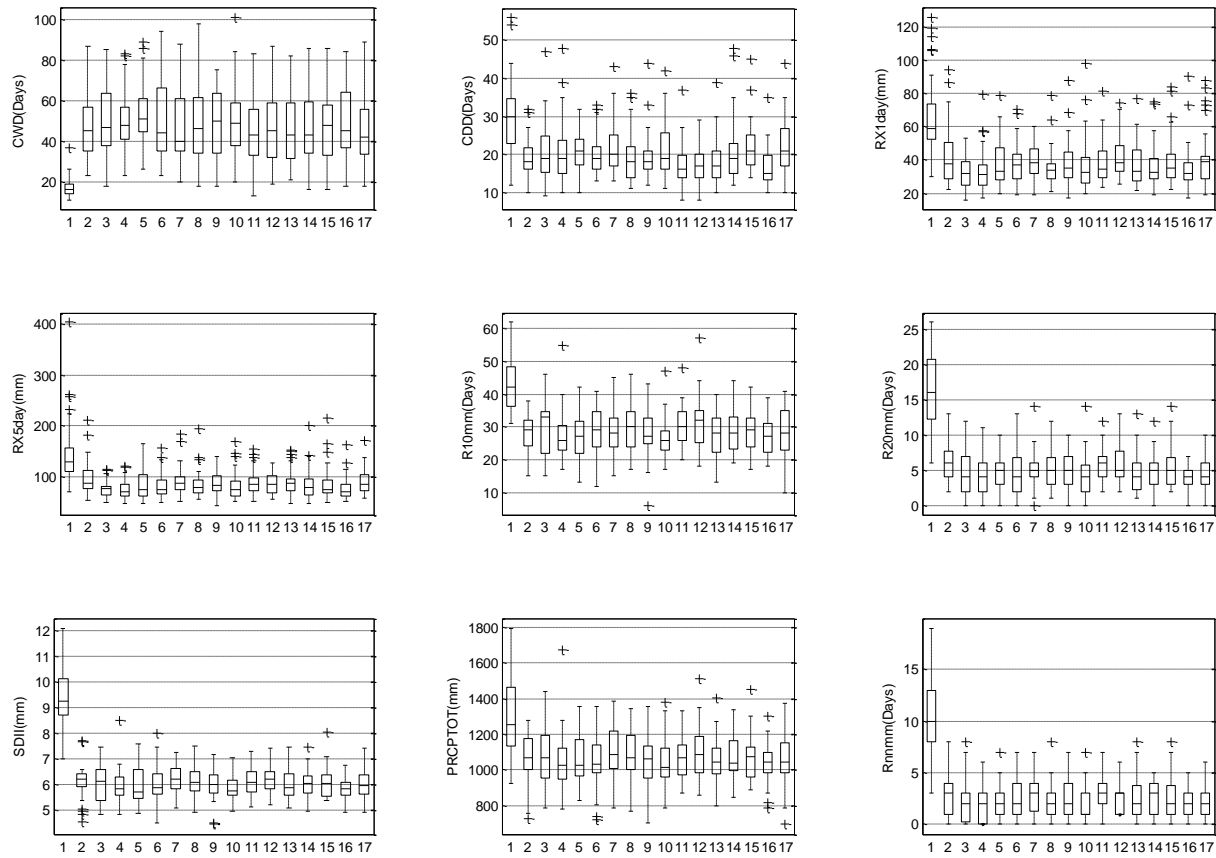


Figure 68: Station 11 WMO indices bias evaluation.

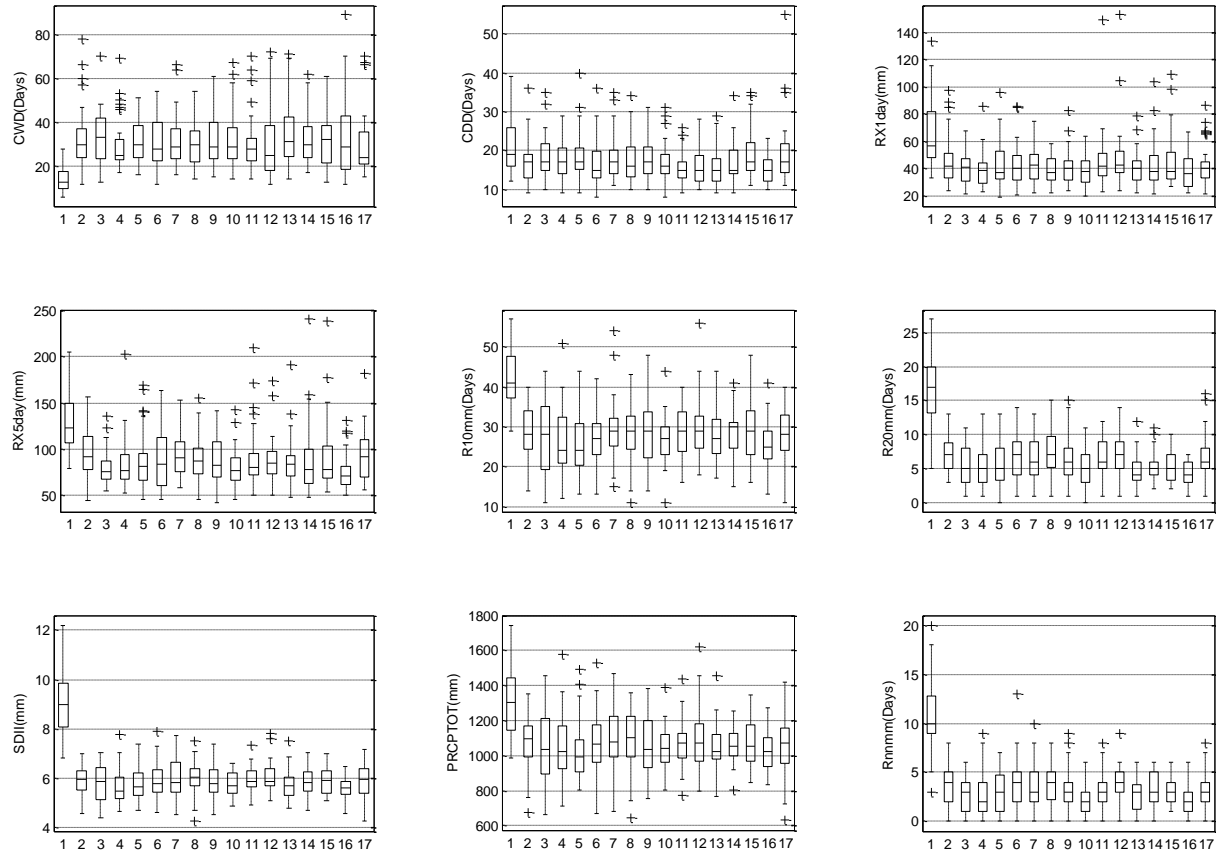


Figure 69: Station 13 WMO indices bias evaluation.

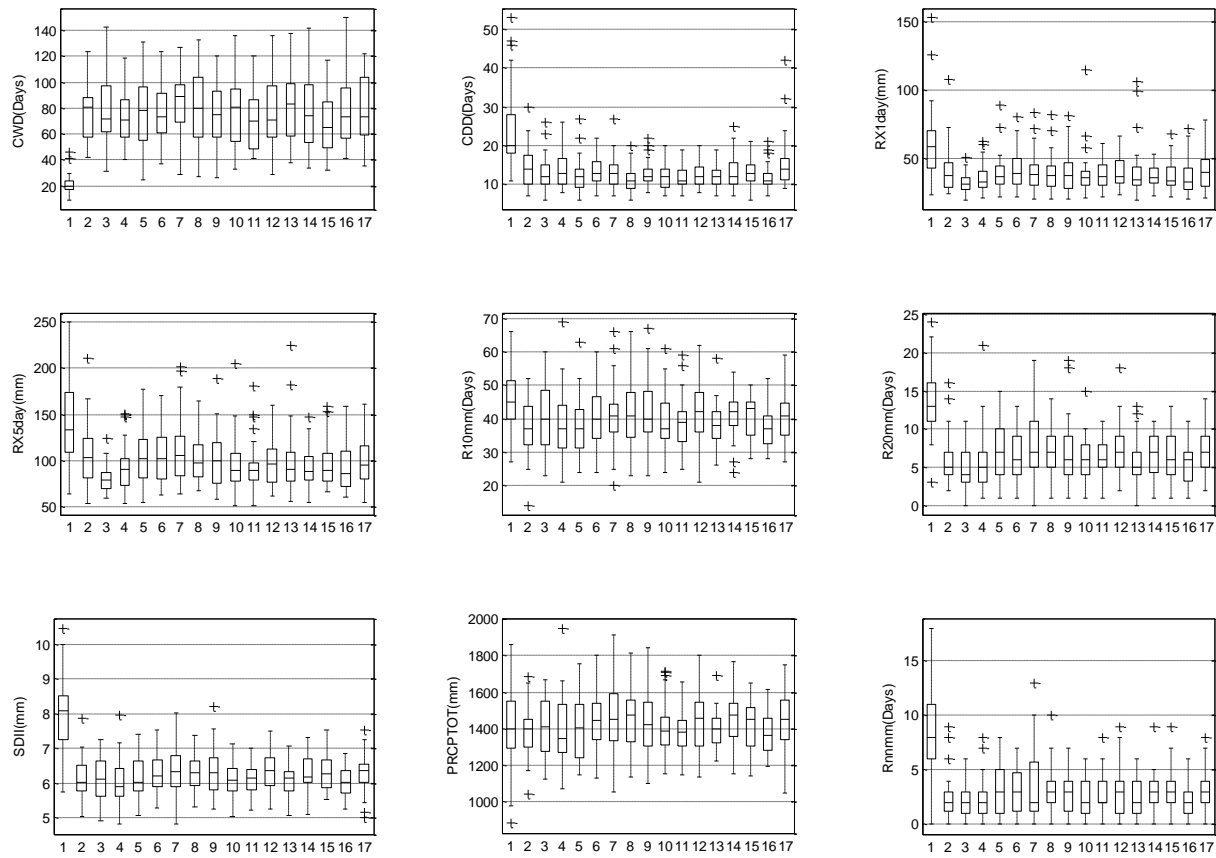


Figure 70: Station 14 WMO indices bias evaluation.

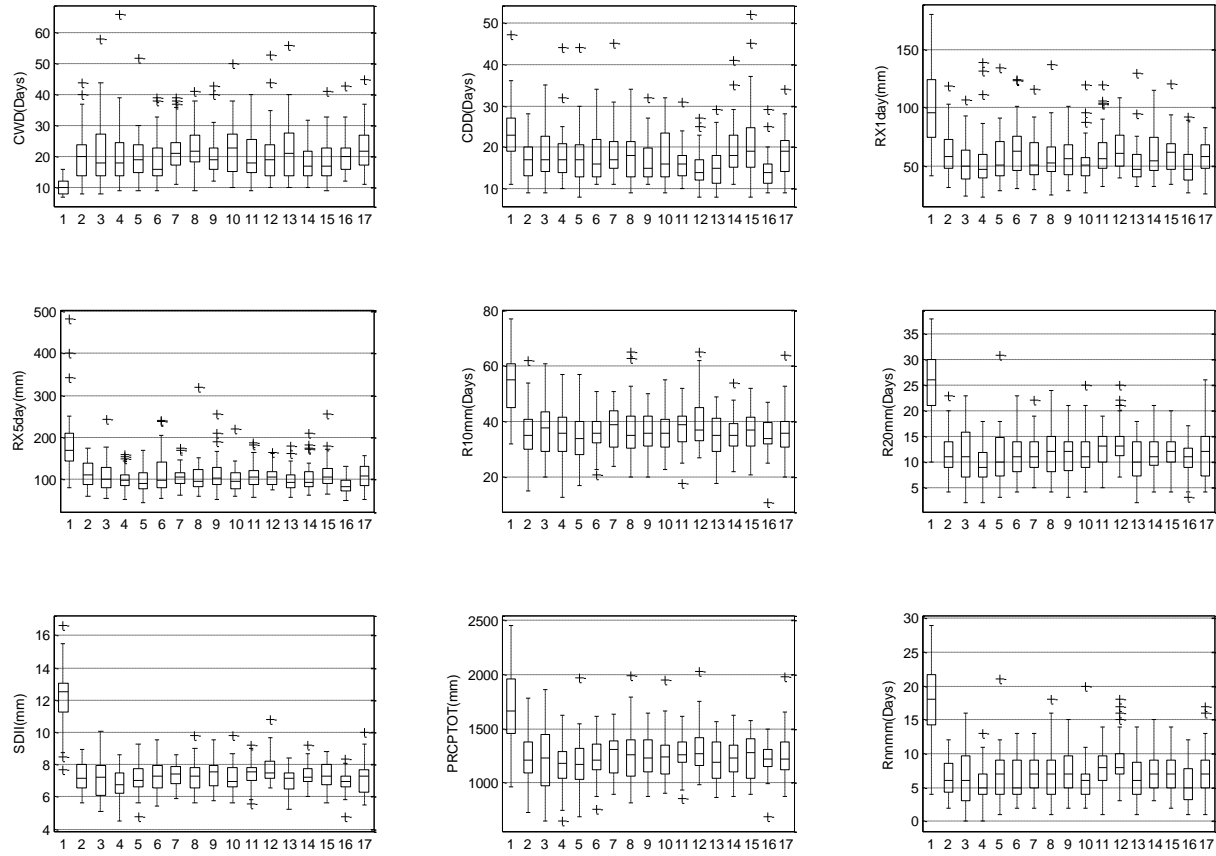


Figure 71: Station 15 WMO indices bias evaluation.

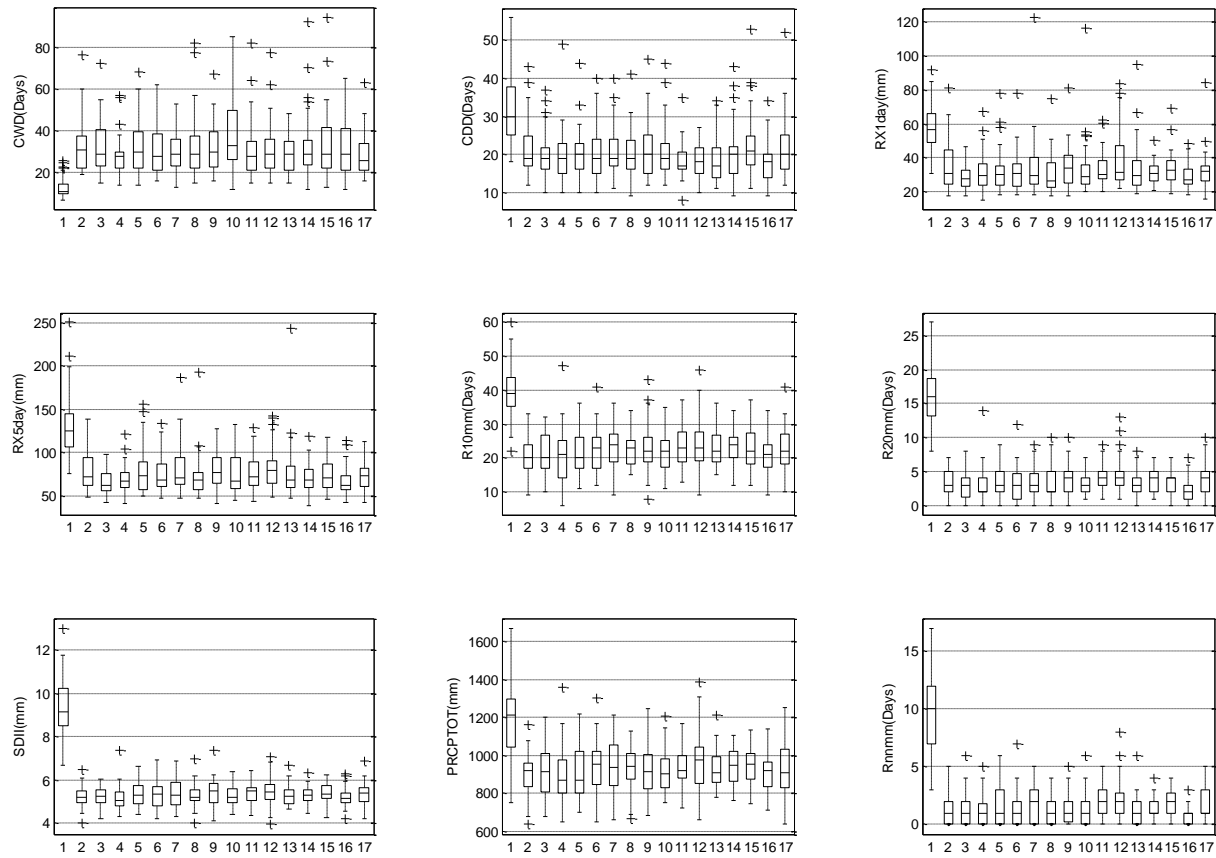


Figure 72: Station 16 WMO indices bias evaluation.

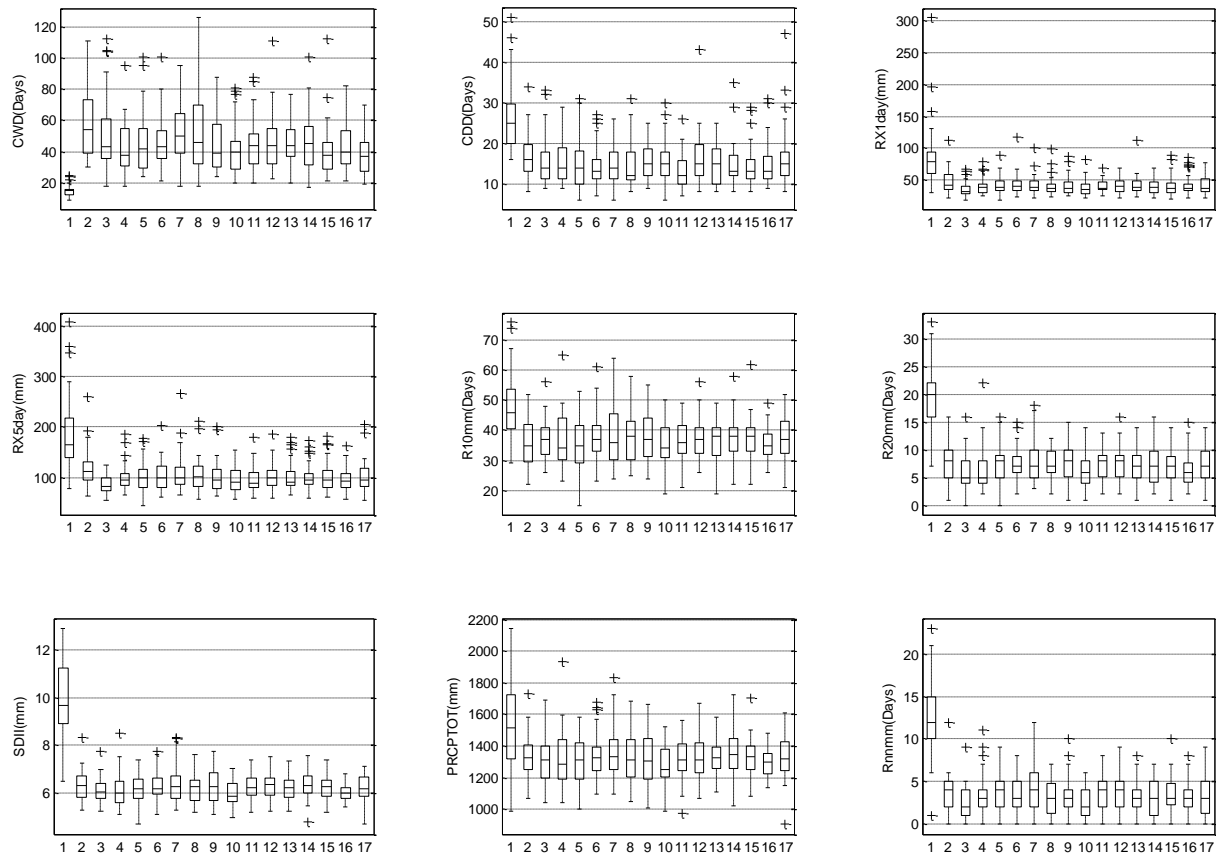


Figure 73: Station 17 WMO indices bias evaluation.

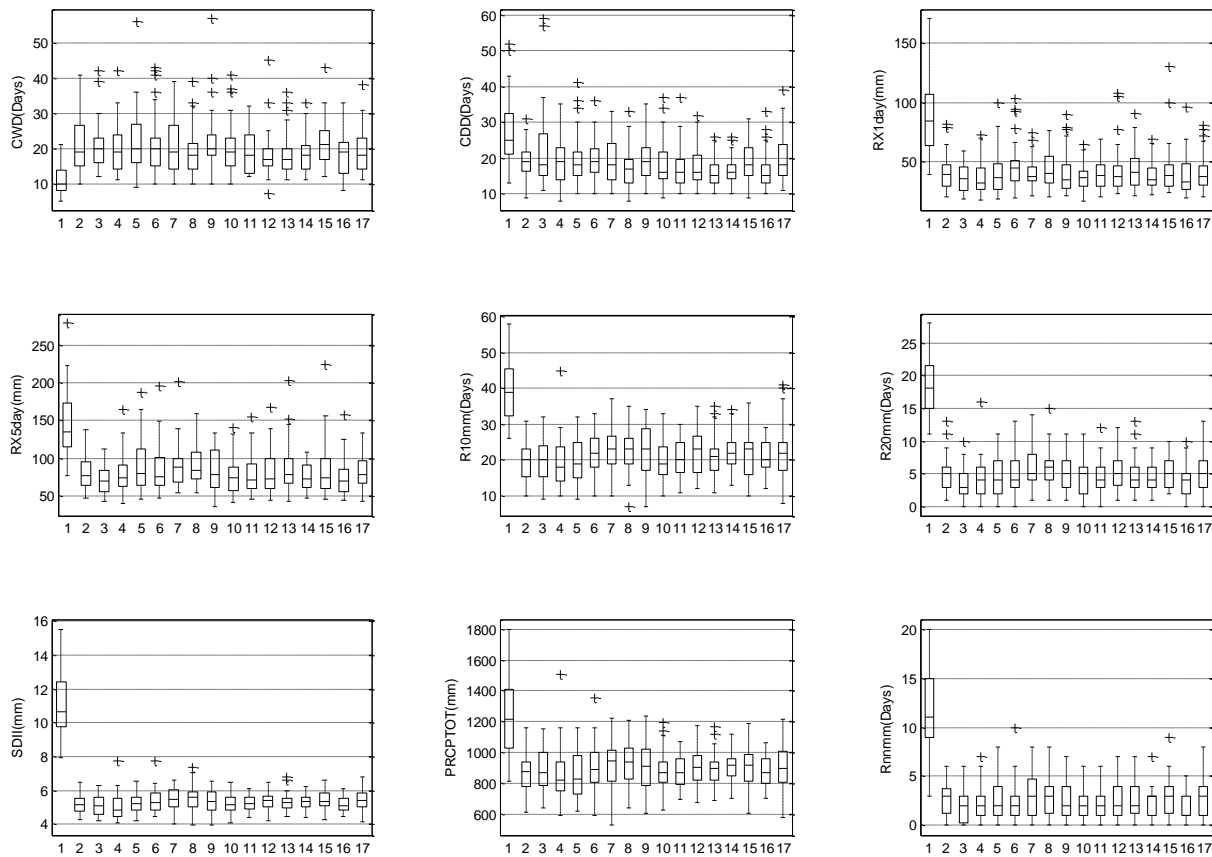


Figure 74: Station 18 WMO indices bias evaluation.

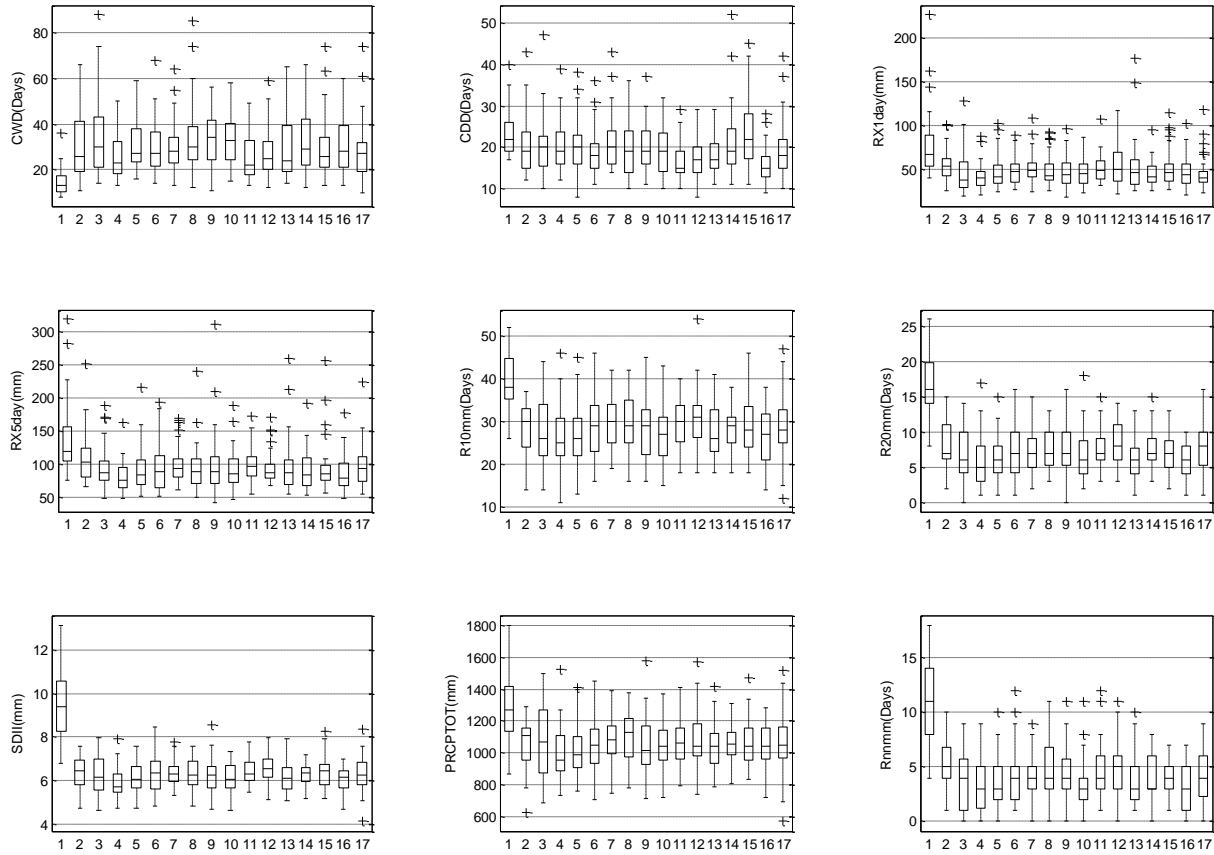


Figure 75: Station 19 WMO indices bias evaluation.

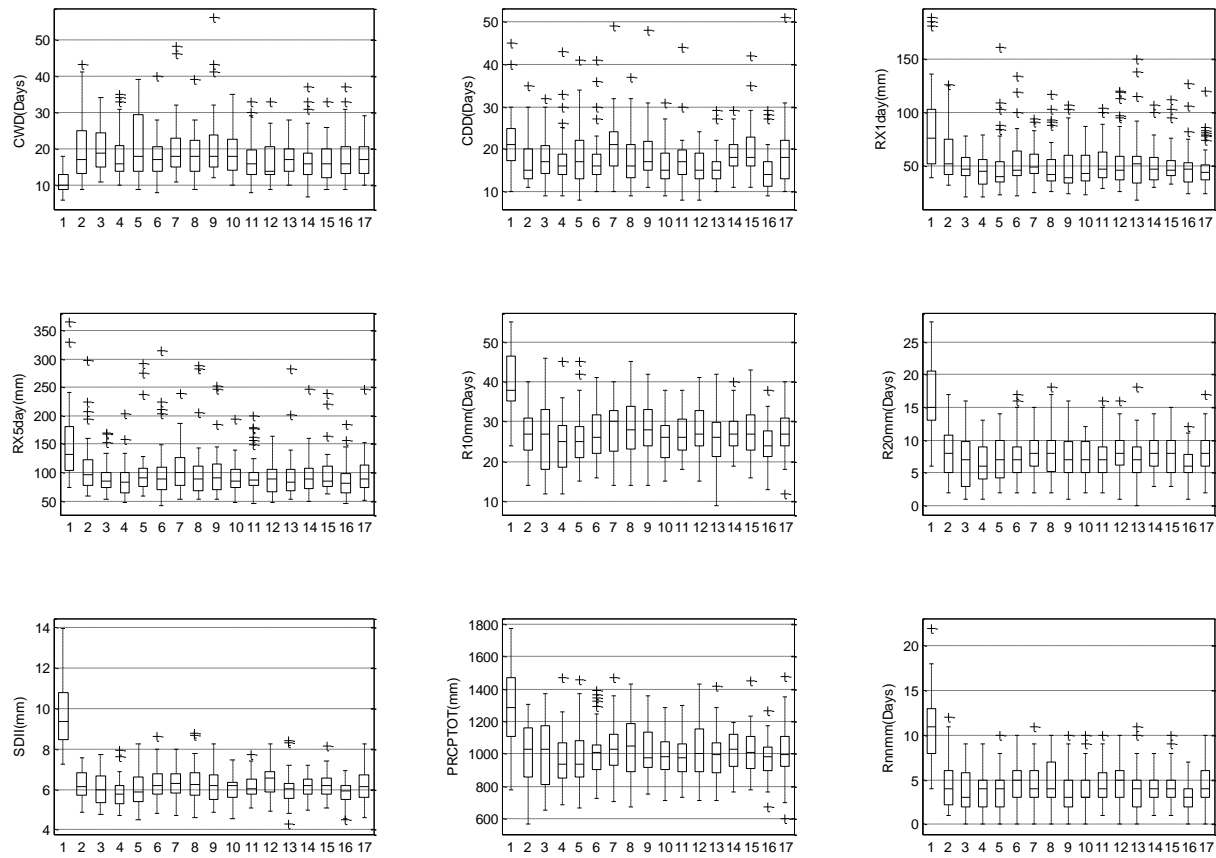


Figure 76: Station 21 WMO indices bias evaluation.

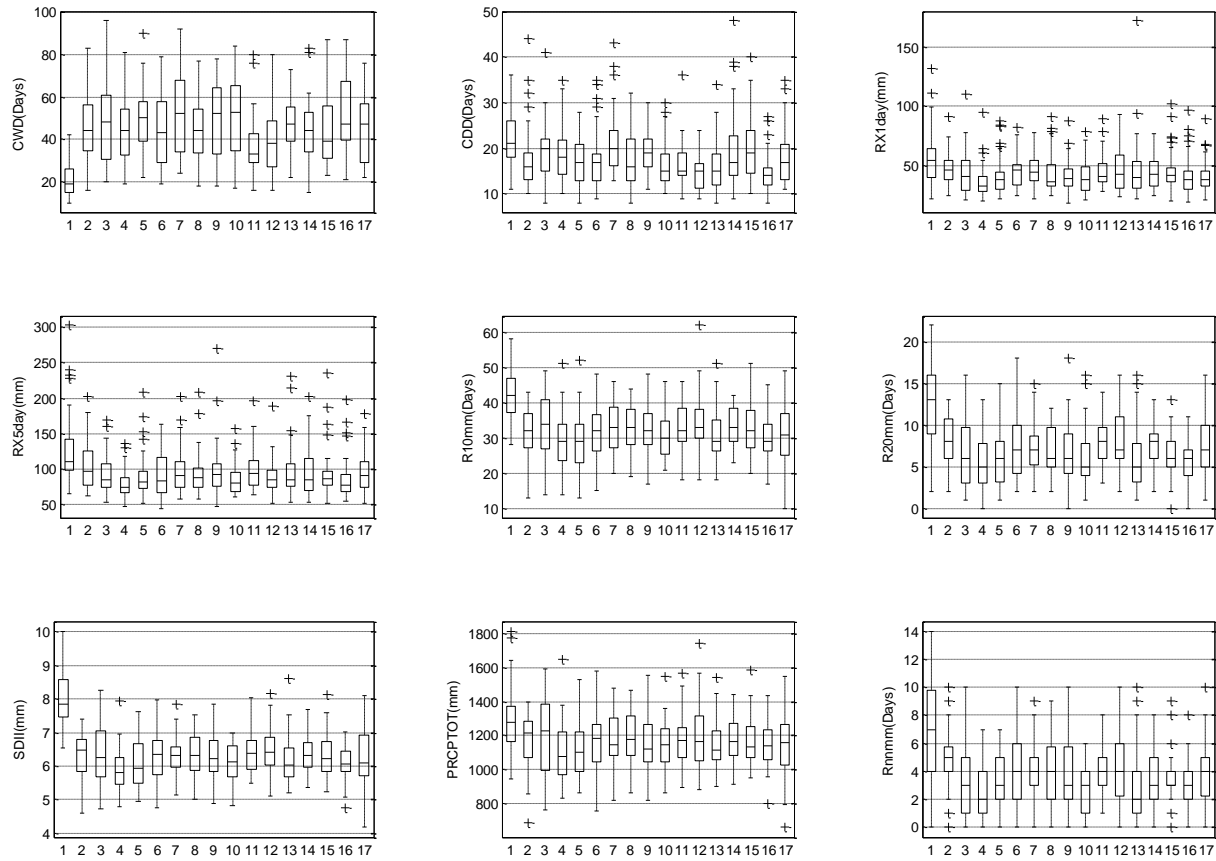


Figure 77: Station 22 WMO indices bias evaluation.

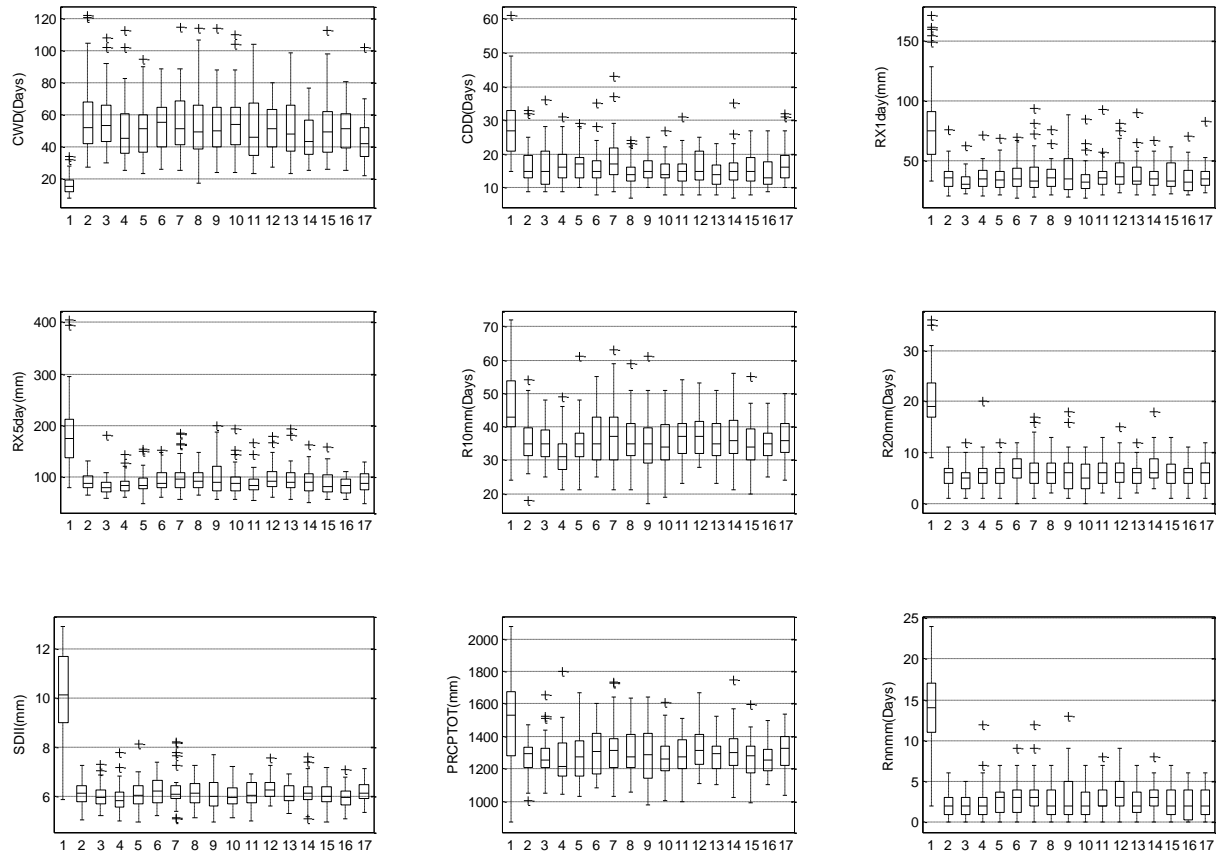


Figure 78: Station 23 WMO indices bias evaluation.

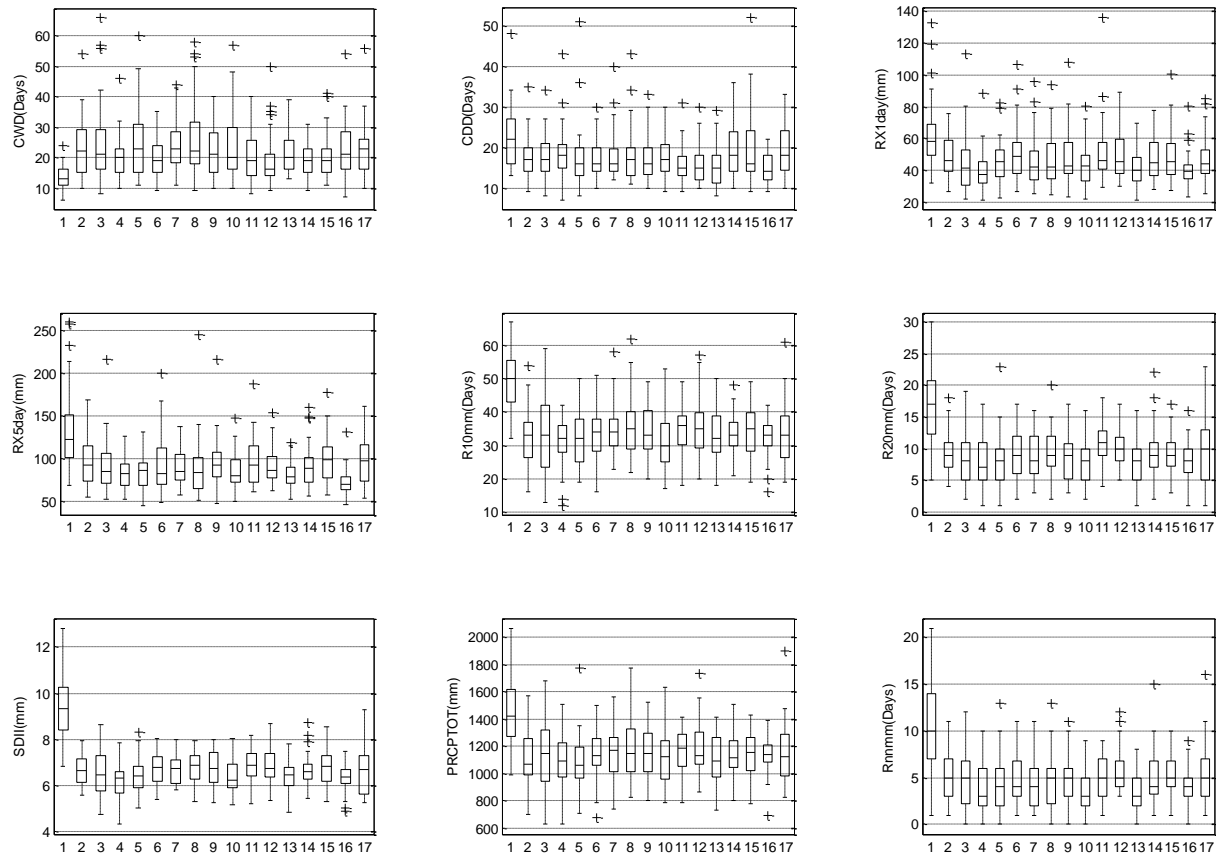


Figure 79: Station 24 WMO indices bias evaluation.

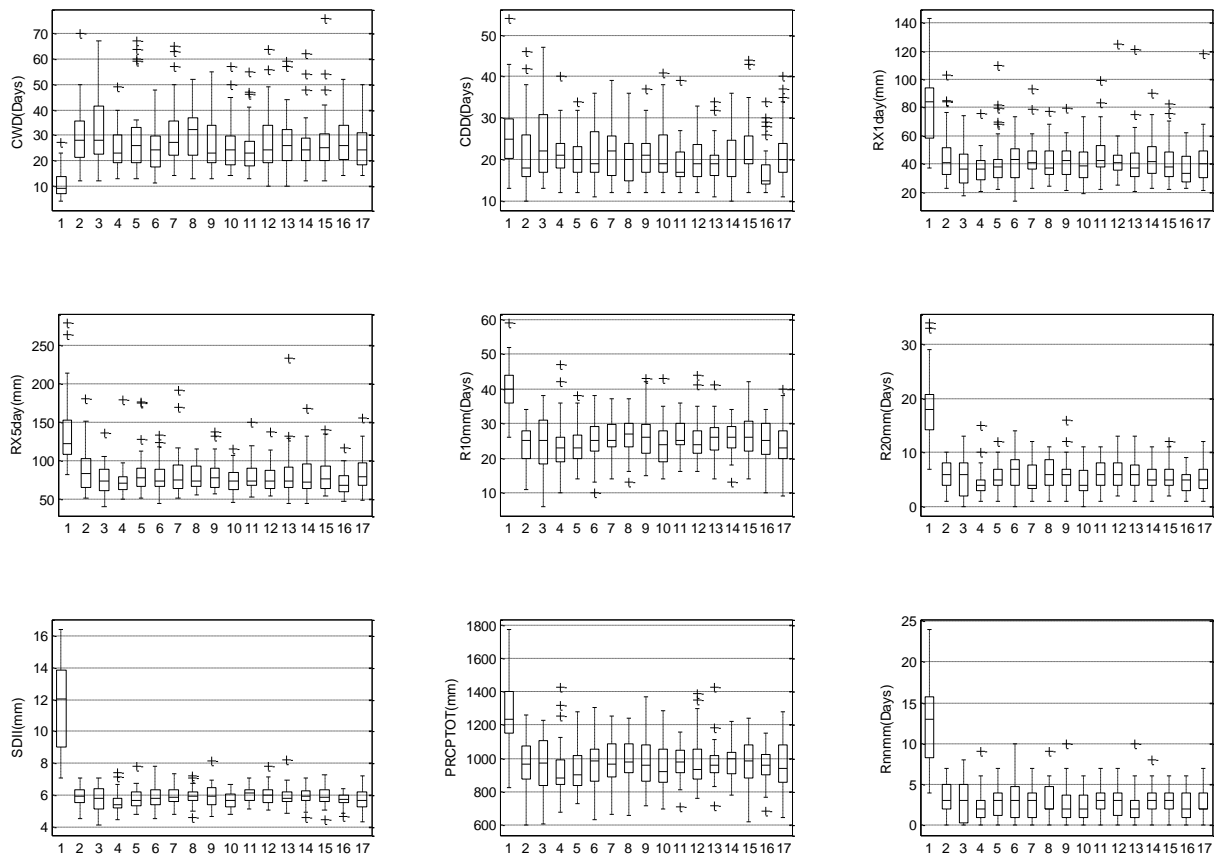


Figure 80: Station 26 WMO indices bias evaluation.

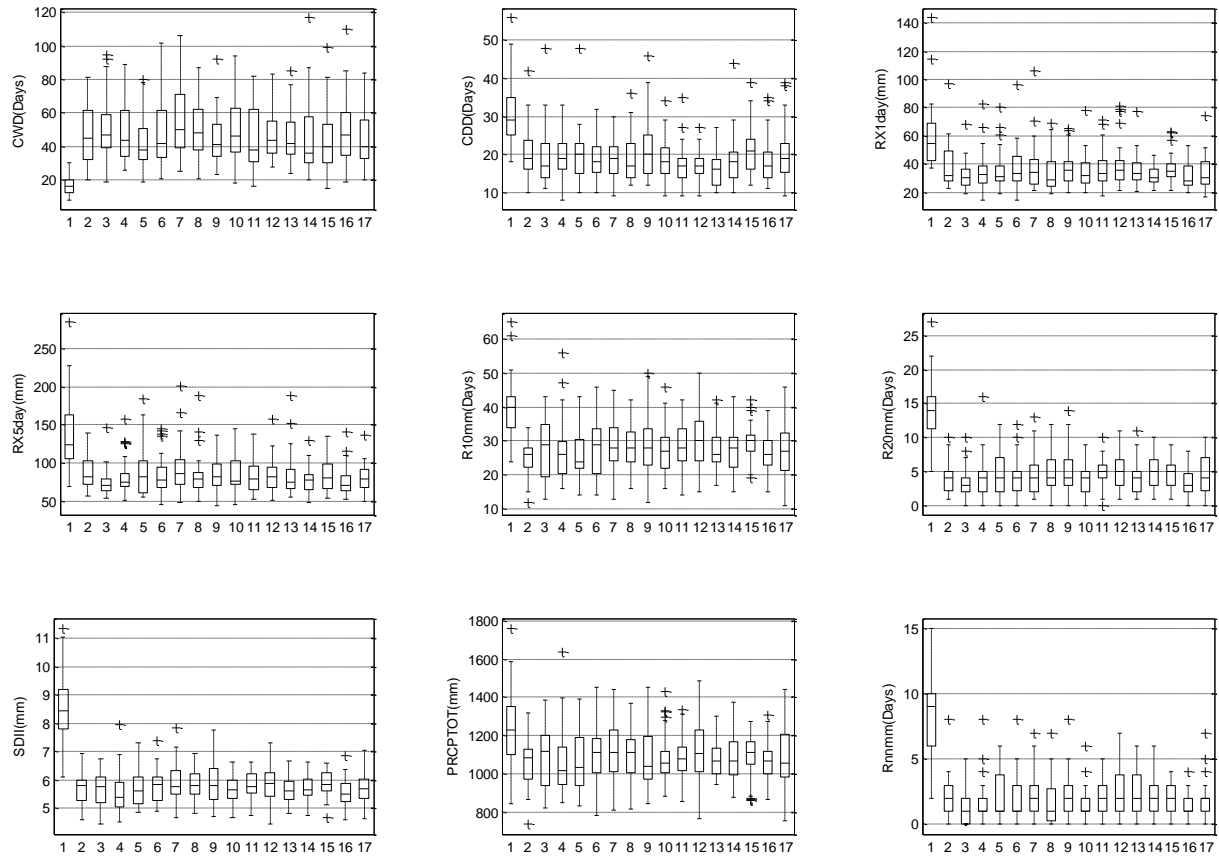


Figure 81: Station 27 WMO indices bias evaluation.

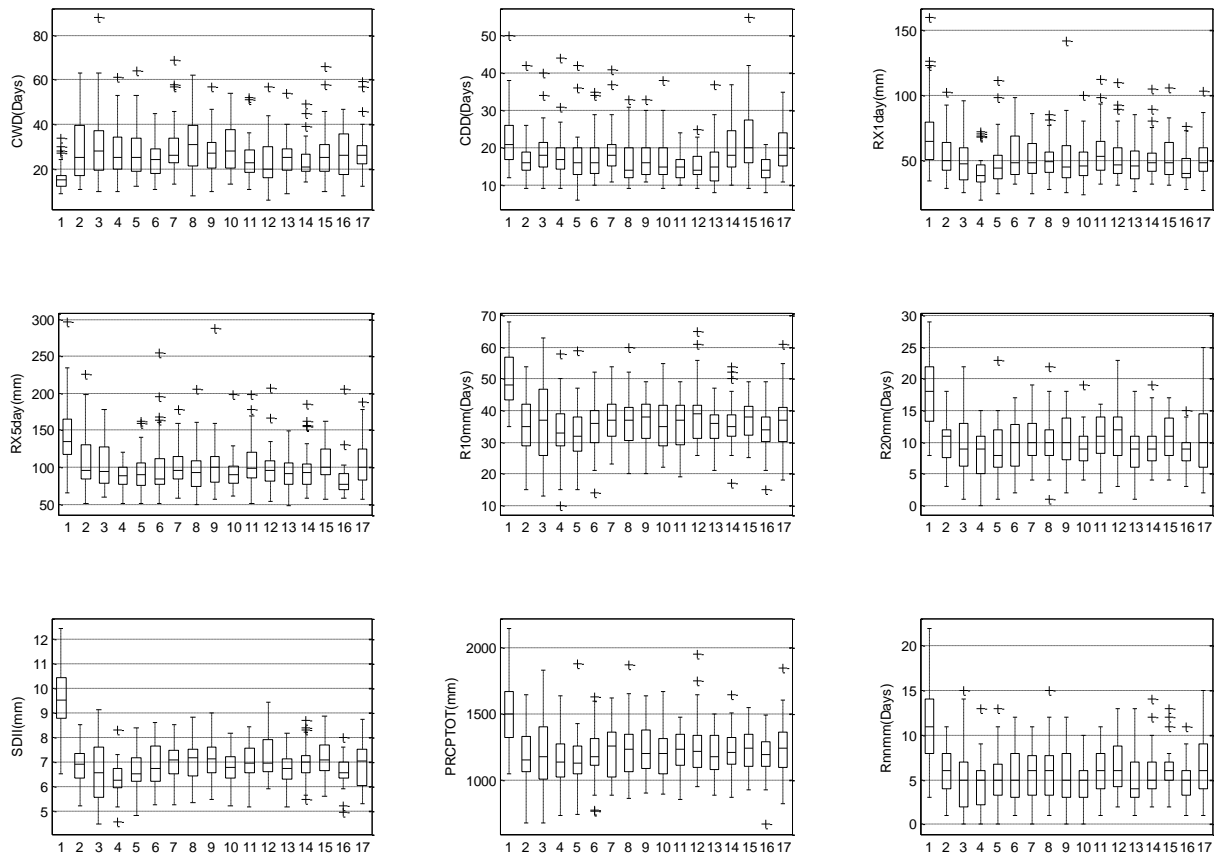


Figure 82: Station 28 WMO indices bias evaluation.

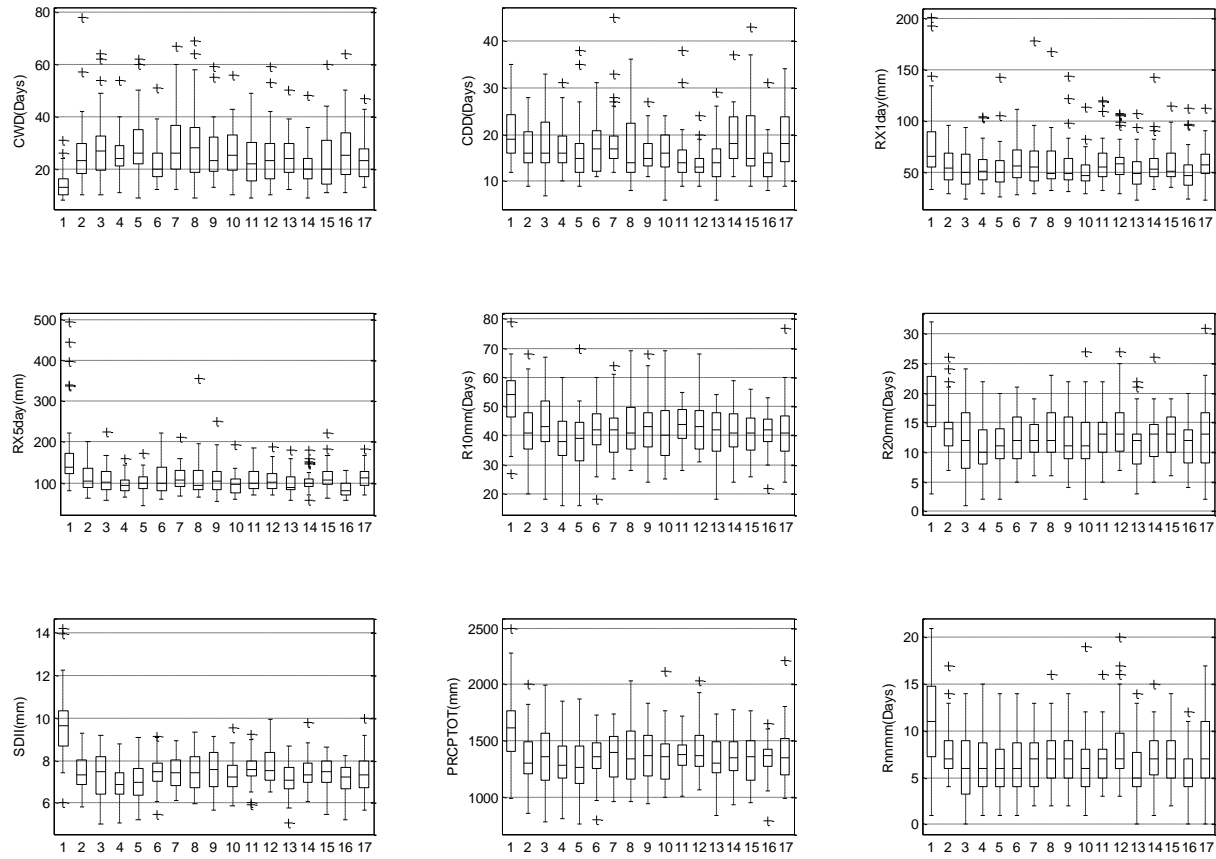


Figure 83: Station 29 WMO indices bias evaluation.

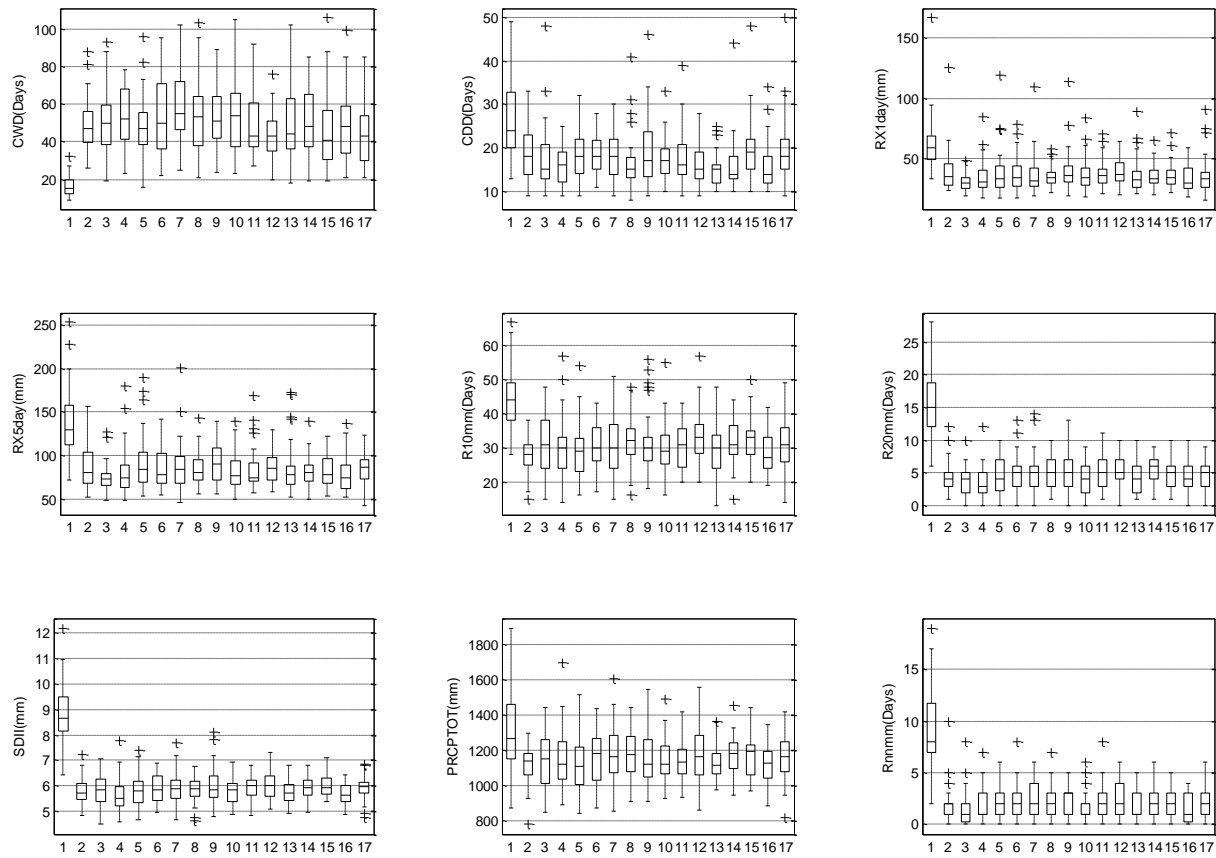


Figure 84: Station 30 WMO indices bias evaluation.

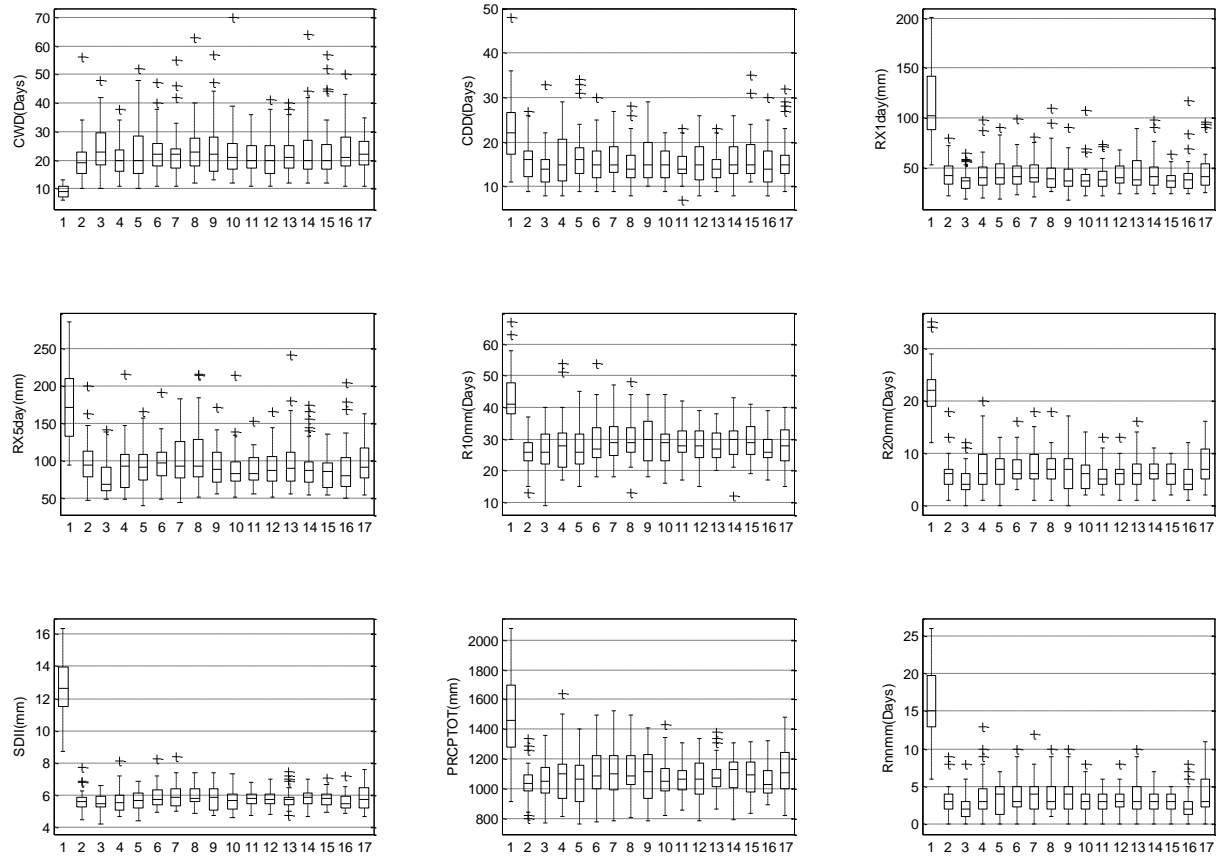


Figure 85: Station 31 WMO indices bias evaluation.

**Appendix C: WMO bias corrected indices performance measures**

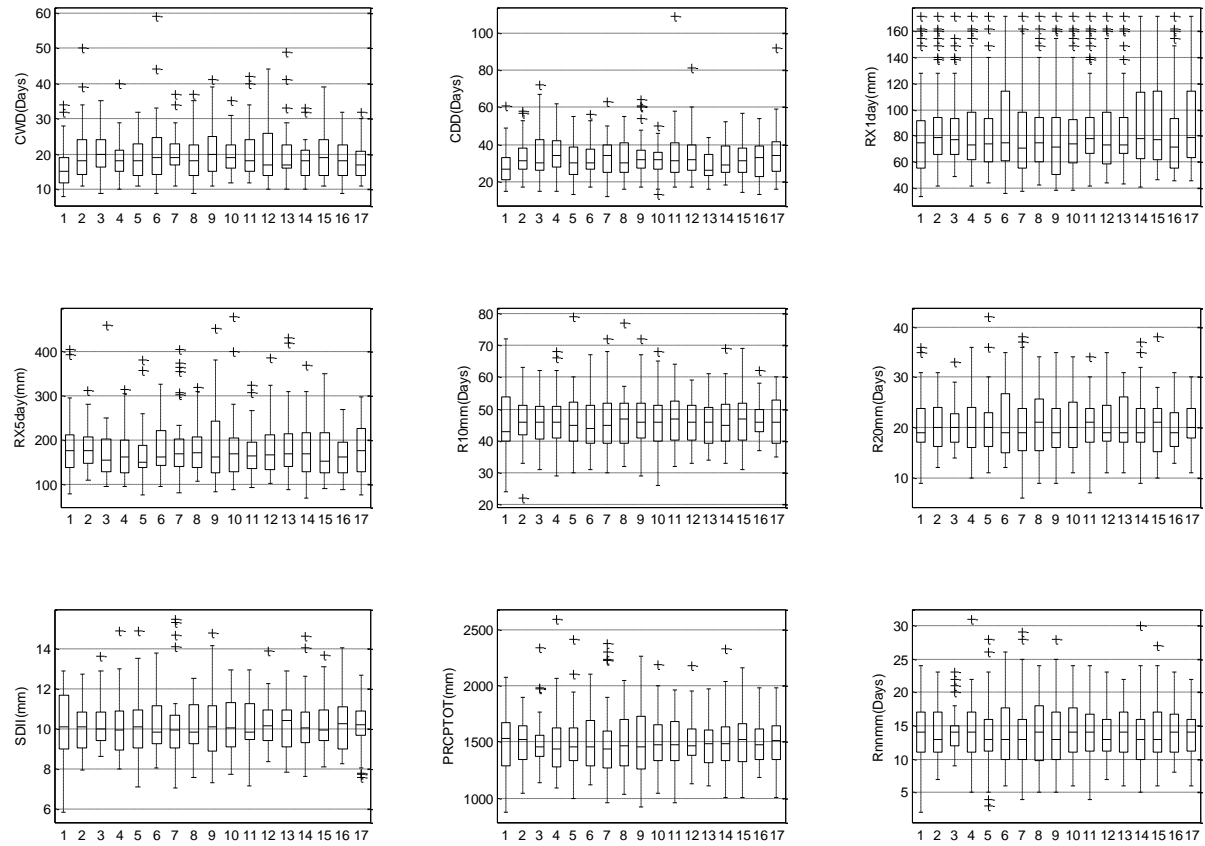


Figure 86: Station 1 WMO indices bias evaluation after quantile mapping.

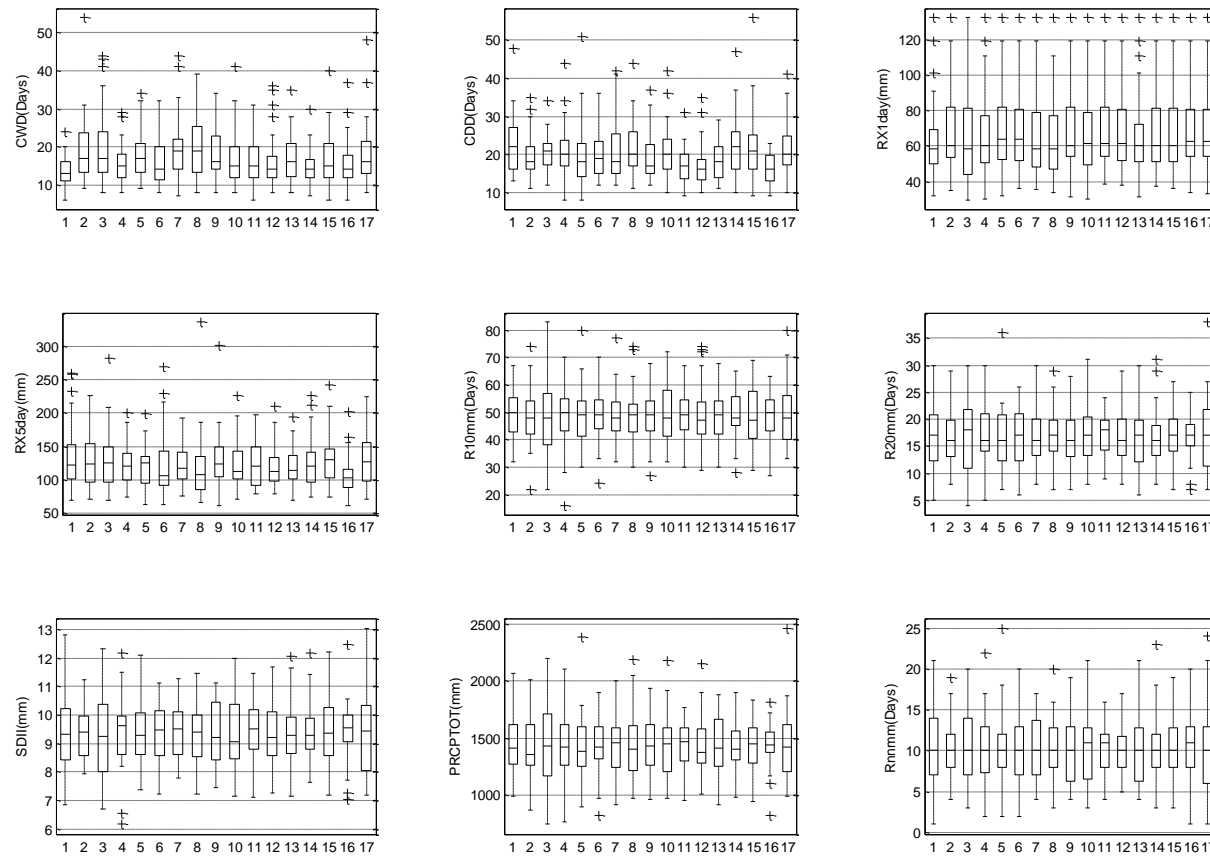


Figure 87: Station 2 WMO indices bias evaluation after quantile mapping.

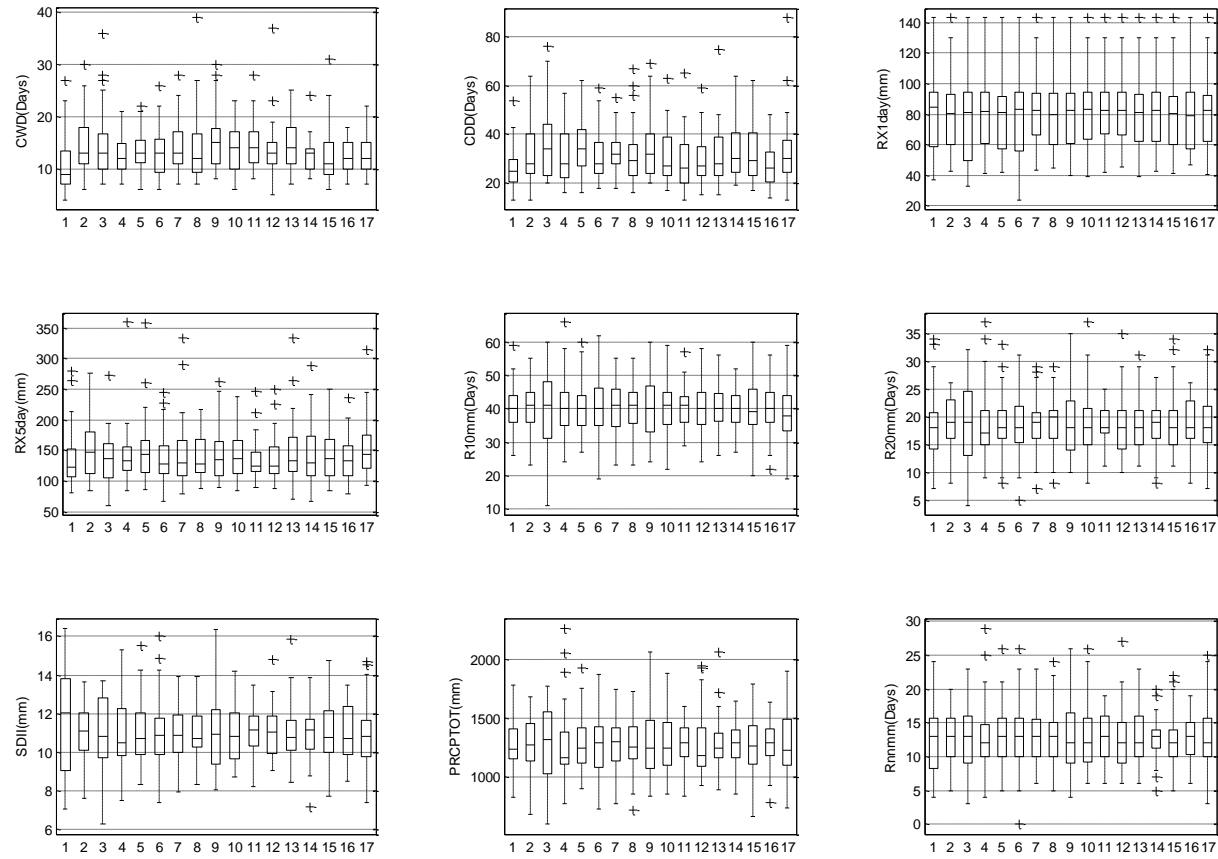


Figure 88: Station 4 WMO indices bias evaluation after quantile mapping.

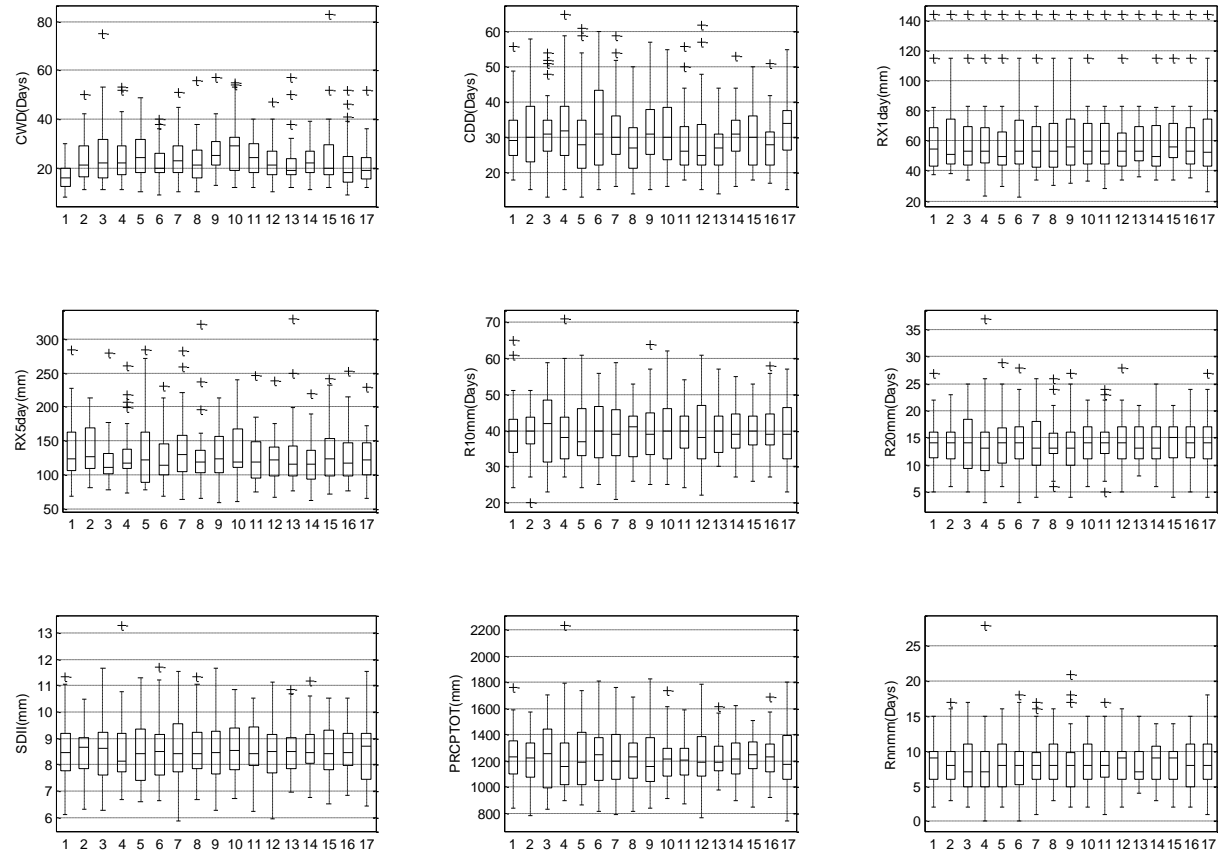


Figure 89: Station 5 WMO indices bias evaluation after quantile mapping.

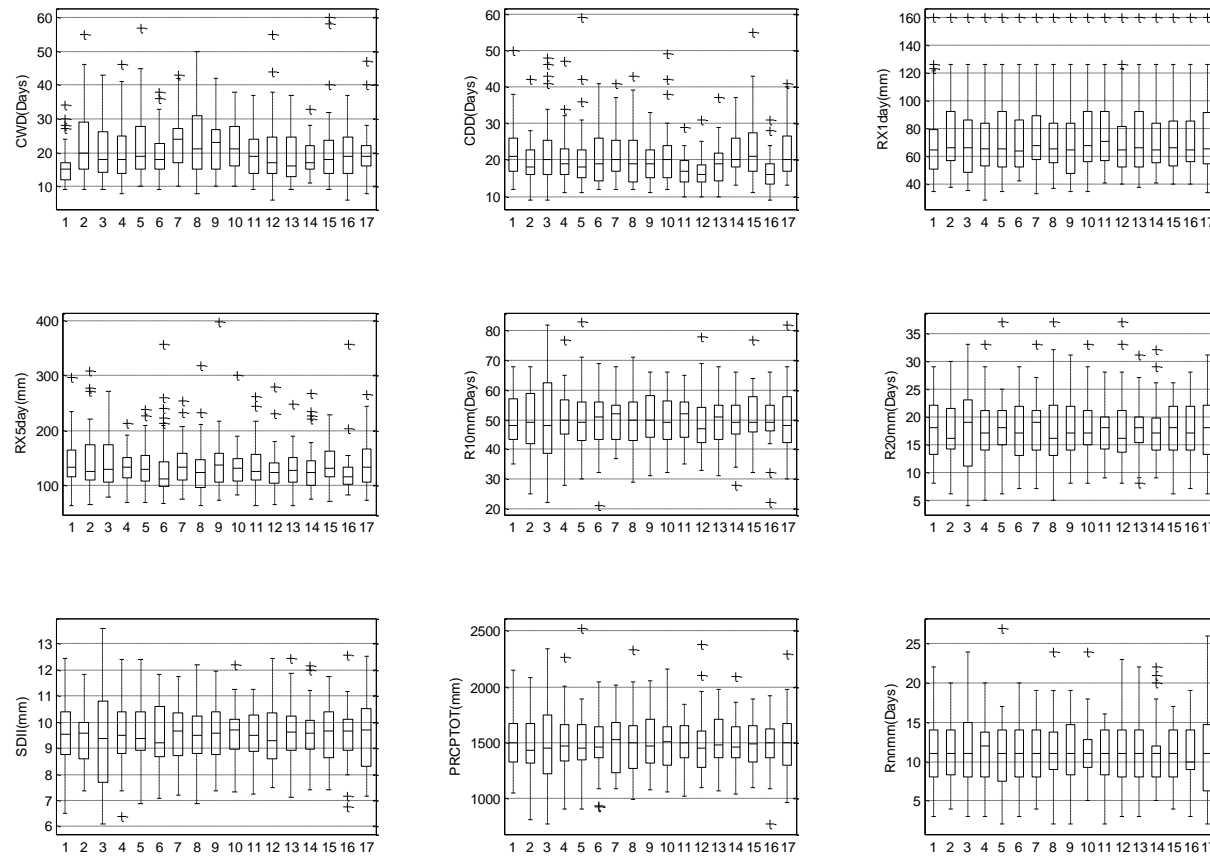


Figure 90: Station 6 WMO indices bias evaluation after quantile mapping.

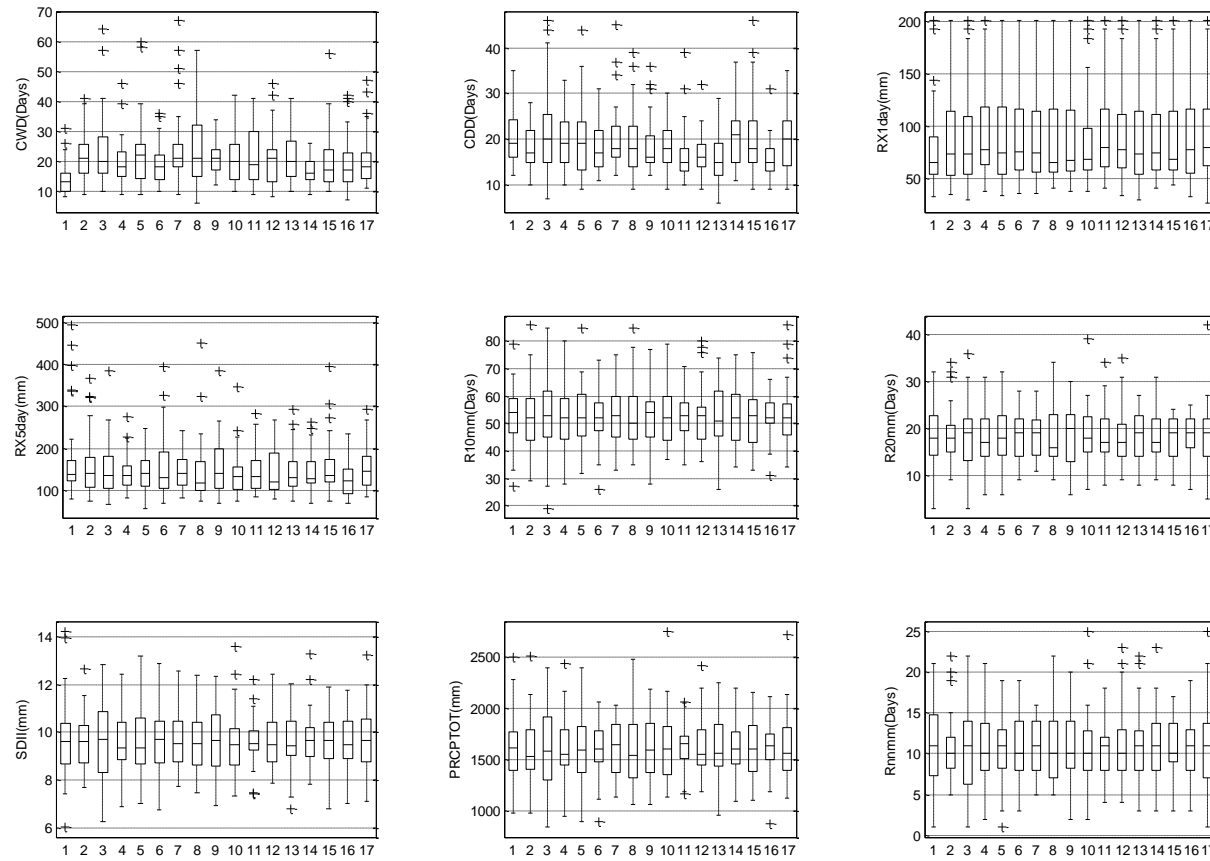


Figure 91: Station 7 WMO indices bias evaluation after quantile mapping.

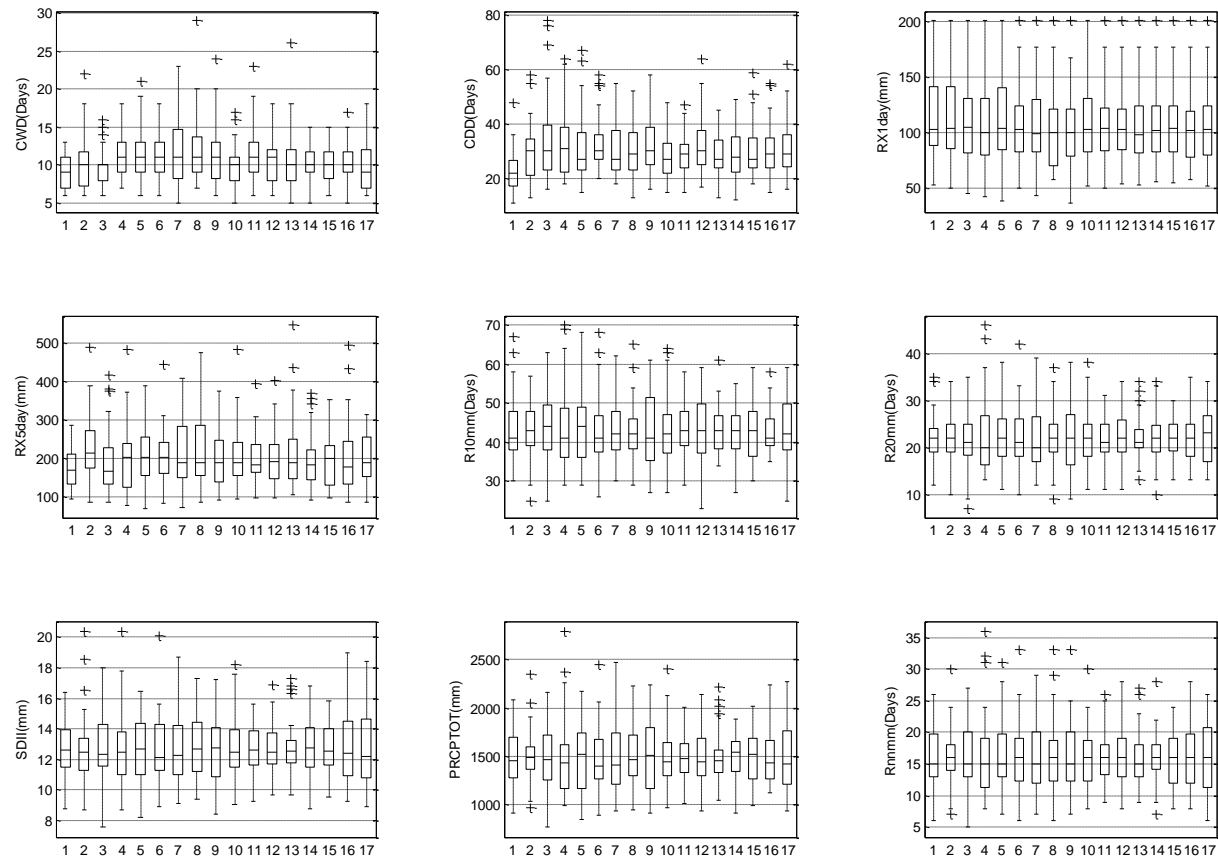


Figure 92: Station 9 WMO indices bias evaluation after quantile mapping.

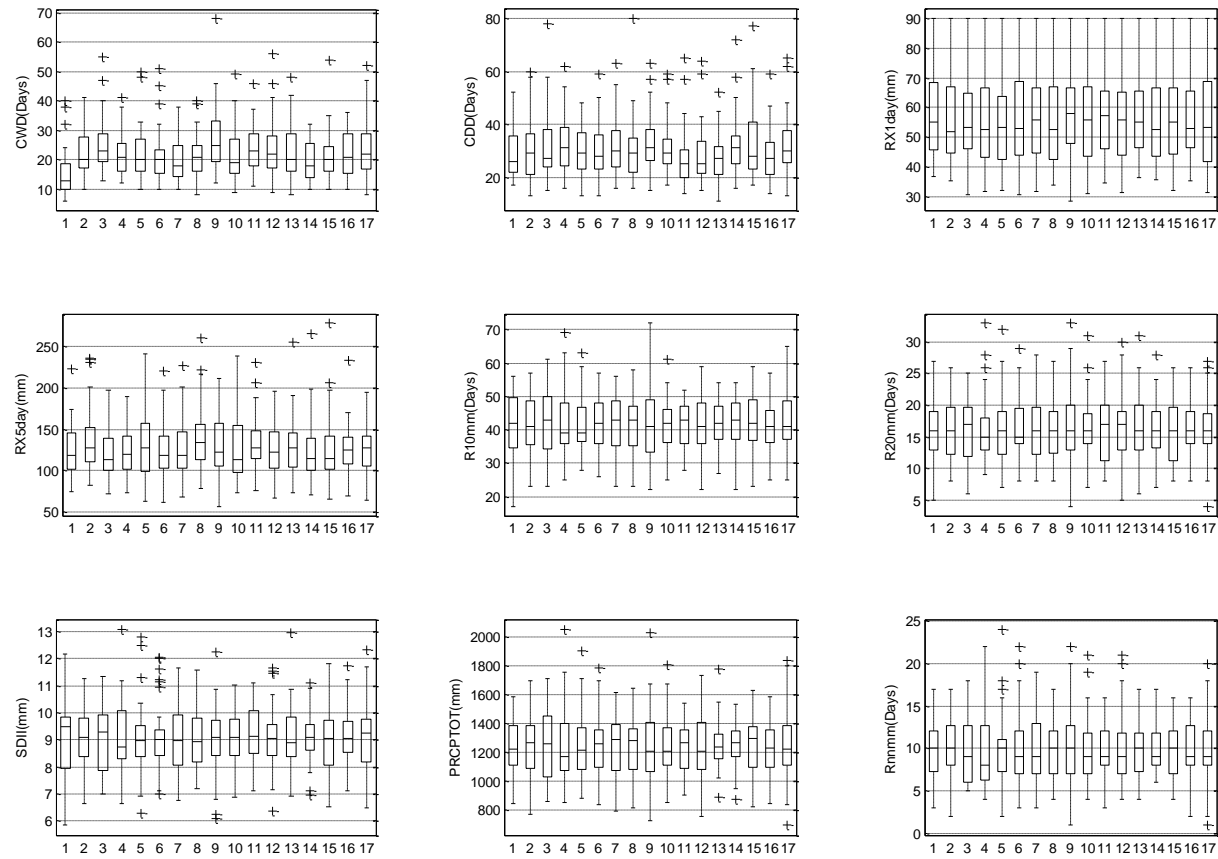


Figure 93: Station 10 WMO indices bias evaluation after quantile mapping.

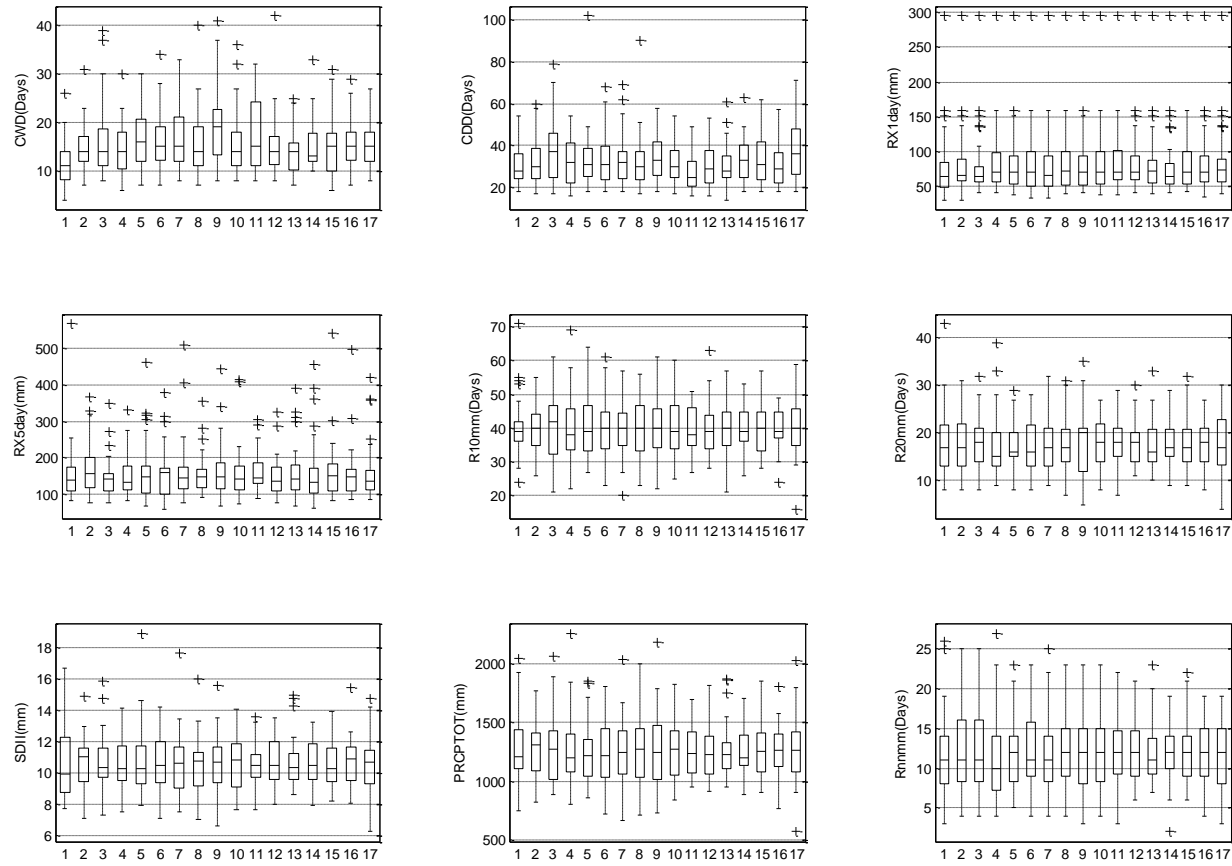


Figure 94: Station 11 WMO indices bias evaluation after quantile mapping.

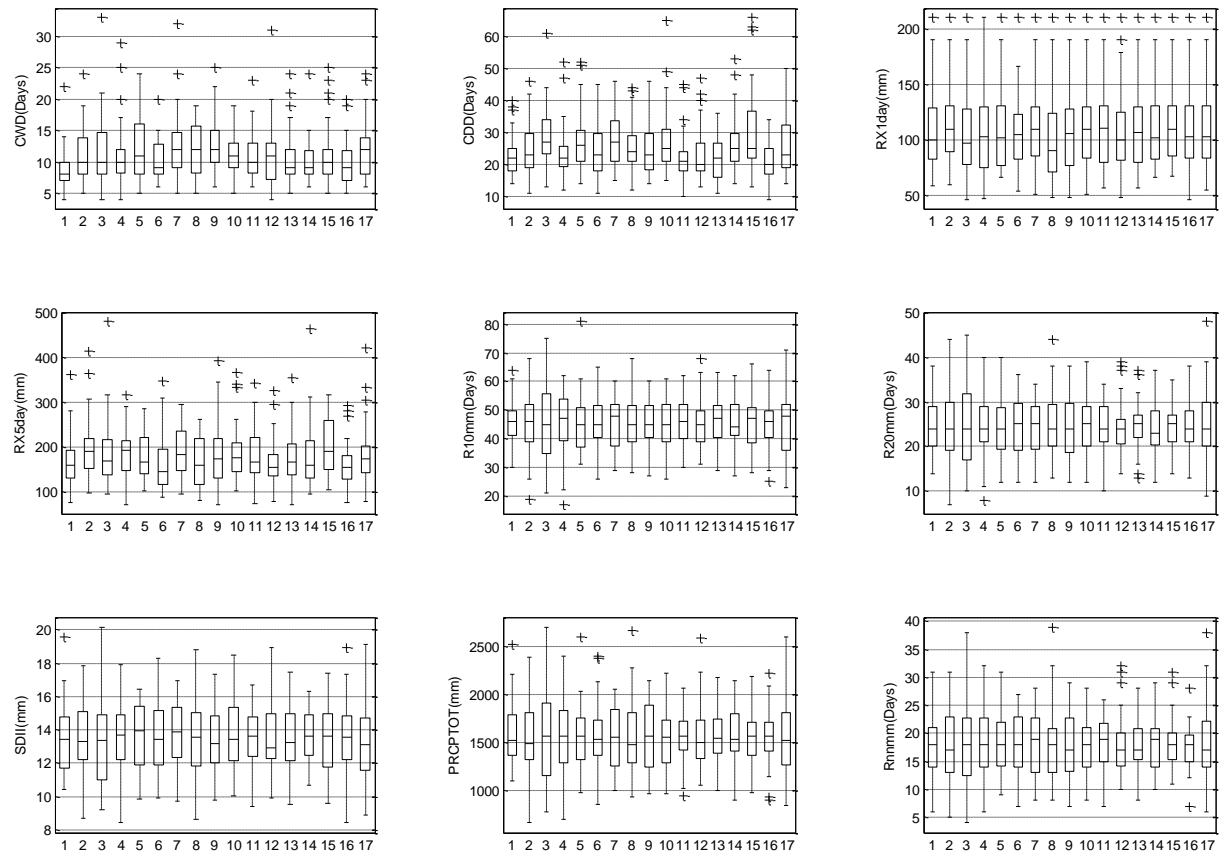


Figure 95: Station 13 WMO indices bias evaluation after quantile mapping.

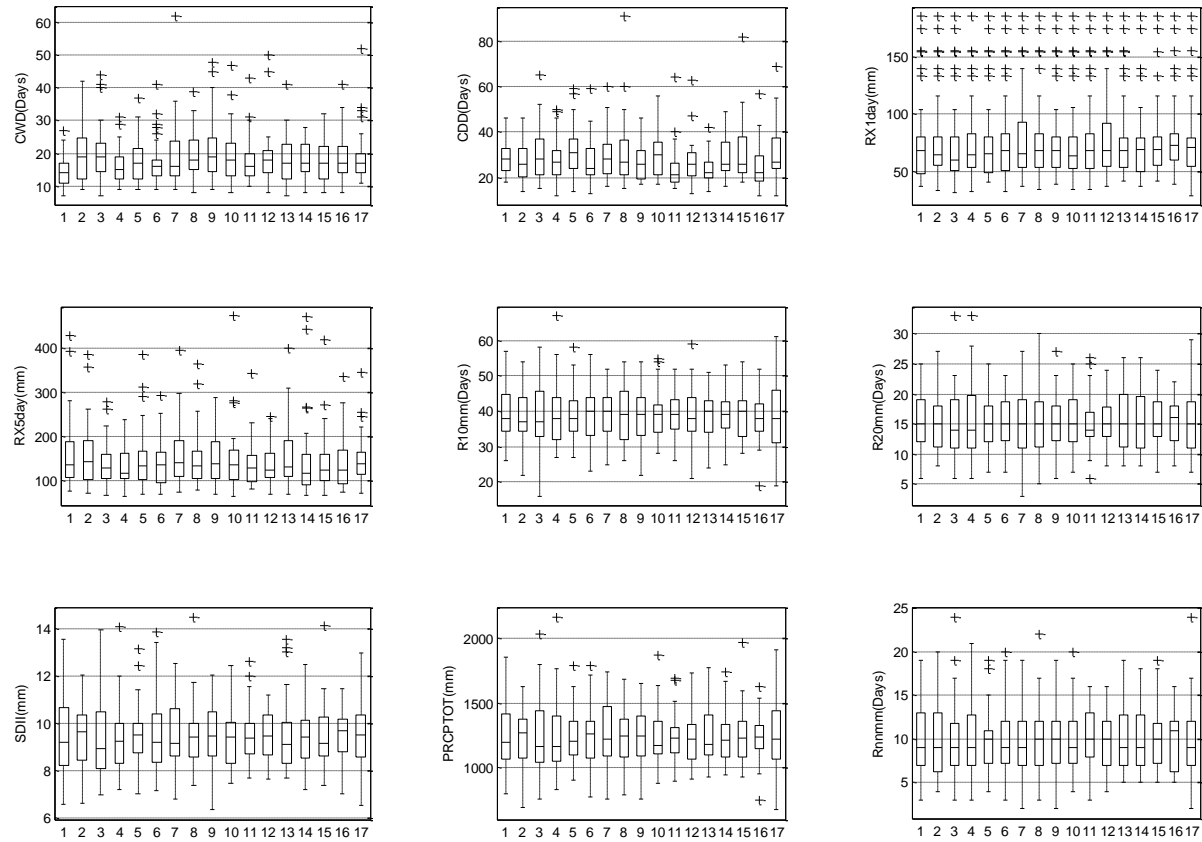
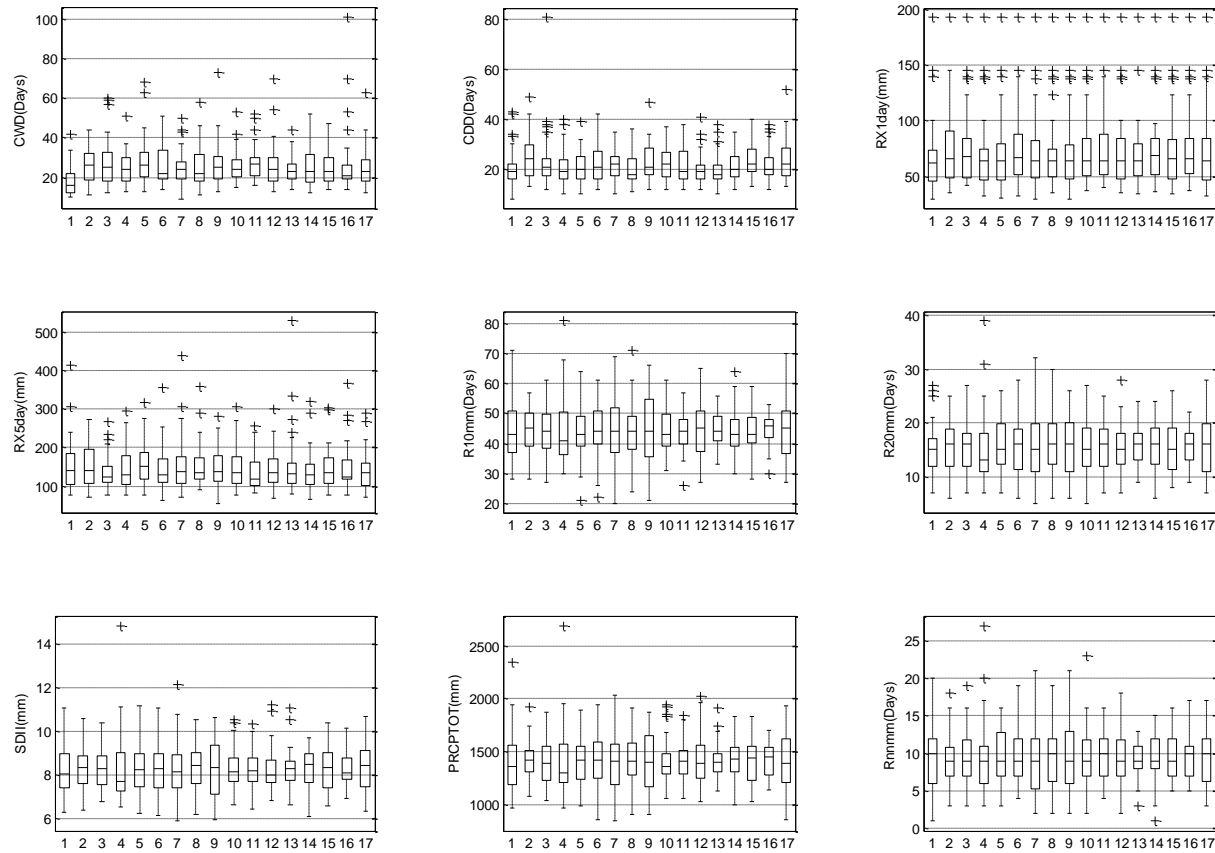


Figure 96: Station 14 WMO indices bias evaluation after quantile mapping.



**Figure 97: Station 15 WMO indices bias evaluation after quantile mapping.**

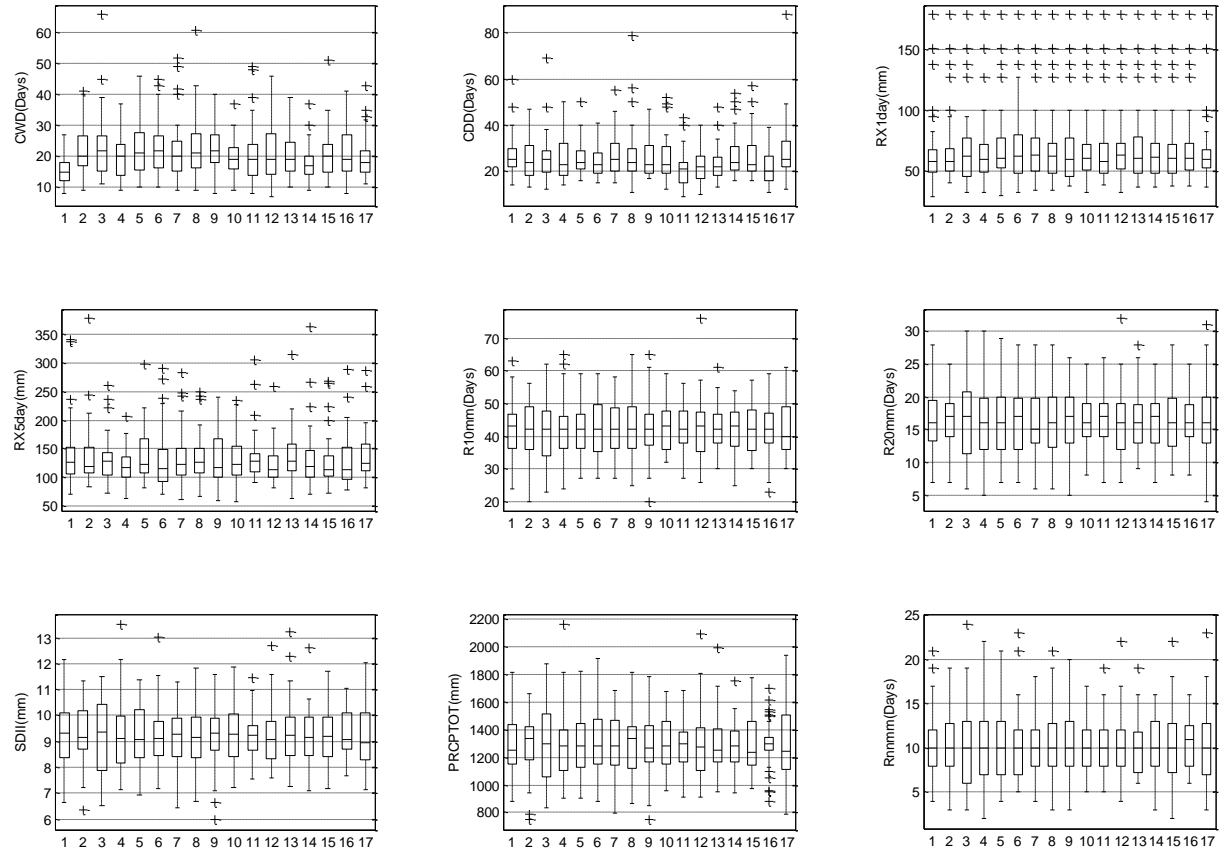
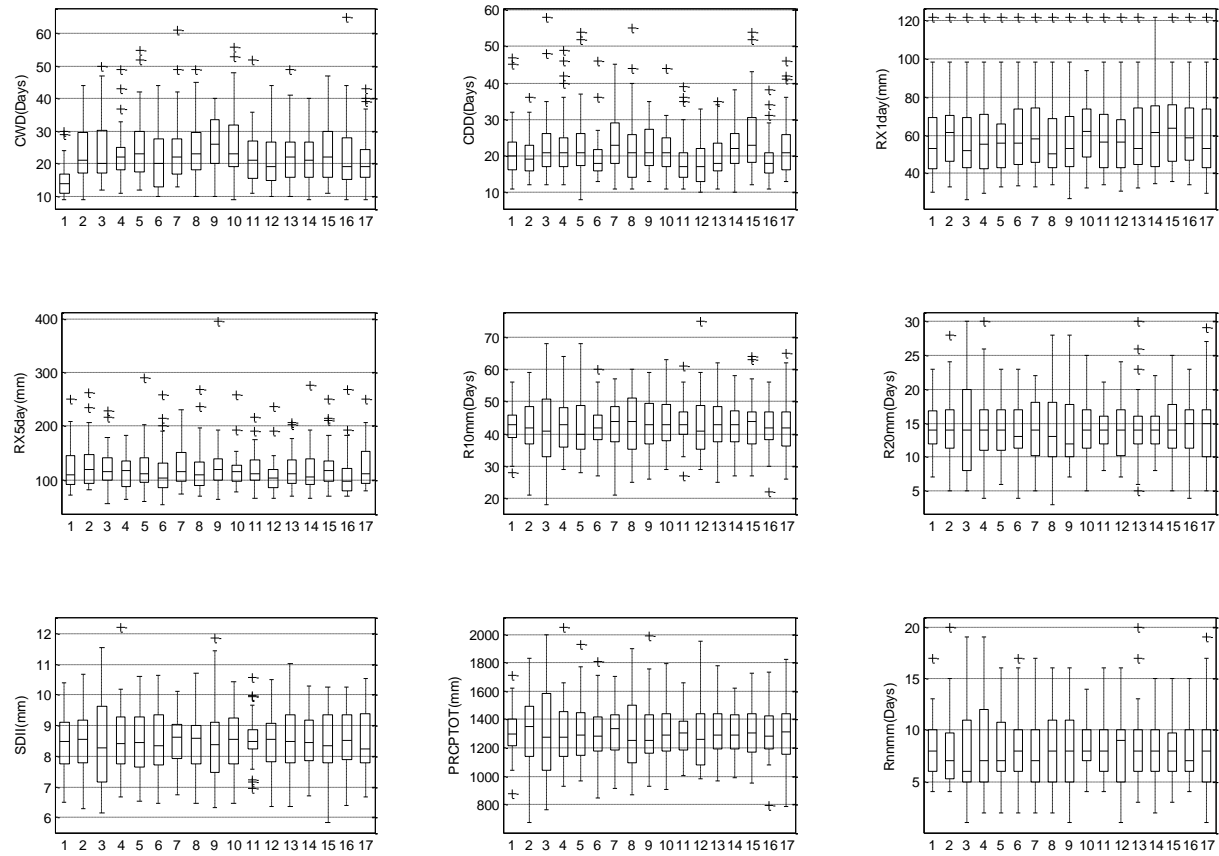


Figure 98: Station 16 WMO indices bias evaluation after quantile mapping.



**Figure 99: Station 17 WMO indices bias evaluation after quantile mapping.**

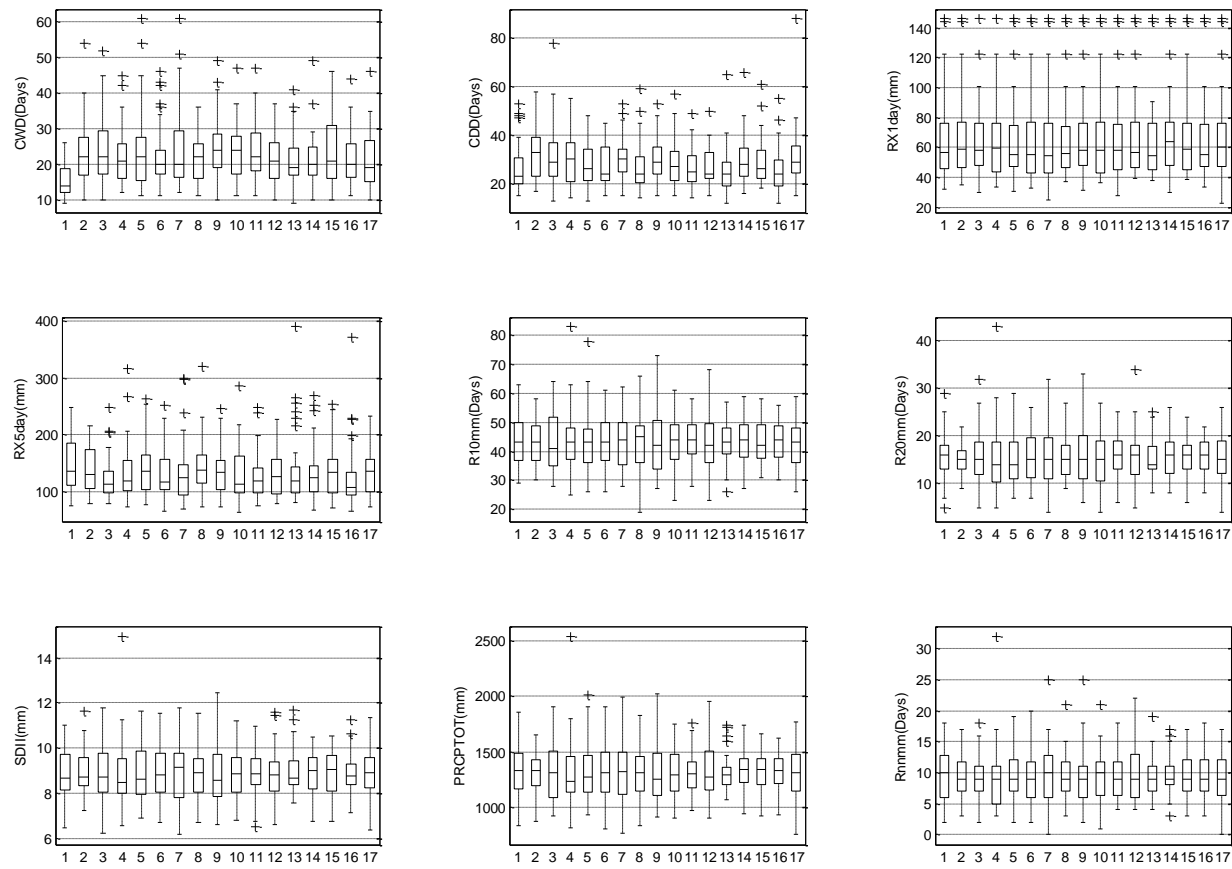


Figure 100: Station 18 WMO indices bias evaluation after quantile mapping.

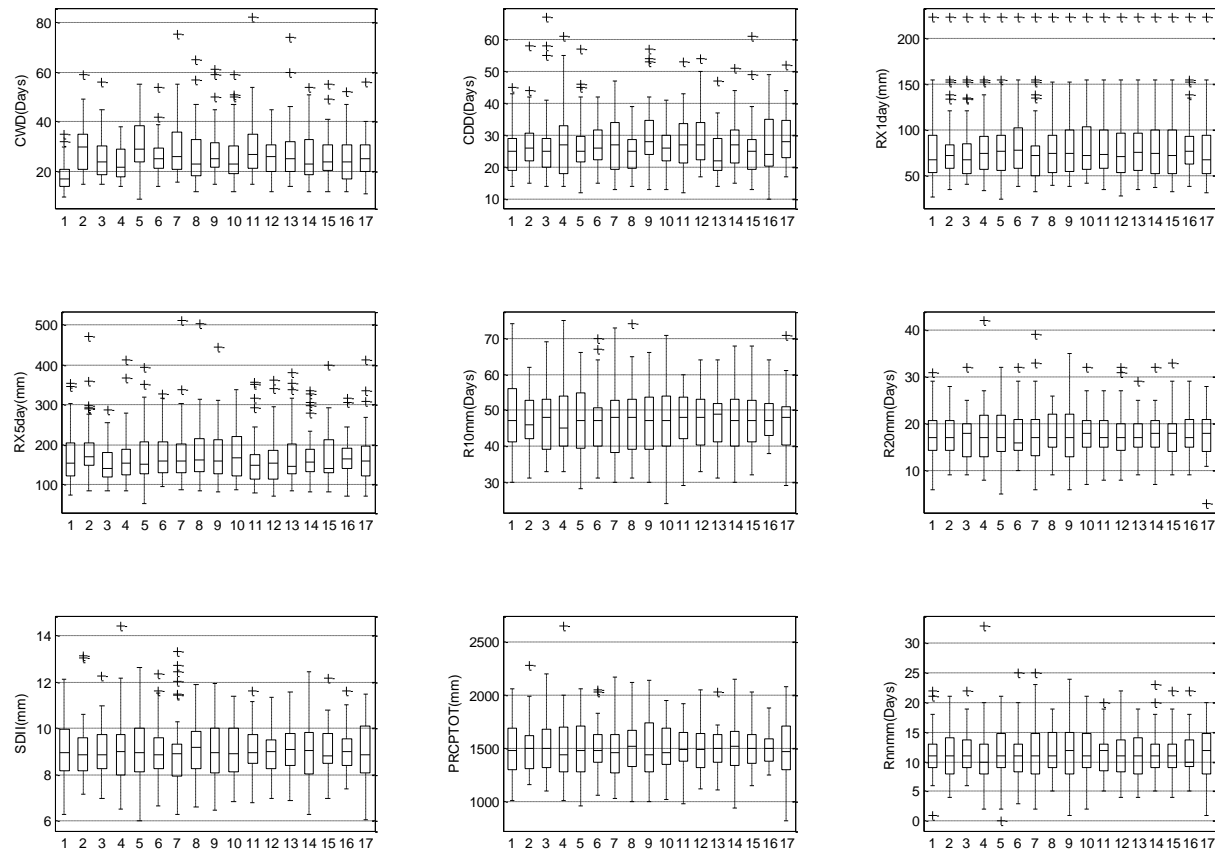


Figure 101: Station 19 WMO indices bias evaluation after quantile mapping.

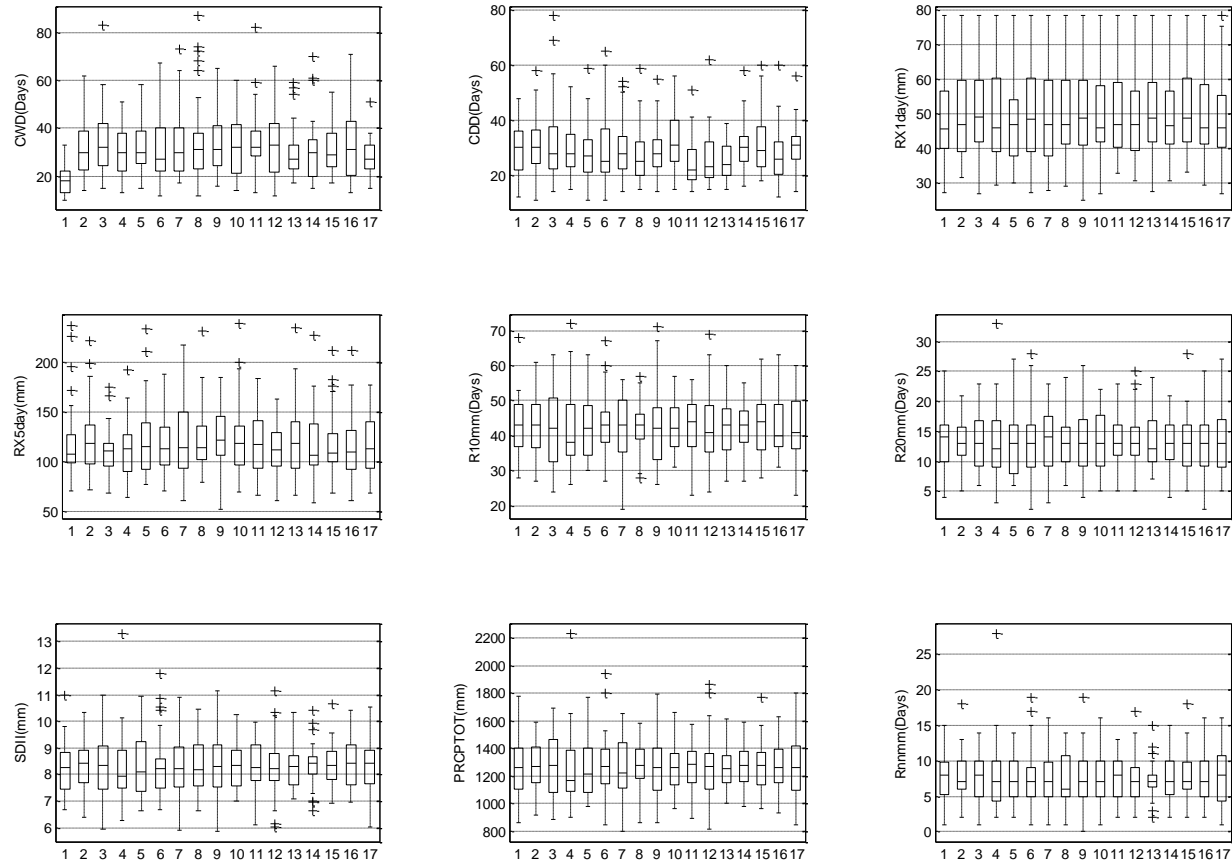


Figure 102: Station 21 WMO indices bias evaluation after quantile mapping.

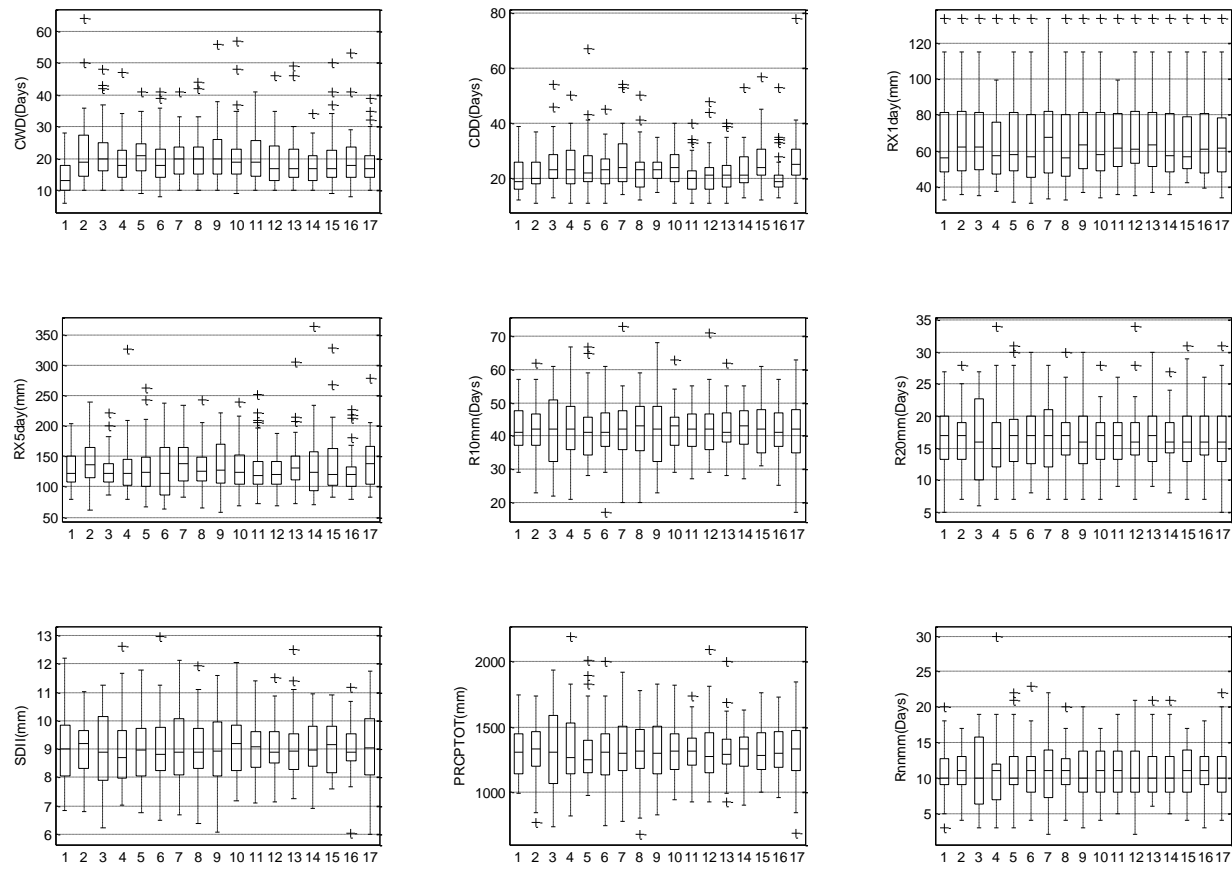


Figure 103: Station 22 WMO indices bias evaluation after quantile mapping.

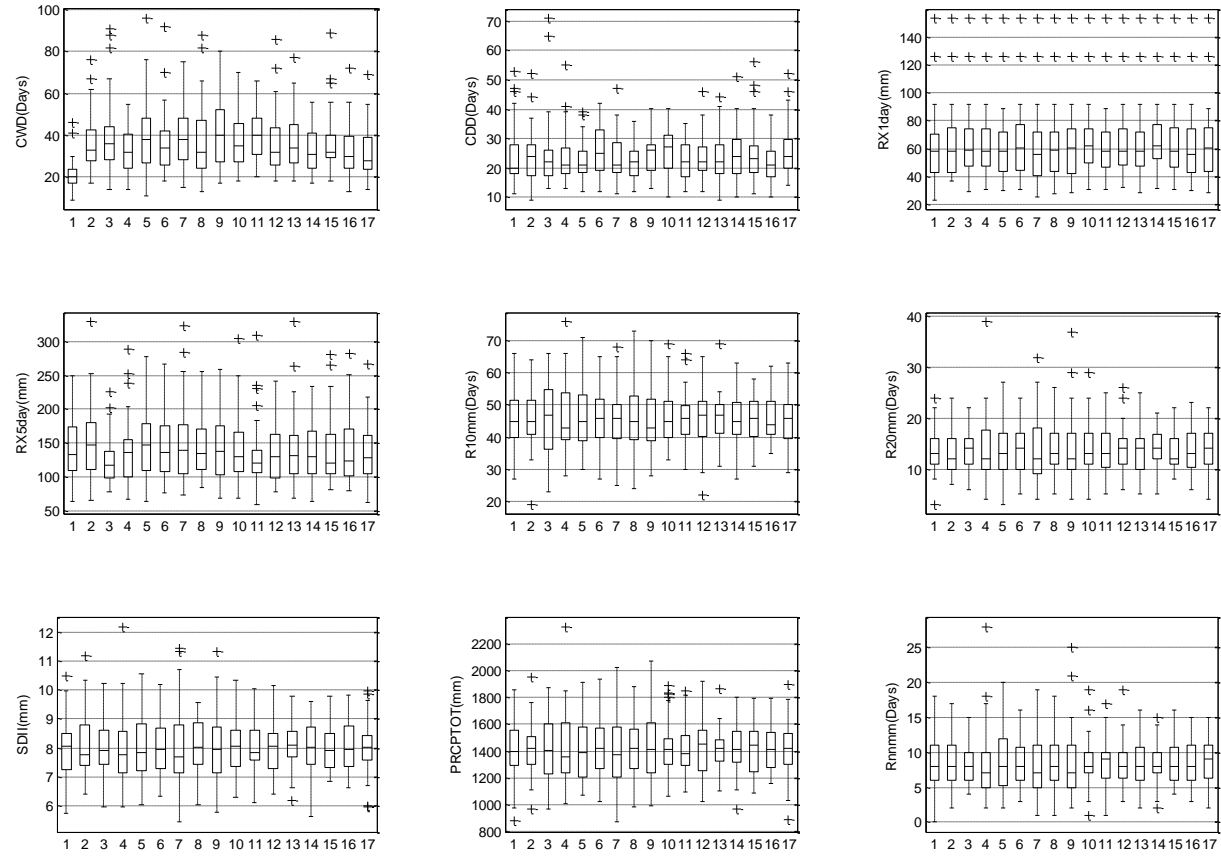
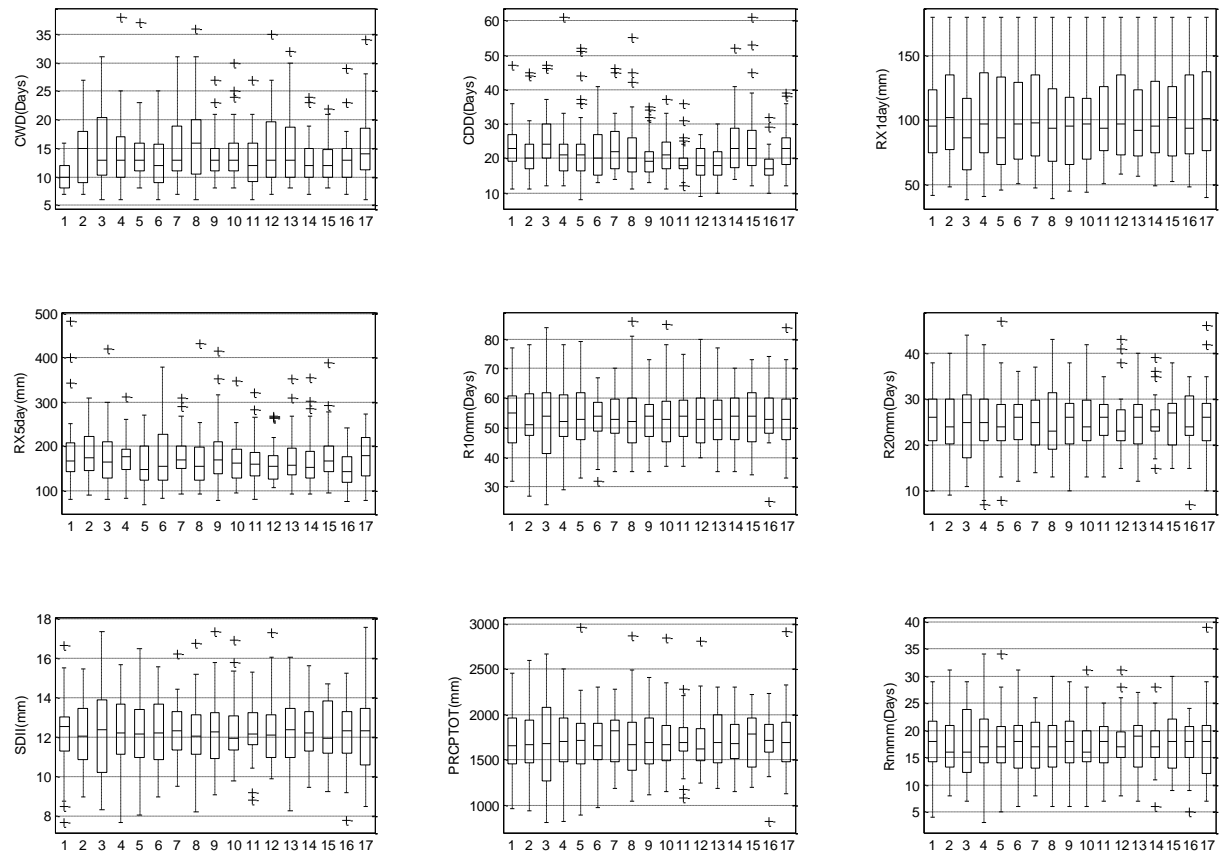


Figure 104: Station 23 WMO indices bias evaluation after quantile mapping.



**Figure 105: Station 24 WMO indices bias evaluation after quantile mapping.**

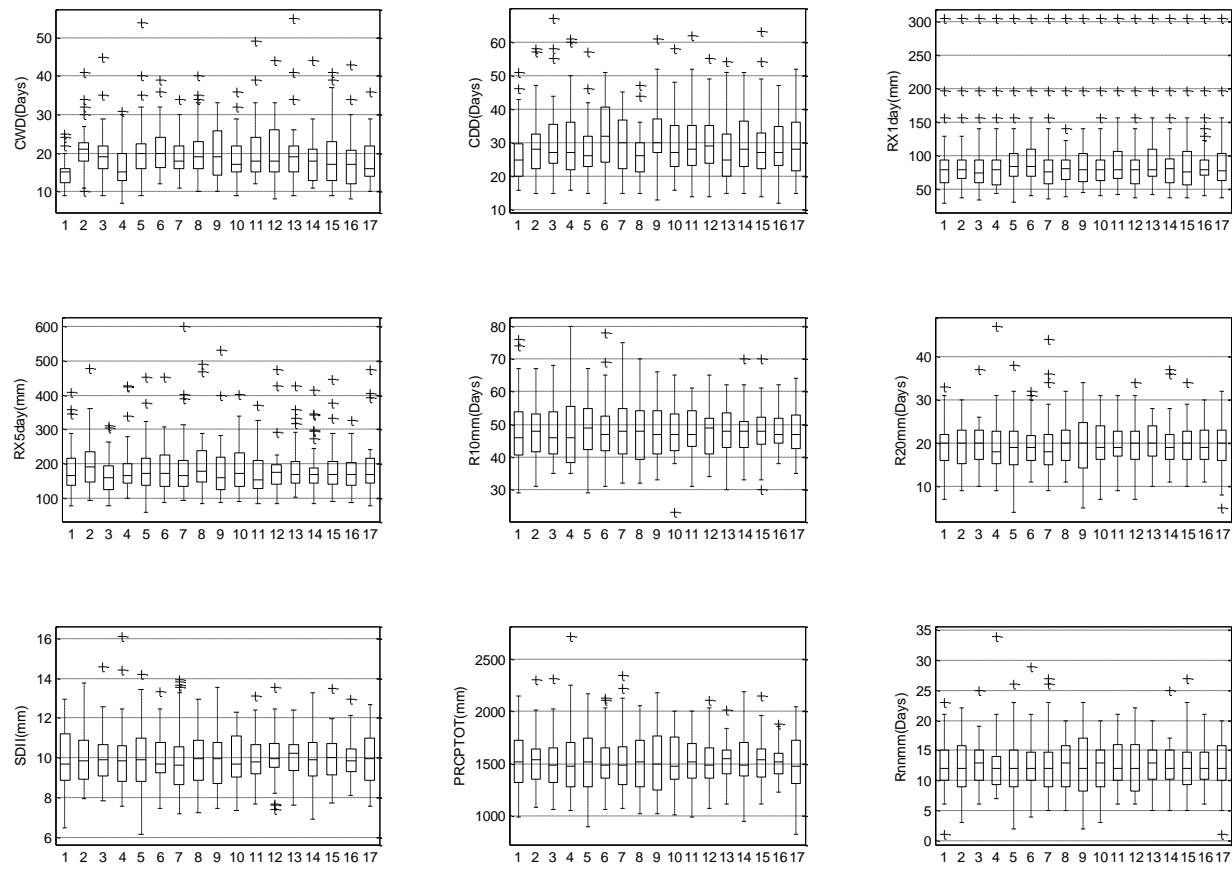


Figure 106: Station 26 WMO indices bias evaluation after quantile mapping.

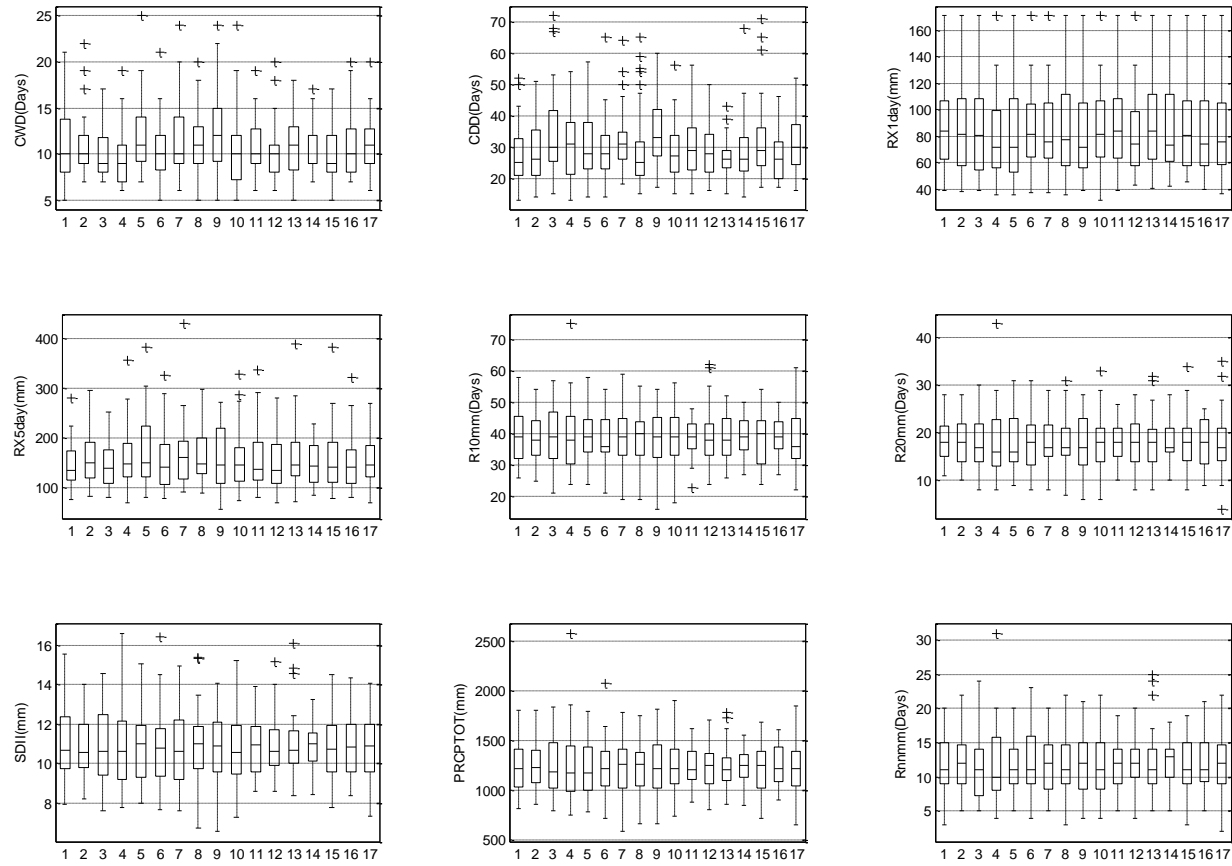


Figure 107: Station 27 WMO indices bias evaluation after quantile mapping.

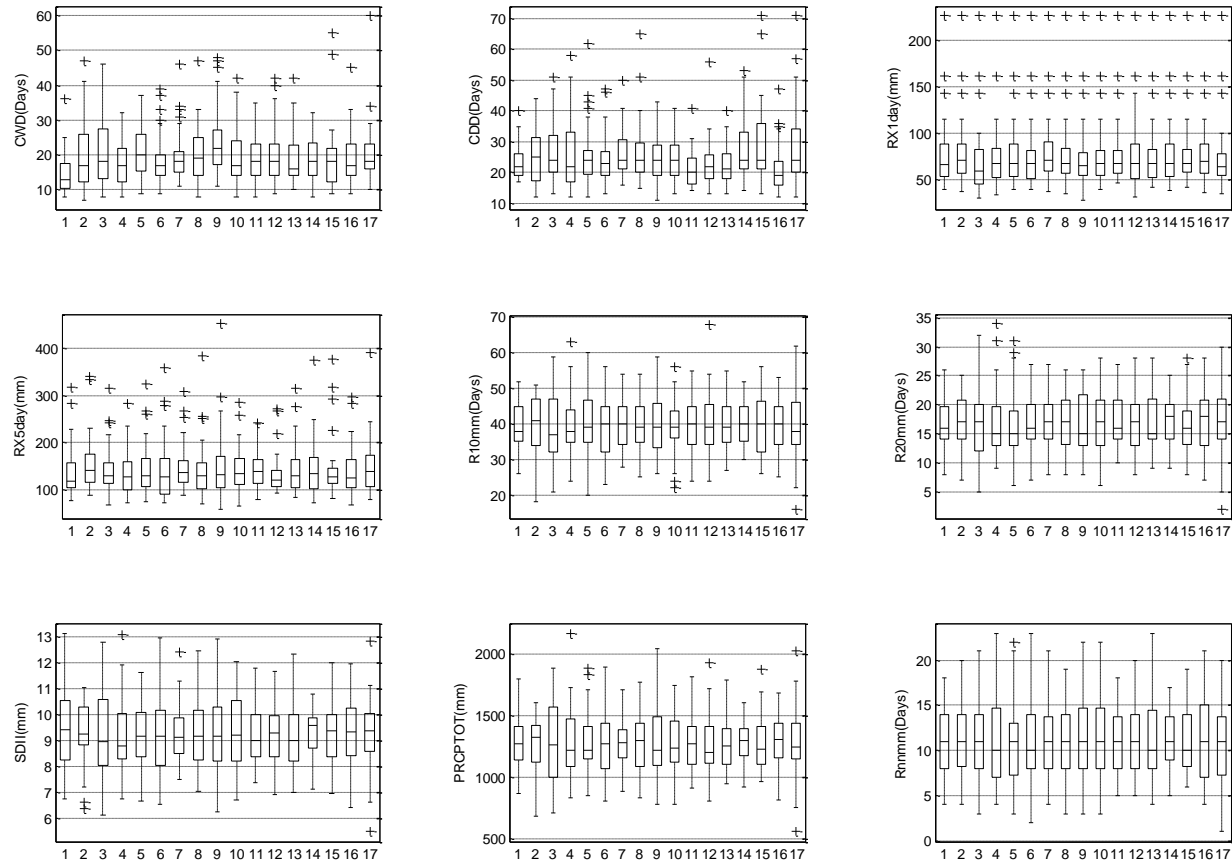


Figure 108: Station 28 WMO indices bias evaluation after quantile mapping.

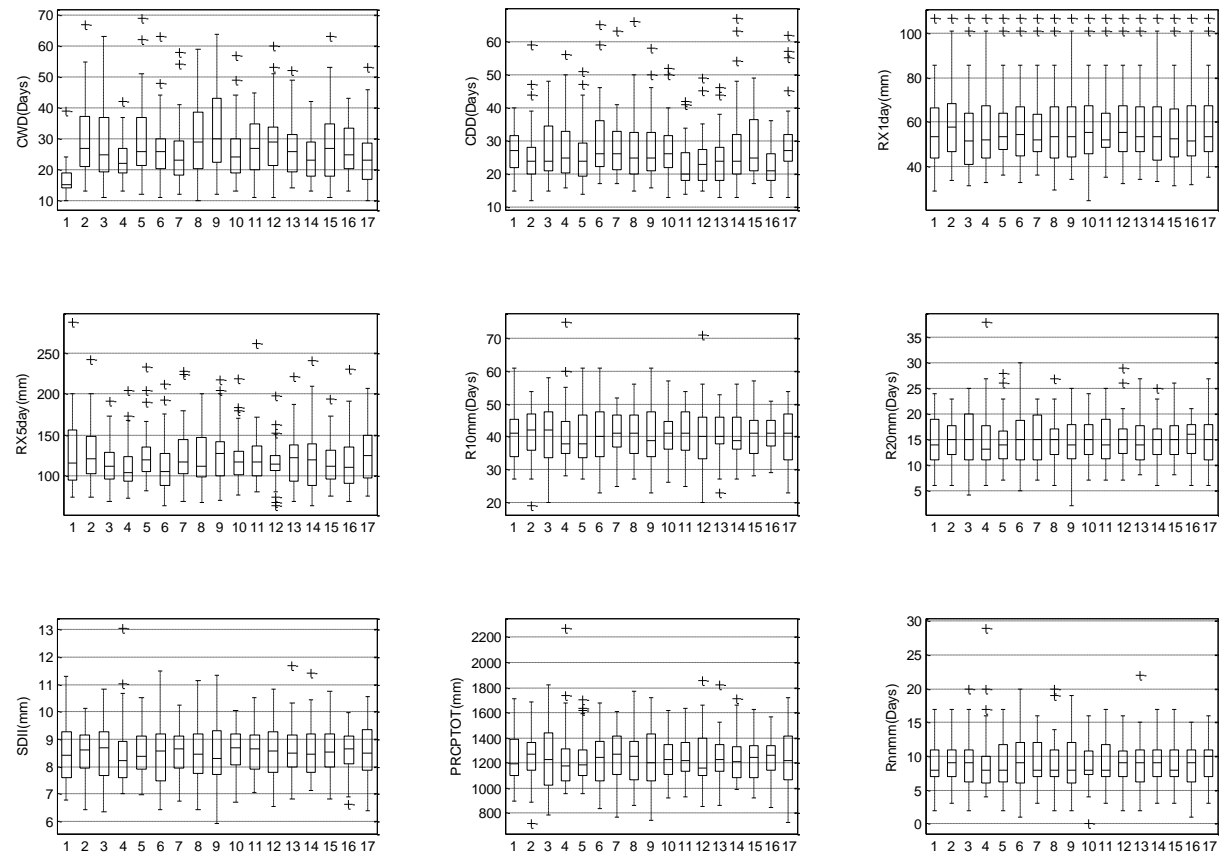


Figure 109: Station 29 WMO indices bias evaluation after quantile mapping.

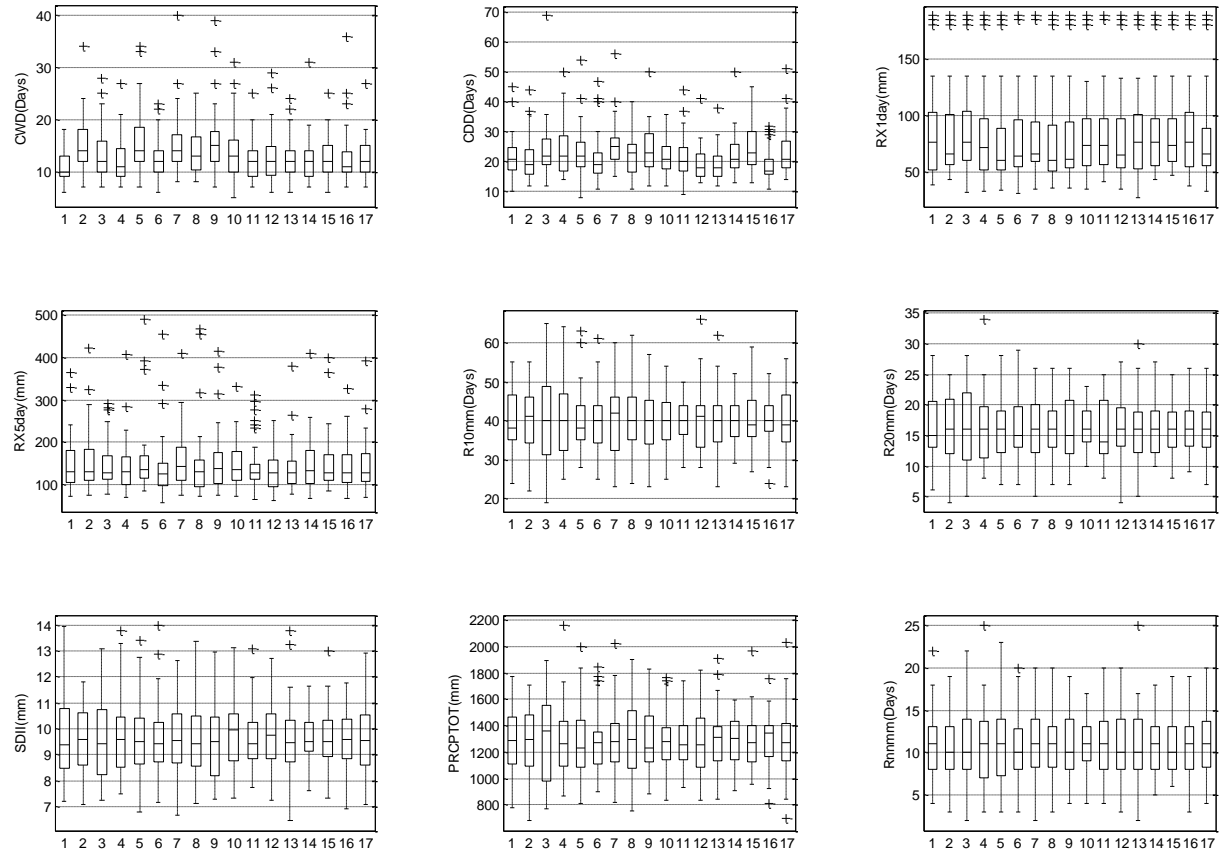


Figure 110: Station 30 WMO indices bias evaluation after quantile mapping.

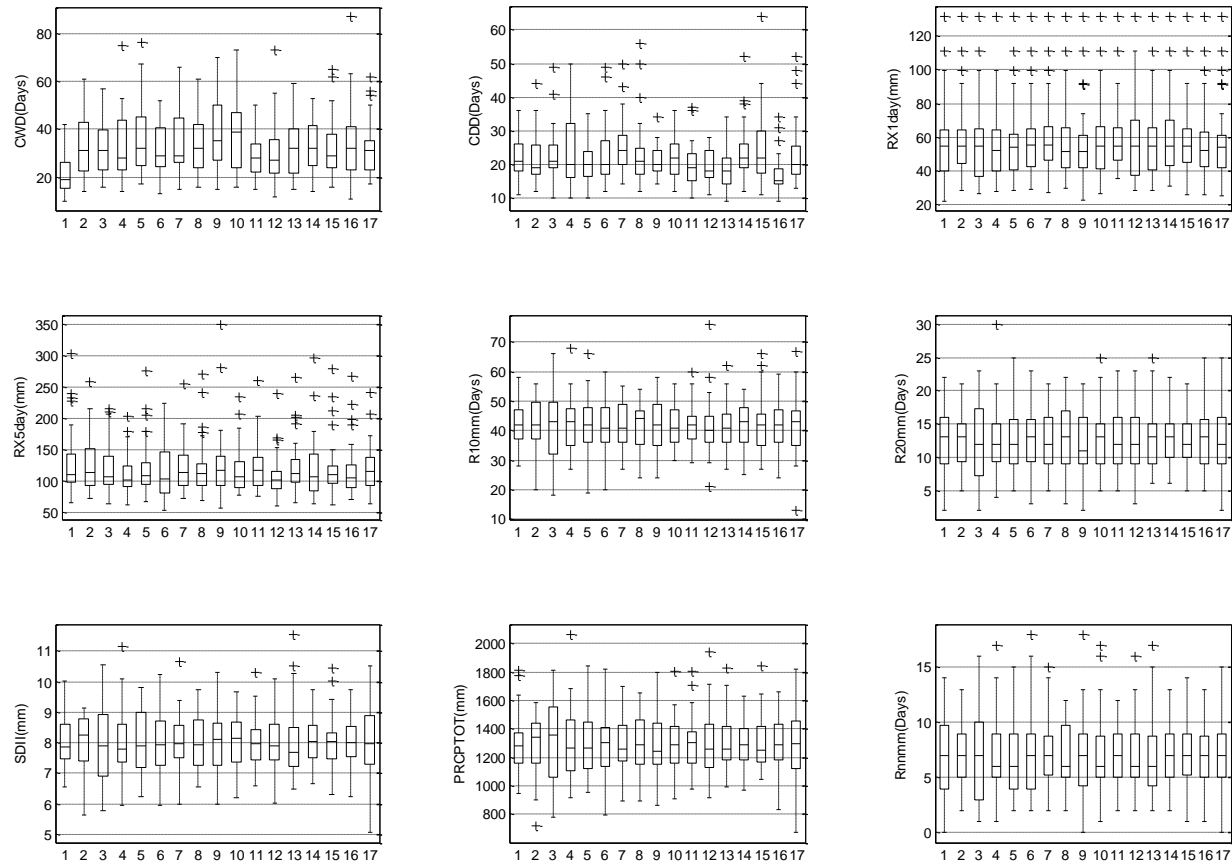


Figure 111: Station 31 WMO indices bias evaluation after quantile mapping.

## References

- Arisz, H., & Burrell, B. C. (2006). *Urban Drainage Infrastructure Planning and Design*. New Burnswick: IEEE.
- Bates, B., Kundzewicz, Z., Wu, S., & Palutikof, J. (2008). *Climate Change and Water: Technical Paper of the Intergovernmental Panel on Climate Change*, . Geneva, Switzerland: IPCC Secetariat.
- Brekke, L. (2013). *Addressing Climate Change in Long-Term Water Resources Planning and Managment*. Washington DC: U.S. Army Corps of Engineers.
- Brekke, L. D., Kiang, J. E., Olsen, J. R., Pulwarty, R. S., Raff, D. A., Turnipseed, D. P., et al. (2009). *Climate Change and Water Resources Management*:. Virginia: USGS.
- Carpenter, A., & Provorse, C. (1998). *The World Almanac of the U.S.A*. The United States Geological Survey.
- Chernick, M. (2007). *Bootstrap Methods: A Guide for Practitioners and Researchers*. Wiley-interscience.
- Chung, F. P. (2010). DFG USGS and USFWS Downscaling Workshop. *Experience with Downscaling Techniques at DWR*. California: Department of Water Resources State of California.
- CIG, C. I. (2008). *About PDO*. (CIG) Retrieved from CSES: <http://cses.washington.edu/cig/pnwc/aboutpdo.shtml>
- CIG, C. I. (2011). *Climate Variability*. (Center for Science in the Earth System) Retrieved Februrary 6, 2013, from Climate Impacts Group: <http://cses.washington.edu/cig/pnwc/clvariability.shtml>

- Claussen, M. (1998). *Climate modeling for Earth System Modelling: Concepts and Experiments*. Journals of Meteorology (NF)36.
- Davison, A., & Hinkley, D. (1997). *Bootstrap Methods and their Applications*. Cambridge University Press.
- Denault, C., Miller, R., & Lence, B. (2002). Climate Change and Drainage Infrastructure Capacity in an Urban. *Journal of the American Water Resources Association*, 42(3): 685-697.
- Durkee, J. D., Frye, J. D., Fuhrmann, C. M., Lacke, M. C., Jeong, H. G., & Mote, T. L. (2007). *Effects of the North Atlantic Oscillation on precipitation-type*. Theoretical and Applied Climatology.
- Easterling, D., Meehl, G., Parmesan, C., Changon, S., Karl, T., & Mearns, L. (2000). *Climate extremes: observations, modeling, and impacts*. Science.
- Efron, B. (1979). *Bootstrap methods: another look at the jackknife*. Ann. Stat.
- Efron, B., & Gong, G. (1983). *A leisurely look at the bootstrap, the jackknife, and cross validation*. Am. Stat.
- Efron, B., & Tibshirani, R. (1993). *An Introduction to the Bootstrap*. London: Chapman and Hall.
- Enfield, D. B., Mestas-Núñez, A. M., & Trimble, P. J. (2001). The Atlantic Multidecadal Oscillation and its Relation to Rainfall and River Flows in the Continental U.S. *Geophysical Research Letters*, 28(10): 2077-2080.
- Gershunov, A., & Barnett, T. (1998). *Interdecadal Modulation of ENSO Teleconnections*. American Meteorologic Society.
- Hamlet, A. (2011). *Impacts of Climate Variability and Climate Change on Transportation Systems*. Seattle: Washington University.

- Hurrell, J. W., Kushnir, Y., Ottersen, G., & Visbeck, M. (2003). The North Atlantic Oscillation: Climatic Significance and Environmental Impact. *National Center for Atmospheric Research, 134*, 98(23): 69-94.
- IPCC. (2000). *Summary for Policymakers: Emission Scenarios*. Intergovernmental Panel on Climate Change.
- IPCC. (2007). *The Physical Science Basis. Summary for Policymakers*. New York: Cambridge University Press.
- IPCC. (2011, ovember 28). *Criteria for Selecting Climate Scenarios*. (IPCC) Retrieved Februrary 6, 2013, from Data Distribution Centre: [http://www.ipcc-data.org/ddc\\_scen\\_selection.html](http://www.ipcc-data.org/ddc_scen_selection.html)
- Jain, S., & Lall, U. (2001). *Floods in a changing climate: Does the past represent the future?* Water Resources Reasearch.
- Katz, R., Parlange, M., & Naveau, P. (2002). *Statistics of Extremes in Hydrology*. ELSEVIER; Advances in Water Resources.
- Knight, J., Folland, C., & Scaife, A. (2006). *Climate impacts of the Atlantic Multidecadal Oscillation*. Geophysical Research Letters.
- Lemmen, D., Warren, F., Lacroix, j., & Bush, E. (2007). *From impacts to adaption: canada in a changing climate*. Government of Canada.
- Madsen, T., Group, F., Wilcox, N., & Center, E. A. (2012). *When It Rains, It Pours: Global Warming and the Increase in Extreme Precipitation*. Environment America Research and Policy Center.
- Mailhot, A., & Duchesene, S. (2010). Design cruiteria of urban drainage infrastructures under climate change. *Journal of Water resource planning and managment*, 136: 201-208.

- Maurer, P., E., Brekke, L., Pruitt, T., & Duffy, P. (2007). *'Fine-resolution climate projections enhance regional climate change impact studies'*. Eos Trans. AGU.
- Melillo, J., & Peterson, T. (2009). *Global Climate Change Impacts in the United States*. New York: Cambridge University Press.
- Moss, R., Edmonds, J., Hibbard, K., Manning, M., Rose, S., Van Vuuren, D., et al. (2010). The next generation of scenarios for climate change research and assesment. *Nature*, 463: 747-756.
- Nielsen, K. (2011). Quantification of climate change effects on extreme precipitation used for high resolution hydrologic design. *Urban Water Journal*, 9:2, 57-64.
- Null, J. (2012, November 15). *El Niño and La Niña Years and Intensities*. Retrieved from GG Weather: <http://ggweather.com/enso/oni.htm>
- Obeyskera, J., Trimble, P., Neidrauer, C., Strowd, T., Hall, C., & Pathak, C. (2006). *Consideration of Long-Term Climatic Variation in SFWMD Planning and Operations*. South Florida Water Managment District.
- Overeem, A., Buishand, A., & Holleman, I. (2008). *Rainfall depth-duration-frequency curves and their uncertainties*. Journal of Hydrology.
- Riorbdan, R. (2008, December 8). *Natural Geography*. Retrieved 10 12, 2013, from [www.landscape.org](http://www.landscape.org): [http://www.landscape.org/florida/natural\\_geography/](http://www.landscape.org/florida/natural_geography/)
- RMetS, R. M. (2009). Climate extremes: progress and future directions. *International journal of climatology*, 29: 317-319.
- Ropelewski, C. F., & Halpert, M. (1986). North American Precipitation and Temperature Patterns Associated with the El Niño/Southern Oscillation (ENSO). *Journal of Climate*, 114(12): 268-284.

- Rosenburg, E., Keys, P., Booth, D., Hartley, D., Burkley, J., Stienmann, A., et al. (2010). Precipitation extremes and the impacts of climate change on stormwater infrastructure in Washington State. *Climate Change*, 102: 319-349.
- Rosenzwei, C., Solecki, W. D., Hammer, S. A., & Mehrotra, S. (2011). *Climate Change and Cities: First Assessment Report of the Urban Climate Change Research Network*. USA: Cambridge University Press.
- Scott, M. (2010, August 2). *Will Hurricanes Change as the World Warms?* Retrieved January 9, 2012, from Climate Watch Magazine: <http://www.climatewatch.noaa.gov/article/2010/will-hurricanes-change-as-the-world-warms-2>
- Tank, A., Zwiers, F., & Zhang, X. (2009). *Guidelines on the analysis of extremes in a changing climate in support of informed decisions for adaptation*. Climate data and monitoring.
- Teegavarapu, R. (2013). *Climate change-sensitive hydrologic design under uncertain future*. Boca Raton: Journal of Hydrology.
- Teegavarapu, R. S. (2012). *Assessment and Evaluation of NEXRAD-based Rainfall Estimates in South Florida Water Management District*. Boca Raton : Florida Atlantic University.
- Teegavarapu, R., Goly, A., & Obeysekera, O. (2013). Influences of Atlantic multidecadal oscillation phases on spatial. *Journal of Hydrology*, 495: 74-93.
- Viner, D. P. (2011, November 28). *What is a GCM?* (IPCC) Retrieved February 6, 2013, from Data Distribution Centre: [http://www.ipcc-data.org/ddc\\_gcm\\_guide.html](http://www.ipcc-data.org/ddc_gcm_guide.html)
- Visbeck, M. H., Hurrell, J. W., Polvani, L., & Cullen, H. M. (2001). *The North Atlantic Oscillation: Past, present, and future*. PNAS.

- Wilby, R., Charles, S., Zorita, E., Timbal, B., Whetton, P., & Mearns, L. (2004). *Guidelines for use of climate scenarios developed from statistical downscaling models*. USA: National center of atmospheric research.
- Wilks, D. (2006). *Statistical Methods in the Atmospheric Sciences*. Department of Earth and Atmospheric Sciences Cornell University.
- Willems, P., Arnberjerg-Nielson, K., Olsson, J., & Nguyen, V. (2011). Climate Change Impacts assesment on urban rainfall extremes and urban drainage: Methods and shortcomings. *Atmospheric Research*, 103: 106-118.
- Zhang, X., Zwiers, F., Hegerl, G., Lambert, F., Gillett, N., Solomon, S., et al. (2007). *Detection of human influence on 20th century precipitation trends*. Nature.